

UNIVERSITY OF TRENTO - Italy  
Department of Civil, Environmental  
and Mechanical Engineering



Doctoral School in Civil, Environmental and Mechanical Engineering  
Topic 1. Civil and Environmental Engineering - XXX cycle 2016/2017

Doctoral Thesis - July 2018

Gianni Schiro

**Timber composite solutions for high performance new  
diaphragms and structural rehabilitation  
of existing floors**

**Supervisors**

Prof. Maurizio Piazza, DICAM - University of Trento

Dr. Ivan Giongo, DICAM - University of Trento

Credits of the cover image: Gianni Schiro

University of Trento  
Doctoral School in Civil, Environmental and Mechanical Engineering  
*<http://web.unitn.it/en/dricam>*  
Via Mesiano 77, I-38123 Trento  
Tel. +39 0461 282670 / 2611 - *[dicamphd@unitn.it](mailto:dicamphd@unitn.it)*

*Ai miei genitori e a tutti quelli  
che hanno saputo credere in me*



## ABSTRACT

The main aim of this research work was to deepen the understanding of the mechanical behaviour of timber-to-timber composite (TTC) floors with incomplete interaction in order to develop, design and test high performance solutions. Several types and arrangements of connections and different timber products, made from both softwood and hardwood species, were considered for the realisation of diaphragms suitable for a wide range of structural applications.

An original assembly procedure, developed at the University of Trento, was adopted in the optimization process of these technical solutions. Such innovative procedure allows the designers to pre-stress and camber composite timber elements by simply relying on screw type connectors. The experimental tests presented in this thesis positively contributed to the calibration and validation of this assembly technique, confirming the method applicability. The test results were consistent with the numerical and analytical models, in terms of uplifts, stress levels and overall mechanical performance. The benefits from adopting the above-mentioned procedure appeared to be persistent over time, as the result of an experimental test where four composite specimens, 5.4 m long, were loaded out-of-plane and subjected to continuous monitoring under controlled environmental conditions for a period of two years.

The research program was organized into two phases. The first phase was dedicated to the study of alternative strategies for retrofit interventions on timber diaphragms in historical heritage buildings. An extensive experimental campaign on the out-of-plane behaviour of the retrofitted diaphragms was performed in order to evaluate the effectiveness of the different techniques analysed. Specifically, hybrid solutions that coupled the reduced weight of softwood elements with the strength of hardwood components by means of different types of fasteners, were compared with “more common” timber-to-timber strengthening techniques. A large number of tests, covering fourteen configurations obtained by changing fasteners type, fastener arrangement and timber products, were performed to maximize the performance (cost/effectiveness) of

the retrofit techniques. Test outcomes included characterization of stiffness, strength, static ductility and residual strength of the connection systems as well.

The second phase of the program was devoted to the development of solutions for newly constructed diaphragms, either for new building applications or replacement of damaged/inadequate existing floors. The second phase research work included the design and testing of prefabricated timber-to-timber composite floor modules to be assembled by using laminated veneer lumber (LVL) made of beech wood. Full scale tests were performed on 6 m long and 10 m long modules, respectively designed for residential areas and offices. In addition to the full-scale testing of the modules, the connection system optimization was performed by referring to different types of test protocols, including both push-out and pull-out testing.

# INDEX

Abstract .....	3
1 Introduction .....	9
1.1 Thesis outline .....	13
1.2 References .....	15
2 An innovative procedure for pre-stressing and cambering timber composite beams .....	19
2.1 Introduction .....	19
2.2 Analytical formulation.....	21
2.3 Numerical model .....	28
2.4 Model comparison .....	28
2.5 Experimental validation.....	33
2.6 Parametric analysis.....	41
2.6.1 Influence of connection stiffness and compression force on the final camber value.....	41
2.6.2 Analysis of the deformation: flexural deformation and rigid body rotation.	43
2.6.3 Influence of the fastener arrangement on the final camber .....	44
2.7 Conclusions .....	49
2.8 References .....	50
3 Testing of timber-to-timber screw-connections in hybrid configurations .....	53
3.1 Introduction .....	53
3.2 Connection tests .....	55
3.2.1 Test configuration and geometry .....	55
3.2.2 Timber elements .....	57
3.2.3 Connectors.....	57
3.2.4 Test setup and instruments .....	60
3.2.5 Estimation of connection mechanical parameters .....	61
3.2.6 Experimental results .....	62
3.2.7 Comparison between experimental results and theoretical models .....	66
3.3 Experimental result comparison .....	70

---

3.3.1	Comparison parameter: screw configuration.....	70
3.3.2	Comparison parameter: timber product combination (hybrid solutions)..	72
3.3.3	Comparison parameter: screw typology (ST & DT) .....	74
3.3.4	Comparison parameter: timber product arrangement and failure mode...	75
3.3.5	Comparison parameters: ductility and residual strength.....	77
3.4	Considerations on practical issues .....	79
3.5	Conclusions .....	80
3.6	Annex: Formulas and parameters for theoretical values calculation .....	82
3.6.1	A: Theoretical load-bearing capacity calculation .....	82
3.6.2	B: Theoretical slip modulus calculation .....	85
3.7	References .....	87
4	Experimental tests on timber-to-timber composite floors .....	91
4.1	Introduction .....	91
4.2	Test set-up .....	92
4.3	Test configurations and results .....	95
4.4	Result comparison .....	122
4.4.1	Hardwood-hardwood solutions.....	128
4.4.2	Solutions for retrofit intervention on timber diaphragms .....	130
4.4.3	Hybrid solutions Vs. hardwood-hardwood solutions .....	133
4.5	References .....	137
5	New high-performance TTC floor-modules realized with beech LVL: design and testing.....	139
5.1	Introduction .....	139
5.2	Connection testing .....	141
5.2.1	Pull-out tests .....	142
5.2.2	Fastener preload tests.....	147
5.2.3	Push-out tests.....	153
5.3	Design parameters .....	155
5.4	Numerical and analytical models .....	157

---

5.5	Floor module design .....	159
5.6	Full scale testing .....	163
5.6.1	Floor modules for residential buildings (L = 6 m) .....	163
5.6.2	Floor module for office areas, schools and restaurants (L = 10 m) ....	185
5.7	Conclusions .....	201
5.8	References .....	204
6	Long-term out-of-plane testing of pre-stressed timber composite floors .....	205
6.1	Introduction .....	205
6.2	Test configurations .....	206
6.2.1	Specimen configurations .....	206
6.2.2	Connection properties.....	209
6.2.3	Design loads and parameters .....	211
6.3	Test set-up and instrument arrangement.....	212
6.4	Experimental results .....	214
6.4.1	Assembly procedure .....	214
6.4.2	Specimen loading (short-term).....	217
6.4.3	Specimen loading (long-term).....	219
6.5	Prediction of the long-term behaviour.....	221
6.6	Conclusions .....	226
6.7	References .....	227
7	Conclusions .....	229



---

# 1 INTRODUCTION

When people refer to timber composite floors, they generally refer to timber-concrete composite (TCC) structures. This construction technique is well-established and used both for the retrofit of existing timber floors (Turrini and Piazza 1983a, b; Ceccotti 1995) and for the realisation of new diaphragms. As stated by Yeoh et al. in [4], the development of TCC systems in Europe started after the World Wars, as a consequence of a shortage of steel for reinforcement in concrete. Over the years, this technique has been subjected to many improvements, since the first ad-hoc connection system was patented by Muller in 1922 [5]. Several research works are available in literature regarding the development of more and more specialized connections [6] and addressing the study of both short-term [7] and long-term [8] flexural behaviour of TCC elements. Historically, timber-concrete floors were realised by using softwood elements, typically glue-laminated or solid timber beams, and a reinforced concrete slab. The availability of “new engineered wood products” such as laminated veneer lumber (LVL) beams made of European beech [9], has successfully contributed to the development of new research activities on TCC floors, as demonstrated by the experiences reported in [10] and [11].

With reference to the design approach, the effects of an incomplete connection between the elements of a composite beams were firstly analysed by Newmark in 1951 [12]. He developed a linear-elastic theoretical model for composite beams with incomplete interaction based on the results of a series of bending tests on steel-to-concrete composite systems carried out in 1943. A simplified solution was subsequently studied by Möhler in 1956 [13] and adopted by the Eurocode 5 – Annex B: mechanically joined beams [14]. This method, better known as  $\gamma$  *method*, permits to define the effective bending stiffness  $(EJ)_{ef}$  of composite beams starting from the linear properties of the elements and the shear stiffness of the connection, which is supposed to be equally distributed along the span. An alternative formulation for the elasto-plastic analysis of

composite structures was proposed by Frangi and Fontana [15]. However, the linear-elastic solution is widely used for the design of composite beams [4].

The success of TCC floors relies on its effectiveness in increasing both the in-plane (lateral loads) and the out-of-plane (gravity loads) performance of existing timber floors. It is widely known that horizontal diaphragms play a key role in the dynamic behaviour of masonry buildings [16]. Post-earthquake damage assessment has shown that unreinforced masonry (URM) building failures are frequently related to the absence of wall-to-wall connectivity, but also to inadequate diaphragms stiffness (in-plane) and lack of connections between floor/roof and lateral walls [17]. This leads to the substantial incapability of masonry buildings to behave as a box. Consequently, diaphragms in URM buildings are required to fulfil three principal functions. First of all, they have to support the design actions (vertical loads) without deflecting excessively. Secondly, they have to provide an effective restraint to the out-of-plane loaded walls, avoiding their overturning along the weak direction. Furthermore, if sufficiently stiff, horizontal diaphragms can provide load distribution among shear walls. The potential improvement of floor performance with respect to each of the aforementioned functions makes this technique very useful in the field of the structural rehabilitation of historical buildings.

However, in spite of the widespread use in the past of reinforced concrete slab for the upgrading of existing timber diaphragms, some limitations have to be considered in light of the acquired experience. Post-seismic reports, after the sequence of earthquakes that struck the Italian regions of Umbria and Marche in 1997, highlighted severe damages on retrofitted masonry buildings. Failures have frequently been attributed to the “excessively stiff response” of horizontal diaphragms, to the mass-increase associated with the interventions based on concrete use and to the detrimental effect resulting from the introduction of concrete curbs inside the wall thickness. Such aspects have proven to negatively affect for the seismic vulnerability of masonry buildings, especially when the quality of the original construction is particularly poor (Parisi and Piazza 2007; Binda and Saisi 2005).

As designers, we have the possibility and the responsibility to learn from past mistakes in order to develop more effective retrofit solutions that are able to satisfy both the current safety requirements and the principles of compatibility and reversibility. The past shortcomings in the regulations, lack of knowledge and sensitivity towards cultural heritage resulted in invasive and detrimental interventions. With reference to timber floors and roofs, there are several examples where the old diaphragms were removed and superseded by new technical solutions (Parisi and Piazza 2007). However, in many cases these renovated structures performed poorly during severe seismic events

confirming that, where possible, it is advisable to maintain the original structural concept avoiding considerable weight increase and significant stiffness/overstrength redistribution, especially at the upper floor levels.

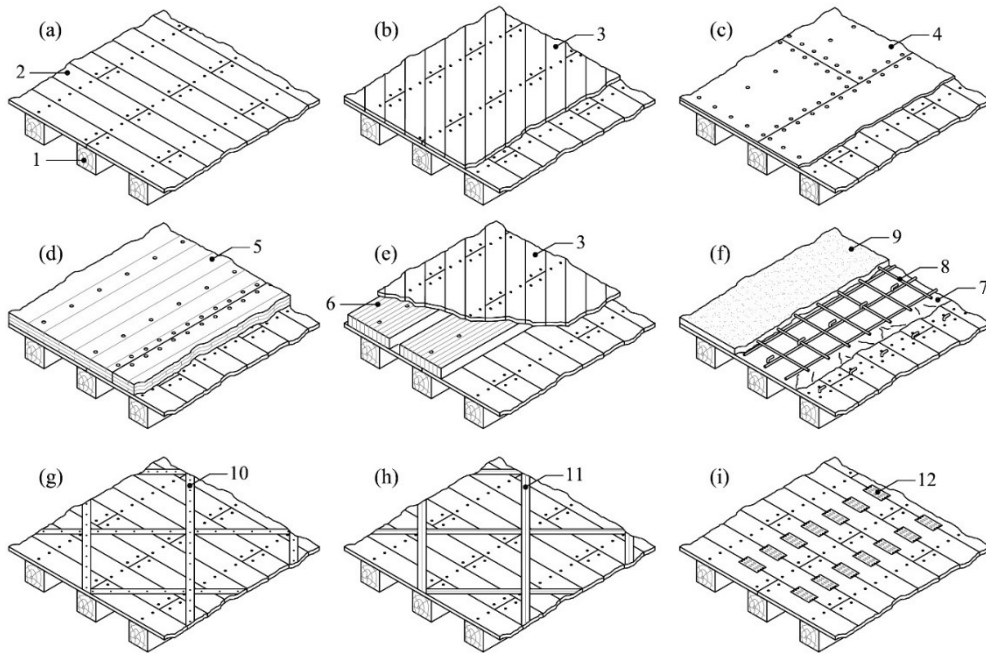
As several aspects are to be considered in the design process of a retrofit intervention, the definition of the “best technique” is rarely possible, but pros and cons of different strategies have to be evaluated and compared on a case-by-case basis. Therefore, the first step of the design approach should necessarily concern the evaluation of the state of conservation of the existing structure, trying to point out the “structural weaknesses” of the system. In many cases, retrofit interventions on existing timber floors have to deal with issues related to out-of-plane displacements due to service loads, irreversible creep deformations and vibration performance. Furthermore, diaphragms should be able to guarantee adequate in-plane strength and stiffness. With the exception of few peculiar scenarios, such as destination changes or severe material degradation, floor structural deficiencies are mostly related to the diaphragm flexibility rather than insufficient strength (Schiro et al. 2017).

Several retrofit techniques aimed at enhancing the mechanical behaviour of existing timber floors are available in literature. A selection of strategies is proposed in Figure 1-1 ([17], [20], [21] and [22]). These solutions differ from each other for many aspects including: expected performances (in terms of both strength and stiffness), mass increase, invasiveness, costs, material compatibility and reversibility level [23].

There are strategies (e.g. solutions *b*, *c*, *g*, *h* and *i* of Figure 1-1) aimed at enhancing exclusively the in-plane behaviour of timber diaphragms. Generally, these techniques are characterised by limited load increases and a good level of reversibility (especially when “dry” solutions are considered).

On the other hand, retrofit techniques such as solutions *d*, *e* and *f* of Figure 1-1 allow the designers to simultaneously improve both the in-plane and the out-of-plane behaviour of existing wooden floors. In such cases, the out-of-plane stiffening can be evaluated by means of the above-mentioned theory on composite beam with incomplete interaction.

The potentialities of timber-to-concrete composite systems (solution *f*) were widely discussed on this introduction. However, as demonstrated by the analysis of recent earthquake disasters, several limitations may be attributed to this technique. With the aim of avoiding considerable mass increases, alternative strategies are represented by solutions *d* and *e* of Figure 1-1, where the concrete slab is replaced with timber-based elements. Furthermore, thanks to the possibility of employing screw-type fasteners (dry solution), these techniques are considered to be less invasive with respect to TCC solutions.



- |                                  |  |                        |
|----------------------------------|--|------------------------|
| 1. Original joist                | 5. Cross laminated timber (CLT) panel or laminated veneer lumber (LVL) panel | 8. Steel reinforcement |
| 2. Original floorboards          | 6. Glulam or LVL plank   | 9. Concrete slab       |
| 3. Additional diagonal sheathing | 7. Waterproof sheath   | 10. Metal straps       |
| 4. Structural wood-based panel   | 8. Steel reinforcement   | 11. FRP – CFRP straps  |
|                                  |  | 12. Nail plates        |

*Figure 1-1 Strengthening and stiffening solutions: a) original floor; b) additional diagonal sheathing; c) structural wood-based panels; d) CLT/LVL panels; e) timber planks and additional diagonal sheathing; f) concrete slab; g) metal straps; h) FRP/CFRP straps; i) nail plates*

However, to the best knowledge of the author, a very limited number of works are available in literature on the mechanical behaviour of timber-to-timber composite (TTC) structures ([20] and [25]). The thesis work presented herein, is aimed at reducing the gap of knowledge on TTC systems and was carried out within the framework of a wide research effort on timber-to-timber solutions that was undertaken by the University of Trento in the late 2000s.

## 1.1 THESIS OUTLINE

The research work has been organized into two parts. The first phase was dedicated to the study of alternative strategies for retrofit interventions on timber diaphragms in historical heritage buildings. The second phase of the thesis program was devoted to the development of solutions for newly constructed diaphragms, either for new building applications or replacement of damaged/inadequate existing floors.

### ***CHAPTER 2: An innovative procedure for pre-stressing and cambering timber composite beams***

An original assembly procedure, developed at the University of Trento, is analysed in Chapter 2. Such innovative technique permits the builders to pre-stress and camber composite beams by simply relying on the pressure generated by screw-fasteners. An analytical formulation able to describe both the stress and the strain state resulting from the implementation of this procedure is presented. To validate the theoretical approach, a numerical model is developed through a finite element software. The nonlinear staged construction analysis is employed [1] to reproduce the sequential insertion of the connectors during the assembly procedure. A general good correlation is observed between the results of the analytical formulation and the numerical model. To prove both the applicability and the potentiality of this assembly technique, two experimental tests on timber-to-timber composite beam 6.4 m span are presented in Chapter 2. The outcomes are consistent with the numerical and analytical models, in terms of uplifts, stress levels and overall mechanical performance.

### ***CHAPTER 3: Testing of timber-to-timber screw-connections in hybrid configurations***

The goal of Chapter 3 is to evaluate the mechanic performance of connection configurations that are intended for use in the field of timber-to-timber composite structures where the fasteners may be inserted at an angle to the grain other than 90° and may connect different timber products and/or elements from different timber species. To this purpose, the results of fifty-eight pushout tests [24] covering fourteen different configurations are presented in this Chapter. Result comparisons regarding connection stiffness, strength, static ductility, residual strength and failure mode are provided.

### ***CHAPTER 4: Experimental tests on TTC floors***

In this Chapter, the results of seventeen full-scale bending tests on timber-to timber composite beams, 6.4 m span, assembled with the above-mentioned procedure are

presented. Essentially, the aim of these tests is two-fold. The first goal is to investigate the mechanical behaviour of TTC beams designed for newly constructed high-performance diaphragms. The second one is to evaluate the performance of alternative strategies for retrofit interventions on timber diaphragms in historical heritage buildings affected by large deformations

### ***CHAPTER 5: New high-performance TTC floor-modules realized with beech LVL: design and testing***

The main purpose of Chapter 5 is to develop high-performance solutions for prefabricated timber-to-timber composite floor modules to be realized by using laminated veneer lumber (LVL) made of beech wood. The cambering and pre-stressing procedure, analysed in Chapter 2, is used in this section to maximize floor efficiency and exploit the remarkable strength properties of hardwood products. Two modules characterised by different service load and span (6 m and 10m) are designed and tested out-of-plane. As to better understand the mechanical behaviour of the connection system that is regarded as the most suited to guarantee the best floor performance, a series of tests including pull-out tests, screw pressure tests and push-out tests are reported.

### ***CHAPTER 6: Long-term out-of-plane testing of pre-stressed timber composite floors***

Chapter 6 is dedicated to the study of the rheological behaviour of timber-to-timber composite beams assembled with the innovative assembly technique thoroughly analysed in this document. To this purpose, four experimental tests on the long-term behaviour (out-of-plane) of TTC beams 5 m span are presented [25]. The specimens were subjected to uniformly distributed loading (vertical load) in a climatic controlled chamber. In this section, the effects of different fastener configurations on the long-term behaviour of timber composite structures are investigated.

### ***CHAPTER 7: Conclusions***

A summary of the main findings and conclusions of the research work are reported in the final Chapter.

## 1.2 REFERENCES

- [1] Turrini, G., Piazza, M. (1983a) Static behaviour of timber-concrete composite structures. *Recuperare*, vol. 6, pp. 214–225 (in Italian).
- [2] Turrini, G., Piazza, M. (1983b) A technique for stiffness and strength upgrading of wooden floors. *Recuperare*, vol. 5, pp.224–237 (in Italian).
- [3] Ceccotti, A. (1995) Timber-concrete composite structures. Timber engineering STEP 2, H. Blass, et al., ed., 1st Ed., Centrum Hout, Netherlands, E13/1–E13/12.
- [4] Yeoh D., Fragiaco M., De Franceschi M., Heng Boon K. (2011) State of the Art on Timber-Concrete Composite Structures: Literature Review. *American Society of Civil Engineering* DOI: 10.1061/(ASCE)ST.1943-541X.0000353.666666.
- [5] Muller, P. (1922) Decke aus hochkantig stehenden Holzbohlen oder Holzbrettern und Betondeckschicht. Patentschau aus dem Betonbau und den damit verwandten Gebieten, Auszüge aus den Patentschriften, Beton und Eisen, H. XVII, S. 244 (in German).
- [6] Lukaszewska E., Johnsson H., Fragiaco M. (2008) Performance of connections for prefabricated timber–concrete composite floors. *Materials and Structures*, vol. 41, pp. 1533-1550.
- [7] Piazza M., and Ballerini M. (2000) Experimental and numerical results on timber-concrete composite floors with different connection systems. *Proceedings of the World Conference on Timber Engineering*, Whistler Resort, British Columbia, Canada.
- [8] Ceccotti A., Fragiaco M., Giordano S. (2007) Long-term and collapse tests on a timber-concrete composite beam with glued-in connection. *Materials and Structures*, vol. 40, issue 1, pp. 15-25.
- [9] Knorz M., Van de Kuilen J-W. (2012) Development of a high-capacity engineered wood product - LVL made of European beech (*Fagus Sylvatica* L.). *In proceeding of the World Conference on Timber Engineering (WCTE) 2012*, Auckland, New Zealand.
- [10] Yeoh D., Fragiaco M., Ghafar H. A., Buchanan A., Deam B., Crews K. (2008) LVL-Concrete Composite Floor Systems: An Effective Solution for Multi-storey Timber Buildings. *Proceeding of the Australasian Structural Engineering Conference*, Melbourne, Australia.
- [11] Sebastian W., Mudie J., Cox G., Piazza M., Tomasi R., Giongo I. (2016) Insight into mechanics of externally indeterminate hardwood–concrete composite beams. *Construction and Building Materials*, Volume 102, Part 2, pages: 1029 – 1048.

- [12] Newmark N.M., Siess C.P., Viest I.M. (1951) Test and analyses of composite beams with incomplete interaction. *Proceedings, Society for Experimental Stress Analysis*, vol. 9, no. 1, pp. 75-92, University of Illinois, Urbana, Illinois.
- [13] Möhler, K. (1956) On the load carrying behaviour of beams and columns of compound sections with flexible connections. *Habilitation*, Technical University of Karlsruhe, Germany (in German).
- [14] European Committee for Standardization (2014). EN 1995-1-1:2004+A2:2014: Eurocode 5 - Design of timber structures, Part 1-1, General - Common rules and rules for buildings. CEN, Brussels, Belgium.
- [15] Frangi, A., and Fontana, M. (2003) Elasto-plastic model for timber–concrete composite beams with ductile connection. *Structural Engineering International*, vol. 13, pp. 47–57.
- [16] Tomažević M. (1991) The influence of rigidity of floors on the seismic behaviour of old stone-masonry buildings. *European earthquake engineering*.
- [17] Oliver S. J. (2010) A design methodology for the assessment and retrofit of flexible diaphragms in unreinforced masonry buildings. *SESOC Journal*, vol. 23, pp.19 – 49.
- [18] Parisi M. A., Piazza M. (2007) Restoration and Strengthening of Timber Structures: Principles, Criteria, and Examples. *Practice Periodical on Structural Design and Construction*, vol. 12. Issue 4.
- [19] Binda L., Saisi A. (2005) Research on historic structures in seismic areas in Italy. *Progress in Structural Engineering Material*, vol. 7, pp. 71-85.
- [20] Giongo I., Piazza M., Tomasi R. (2012) Out of plane refurbishment techniques of existing timber floors by means of timber to timber composite structures. *Proceedings of the World Conference on timber Engineering (WCTE)*, Auckland, New Zealand.
- [21] Gattesco N., Macorini L. (2014) In-plane stiffening techniques with nail plates or CFRP strips for timber floors in historical masonry buildings. *Construction and Building Materials*, vol. 58, pp. 64-76.
- [22] Tomasi R., Baldessari C., Piazza M. (2009) The refurbishment of existing timber floors: characterisation of the in-plane behaviour. *Proceedings of the Prohitech Conference, Rome, Italy*
- [23] Schiro G., Rizzi E., Piazza M. (2017) Interventions aimed at reducing the excessive deformability of timber floors: strengthening and stiffening techniques according to the new Italian code (NTC). *Proceedings of the XVII ANIDIS (Italian National Association of Earthquake Engineering) conference*, Pistoia, Italy (in Italian).

- 
- [24] Schiro G., Giongo I., Sebastian W., Riccadonna D., Piazza M. (2018) Testing of timber-to-timber screw-connections in hybrid configurations. *Construction and Building Materials*, vol. 171, pp. 170-186.
  - [25] Giongo I., Schiro G., Piazza M., Tomasi R. (2016) Long-term out-of-plane testing of timber floors strengthened with innovative timber-to-timber solutions. *Proceedings of the World Conference on timber Engineering (WCTE)*, Vienna, Austria.



---

## **2 AN INNOVATIVE PROCEDURE FOR PRE-STRESSING AND CAMBERING TIMBER COMPOSITE BEAMS**

### **2.1 INTRODUCTION**

As mentioned in the introduction, retrofit interventions on existing timber floors must deal with issues concerning excessive out-of-plane displacements due to service loads, irreversible creep deformations and vibration performance. Furthermore, diaphragms should be able to guarantee adequate in-plane strength and stiffness to prevent the collapse of out-of-plane loaded walls and redistribute inertial force among the in-plane loaded piers [1]. With the exception of few peculiar scenarios, such as a change in the building use or severe material degradation, floor structural deficiencies are mostly related to the diaphragm flexibility rather than insufficient strength. As illustrated in the introductory chapter of this document, several retrofit techniques are available in literature aimed at improving both the in-plane and the out-of-plane response of existing wooden floor.

Considering the timber-to-timber composite techniques presented in Figure 1-1 (d and e), a strategy to optimise the potentialities of such solutions is analysed in this Chapter. More specifically, to increase the performance of these structural systems, an original assembly procedure, developed at the University of Trento [3], was improved and implemented on real applications.

As will be present in the following, this technique permits to pre-stress and camber composite timber elements by simply relying on screw type connectors arranged in a specific configuration (no additional external supports are required). The potentiality shown by this technique makes it a valid option for the retrofit of vintage timber floors. Basically, by applying this assembly method it is possible to reduce the effects of

irreversible deformation and to improve the out-of-plane response of existing diaphragms without significantly increasing the weight. In addition, use of this technique seems to be even more promising when it aimed at the development new timber diaphragms characterized by extremely high mechanical performance. In order to understand the operating principle of this assembly method, a schematic description is reported below.

Figure 2-1-a shows a simply supported composite beam, where the screw-fasteners connecting the two beam-components, are inserted at a  $90^\circ$  angle to the beam axis. In such configuration, all the compression force arising from the pressure generated by the screws [2] is self-equilibrated and consequently the beam is undeformed. Once external loading is applied, as in Figure 2-1-b, the beam starts to sag and the force system exchanged by the two beam-components reproduces that of Figure 2-1-c. Conversely, if the screws are inserted as in Figure 2-1-d, the equilibrium is only possible if the two contact surfaces at the component interface exchange shear forces (Figure 2-1-e) that are opposite to those reported in Figure 2-1-c and that consequently result in a beam deflection opposite to that in Figure 2-1-b.

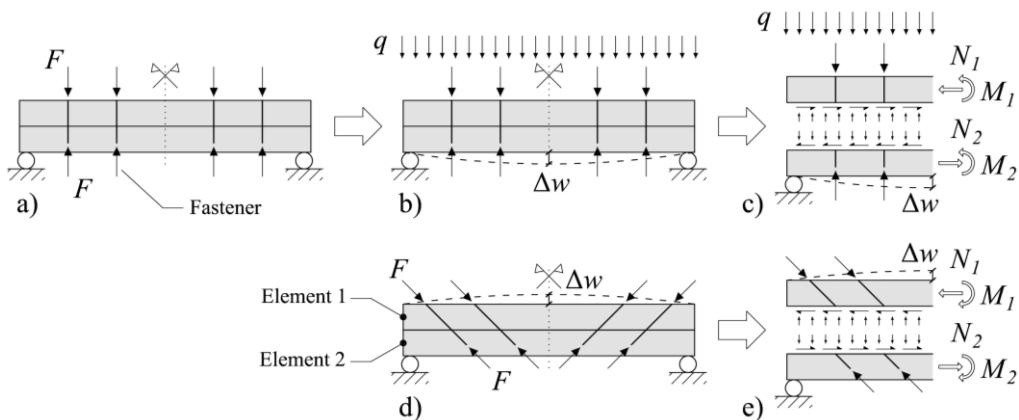


Figure 2-1 Cambering principles for composite beam with imperfect interaction

As regards the screw configuration showed in Figure 2-1-d, the benefits in terms of upward camber ( $\Delta w_{CP}$ ) were firstly demonstrated by Giongo et al. in [3] where three specimens, 4 m long, were assembled by the overlapping of two glulam beams ( $100 \times 100 \text{ mm}^2$ ). The connection between the two timber elements was realised by using equally-spaced double-threaded screws inclined at  $45^\circ$  to the beam axis. The fastener insertion order that allows the designers to exploit the full potential of this assembly technique, is reported in Figure 2-2. The fasteners are to be inserted symmetrically by starting from the midspan position and proceeding towards the beam supports (Figure

2-2-a). This means that two connectors placed at the same distance from the midspan section but in opposite positions, are considered as inserted “almost simultaneously”. In such way, it is possible to exploit the problem symmetry by considering the simply supported composite structure as a cantilever (Figure 2-2-b).

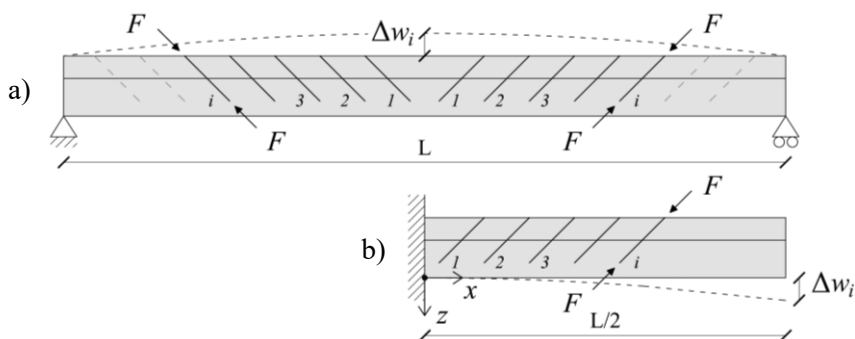


Figure 2-2 Schematics of the cambering and pre-stressing procedure

Throughout the thesis, the acronym *CP* procedure will be used to refer to the peculiar assembly technique that permits to camber and pre-stress a composite beam by solely using inclined screw fasteners as in Figure 2-2.

## 2.2 ANALYTICAL FORMULATION

A theory to predict the behaviour of composite beams with incomplete interaction was originally proposed by Newmark et al. in the early 1940's ([4] and [5]), based on the following assumptions:

1. linear elastic materials for both elements;
2. small displacements and deformations;
3. the two beam elements are characterised by the same vertical displacement and thus the same curvature;
4. linear strain distribution over the cross-section height for both elements;
5. linear load-slip relation for the connection fasteners;
6. fasteners uniformly distributed along beam axis;
7. element cross-sections are constant along the beam axis;
8. negligible element shear deformation.

Starting from the equilibrium conditions applied to the infinitesimal segment of composite beam reported in Figure 2-3 and considering the displacement compatibility

between the elements and the material constitutive laws, a differential equation for the internal force transmitted through the shear connection was developed by Newmark et al. in [4].

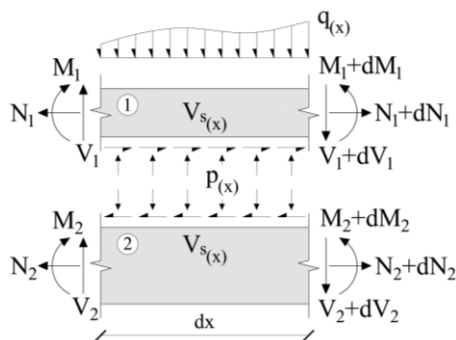


Figure 2-3 Internal equilibrium of the composite beam

The general problem is described by the second order differential equation with constant coefficients reported below:

$$\frac{d^2 N_1}{dx^2} - C_1^2 N_1 = C_2 M \quad (\text{Eq. 1})$$

where  $N_1 = N_1(x)$  is the axial load in the upper element of the composite structure,  $M = M(x)$  is the external bending moment and  $C_1$  and  $C_2$  are constants defined as:

$$C_1 = \sqrt{\frac{k_c (EJ)_\infty}{(EA)_0 (EJ)_o}} \quad (\text{Eq. 2})$$

$$C_2 = \frac{k_c a}{(EJ)_o} \quad (\text{Eq. 3})$$

$(EJ)_0$  and  $(EJ)_\infty$  are, respectively, the flexural stiffness of a composite beam with no interaction and complete interaction,  $(EA)_0 = [\sum 1/(EA)_j]^{-1}$ ,  $a$  is the distance between the barycentre of the two element cross-sections and  $k_c$  is the shear stiffness of the connection per unit length (uniformly distributed along beam axis). In the following discussion, the subscript  $j = 1$  will be used to indicate the upper element and

$j = 2$  will be used for the lower element. As will be presented hereafter, from the solution of (Eq. 1) it is possible to derive all other significant quantities such as the internal actions ( $M_j$ ,  $N_j$  and  $V_j$ ), the interface slip  $\delta$  between the two elements and the relevant shear force transmitted per unit length  $V_s$ .

Considering now the assembly procedure described in the introduction chapter, during the sequential insertion of the fasteners, there is no external moment acting on the composite beam ( $q = 0$ ). Consequently, the imposition of the equilibrium on the infinitesimal composite element (Figure 2-3) produces:

$$N_1 + N_2 = 0 \quad (\text{Eq. 4})$$

$$V_1 + V_2 = 0 \quad (\text{Eq. 5})$$

$$M_1 + M_2 - N_1 a = 0$$

The equilibrium equations for element 1 are (the higher-order terms may be neglected):

$$\frac{dN_1}{dx} = -V_s \quad (\text{Eq. 6})$$

$$\frac{dV_1}{dx} = p \quad (\text{Eq. 7})$$

$$\frac{dM_1}{dx} = V_1 - V_s \frac{h_1}{2} \quad (\text{Eq. 8})$$

The CP procedure relies on a sequential insertion of the fasteners. Hence the level of interaction between the two elements, evidenced by the shear stiffness at the element interface, should be time-dependent and vary along the beam axis. Because all the materials forming the compound structure are linear elastic, it is possible to employ the linear superposition principle. In this way, the effects (in terms of stress and strain) introduced by each fastener can be taken in to account separately.

By considering a cantilever compound beam as the one in Figure 2-4, after the insertion of the  $i$ -th fastener ( $i$ -th couple of fasteners if the simply supported beam is considered), the connection stiffness still varies along the beam axis due to the beam part where the fasteners are yet to be inserted. To try and solve this problem one could think of cutting the cantilever right behind the last connector inserted. The part with the fasteners can

be deemed as a composite beam with uniformly distributed connection stiffness  $k_c$  while the remaining part can be treated as a rigid appendix.

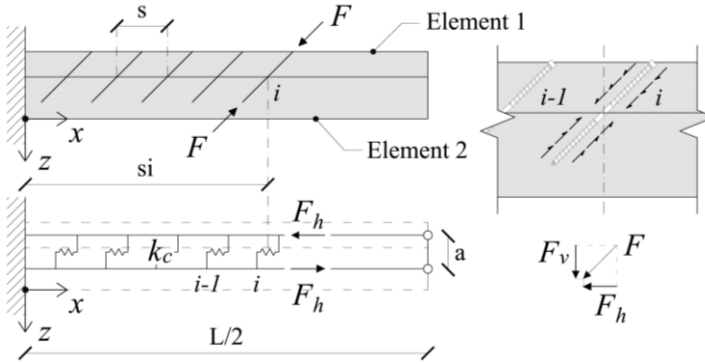


Figure 2-4 CP Procedure: static scheme

By acknowledging that there is no external moment acting on the composite beam during the assembly procedure, (Eq. 1) can be solved by imposing the following boundary conditions (Figure 2-4):

$$\frac{dN_{1,i}}{dx} \Big|_{x=0} = 0 ; N_{1,i} \Big|_{x=si} = -F_h \quad (\text{Eq. 9})$$

For  $0 \leq x \leq si$ , the axial load in the upper element of the composite structure due to the insertion of the  $i$ -th fastener is:

$$N_{1,i}(x) = -F_h \frac{\cosh(C_1 x)}{\cosh(C_1 si)} \quad (\text{Eq. 10})$$

Otherwise, for  $si < x \leq L/2$  the axial load produced by the  $i$ -th connector is zero.

As regards the vertical displacement component  $w(x)$ , starting from assumptions 3 and 4, and taking into account 0, the following second order differential equation can be defined:

$$\frac{d^2 w}{dx^2} = -\frac{M_1}{(EJ)_1} = -\frac{N_1 a}{(EJ)_o} \quad (\text{Eq. 11})$$

In accordance with the external constraints, the boundary conditions are:

$$\frac{dw}{dx} \Big|_{x=0} = 0 ; w \Big|_{x=0} = 0 \quad (\text{Eq. 12})$$

Consequently, for  $0 \leq x \leq si$ , the vertical displacements originated from the external pressure introduced by the  $i$ -th fastener is:

$$w_i(x) = \frac{F_h a}{C_1^2 (EJ)_0} \cdot \frac{\cosh(C_1 x) - 1}{\cosh(C_1 si)} \quad (\text{Eq. 13})$$

In order to determine the entire cambering value  $\Delta w_i$ , the scheme reported in Figure 2-5 has to be considered.

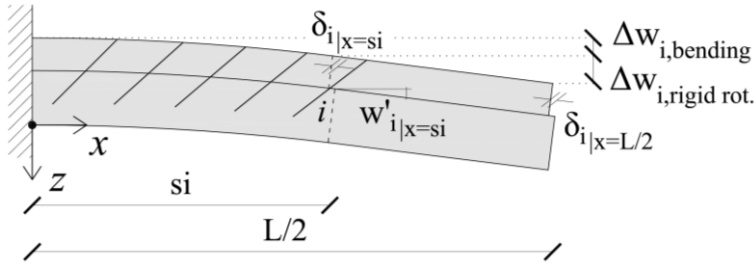


Figure 2-5 Deformed shape of the composite beam after the insertion of the  $i$ -th fastener

In particular, if one considers the cantilever composite beam in Figure 2-5, the vertical deflection produced by the  $i$ -th fastener is the result of two main contributions: the bending deformation  $\Delta w_{i,bending}$  of the portion between  $x = 0$  and  $x = si$ , and the rigid body rotation  $\Delta w_{i,rigid\ rot}$  of the free part of the beam. As a result, the total value of camber  $\Delta w_{i|x=L/2}$  due the insertion of the  $i$ -th fastener is:

$$\begin{aligned} \Delta w_{i|x=L/2} &= \Delta w_{i,bending} + \Delta w_{i,rigid\ rot}. = \\ &= w_{i|x=si} + \frac{dw_i}{dx} \Big|_{x=si} \left( \frac{L}{2} - si \right) \end{aligned} \quad (\text{Eq. 14})$$

Then, by substituting (Eq. 13) in (Eq. 14):

$$\Delta w_{i|x=L/2} = \frac{F_h a}{C_1^2 (EJ)_0} \left[ 1 + \frac{C_1 \sinh(C_1 s i) (L - 2s i) - 2}{2 \cosh(C_1 s i)} \right] \quad (\text{Eq. 15})$$

As already mentioned, in order to evaluate the beam camber at the end of the assembly procedure  $\Delta w_{|x=L/2}$ , the linear superposition principle may be used. By acknowledging that a constant fastener spacing  $s$  is assumed:

$$\begin{aligned} \Delta w_{|x=L/2} &= \sum_{i=1}^N \Delta w_{i|x=L/2} = \\ &= \sum_{i=1}^N \frac{F_h a}{C_1^2 (EJ)_0} \left[ 1 + \frac{C_1 \sinh(C_1 s i) (L - 2s i) - 2}{2 \cosh(C_1 s i)} \right] \end{aligned} \quad (\text{Eq. 16})$$

Where  $N$  is the number of connectors in the cantilever composite beam. In cases where the fasteners are arranged in multiple rows, the evaluation of  $k_c$  (shear stiffness) and  $F_h$  (i.e. the horizontal component of the compression force yielded by the fasteners) should reflect the presence of multiple fasteners at the same  $x$ -location.

From the definition of axial force  $N_{1,i}$  and vertical displacement  $w_i$ , and by taking into account the equilibrium equations reported previously, all the others quantities may be derived. A summary of formulas for the cambering and pre-stressing of composite beams with incomplete interaction is reported in Table 2-1.

Table 2-1 Summary of formulas for the CP procedure of composite beams

$$N_1(x) = -N_2(x) = \sum_{i=1}^N \begin{cases} -F_h \frac{\cosh(C_1 x)}{\cosh(C_1 s_i)} & 0 \leq x \leq s_i \\ 0 & s_i < x \leq L/2 \end{cases} \quad (\text{Eq. 17})$$

$$V_1(x) = -V_2(x) = \sum_{i=1}^N \begin{cases} F_h C_1 \frac{\sinh(C_1 x)}{\cosh(C_1 s_i)} \left[ \frac{h_1}{2} - a \frac{(EJ)_1}{(EJ)_0} \right] & 0 \leq x \leq s_i \\ 0 & s_i < x \leq L/2 \end{cases} \quad (\text{Eq. 18})$$

$$M_1(x) = \sum_{i=1}^N \begin{cases} -F_h a \frac{(EJ)_1 \cosh(C_1 x)}{(EJ)_0 \cosh(C_1 s_i)} & 0 \leq x \leq s_i \\ 0 & s_i < x \leq L/2 \end{cases} \quad (\text{Eq. 19})$$

$$M_2(x) = \sum_{i=1}^N \begin{cases} -F_h a \frac{(EJ)_2 \cosh(C_1 x)}{(EJ)_0 \cosh(C_1 s_i)} & 0 \leq x \leq s_i \\ 0 & s_i < x \leq L/2 \end{cases} \quad (\text{Eq. 20})$$

$$V_s(x) = \sum_{i=1}^N \begin{cases} F_h C_1 \frac{\sinh(C_1 x)}{\cosh(C_1 s_i)} & 0 \leq x \leq s_i \\ 0 & s_i < x \leq L/2 \end{cases} \quad (\text{Eq. 21})$$

$$\delta(x) = \sum_{i=1}^N \begin{cases} \frac{F_h C_1 \sinh(C_1 x)}{k_c \cosh(C_1 s_i)} & 0 \leq x \leq s_i \\ \frac{F_h C_1 \tanh(C_1 s_i)}{k_c} & s_i < x \leq L/2 \end{cases} \quad (\text{Eq. 22})$$

$$p(x) = \sum_{i=1}^N \begin{cases} F_h C_1^2 \frac{\cosh(C_1 x)}{\cosh(C_1 s_i)} \left[ \frac{h_1}{2} - a \frac{(EJ)_1}{(EJ)_0} \right] & 0 \leq x \leq s_i \\ 0 & s_i < x \leq L/2 \end{cases} \quad (\text{Eq. 23})$$

## 2.3 NUMERICAL MODEL

A numerical model was developed through the finite element software SAP2000 [6]. As schematized in Figure 2-6, the composite beam was simulated by using linear elastic frame elements, while the fasteners were reproduced by inclined nonlinear link elements [3]. Vertical inextensible rods were introduced to maintain the distance between the frame elements unaltered during the analysis (deformation orthogonal to the grain is neglected).

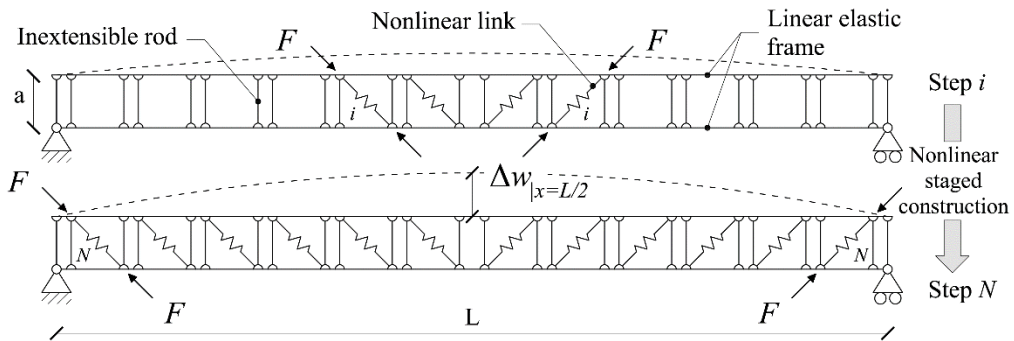


Figure 2-6 Numerical model

To reproduce the sequential insertion of the fasteners during the CP procedure, the *nonlinear staged construction* function was employed [6]. As a result, the total number of nonlinear links changed at every step (with the number of steps  $i=1-N$ ). The compression force exerted by the screws was schematized as a self-balanced system of forces  $F$  as showed in Figure 2-6.

As the analytical formulation is based on the hypothesis of a constant spacing between the fasteners (constant shear stiffness  $k_c$  per unit length), use of numerical modelling was necessary to study the influence of a variable connector spacing. The finite element (FE) model was also employed to analyse the behaviour of the cambered, pre-stressed composite beam under vertical loading (via pushover analysis).

## 2.4 MODEL COMPARISON

A discussion of the results of the numerical and analytical models is given in this paragraph. In order to compare the outcomes of the models in terms of internal actions, interface slip, exchanged shear force and vertical uplift, a case study was selected (Figure 2-7).

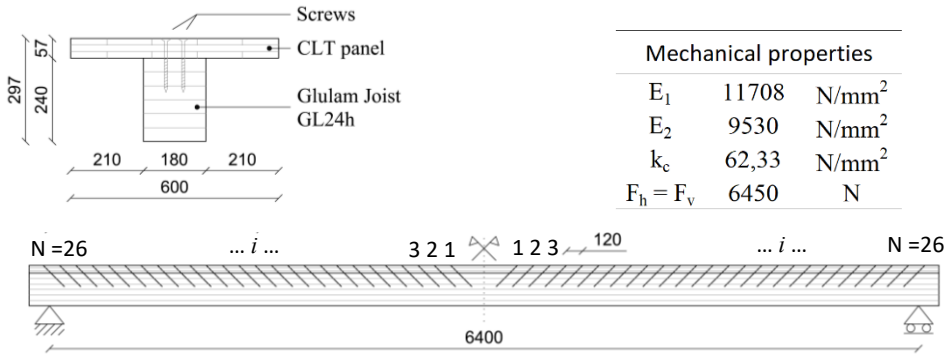
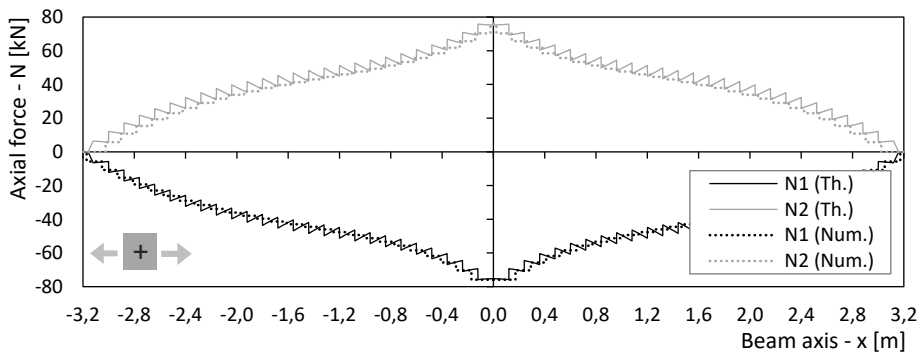


Figure 2-7 Composite beam: case study

With reference to Figure 2-7, the case study presented in this section regards a simply supported composite floor module. The length of the composite floor is 6700 mm (6400 m span). The structure comprises a softwood 3-layers cross laminated timber panel 600 x 6400 mm<sup>2</sup> (19 + 19 + 19 = 57 mm thick) and a glulam joist GL24h 180 x 240 mm<sup>2</sup> made from grade GL24h glulam timber. A constant fastener spacing ( $s = 120\text{ mm}$ ) was considered in the analysis, with a shear stiffness per unit length equal to  $k_c = 62.33\text{ N/mm}^2$ . As regards the compression force exerted by the connectors, the following components were considered in the models:  $F_h = F_v = 6450\text{ N}$ .

The internal action diagrams  $N_i(x)$ ,  $V_i(x)$  and  $M_i(x)$  for the elements of the composite structure at the end of the CP procedure are reported in Figure 2-8.



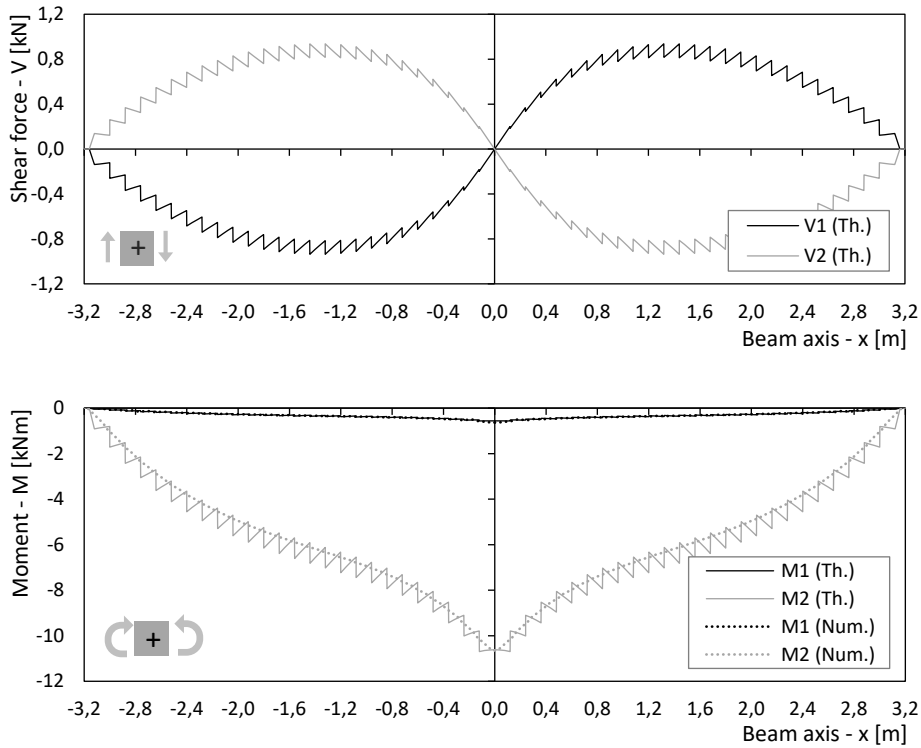


Figure 2-8 Case study: internal actions at the end of the CP procedure

With reference to the axial force and the bending moment acting along the elements of the composite beam, the results of the numerical model (dotted line) are in good agreement with those obtained by means of the analytical formulation (continuous line). At the end of the assembly procedure, the maximum values of normal stress were registered at the mid-span section of the composite structure. As visible from Figure 2-9, despite the presence of the axial tension force  $N_2$  in the lower element, the bottom side of element 2 is compressed due to the effect produced by the bending moment  $M_2$ . With reference to the flexural behaviour of TTC/TCC composite beams under uniformly distributed loading, the ultimate strength of the system is reached by formation of a crack that starts from the bottom mid-span and propagated towards one of the supports [12]. The stress state resulting from the adoption the assembly technique discussed herein (Figure 2-9) determines an increase in the load bending capacity of the composite structure.

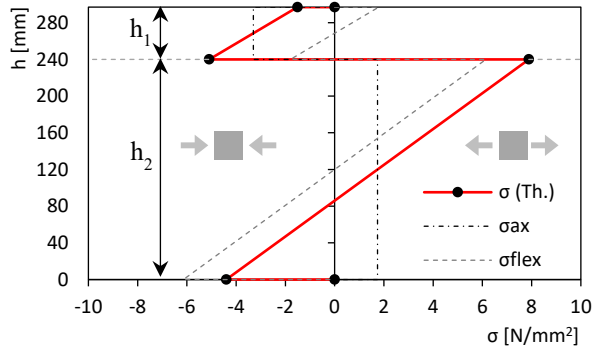


Figure 2-9 Normal stress distribution over the mid-span cross section at the end of the CP procedure

Figure 2-10-a reports the total uplift measured at midspan after the insertion of each couple of fasteners ( $i = 1..N$ ). A 2.20% variation in the final camber value between the analytical solution and the numerical model was registered. Figure 2-10-b plots the percentage contribution of each couple of connectors to the final vertical displacement. With an uplift increase of 0.97 mm registered in the analytical model (5.13% of the total), the most effective couple of fasteners was the eleventh. The dashed line in Figure 2-10-b isolates the bending contribution from the rigid rotation contribution.

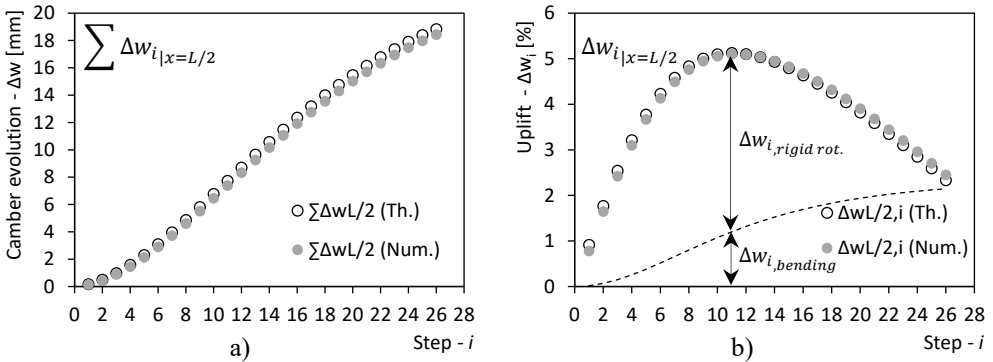


Figure 2-10 Case study: camber evolution

Figure 2-11-a shows the shear force acting at the interface surface at the end of the fastener insertion. Given the symmetry of the problem, only half beam was reported in the diagrams. The interface slip between the elements is plotted in Figure 2-11-b. A 12.01% variation in the slip at the support ( $x = 3.2\text{ m}$ ) was registered between the models.

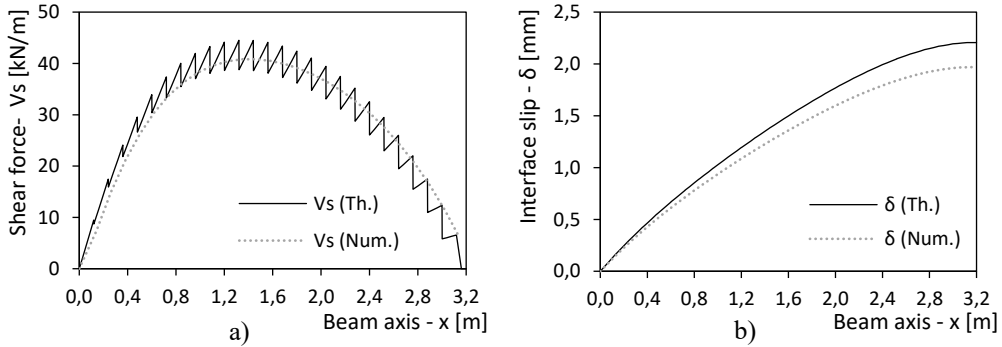


Figure 2-11 Case study: a) shear force and b) interface slip at the end of the CP procedure

Figure 2-12-a plots the interface slip over the beam length calculated after the insertion of each  $j$ -th couple of fasteners (continuous grey lines). The black dashed line reveals the value of slip at a certain location when the fastener is inserted at that very same location. Hence, the actual slip endured by the fasteners  $\Delta_j$  during the CP procedure can be estimated (Figure 2-12-a) as the difference between the solid red line and the dashed black line. The result is showed in Figure 2-12-b. In this way the stress-strain state on the connection system at the end of the CP procedure may be fully established.

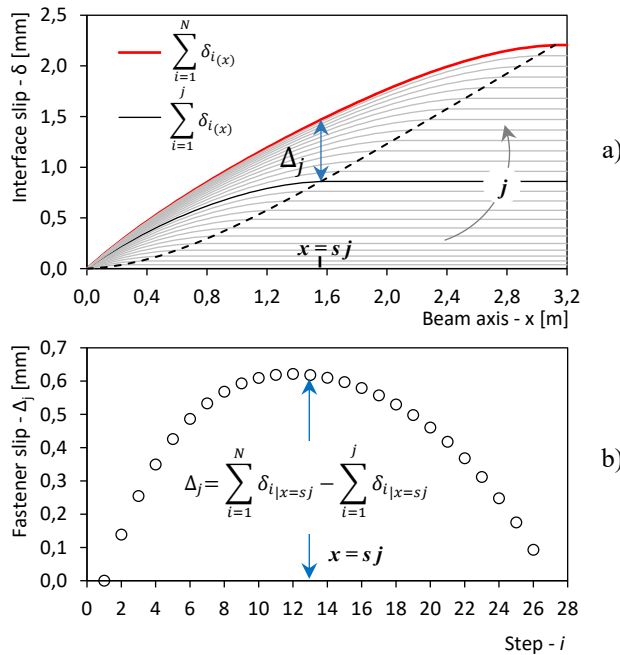


Figure 2-12 a) interface slip after the insertion of each couple of fasteners; b) fastener slip

## 2.5 EXPERIMENTAL VALIDATION

More than 30 full-scale tests on timber-to-timber composite floors, from 4 m to 10 m span, have been carried out at the Laboratory of the Department of Civil, Environmental and Mechanical Engineering (DICAM) of the University of Trento (Italy) over the last years [12], [7]. Several aspects were investigated, including the applicability of the pre-stressing and cambering procedure, the validation of the numerical and the analytical models presented in the previous sections and the out-of-plane flexural behaviour of structures assembled with the CP procedure (both the ultimate limit state and the long-term behaviour [7] of the composite structures were investigated).

Two of these tests are presented in this section: test A and B. The geometry layout, as well as the element types and the fastener arrangement, reproduce exactly those reported in Figure 2-7. Concerning the connection system, two screw types were adopted: double threaded (DT) screws and single threaded (ST) screws (Figure 2-13).

Test A | Double threaded screw (DT) 8.5 x 150 mm [9]



Test B | Single threaded screw (ST) 10 x 220 mm [10]



Figure 2-13 Experimental validation: screw types

As visible from Figure 2-7, the screws were inserted at a 45° angle to the grain. Therefore, for the insertion of single threaded (ST), groove cuts were provided to ensure an adequate contact surface between the washers and CLT panel surface ([7], [8])

Prior to the execution of the full-scale tests, a series of preliminary investigations were performed to determine the MoE and the density of the timber elements, as well as the mechanical behaviour of the connections [8]. The compression forces  $F$  due to the pressure generated by the screws was determined according to the formulation proposed by [11]:

$$F = \gamma \cdot (d \cdot l_{th})^\alpha \rho^\beta \cdot \varphi \quad (\text{Eq. 24})$$

Where  $F$  is the resultant pressure generated by the fastener [N],  $d$  is the connector diameter [mm],  $l_{th}$  is the threaded part length [mm] (for double-threaded screws  $l_{th}$  is

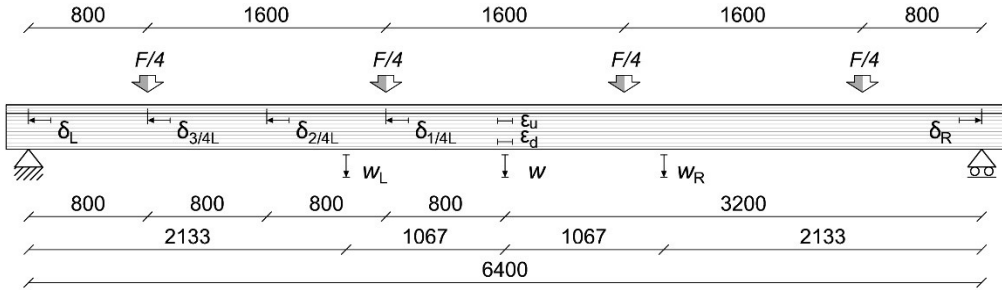
the length of one of the threads),  $\rho$  is the wood density,  $\alpha$ ,  $\beta$ ,  $\gamma$  are experimental parameters ( $\alpha = 3/5$ ,  $\beta = 20/7$ ,  $\gamma = 2.67 \cdot 10^{-6}$  according to [11]) and  $\varphi$  is a coefficient depending on the screw typology ( $\varphi \approx 0.5$  for single screw value,  $\varphi \approx 1$  for double screws value).

The mechanical properties of timber elements and the connector parameters [8] are reported in Table 2-2, where  $E_i$  is the modulus of Elasticity,  $\rho_i$  is the mean density,  $k_s$  is the slip modulus per shear plane for a single fastener (shear-tension configuration) and  $F$  is the compression force generated by the screw (one device).

*Table 2-2 Mechanical properties of timber elements and connector systems*

Element	Property	Test A	Test B
Panel (1)	$E_1$ [N/mm <sup>2</sup> ]	11353	11708
	$\rho_{m,1}$ [kg/m <sup>3</sup> ]	457.12	458.24
Joist (2)	$E_2$ [N/mm <sup>2</sup> ]	9638	9530
	$\rho_{m,2}$ [kg/m <sup>3</sup> ]	418.05	421.50
Connection	$k_s$ [N/mm]	9773	3740
	$F$ [N]	2940	4560

Each test was monitored both during the assembly phase (pre-stressing and cambering procedure) and during the loading. In the second phase, the specimens were subjected to a monotonic quasi-static loading under displacement control until the failure of the samples. A six-point bending test scheme was selected in order to simulate a uniform distributed load on the floor. The load was applied through a hydraulic actuator and was monitored by a 1000 kN load cell. The imposed displacement rate was set to 0.05 mm/s. The instrument arrangement is showed in Figure 2-14. Specifically, the vertical deflection ( $w$ ,  $w_L$ ,  $w_R$ ) was monitored through the installation of four linear displacement transducers (LDT) positioned at the mid-span ( $2x$ ) and at a distance of  $L/3$  from the end of the composite beam. The panel-to-joist interface slips ( $\delta_L$ ,  $\delta_{3/4L}$ ,  $\delta_{2/4L}$ ,  $\delta_{1/4L}$ ,  $\delta_R$ ) were measured by means of four LDTs positioned as in Figure 2-14. Additionally, linear strain gauge sensors were used to define the strain profile ( $\varepsilon_u$ ,  $\varepsilon_d$ ) at the mid-span cross section of the joist.



Instruments:

$\delta_L, \delta_{3/4L}, \delta_{2/4L}, \delta_{1/4L}, \delta_R$ : linear displacement transducer (LDT) – 50 mm

$w(2x), w_L, w_R$ : linear displacement transducer (LDT) – 300 mm

$\epsilon_u, \epsilon_d$ : Linear strain gauge sensor – 100 mm

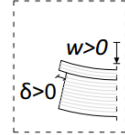


Figure 2-14 Test setup and instrument arrangement

The setup used for the testing the flexural response of the floor-specimens, is showed in Figure 2-15. Polyethylene plates were fixed to 20 x 600 mm<sup>2</sup> steel plates and inserted between the loading-rig and the CLT panel surface in order to increase the contact area (so as to avoid local crushing perpendicular to the grain) and to reduce friction.

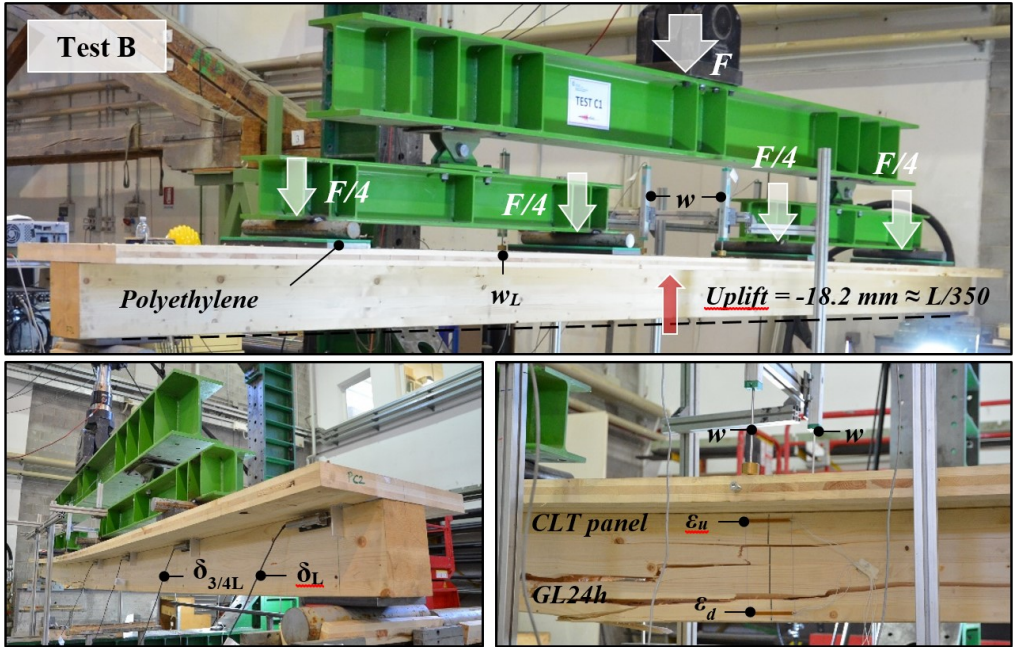


Figure 2-15 Test setup and instrument configuration

The test results are summarized in Table 2-3, where  $\Delta w_{CP}$  is the final camber measured at the end of the CP procedure;  $q_0$  is the equivalent uniformly distributed load necessary to induce a midspan displacement variation equal to  $\Delta w_{CP}$ ;  $F_{max}$  and  $q_{max}$  are, respectively, the maximum force and the equivalent uniformly distributed load; and  $w_{max}$  is the midspan deflection corresponding to the maximum load. Every displacement value was measured with reference to the initial condition (i.e. self-weight applied only).

Table 2-3 Test results

		Test A	Test B
$\Delta w_{CP}$	[mm]	8.35	18.22
$q_0$	[kN/m <sup>2</sup> ]	3.38	6.51
$F_{max}$	[kN]	87.90	90.29
$q_{max}$	[kN/m <sup>2</sup> ]	22.89	23.51
$\Delta w_{CP}(\text{Th.})$	[mm]	7.82 (-6.35%)	18.84 (+3.40%)
$\Delta w_{CP}(\text{Num.})$	[mm]	7.42 (-11.14%)	18.43 (+1.15%)

Thanks to the higher pressure developed by the ST screws with washers (see [11] for insight about the compression force generated by different types of screw) and also thanks to the minor shear stiffness of such fasteners, test B exhibited a significantly larger uplift than test A (+118.63%). The camber value reached in test B was comparable (but in the opposite direction) to the deformation limit usually assumed for the serviceability limit state ( $\Delta w_{CP,B} = L/351$ ).

Figure 2-16 presents the results of the six-point bending tests in terms of force Vs. displacement at the midspan. The effect of the assembly procedure is reflected by having the starting points on the negative side of the x-axis.

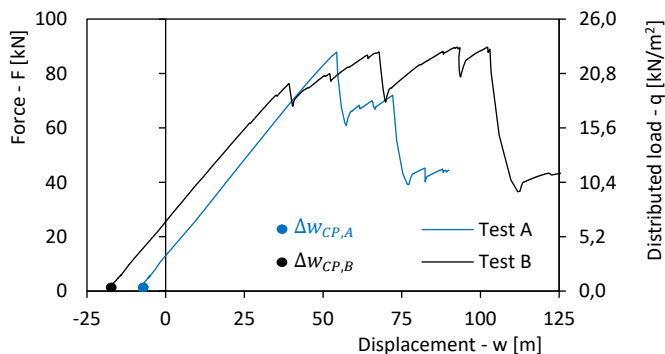


Figure 2-16 Load-displacement curves of tested specimens

A remarkable equivalent distributed load  $q_0$  was necessary for both specimens in order to induce a midspan displacement variation that nulled the initial camber value  $\Delta w_{CP}$ . More specifically, a value of  $q_0$  equal to  $6.51 \text{ kN/m}^2$  was registered in test B, approximately twice the value reached in test A ( $3.38 \text{ kN/m}^2$ ). A collapse mode similar to that reported in Figure 2-15 was detected for all tests. Approximately the same maximum force was applied in the bending tests. However, in test B the collapse was anticipated ( $w \approx 40 \text{ mm}$ ) by a crack opening that started from a defect located in the lower portion of the joist. A residual capacity greater than  $10 \text{ kN/m}^2$  was registered in both tests after the failure.

Table 2-4 compares the bending stiffness of the composite systems  $(EJ)_{Exp}$  with the reference values of  $(EJ)_0$  and  $(EJ)_\infty$ . The specimens showed an efficiency of 80% in test A and 0.72% in test B, where the efficiency  $\eta$  of the the connection system was defined as:

$$\eta = \frac{(EJ)_{Exp} - (EJ)_0}{(EJ)_\infty - (EJ)_0} \quad (\text{Eq. 25})$$

Finally, the bending stiffness of the composite elements was analytically evaluated  $(EJ)_{Ef,EC5}$  by means of the method provided by the Eurocode 5 – Annex B [14]. As showed in Table 2-4, a good correlation between the analytical flexural stiffness and the experimental evidence was registered.

Table 2-4 Bending stiffness of the composite systems

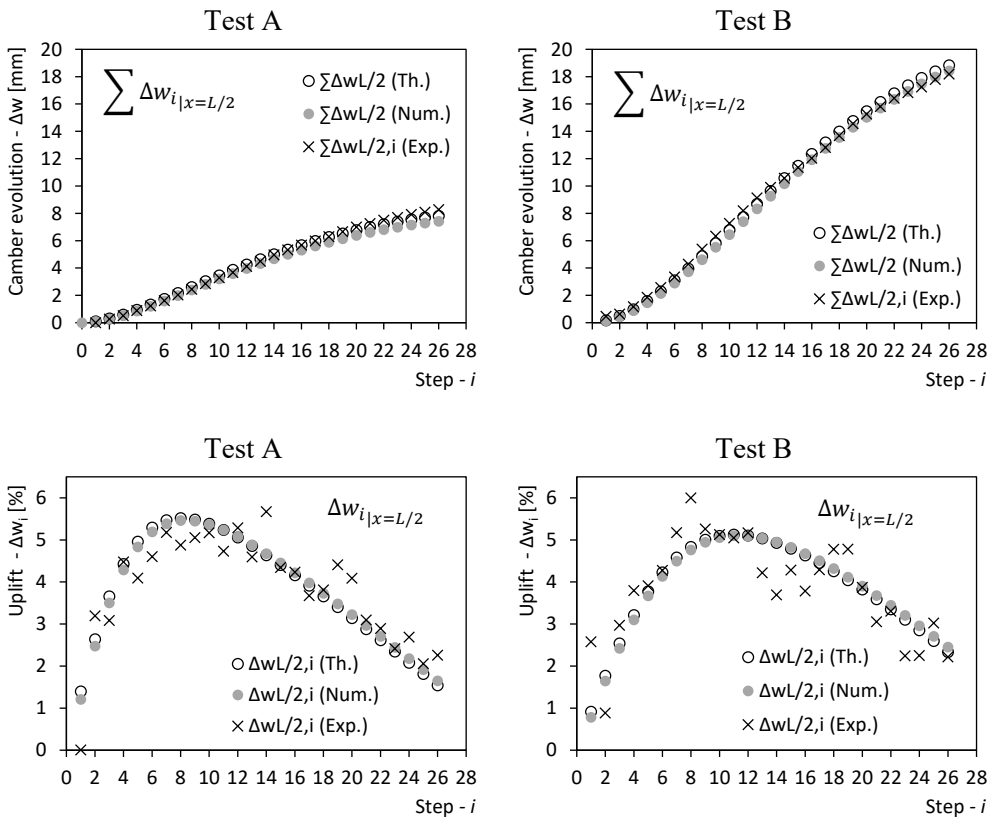
Bending stiffness $\cdot 10^{12}$		Test A	Test B
$(EJ)_0$	[Nmm <sup>2</sup> ]	2.10	2.08
$(EJ)_\infty$	[Nmm <sup>2</sup> ]	5.62	5.65
$(EJ)_{Exp}$	[Nmm <sup>2</sup> ]	4.92	4.65
$\eta$		0.80	0.72
$(EJ)_{Ef,EC5}$	[Nmm <sup>2</sup> ]	4.95 (+0.62%)	4.28 (-7.96%)

With reference to the CP procedure, Figure 2-17 plots a comparison between the experimental results (Exp) and the deformation state predicted by the theoretical (Th) and the numerical (Num) models. Despite the natural variation of the mechanical properties inside timber elements associated with the presence of density gradient, sloping grain, knots or knothole, a generally good correlation between models and experimental data was observed. In particular, the analytical formulation provided camber values ( $\Delta w_{CP}$ ) ranging between  $-6.35\%$  (test A) and  $+3.40\%$  (test B). The

larger difference observed for test A partially reflects the higher uncertainty associated with the estimation of the compression force exerted by DT screws [11]. Further research is needed to provide a better estimation of such parameter.

As expected, the measured screw effectiveness ( $\Delta w_i$ ) was maximum at those locations far from the supports and the beam centre. Additionally, the actual  $\Delta w_i$  profile observed in both test A and B corresponded with a good level of approximation to the profiles predicted by the models.

As for the interface slip  $\delta$  between the CLT panel and the GL24h joist, the numerical model proved to be the best tool (the values reported in Figure 2-17 refer to the end of the assembly procedure).



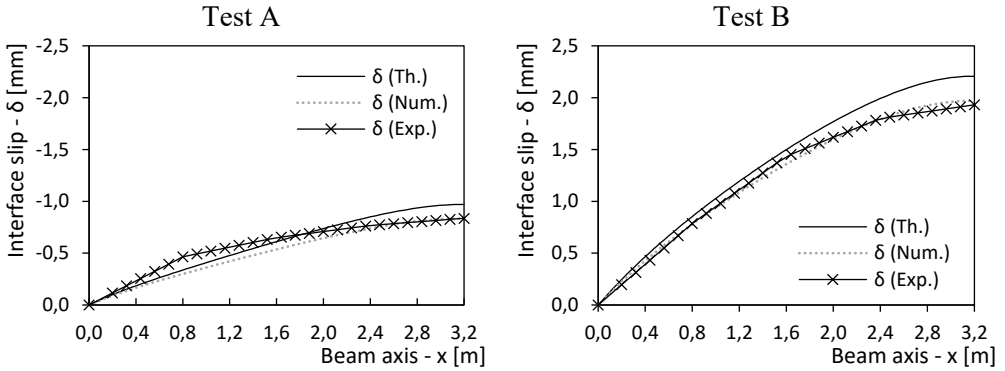


Figure 2-17 Experimental validation: CP procedure

Figure 2-18 plots the interface slip Vs. vertical displacement recorded by the LDTs arranged along the beam axis from the initial cambering phase to the failure. The higher slip/displacement ratio observed during the cambering phase when compared to the loading phase is related to the lower flexural stiffness of the composite beam yet to be completed with all the fasteners . Despite a vertical deflection greater than 100 mm, the interface slips remained negative, as proof of the high level of interaction reached between the elements (i.e. effective element coupling).

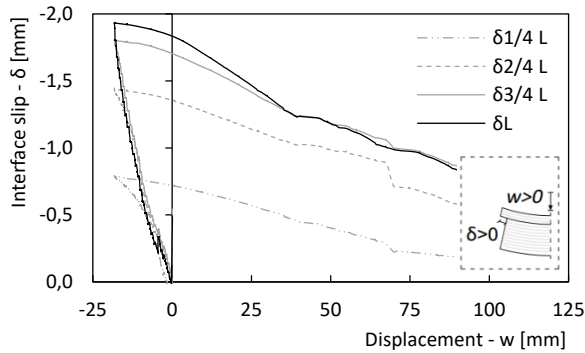


Figure 2-18 Test B: interface slip Vs. vertical displacement

The axial force and the bending moment acting at the midspan during the assembly procedure were defined considering the record from the linear strain gauge sensors and taking into account the moduli of elasticity reported in Table 2-2. As expected, the joist was subjected to combined tension bending. As shown in Figure 2-19-b, a good estimation of the bending moment was obtained by both analytical and numerical

models. As for the axial force, an unexpected compression force on the joist was registered up to the insertion of the third “couple” of fasteners.

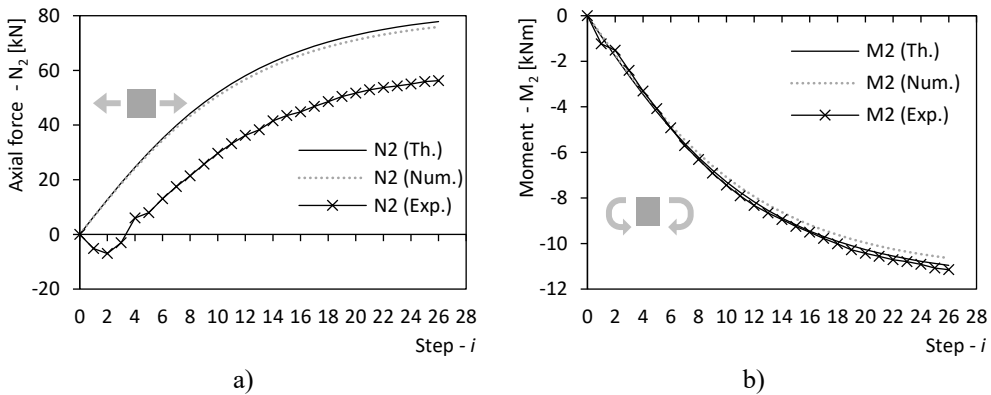


Figure 2-19 Test B: a) axial force and b) bending moment in the joist at the midspan cross section during the CP procedure

With reference to the test B, Figure 2-20 shows the normal stress profile at midspan throughout both test phases. It can be observed how, during the CP procedure (continuous grey line), the neutral axis of the joist moved downwards from the centre of the cross section. Interestingly, the stress profile measured at the end of the screw insertion ( $\sigma_{CP,B}$ ) and the profile predicted by the analytical formulation ( $\sigma_{CP,(Th.)}$ ) are remarkably close to each other. Turning the attention to the experimental results from the loading phase, a gradient change in the normal stress profile was observed ( $\sigma_{F,B}$ ). Unfortunately, after the first crack opening in the joist element ( $w \approx 40$  mm), damage at the linear strain gauge sensors occurred, that resulted in a signal loss.

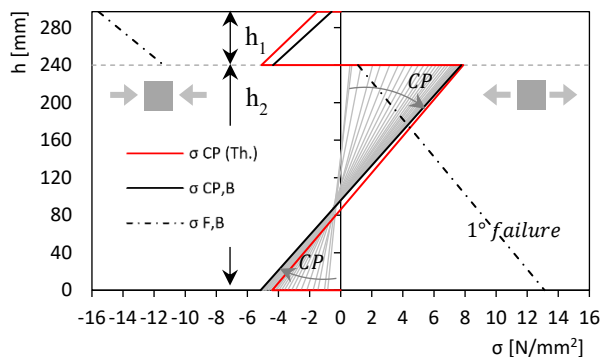


Figure 2-20 Test B: experimental normal stress at the midspan

Alternatively to the simply supported scheme assumed for the assembly procedure (Figure 2-14), the adoption of a modified scheme where the supports are moved inward (e.g. at 1/3 of the module span) would allow the builders to take advantage of self-weight to increase the increment CP procedure effectiveness. However, such possibility was not investigated in this experimental campaign.

## 2.6 PARAMETRIC ANALYSIS

In this section, a series of parametric analyses are presented. Considering the good correlation observed between the results from the analytical and the numerical models, the first one was assumed as the reference tool. However, due to the limitation of the analytical formulation (constant fastener spacing is required), the numerical model was used in this section where a variable spacing of the connectors was analysed.

The following case study was considered as reference for the parametric study (see Table 2-5).

*Table 2-5 Reference case study for the parametric analyses*

Reference model: TTC beam (5 m span)	
Element 1	Softwood CLT panel 500 x 57 mm <sup>2</sup> (3 layers) $E_1 = 11000 \text{ N/mm}^2$
Element 2	Softwood C24 joist 100 x 140 mm <sup>2</sup> $E_2 = 11000 \text{ N/mm}^2$
Interlayer	Non-structural floorboard 20 mm thick
Connection	$s = 150 \text{ mm}$ (N=16) $k_s = 15000 \text{ N/mm}$ $F_h = F_v = 5000 \text{ N}$

### 2.6.1 INFLUENCE OF CONNECTION STIFFNESS AND COMPRESSION FORCE ON THE FINAL CAMBER VALUE

Several typologies of fastener are available on the market for creating timber-to-timber composite structures. They differ from each other for thread geometry and type, head, tip, diameter, length, washer. As a result, different mechanical performances are provided by the fasteners.

Figure 2-21 shows the relation between the final camber  $\Delta w_{CP}$  and the mechanical properties of the connection system. A percentage variation from -50% to 50% in the

shear stiffness  $K_s$  and the compression force  $F$  was alternatively considered (the values reported in Table 2-5 were taken as references).

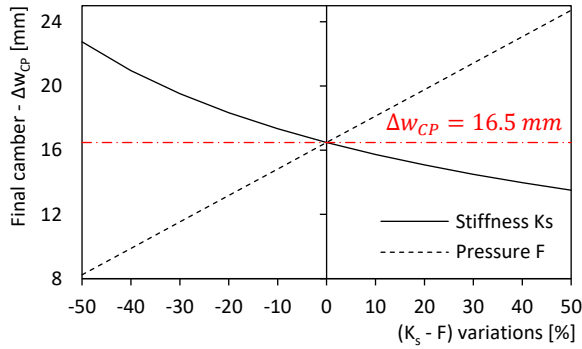
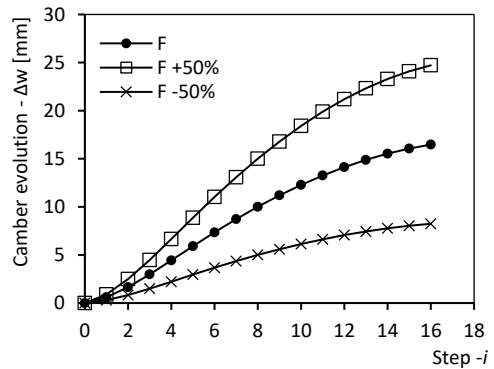
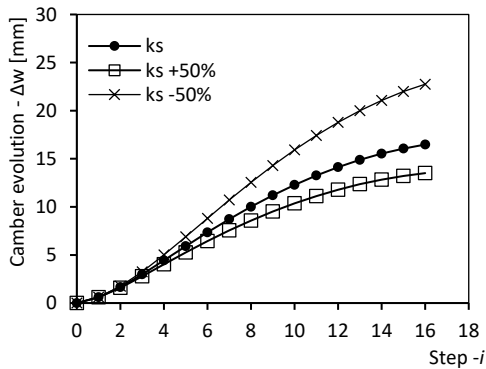


Figure 2-21 Final camber vs percentage variations of connection stiffness and compression force

As expected, an increase in the compression force developed by the fasteners results in a linear increase of the final camber. Contrarily, an increase of the shear stiffness results in a decrease of the uplift reached, although with a less pronounced trend. Further details are provided in Figure 2-22.



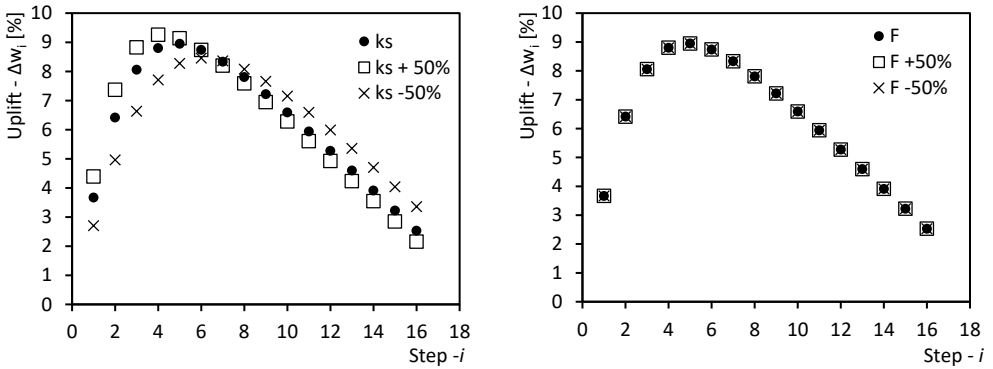


Figure 2-22 Parametric analysis results

**2.6.2 ANALYSIS OF THE DEFORMATION: FLEXURAL DEFORMATION AND RIGID BODY ROTATION**

As previously mentioned, the vertical uplift of the composite structure can be divided into two main contributions: the actual bending of the beam portion with the fasteners inserted and the rigid rotation of the external part of the beam with no fasteners inserted. The two components are isolated from each other in Figure 2-23.

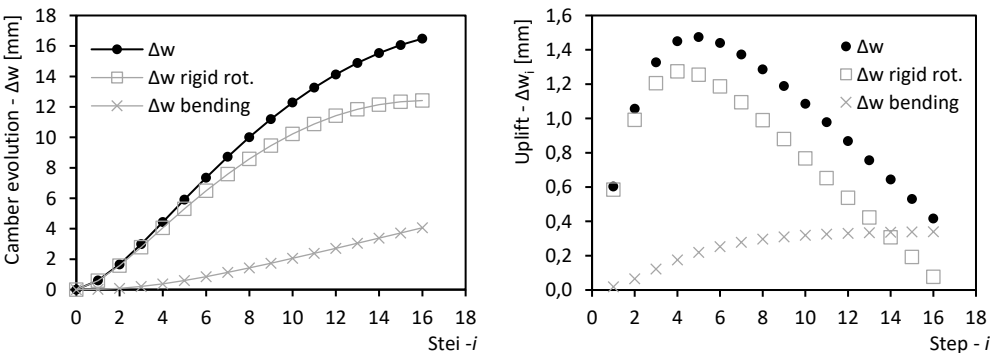


Figure 2-23 Bending and rigid rotation contribution to total camber

As result, 75.34% of the final camber is related to the rigid rotation contribution. Not surprisingly, the effectiveness of the last fasteners ( $i \geq 14$ ) is mostly related to the bending contribution, as the length of the free part of the beam is considerably reduced.

As visible from Figure 2-24, the magnitude of the bending contribution showed no sensitivity to a variation in the fastener spacing  $s$ . Conversely, a reduction in the fastener spacing results in an increase of the contribution given by the rigid body rotation.

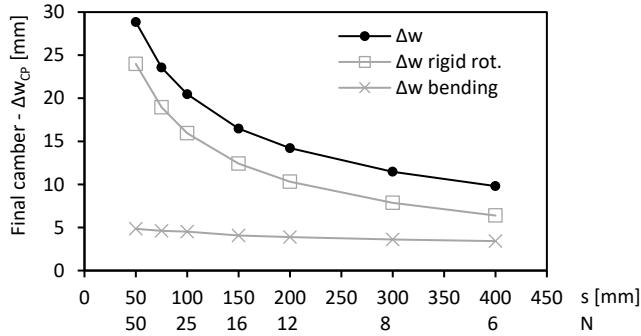


Figure 2-24 Influence of the fastener spacing on the camber value components

### 2.6.3 INFLUENCE OF THE FASTENER ARRANGEMENT ON THE FINAL CAMBER

In this section, the influence of a variable fastener spacing on the cambering and prestressing procedure was analysed. As shown in Figure 2-25, three different fastener configurations were considered:

- S1:  $s = 150 \text{ mm}$  along the whole beam ( $N = 16$ );
- S2:  $s = 150 \text{ mm}$  in the internal part and  $s = 75 \text{ mm}$  in the external part ( $N = 24$ );
- S3:  $s = 75 \text{ mm}$  in the internal part and  $s = 150 \text{ mm}$  in the external part ( $N = 24$ ).

Differently from the previous sections, the following connection properties were considered in the analysis:  $k_s = 15800 \text{ N/mm}$  and  $F_h = F_v = 4300 \text{ N}$ .

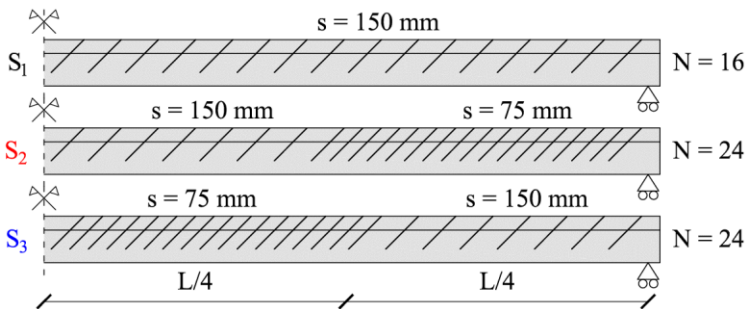


Figure 2-25 Fastener spacing configurations:  $S_1$ ,  $S_2$  and  $S_3$

The outcomes of the assembly procedure are shown in Figure 2-26. As a result, an +50% increase in the total number of fasteners in the external part of the beam ( $S_2$

configuration) produced a +18.03% variation in the uplift. Conversely, the same +50% fastener addition in the central part of the composite system (S<sub>3</sub> configuration) resulted in a +30.44% variation of the final camber.

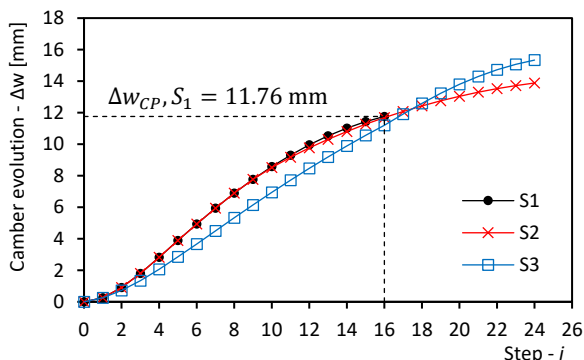


Figure 2-26 Influence of a variable fastener spacing on the camber evolution

Figure 2-27 shows the percentage contribution of each couple of connectors to the final vertical displacement. As reference to the S<sub>2</sub> configuration, a reduced efficiency of the additional fasteners inserted in the external portions ( $i \geq 16$ ) of the composite beam was observed. On the contrary, a more uniform contribution was registered in test S<sub>3</sub>.

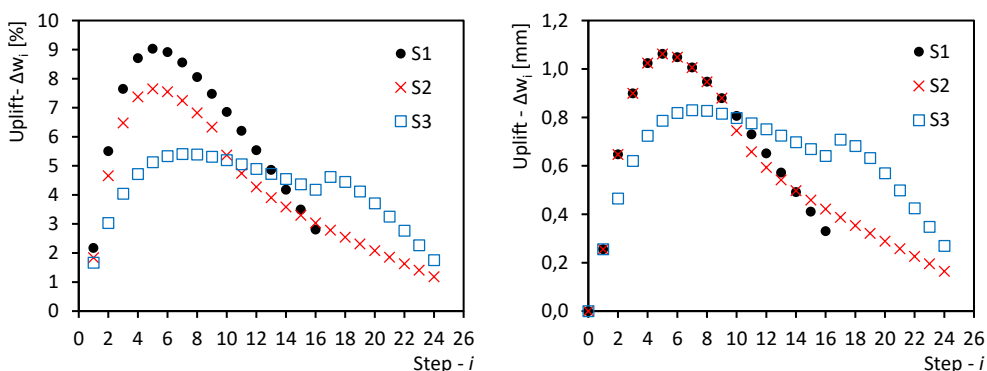


Figure 2-27 Influence of a variable fastener spacing on the contribution offered by each couple of devices

To better understand the influence of a variable connector spacing on the effects introduced by the assembly procedure, the final bending moment acting on the joist element is reported in

Figure 2-28.

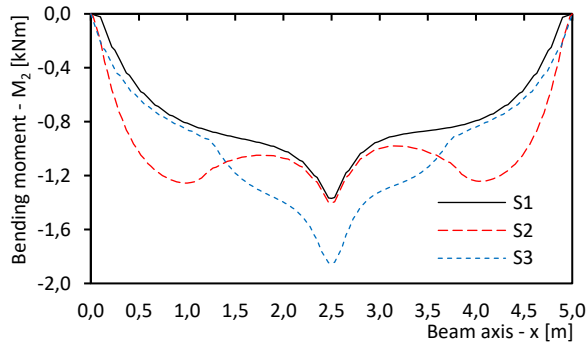


Figure 2-28 Bending moment acting on the joist element for different fastener configurations

As illustrated in

Figure 2-28, an increase in the fastener number in the lateral parts of the beam results in an increase in the internal moment (and curvature) acting on the beam near the supports, with the moment at the midspan remaining unchanged. Consistently with the diagrams showed in Figure 2-29, the deformed shape of the composite beams is plotted in Figure 2-29.

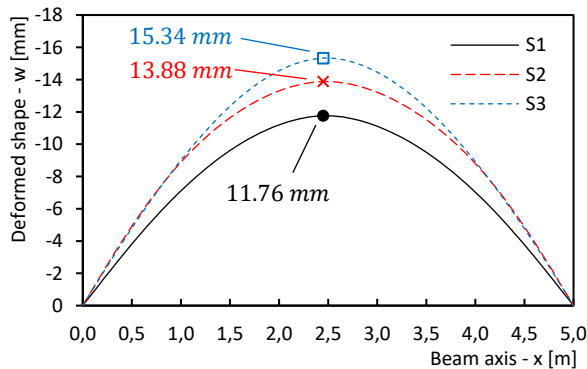


Figure 2-29 Deformed shape at the end of the CP procedure for different fastener configurations

Whit reference to a composite beam (5 m span) with a fastener spacing equal to 75 mm in the central part and 150 mm in the external parts (Figure 2-30), the effects produced by a variation in the connector distribution (moving the fastener from the inner part to the external part and vice versa) was analysed in the following.

Considering a constant number of fasteners ( $N = 16$ ), the subsequent configurations were studied:

- $S = 16 + 0$  (no fasteners in the external parts);
- $S = 12 + 4$
- $S = 8 + 8$
- $S = 4 + 12$
- $S = 0 + 16 = S_1$  (constant 150 mm spacing along the whole beam);

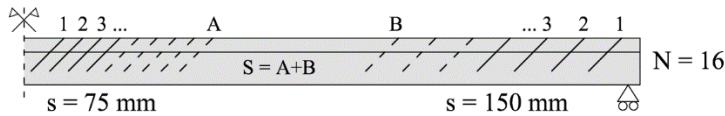


Figure 2-30 Fastener configurations

According to the results of the numerical model (Figure 2-31), despite the profiles of uplift introduced by each couple of fasteners differ from one configuration to the other, the values of the final camber did not differ significantly.

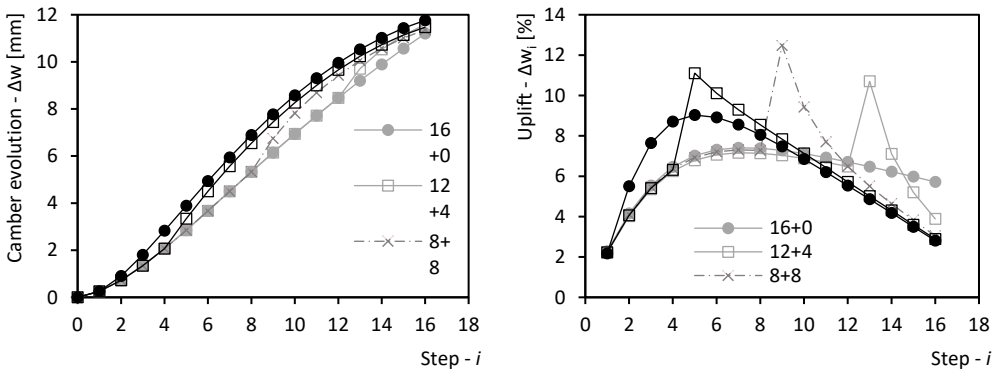


Figure 2-31 Camber evolution for different fastener configurations

Differently, as reported in Figure 2-32, the bending moment profile acting on the joist element of the composite system, and consequently the curvature, depends on how the connectors were arranged along the beam. More specifically, going from the combination with constant fastener spacing along the whole beam ( $S = S_1$ ) to the combination with no fasteners inserted in the lateral parts ( $S = 16 + 0$ ), a bending moment (maximum values) variation of +32.36% was registered.

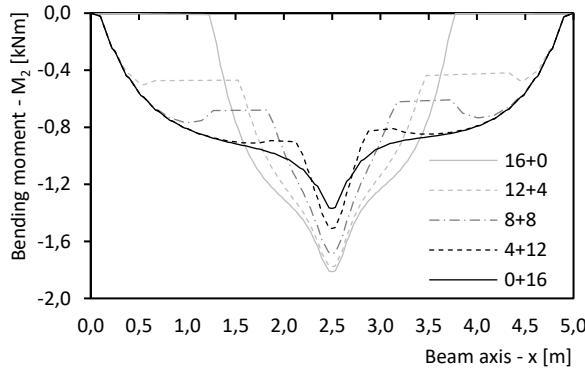


Figure 2-32 Bending moment acting on the joist element at the end of the CP procedure for different fastener configurations

Figure 2-33 plots the vertical beam deflection at the end of the assembly procedure ( $w_{CP}$ ) and after the application of a distributed load equal to  $5\text{ kN/m}^2$  ( $w_{load}$ ). As visible in the histogram, the maximum downward deflection was registered in the configuration where no fasteners were inserted in the later parts of the composite beam ( $\Delta w_{load} = 28.80\text{ mm}$ ). Conversely, the highest bending stiffness was registered in the configuration where the fasteners were equally distributed along the beam ( $\Delta w_{load} = 15.21\text{ mm}$ ).

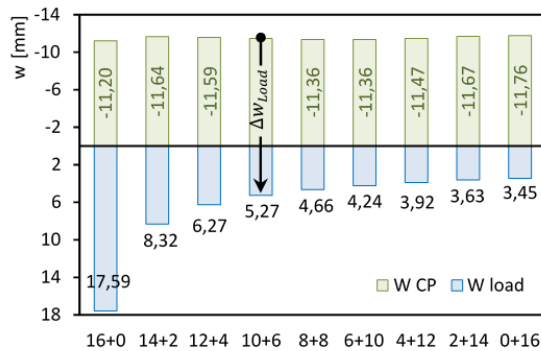


Figure 2-33 Actual deformation at the end of the CP procedure ( $w_{CP}$ ) and after the load application ( $w_{load}$ ) for different fastener configurations

Hence, from the parametric study presented in this section, the configuration with the fasteners equally distributed along the beam axis has proved to be the most performing

solution, considering both the benefits introduced by the CP procedure and the flexural behaviour of the system under imposed load.

## 2.7 CONCLUSIONS

An original assembly procedure (CP procedure), developed at the University of Trento [1], was analysed and validated in this chapter. Such innovative technique allows to pre-stress and camber composite beams by simply relying on the pressure generated by the insertion of screw-fasteners.

The potentiality shown by this assembly method makes it a useful tool for the realisation of high performance new diaphragms. Furthermore, the simplicity of this procedure (e.g. no additional external supports are required), combined with the speed of the implementation (e.g. dry solution) makes this technique suitable also for the rehabilitation of vintage timber floors. By applying this retrofit strategy it is possible to reduce the effects of irreversible deformation accumulated over time (creep phenomena) and improve the out-of-plane behaviour of existing diaphragms without any significant mass increase.

An analytical formulation able to describe both the stress and the strain state resulting from the implementation of this procedure was presented. Successively, a numerical model was developed through a finite element software. The *nonlinear staged construction* function was employed [6] to reproduce the sequential insertion of the connectors during the assembly procedure. A general good correlation was observed between the results of the analytical formulation e the numerical model.

Thirty full-scale tests on timber-to-timber composite floors assembled with the aforementioned procedure have been carried out at the Laboratory of the Department of Civil, Environmental and Mechanical Engineering (DICAM) of the University of Trento (Italy) over the last five years. Two tests (out of thirty) were selected and presented in this section with the aim of proving the applicability and the potentiality of the pre-stressing and cambering procedure. The experimental tests positively contributed to the calibration and validation of this assembly technique, confirming the method applicability. The test outcomes were consistent with the numerical and analytical models presented herein, in terms of uplifts, stress levels and overall mechanical performance. The results of the entire experimental campaign (thirty full-scale tests) are presented in the subsequent chapters.

A parametric study was performed in order to better understand the effects of different fastener configurations on the mechanical behaviour of composite systems assembled

with the assembly procedure. The configuration with the fasteners equally distributed along the beam axis has proved to be the most performing solution, considering both the benefits introduced by the CP procedure and the flexural behaviour of the system under vertical load.

## 2.8 REFERENCES

- [1] Schiro G., Rizzi E., Piazza M. (2017) Interventions aimed at reducing the excessive deformability of timber floors: strengthening and stiffening techniques according to the new Italian code (NTC). *Proceedings of the XVII ANIDIS (Italian National Association of Earthquake Engineering) conference*, Pistoia, Italy (in Italian).
- [2] Giongo I., Piazza M., Tomasi R. (2013) Investigation on the self-tapping screws capability to induce internal stress in timber elements. *Advanced Material Research*, vol. 778, pp. 604-611.
- [3] Giongo I., Piazza M., Tomasi R. (2012) Cambering of timber composite beams by means of screw fasteners. *Journal of Heritage Conservation*, vol. 32, pp. 133-136.
- [4] Newmark N.M., Siess C.P., Viest I.M. (1951) Test and analyses of composite beams with incomplete interaction. *Proceedings, Society for Experimental Stress Analysis*, vol. 9, no. 1, pp. 75-92, University of Illinois, Urbana, Illinois.
- [5] Newmark N.M., Siess C.P. (1942) Moment in I-beam bridge. Bulletin series n.336, University of Illinois, Urbana, Illinois.
- [6] CSI [Computers and Structures Inc.] (2004) CSI Analysis Reference Manual For SAP2000®, ETABS®, and SAFE®. *CSI, Berkeley*.
- [7] Giongo I., Schiro G., Piazza M., Tomasi R. (2016) Long-term out-of-plane testing of timber floors strengthened with innovative timber-to-timber solutions. *Proceedings of the World Conference on timber Engineering (WCTE)*, Vienna, Austria.
- [8] Schiro G., Giongo I., Sebastian W., Riccadonna D., Piazza M. (2018) Testing of timber-to-timber screw-connections in hybrid configurations. *Construction and Building Materials*, vol. 171, pp. 170-186.
- [9] ETA (European Technical Approval) 12/0121: HECO-TOPIX-T and HECO-TOPIX-CC self-tapping screws.
- [10] ETA (European Technical Approval) 11/0190: Würth self-tapping screws.

- [11] Giongo I., Piazza M., Tomasi R. (2013) Investigation on the self-tapping screws capability to induce internal stress in timber elements. *Advanced Material Research*, vol. 778, pp. 604-611.
- [12] Giongo I., Piazza M., Tomasi R. (2012) Out of plane refurbishment techniques of existing timber floors by means of timber to timber composite structures. *WCTE 2012 – World conference on timber engineering*
- [13] Giongo I. (2016) Study on timber compression forces induced by self-tapping screw fastener. *European Journal of Wood and Wood Products*, vol. 74, pp. 473-475.
- [14] European Committee for Standardization (2014). EN 1995-1-1:2004+A2:2014: Eurocode 5 - Design of timber structures, Part 1-1, General - Common rules and rules for buildings. CEN, Brussels, Belgium.



---

## 3 TESTING OF TIMBER-TO-TIMBER SCREW- CONNECTIONS IN HYBRID CONFIGURATIONS

### 3.1 INTRODUCTION

Several typologies of self-tapping screws (for use in timber constructions) covering a wide variety of structural applications have been developed over the past two decades and are currently available on the market [1]. A possible way to classify them can be to refer to the fastener threaded part. Three main classes can be identified, namely partially threaded screws (also referred to as single-threaded screws, ST), double threaded screws (DT) and fully-threaded screws (FT, also referred to as all-threaded screws). There are also screws that do not neatly fit into either of these three categories, as they are designed for special purposes like coupling timber with other materials, such as concrete or steel. In contrast to other connector types (e.g. lag screws), there is currently no harmonized standard that establishes the requirements for structural screws. Consequently, each of the three classes (ST, DT and FT) includes fasteners that differ from each other for thread, head and tip geometry. The mechanical properties are provided by the producers in the product standards (e.g. European Technical Assessment, ETA: [22], [23], [24] and [25]).

It is evident that when such connectors are used in configurations that are not specifically described by the product standards, their performance needs to be evaluated experimentally [2]. Extrapolation of the results from other “similar” fastener types is inadvisable, unless these extrapolations are proof-checked by testing. For example, in Eurocode 5 [15] it is advised that the slip modulus of a timber-concrete connection is taken as double the value of the modulus calculated by means of the formula given for a parallel timber-timber connection. That is because an approach has not yet been developed specifically for timber-concrete connections. Hence, in the status quo, these

timber-timber extended predictions are backed up by tests on the timber-concrete connections under consideration.

The present chapter focuses on connection configurations that are intended for use in the field of timber-to-timber composite structures where the fasteners may be inserted at an angle to the grain other than  $90^\circ$  and may connect different timber products (e.g. solid sawn timber with cross laminated timber) and/or elements from different timber species (e.g. softwood elements with hardwood elements). Extensive details on the tested configurations and the purposes they are designed for, will be provided in section 2.

Structural solutions in which DT and FT screws are loaded in a combination of shear and tension are becoming more common. Interesting studies into the mechanical performance of such connections (softwood) can be found in the literature ([3] and [4]), where formulations to evaluate connection strength and stiffness are also proposed. However, to the best of the author's knowledge there are no data available on ST screws loaded in a shear-tension configuration, despite available evidence of applications showing advantages from such use [5].

The optimization/specialization process that leads to widening of the timber fastener range also involves timber as a construction material. Wood based structural products now include solid sawn timber, glued-laminated timber, laminated veneer lumber and cross-laminated timber. "New" wood species (such as poplar, oak, birch and beech) are being actively considered for structural purposes by the construction industry (see [6], [7] and [8]) and will soon compete with the traditional (for construction) softwood species (e.g. pine, spruce, larch). This will only be really possible once the performance of mechanical connections realized with these new products (often characterized by very high density values) has been thoroughly investigated and sound analytical formulations to predict their behavior have been developed.

Studies including [9] – [12] have provided first insights that will help close the gap between the availability of new engineered components in renewable materials with high mechanical performance and the wide application of these components in real construction projects.

In the following sections of this chapter, the outcomes of an extensive experimental campaign on short-term testing of timber screw-connections comprising specimens realized with multiple combinations of timber products (hybrid configurations), screw types and screw configurations, will be presented. The specimens and tests are first described, following which interpretation of the results to infer connection properties on strength, stiffness and ductility will be presented. At the end of this chapter, conclusions are drawn.

## 3.2 CONNECTION TESTS

### 3.2.1 TEST CONFIGURATION AND GEOMETRY

The experimental campaign was carried out at the laboratory of the Department of Civil, Environmental and Mechanical Engineering (DICAM) of the University of Trento and totalled 58 pushout tests covering 14 configurations. Different solutions were investigated in order to characterise the mechanical behaviour, in terms of stiffness, strength, static ductility and residual strength of connections mainly designed for the realisation of timber-to-timber composite (TTC) floors. The significant parameters that describe the tested samples, such as geometry, materials and joint configuration, are reported in Table 3-1. Note that, within specimens where the screws were inclined at 45°, all screws were parallel to each other (not in an X-formation) to enable exploitation of the beneficial orientation of the screws (shear-tension configuration). As shown in Figure 3-3, the double-shear specimen layouts used during the tests are those commonly employed in pushout tests and consist of a central timber element flanked by two side elements symmetrically disposed. As will be specified hereinafter, for some tests an interlayer element made of timber boards was added. This represented the situation where timber reinforcing elements are positioned on the existing flooring, a common practice in retrofit interventions. Consistently with EN 1995-1-1 [15], the samples were designed in order to avoid failures strictly related to inadequate screw spacing and distances from the edges.

*Table 3-1 Test configurations*

Test ID	n°	App.	Central element	Interl. t <sub>i</sub> [mm]	Side elements	t <sub>s</sub> [mm]
			Type		Type	
PA	4	N	Beech LVL beam	-	CLT panel	57
PB	4	N	Beech LVL beam	-	CLT panel	57
PC	4	N	Beech LVL beam	-	Beech LVL panel	40
PD	5	N	Beech LVL beam	-	Beech LVL panel	40
PE	5	N	Beech LVL beam	-	Beech LVL panel	40
PF	5	R	Spruce Solid wood	20	Beech LVL on its side	50
PG	2	R	Spruce Solid wood	20	Beech LVL on its side	50
PH	3	R	Spruce Solid wood	20	Beech LVL on its side	50
PI	3	N	Spruce Solid wood	-	CLT panel	57
PL	3	N	Spruce Solid wood	-	CLT panel	57
PM	5	R	Spruce Solid wood	20	CLT panel	57
PN	5	R	Spruce Solid wood	20	CLT panel	57
PO	5	R	Spruce Solid wood	20	CLT panel	57
PP	5	R	Spruce Solid wood	20	CLT panel	57

n°: Number of repetitions; App.: application; N: new application; R: Retrofit application

Test ID	n°	App.	Connections		
			Type	Washer	$\alpha$
PA	4	N	DT <sub>A</sub> 8.5x150	-	45°
PB	4	N	ST <sub>A</sub> 10x220	W+GC	45°
PC	4	N	ST <sub>A</sub> 10x160	W+GC	45°
PD	5	N	ST <sub>A</sub> 10x220	SW	45°
PE	5	N	ST <sub>A</sub> 10x220	W	90°
PF	5	R	ST <sub>A</sub> 10x220	W+GC	45°
PG	2	R	ST <sub>A</sub> 10x220	GC	45°
PH	3	R	DT <sub>A</sub> 8.5x190	-	45°
PI	3	N	DT <sub>A</sub> 8.5x150	-	45°
PL	3	N	ST <sub>A</sub> 10x220	W+GC	45°
PM	5	R	DT <sub>B</sub> 8.2x190	-	45°
PN	5	R	ST <sub>B</sub> 10x200	W+GC	45°
PO	5	R	ST <sub>B</sub> 10x200	W	90°
PP	5	R	ST <sub>B</sub> 10x200	-	90°

ST: Single threaded screw; DT: Double threaded screw;  
W: Washer; SW: Special washer; GC: Groove cut

Essentially, the aims of the experimental campaign were two-fold. The first goal was to investigate the mechanical behaviour of connections specifically designed for newly constructed high-performance TTC floors. Hybrid solutions, that coupled the lightness of softwood elements (spruce cross laminated panels), with the strength of hardwood components (beech laminated veneer lumber beams/panels) by means of different types of connectors (tests PA and PB), were compared with “more common” timber-to-timber solutions (tests PI and PL). In addition, hardwood-hardwood configurations were studied (tests PC, PD and PE).

The second goal was to evaluate the performance of connections designed for retrofit solutions on existing timber floors. In order to reproduce realistic scenarios present in historical buildings, only solid wood elements made of spruce were used for the central part of the specimens (instead of using for example glulam). As stated earlier, timber boards were inserted between the central and side elements to simulate an existing flooring. As regards the reinforcing elements (corresponding to the lateral elements of the samples), two different solutions were adopted: softwood cross laminated panels (tests PM, PN, PO and PP) and beech LVL beams arranged on their side (tests PF, PG and PH). The use of a slender beam element with a reduced section instead of a panel enables enhanced out-of-plane performance of timber diaphragms in case of large deformations or where adjacent existing joists exhibit different levels of sagging.

### 3.2.2 TIMBER ELEMENTS

Different timber products obtained from different both softwood and hardwood species were employed in the experimental campaign. For the central components, spruce solid wood graded as strength class C24 [19] and beech laminated veneer lumber (LVL) of grade GL70 [18] were considered. Two types of panel were selected for the side elements: three-layer cross laminated timber (CLT) of 57 mm thickness [21] and beech LVL (w/o cross layers) of 40 mm thickness [20]. In addition, to simulate a further retrofit solution, beech LVL beams (GL70) arranged on their side were used. The mechanical properties and the density (from product documentation and experimental data) of the various elements are reported in Table 3-2.

*Table 3-2 Strength and stiffness properties for timber elements*

Element type and grading			Beech LVL	Spruce Solid wood	Beech LVL panel	Spruce CLT panel
			GL70 [18]	C24 [19]	[20]	[21]
Bending:	$f_{m,k}$	[MPa]	70	24	80	24
Tension:	$f_{t,0,k}$	[MPa]	55	19.2	60	14
	$f_{t,90,k}$	[MPa]	0.6	0.5	1.5	0.12
Compression:	$f_{c,0,k}$	[MPa]	59.4	24	57.5	21
	$f_{c,90,k}$	[MPa]	10.2	2.5	14	2.5
Shear:	$f_{v,k}$	[MPa]	4	3.5	8	3.3
MoE:	$E_{0,mean}$	[MPa]	16700	11500	16800	12000
Density:	$\rho_{mean}$	[kg/m <sup>3</sup> ]	≥ 740	420	800	450-500
Density (experimental):	$\rho_{experim.}$	[kg/m <sup>3</sup> ]	796	460	846	465
	CoV		0.7%	2.7%	0.5%	1.2%

From Table 3-2 it is possible to note that beech LVL panel has better mechanical properties than beech LVL GL70 (with the exception of compression parallel to the grain) despite both being made of beech laminated veneers. Such difference is to be attributed, at least partly, to the different veneer thickness (4 mm for GL70 beams and 3 mm for LVL panels).

### 3.2.3 CONNECTORS

The fasteners employed in the experimental campaign (Figure 3-1) belong to two macro groups: single (or partially) threaded screws ( $ST_A$  [22] and  $ST_B$  [23]) and double threaded screws ( $DT_A$  [24] and  $DT_B$  [25]).

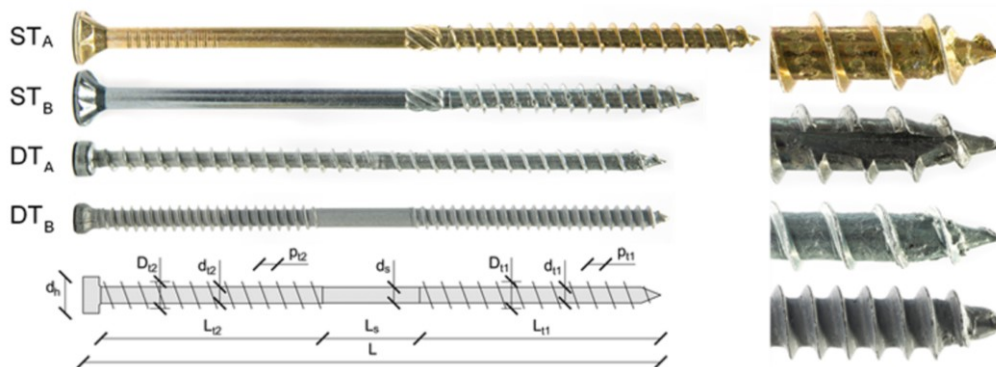


Figure 3-1 Screw types used in the experimental campaign

The geometries of the ST screws were quite similar to each other, with a countersunk head and a milling cutter between the thread and the shank. The main difference between  $ST_A$  and  $ST_B$  fasteners lies in the shape of the tip, with a pronounced cutter on the tip of  $ST_B$ .

As regards the DT connectors, the different diameters ( $D_{i1}$  and  $D_{i2}$ ) and pitches ( $p_{i1}$  and  $p_{i2}$ ) of the two threaded parts, are optimised to generate a pulling and closing effect in the joint.  $DT_B$  screws are characterised by a clearly-distinguishable smooth part at the screw mid-length ( $L_s$ ) and a cylindrical head having a diameter ( $D_h$ ) comparable with  $D_{i2}$  (Table 3-3). Differently,  $DT_A$  screws have a shorter central smooth part ( $L_s$ ), a bigger head diameter ( $D_h$ ) and considerably larger pitches ( $p_{i1}$  and  $p_{i2}$ ).

Table 3-3 Connector geometry and properties

Connector:	$ST_A$ [22]	$ST_B$ [23]	$DT_A$ [24]	$DT_B$ [25]		
$L$ [mm]	220	160	200	190	150	190
$L_{i1}$ [mm]	100	100	80	90	70	80
$d_{i1}$ [mm]	6.3	6.3	6.4	5.3	5.3	5.4
$D_{i1}$ [mm]	10	10	10	8	8	8.2
$p_{i1}$ [mm]	6.6	6.6	5.4	6	6	3.2
$L_s$ [mm]	120	60	120	5	5	30
$d_s$ [mm]	7.2	7.2	7	5.6	5.6	6.3
$L_{i2}$ [mm]	-	-	-	90	70	80
$d_{i2}$ [mm]	-	-	-	5.025	5.025	5.4
$D_{i2}$ [mm]	-	-	-	8.5	8.5	8.9
$p_{i2}$ [mm]	-	-	-	5.68	5.6	3
$d_h$ [mm]	18.5	18.5	18.25	12	12	10
$M_{y,k}$ [Nm]	36	36	36	20	20	19.5
$f_{y,k}$ [Mpa]	600	600	600	900	900	870
$R_{tens,k}$ [kN]	26	26	31.4	18	18	28.6
$f_{ior,k}$ [Nm]	45	45	40	23	23	25.9

The dimensions (Figure 3-1) and the mechanical properties provided by the relevant European Technical Approval (ETA) are summarised in Table 3-3, where  $M_{y,k}$  is the characteristic yield moment,  $f_{y,k}$  is the characteristic yield strength,  $R_{tens,k}$  is the characteristic tensile strength,  $f_{tor,k}$  is the characteristic torsional strength and  $f_{head,k}$  is the characteristic strength of the screw head.

As supplied by the producers, washers with different geometries were adopted. In particular, ST<sub>A</sub> screws were coupled with the washers shown in Figure 3-2-C (top) and ST<sub>B</sub> screws with the washers reported in Figure 3-2-C (bottom). The first type of washers is characterised by a thin section with a countersunk bottom surface, while the second type has a squatter, more compact structure with a totally flat surface at the bottom.

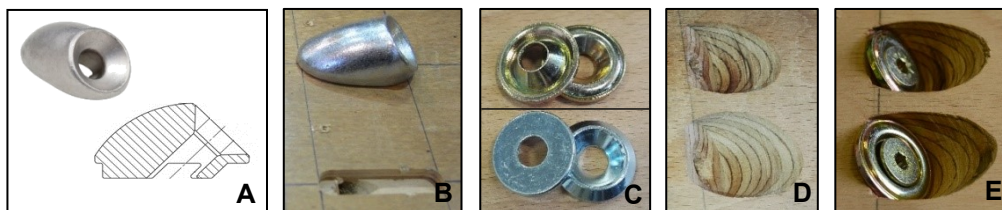


Figure 3-2 Washers and groove cuts

For the configurations where the single threaded screws were inserted at an angle ( $\alpha$ ) different from  $90^\circ$ , groove cuts (GC, Figure 3-2-D) were prepared prior to the assembly of the samples in order to have a wider contact area between the wood and the washer (Figure 3-2-E).

For timber-to-timber hybrid retrofit solutions (where softwood joists are coupled with hardwood reinforcing elements), samples without washers were also tested to verify the necessity of using washers. This additional solution was considered bearing in mind that, because of the high density of wood (see Table 3-2) under the screw heads, failure is determined by thread withdrawal from the softwood element.

As previously mentioned, the washers for single threaded screws that are available on the market, are usually designed for a  $90^\circ$  configuration. As an alternative solution to the groove cuts, the use of washers with a modified geometry could facilitate the assembly operations. However, due to the lack of washers designed ad hoc for timber-to-timber joints with inclined screws, special washers (SW, Figure 3-2-A and Figure 3-2-B) that are designed for steel-to-timber connections were employed. As shown in Figure 3-2-B, a groove cut was nonetheless necessary due to the shape of the bottom

surface of the SW. As will be discussed hereinafter, the design of an optimised washer could result in the complete elimination of groove cuts.

Regarding the double threaded screws selected for the tests, the following remarks can be reported:  $DT_A$  screws compared to  $DT_B$  screws are characterised by a wider pitch for each thread, a shorter smooth part of the shank and a larger diameter of the head (see Figure 3-1 and Table 3-3).

### 3.2.4 TEST SETUP AND INSTRUMENTS

Every test specimen was subjected to quasi-static monotonic loading. According to EN 12512 [16], the constant rate of slip was set equal to 0.05 mm/s (a range between 0.02 mm/s and 0.2 mm/s is recommended by [16]). The setup was designed in order to have maximum displacement values up to 100 mm. Although a slip limit of 30 mm is considered as ultimate condition by [16], where possible, the specimens were pushed up to their actual failure limit state in order to evaluate the residual capacity also for high values of displacement.

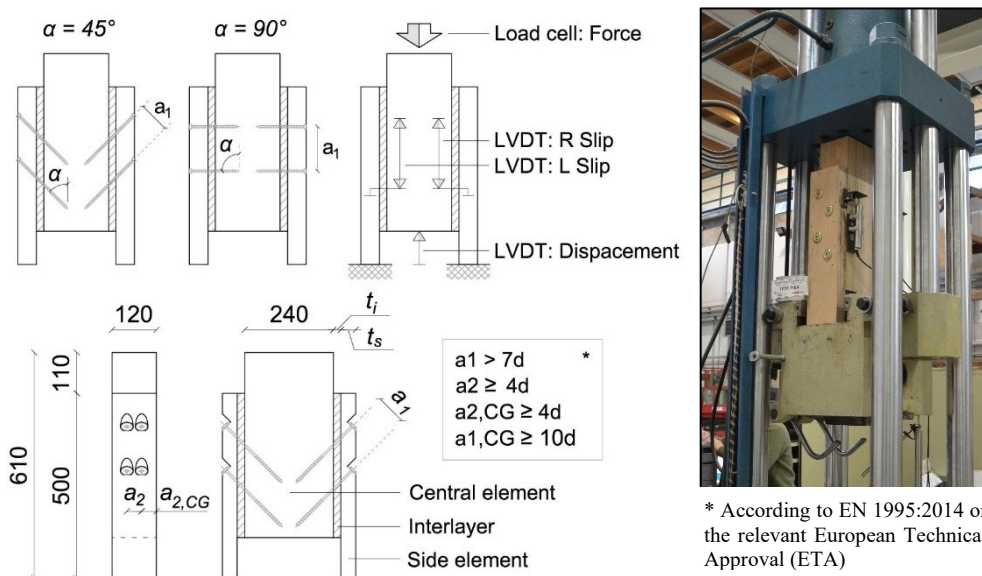


Figure 3-3 Specimen geometry and test setup

The load, introduced by a universal testing machine (Figure 3-3) through a hydraulic actuator, was monitored with a 1000 kN load cell (the values of maximum forces range in the field 80 – 360 kN). Two linear variable differential transformer transducers (LVDTs) were employed (sensitivity of 2 mV/V) to measure the slip between the central

and side elements. A further inductive transducer was introduced to provide alternative measures of the total vertical displacement. The recording was done continuously with a frequency rate of 2 Hz via a multi-channel data recording device.

### 3.2.5 ESTIMATION OF CONNECTION MECHANICAL PARAMETERS

The standards adopted as reference for the evaluation of the connection performance parameters (yield point, secant stiffness, ultimate conditions and static ductility) were EN 12512 [16] and EN 26891 [17].

The slip modulus  $K_s$  of the connections (corresponding to the slip modulus  $K_{ser}$  provided by EN 1995-1-1 [15]) can be calculated by means of the following equation [17]:

$$K_s = \frac{0.4 F'_{max} - 0.1 F'_{max}}{v_{0.4} - v_{0.1}} \quad (\text{Eq. 1})$$

where  $v_{0.1}$  and  $v_{0.4}$  are the connection slips (evaluated for each specimen) corresponding to loading equal to  $0.1 \cdot F'_{max}$  and  $0.4 \cdot F'_{max}$  respectively;  $F'_{max}$  is the mean value of the maximum force values  $F'_{max,i}$  registered for all test repetitions associated with each configuration (consistently with EN 26891 [17], excluding values that deviated by more than 20% from the mean). For each test,  $F'_{max,i}$  is equal to the actual maximum load  $F_{max,R}$  when the corresponding slip value was less than 15 mm, otherwise the load corresponding to a 15 mm slip  $F_{15}$  was used [17].

According to [16], the yield point ( $F_y, v_y$ ) is determined as shown in Figure 3-4. In particular, case A refers to a load-slip curve with two well-defined linear parts, while case B refers to a curve with a pronounced non-linear behaviour. Case C is added to represent tests with a linear-elastic behaviour up to the maximum load.

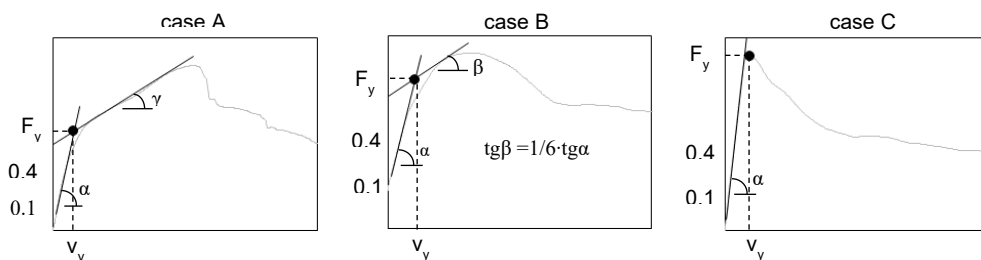


Figure 3-4 Definition of yield point for a load-slip ( $F$ - $v$ ) curve

The ultimate slip  $v_u$  corresponds to the first of the following conditions: failure of the specimen, slip at 0.8 times  $F_{max,R}$  on the descending branch and a slip value of 30 mm [16]. The ductility  $D$  is calculated as the ratio between ultimate slip and yield slip according to [16].

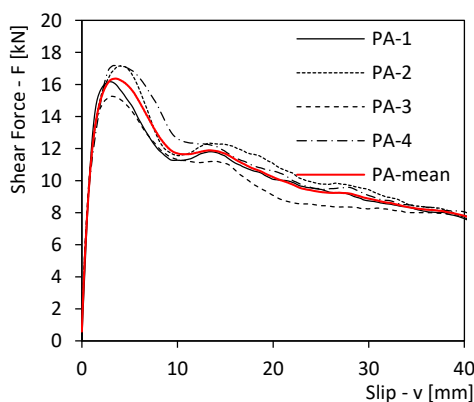
### 3.2.6 EXPERIMENTAL RESULTS

In

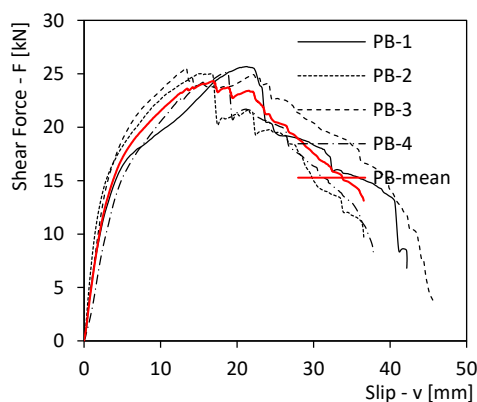
Figure 3-5 the experimental results from each configuration tested are plotted in terms of connection shear force (per single fastener) versus slip (average value from both specimen sides). The red curve in each diagram represents the mean curve of all measured force-slip curves.

Consistently with section 3.2.5, the connection performance parameters (maximum load, slip modulus, yield point and ductility) that were derived from the test data, are also reported in

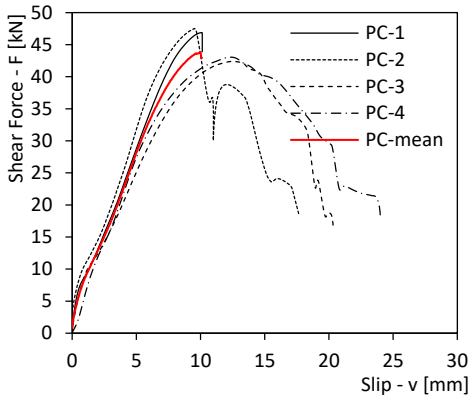
Figure 3-5. For every parameter, the coefficient of variation ( $CoV$ ), is given.



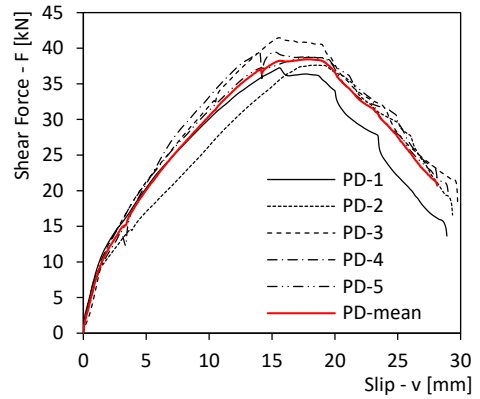
Test PA	Mean	CoV
$F_{max,R}$ [kN]	16.35	4.5%
$K_s$ [N/mm]	13234	3.4%
$F_y$ [kN]	12.98	4.8%
$v_y$ [mm]	0.91	9.2%
$D$	8.53	14.8%



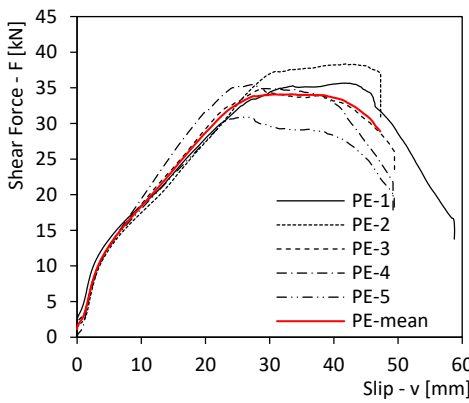
Test PB	Mean	CoV
$F_{max,R}$ [kN]	25.34	1.1%
$K_s$ [N/mm]	5369	23.8%
$F_y$ [kN]	16.13	8.1%
$v_y$ [mm]	3.26	29.0%
$D$	7.76	19.1%



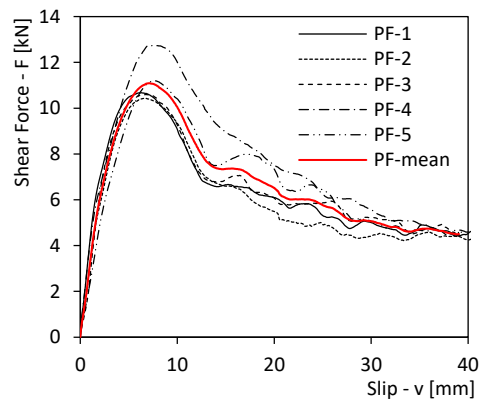
Test PC	Mean	CoV
$F_{\max,R}$ [kN]	44.95	5.0%
$K_s$ [N/mm]	4924	7.3%
$F_y$ [kN]	42.86	8.2%
$v_y$ [mm]	8.20	6.7%
D	-	-



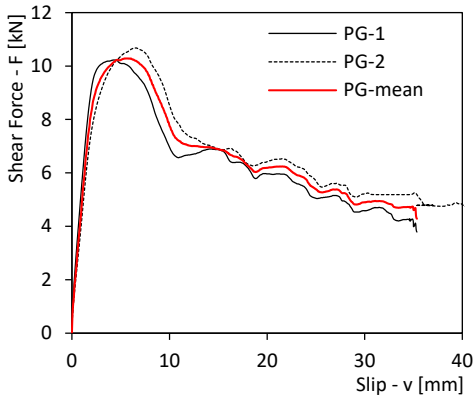
Test PD	Mean	CoV
$F_{\max,R}$ [kN]	38.91	3.9%
$K_s$ [N/mm]	4192	17.9%
$F_y$ [kN]	20.46	17.0%
$v_y$ [mm]	4.54	24.2%
D	5.33	17.3%



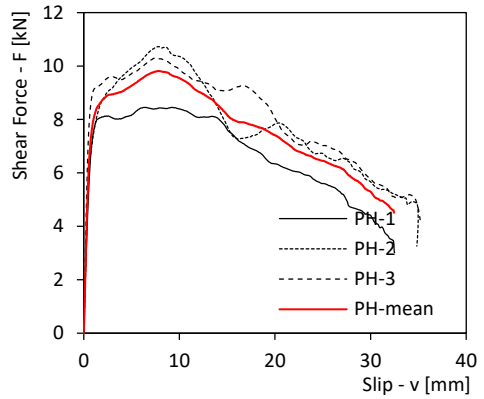
Test PE	Mean	CoV
$F_{\max,R}$ [kN]	35.03	6.8%
$K_s$ [N/mm]	3035	13.6%
$F_y$ [kN]	12.38	7.8%
$v_y$ [mm]	4.12	9.1%
D	7.35	8.9%



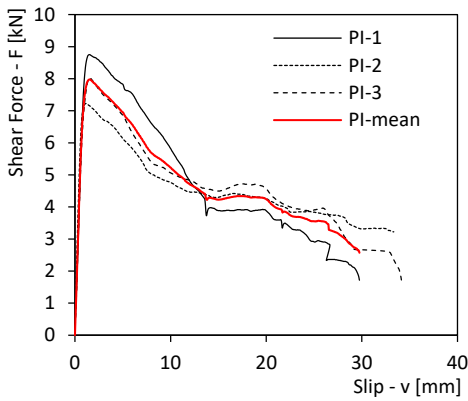
Test PF	Mean	CoV
$F_{\max,R}$ [kN]	11.13	7.6%
$K_s$ [N/mm]	3332	16.7%
$F_y$ [kN]	9.36	6.6%
$v_y$ [mm]	2.91	22.7%
D	4.09	18.5%



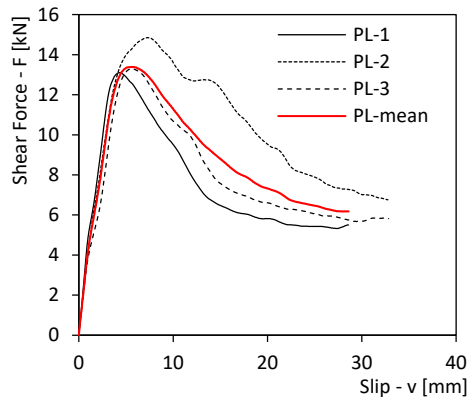
Test PG		Mean	CoV
$F_{max,R}$	[kN]	10.45	2.2%
$K_s$	[N/mm]	4472	14.9%
$F_y$	[kN]	9.01	2.6%
$v_y$	[mm]	1.93	12.8%
D		4.85	5.1%



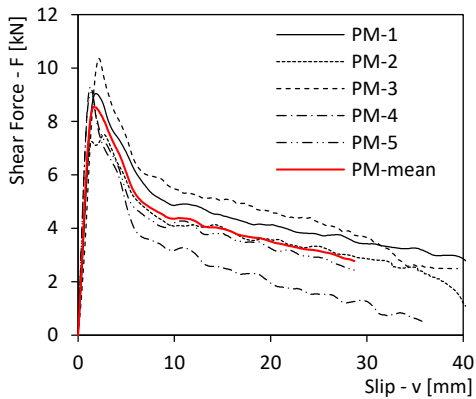
Test PH		Mean	CoV
$F_{max,R}$	[kN]	9.83	10.1%
$K_s$	[N/mm]	13468	20.6%
$F_y$	[kN]	8.59	6.2%
$v_y$	[mm]	0.66	12.5%
D		27.01	24.1%



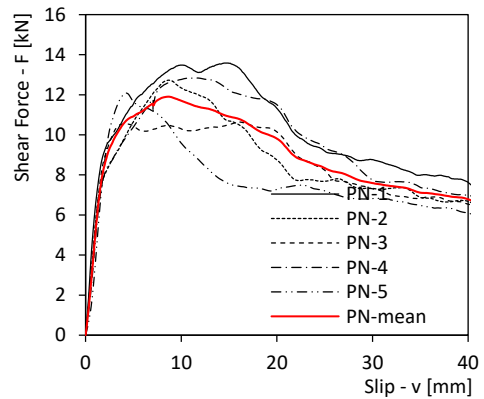
Test PI		Mean	CoV
$F_{max,R}$	[kN]	8.00	7.8%
$K_s$	[N/mm]	9773	12.8%
$F_y$	[kN]	8.00	7.8%
$v_y$	[mm]	1.36	13.0%
D		4.74	14.4%



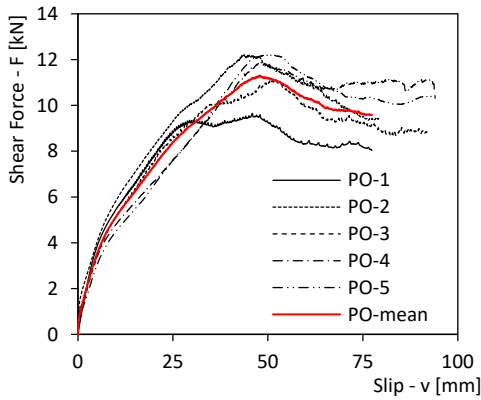
Test PL		Mean	CoV
$F_{max,R}$	[kN]	13.75	5.7%
$K_s$	[N/mm]	3744	20.3%
$F_y$	[kN]	12.59	3.4%
$v_y$	[mm]	3.45	23.3%
D		3.45	32.1%



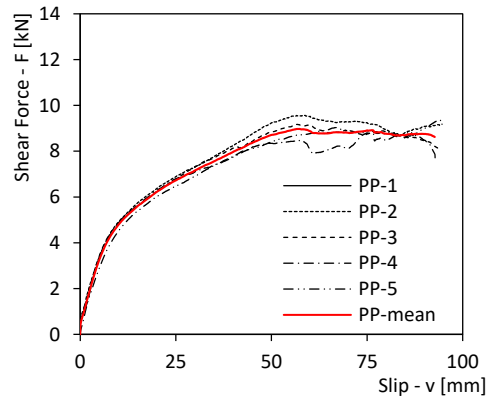
Test PM	Mean	CoV
$F_{max,R}$ [kN]	9.06	10.0%
$K_s$ [N/mm]	7835	28.4%
$F_y$ [kN]	9.06	10.0%
$v_y$ [mm]	1.86	27.5%
D	1.96	11.0%



Test PN	Mean	CoV
$F_{max,R}$ [kN]	12.37	8.0%
$K_s$ [N/mm]	5700	12.4%
$F_y$ [kN]	8.90	12.3%
$v_y$ [mm]	1.68	23.6%
D	12.02	34.3%



Test PO	Mean	CoV
$F_{max,R}$ [kN]	11.41	8.5%
$K_s$ [N/mm]	749	22.6%
$F_y$ [kN]	4.02	9.3%
$v_y$ [mm]	4.94	13.8%
D	6.19	13.1%



Test PP	Mean	CoV
$F_{max,R}$ [kN]	9.22	3.0%
$K_s$ [N/mm]	616	11.8%
$F_y$ [kN]	4.91	3.5%
$v_y$ [mm]	7.57	16.6%
D	4.07	15.8%

Figure 3-5 Experimental results

For the sake of comparison, all the experimental results in terms of maximum load ( $F_{max,R}$ ) and slip modulus ( $K_s$ ), are summarised in Figure 3-6. As will be better described in the comparison paragraphs (see section 3.3), DT screws generally exhibited higher values of stiffness than ST screws, while joints realized with hardwood (especially those where the central element is made of hardwood) resulted in higher connection capacity values when compared to joints where softwood was used.

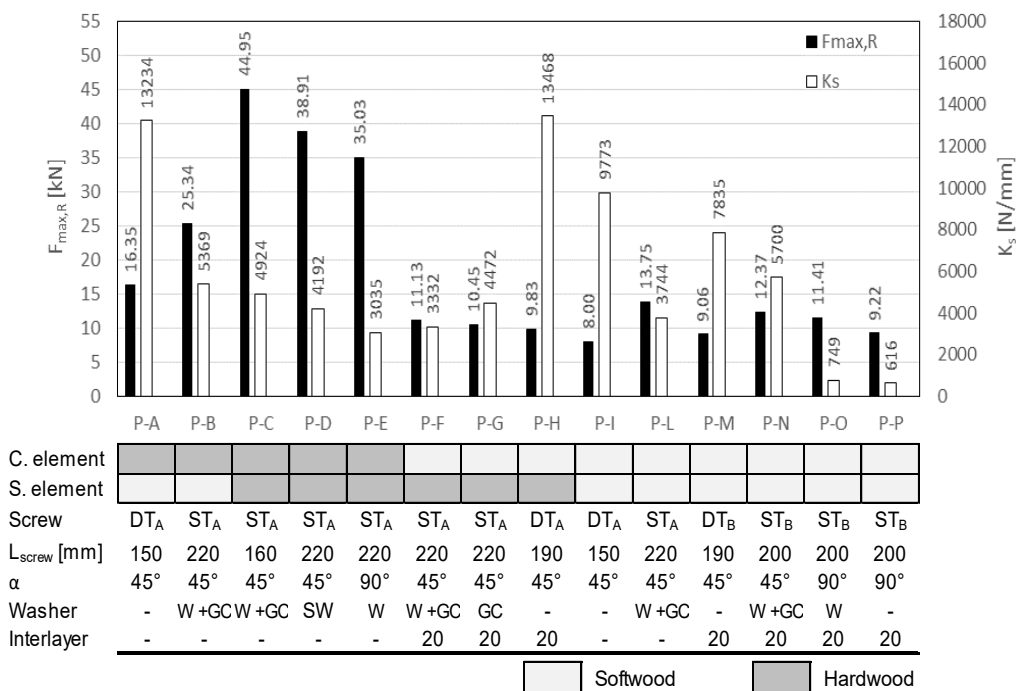


Figure 3-6 Experimental results in terms of maximum load and slip modulus

### 3.2.7 COMPARISON BETWEEN EXPERIMENTAL RESULTS AND THEORETICAL MODELS

In this section, the experimental results in terms of connection capacity and slip modulus are compared to the values predicted by means of theoretical models available in literature.

The characteristic load-bearing capacity ( $F_{max,k,th}$ ) of dowel type connectors subjected to shear loading ( $\alpha = 90^\circ$ ) can be calculated by using the theoretical model included in the EN 1995-1-1[15], which is based on Johansen theory [14]. For fasteners inserted at an angle  $\alpha$  with respect to the shear plane ( $0^\circ \leq \alpha \leq 90^\circ$ ), a theoretical model for the estimation of the connection capacity was proposed by Bejtka and Blaß in [3]. In this

model, the ultimate load of the joints is related not only to the bending strength of the connectors and the embedment strength of the wood elements as in [15], but also to the axial capacity of the fasteners and the friction forces between the timber elements. The different failure modes expected for the configurations where  $0^\circ \leq \alpha \leq 90^\circ$ , are illustrated in Figure 3-7.

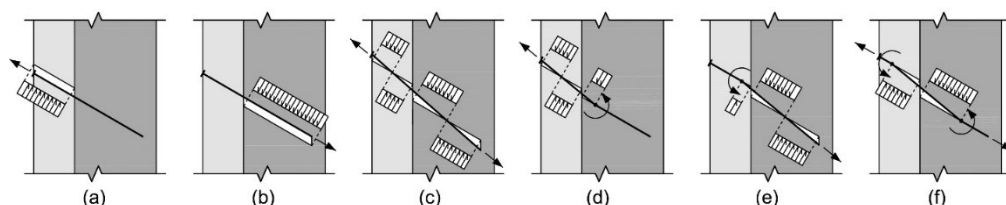


Figure 3-7 Failure modes for inclined fasteners

The theory proposed by Bejtka and Blaß in [3] was applied adopting the following assumption: for those modes where the failure mechanism is mainly governed by the strength properties of just one of the two timber elements (i.e. modes *a*, *b*, *d*, *e*), the axial capacity of the fastener was calculated by considering only the screw-portion within the “actively involved element”. More details on the equations and the parameters used to calculate the theoretical load-bearing capacity are provided in the Annex A to the chapter.

Sensitivity analysis showed negligible sensitivity of the predicted capacity values to small variations (5% - 10%) in timber density and screw yield moment, compatible with observed differences between the experimentally measured parameters and the values provided by product certificates.

By applying the aforementioned theoretical approach (see Annex A), characteristic values (5% percentile) of the connection strength were determined ( $F_{max,k,th}$ ). The characteristic values of the experimental yield strength ( $F_{y,k,exp}$ ) and maximum capacity ( $F_{max,k,exp}$ ), were determined in accordance with Annex D of EN 1990 [26]. The values reported in Figure 3-8 were determined under the following hypotheses: log-normal distribution of the data and coefficient of variation not known from prior knowledge. In cases where the coefficient of variation is not known from prior knowledge, a minimum number of three specimens should be adopted in order to identify the reference log-normal distribution [26]. It is worth mentioning that due to malfunctioning of the data acquisition system, it was not possible to record the results from specimen PG-3 and that means that only two test repetitions were available for PG test type. Consequently, for comparison purpose, the log-normal distribution was determined nonetheless, by adopting the characteristic fractile factor provided by [26] for three-specimen samples.

A comparison between the predicted values and the experimental results is reported in Figure 3-8.

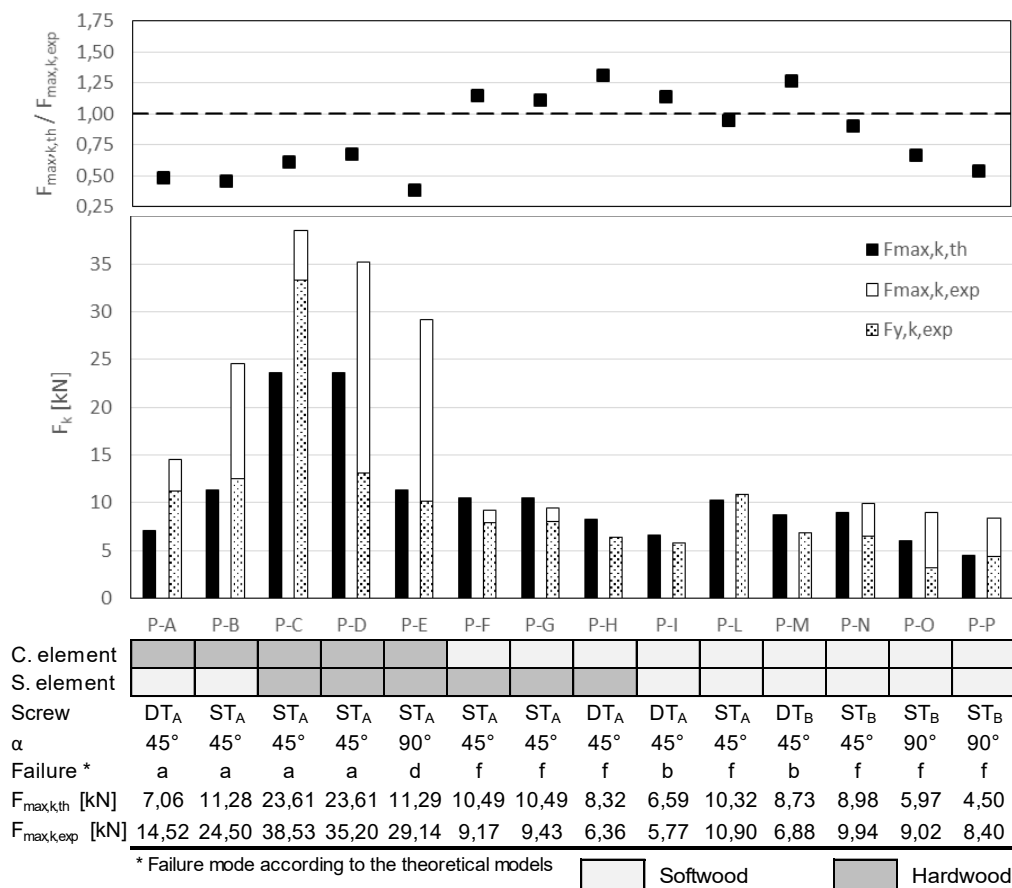


Figure 3-8 Comparison between the experimental and theoretical results in terms of capacity

A significant underestimation of the load carrying capacity can be observed when the central element is made of hardwood. It is worth noting that the formulations available in literature for determining the input parameter required by the theoretical model (e.g. embedment strength, screw withdrawal capacity, screw head pull-through resistance), have been calibrated on wood species characterized by density values not exceeding 650 kg/m<sup>3</sup>. Consequently, further studies are highly recommended in order to improve the calibration of the theoretical model.

The theoretical slip modulus ( $k_{ser,th}$ ) was calculated by using the formulation proposed by Tomasi et al. [4]. For *fastener-to-shear plane* angles ranging between  $0^\circ \leq \alpha \leq 90^\circ$ ,

the slip modulus was determined by considering contributions from both the axial slip modulus and the lateral slip modulus. For DT screws, the axial slip modulus was calculated considering the pull-out of the both threaded parts of the connector [31]. Otherwise, when ST screws were adopted, the axial stiffness was evaluated considering the simultaneous pull-out of the threaded part and the head penetration in the lateral timber element. In determining the lateral slip modulus, the deformation contribution from both timber elements forming the connection was taken into account by adopting the analogy of two springs placed in series (three springs when an interlayer was present). The equations and the parameters used to calculate the theoretical slip modulus are provided in the Annex B to the chapter. In Figure 3-9, the comparison between the experimental and theoretical results in terms of slip modulus is reported.

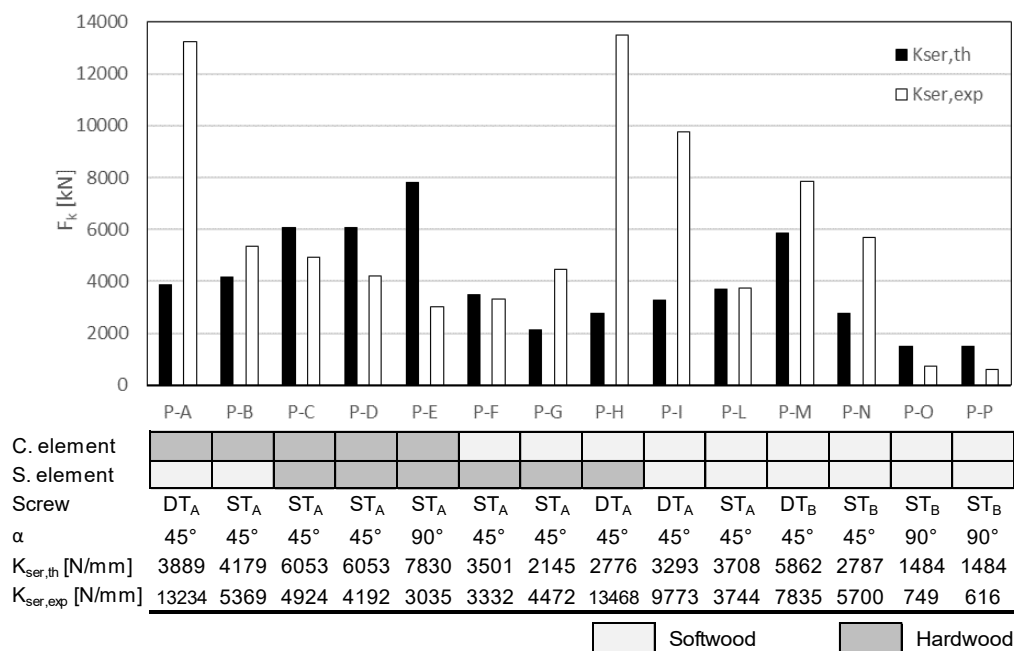


Figure 3-9 Comparison between the experimental and theoretical results in terms of slip modulus

Regardless of the screw-type used, the above mentioned theoretical approach (detail described in Annex B) resulted in an underestimation of the slip modulus not only for hybrid hardwood-softwood specimens with inclined screws (tests PA, PB, PF, PG and PH), but also for softwood-softwood specimens (tests PI, PL, PM, and PN). This difference appeared as more pronounced in the configurations where DT screws were adopted. This was partly attributed to uncertainties associated with the axial stiffness

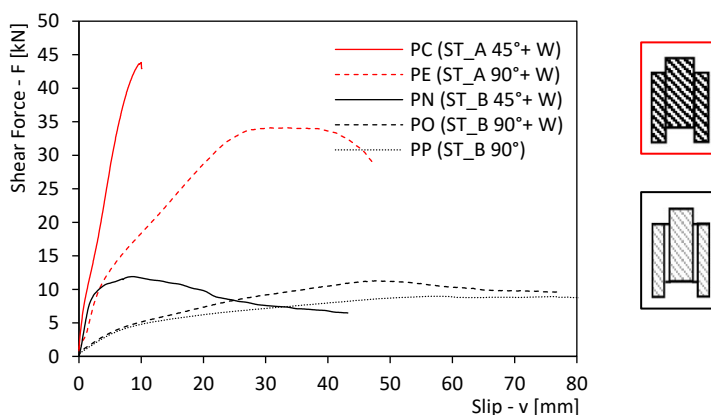
related to the pull-out of the threaded part of screws and the influences of the “pulling and closing effect” generated by the different thread pitch between the front thread and rear thread. Further study aimed at providing better estimations of the axial stiffness values is therefore strongly recommended.

For specimens made exclusively from hardwood (tests PC, PD and PE), a general overestimation of the slip modulus is clearly noticeable, evidencing an excessively strong sensitivity of the formulations currently available to variations in timber density values.

### 3.3 EXPERIMENTAL RESULT COMPARISON

#### 3.3.1 COMPARISON PARAMETER: SCREW CONFIGURATION

As already mentioned in the introduction of this chapter, studies into the influence of the fastener inclination on the mechanical behaviour of screw connections, especially as regards softwood-softwood joints connected by double threaded screws [4] and all-threaded screws [3], are available in literature.



Test (connection)	$F_{\max,R}$ [kN]	$K_s$ [N/mm]
● PE (ST <sub>A</sub> 90°+ W)	35.03	3035
● PC (ST <sub>A</sub> 45°+ W)	44.95	+28% 4924
● PO (ST <sub>B</sub> 90°+ W)	11.41	749
● PN (ST <sub>B</sub> 45°+ W)	12.37	+8% 5700
● PP (ST <sub>B</sub> 90°)	9.22	616

Figure 3-10 Comparisons in terms of screw configurations

In the following, the results from the present test specimens (Figure 3-10) with single threaded screws arranged in different configurations ( $45^\circ$  - shear tension and  $90^\circ$ ) are discussed. In particular, tests PC and PE (red curves) were made of hardwood components, while tests PN, PO and PP (black curves) were made of softwood with the interlayer previously described.

Not surprisingly, significantly higher values of capacity were registered for the specimens where the hardwood was employed.

*Table 3-4 Failure modes*

Test	Failure mode
● PE (ST <sub>A</sub> 90°+ W)	Splitting on the side element with formation of one plastic hinge in the screw
● PC (ST <sub>A</sub> 45°+ W)	Tensile failure of the screw shank
● PO (ST <sub>B</sub> 90°+ W)	Thread withdrawal with formation of two plastic hinges in the screw (rope effect)
● PN (ST <sub>B</sub> 45°+ W)	Thread withdrawal
● PP (ST <sub>B</sub> 90°)	Head penetration with formation of one plastic hinge in the screw (no rope effect)

As reported in Table 3-4, four different types of failure were observed. In particular, the PC tests were characterised by the tensile failure of the screw shank without significant extraction of the threaded part, while for test PN, due to the lower density of softwood, the failure was related to the thread withdrawal. As regards the  $90^\circ$  configurations (Figure 3-11), the maximum load in specimen PE was followed by splitting in the side elements with formation of a plastic hinge in the screw shank. In this case, the washer deformation and the high density of the panel have hindered the formation of the second plastic hinge close to the screw head. Conversely, two clearly-defined plastic hinges were observed in specimen PO. As shown in Figure 3-11, the washer reached the pull-through capacity remaining planar to the panel surface. The absence of the washer in specimen PP allowed the head penetration, thereby avoiding the formation of the second plastic hinge. As already observed in other tests [27], the impact of the rope effect on the mechanical behaviour of the connection is highlighted by comparing specimens PO and PP. In fact, the washer presence in specimen PO permitted to engage the screw withdrawal resistance, resulting in an increase of + 24% in bearing capacity. In addition, the use of washers enabled an increase of the compression force generated by the single threaded screws. As friction between the timber elements is directly proportional to the force perpendicular to the interface, a larger slip modulus (+ 22%) was registered for tests PO (with washers) compared to tests PP (without washers).

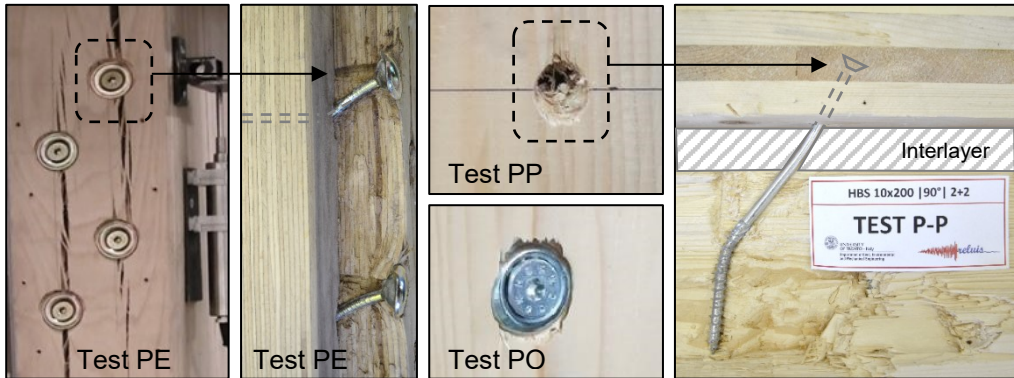


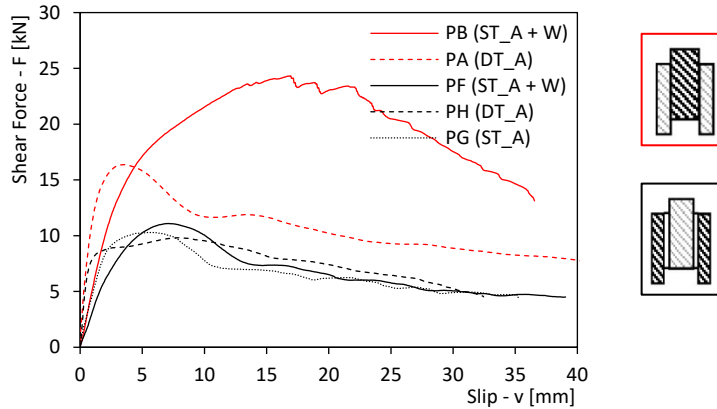
Figure 3-11 Details of 90° test configuration specimens

Unexpectedly, the slip moduli for the ST screws in 45° configurations seemed not to be positively influenced by an increase in the timber density. Actually a stiffness reduction of - 16% was observed when going from test PN (lower density) to test PC (higher density), despite the  $ST_B$  screws in PN had shorter thread length than the  $STA$  screws in PC (while similar screw head diameter). Nonetheless, all 45° configurations (for both hardwood and softwood) showed higher stiffness values than the 90° configurations where the slip modulus appeared to be highly influenced by the embedment strength of the timber elements and consequently by the material density (test PO compared to test PE).

### 3.3.2 COMPARISON PARAMETER: TIMBER PRODUCT COMBINATION (HYBRID SOLUTIONS)

In this section, the results from hybrid solutions (hardwood-softwood) will be discussed. As already mentioned, tests PF, PG and PH were realised in order to investigate the performance of connections designed for retrofit solutions of existing timber floors and therefore an interlayer of wooden boards was inserted.

As observed before, independently from the timber product arrangement, DT screws exhibited a higher stiffness, despite the smaller diameters of DT connectors (Table 3-3) with respect to the ST screws adopted.



Test (connection)	$F_{max,R}$ [kN]	$K_s$ [N/mm]
● PB ( $ST_A$ 45°+ W)	25.34 +55%	5369
● PA ( $DT_A$ 45°)	16.35	13234 +146%
● PF ( $ST_A$ 45°+ W)	11.13 +13%	3332
● PH ( $DT_A$ 45°)	9.83	13468 +304%
● PG ( $ST_A$ 45°)	10.45	4472

Figure 3-12 Comparisons in terms of timber hybrid configurations

When different types of timber elements are coupled, the mechanical behaviour of the connection is generally governed by the component with the lowest density value, especially regarding the failure mode. If the side element is made of hardwood (black curves), failure is strictly related to the thread withdrawal within the central element. Therefore, the maximum load depends on the geometry of the threaded part of the connector used. In this case, the resistance increase of test PF with respect to test PH (+13%) is comparable to the increase in the thread length (+11%), despite the fact that the profiles (external diameters and pitches) of the threaded parts of the two types of connectors are different. It is reasonable that the direct linear proportion between withdrawal capacity and embedment length of the threaded part in softwood [30] is reflected by the whole resistance of the connection.

Another consequence of using hardwood side elements and ST screws is that the removal of the washer (test PG compared to test PF) does not significantly affect the maximum capacity (-6%); on the contrary, an increase in terms of slip modulus was observed (+34%). This might be explained by the difficulty in ensuring even contact between the bottom part of the washer (Figure 3-2-C-up) and the surface of the hardwood side element.

As regards tests PB and PA (red curves), an increase in the resistance was observed when compared to tests PF and PH. This was due to the  $ST_A$  (with washer) screws having a head pull-through resistance larger than the thread pull-out resistance (when inserted into softwood material) and DT screws having the rear-thread withdrawal capacity higher (thanks to the head presence) than the front-thread withdrawal capacity. As expected, the washer coupled with the groove cut resulted in the highest value of strength, as shown by test PB. Concerning DT screws (test PA), head pull-through was anticipated by the thread withdrawal in the side element and this explain the similar values of slip modulus of tests PA and PH. Consequently, where the side elements are made of softwood, a connection with good performance in terms of both stiffness and resistance could be obtained by increasing  $d_h$  of  $DT_A$  screws (Table 3-3).

### 3.3.3 COMPARISON PARAMETER: SCREW TYPOLOGY (ST & DT)

The performance of softwood-softwood specimens assembled with different types of screws (all inclined at a  $45^\circ$  angle to the grain), is compared in Figure 3-13.

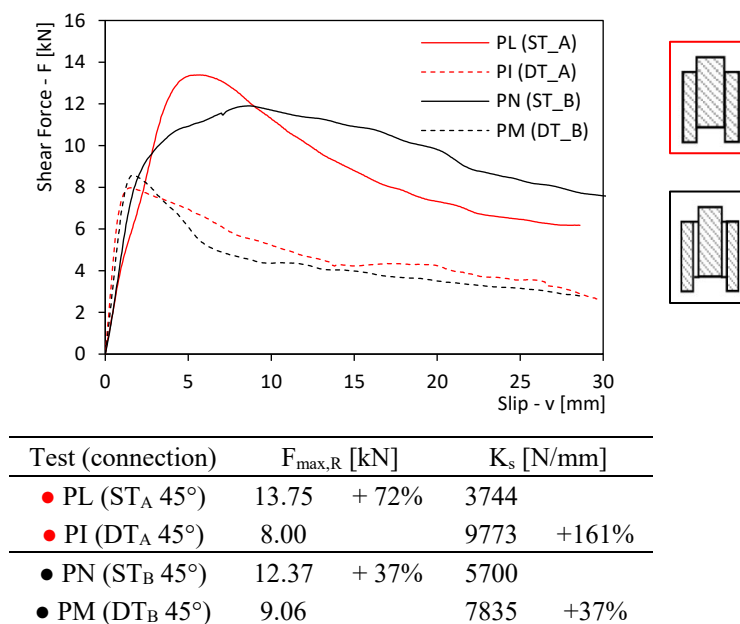


Figure 3-13 Comparisons in terms of screw types

Due to the high pull-through resistance of the washers, both specimens employing ST screws (solid lines) failed due to thread withdrawal. Also the DT specimens (dashed lines) failed due to thread withdrawal in the central element (because of the higher

capacity of the rear threaded part due to the head presence) but with maximum capacity values that are significantly lower than the values obtained from ST screws, owing to the different screw geometry (i.e. thread length and screw diameter).

Despite the different geometry of the connectors (Figure 3-1 and Table 3-3) and the presence of the interlayer, specimens PI and PM (dashed curves) showed a similar mechanical behaviour with a failure mode strictly related to the withdrawal capacity of the threaded part inside the central element. Also in this case, as reported in Table 3-5, the extended thread length of DT<sub>B</sub> when compared with DT<sub>A</sub> screws (+ 14%) resulted in a higher maximum capacity (+ 13%).

*Table 3-5 Characteristic axial withdrawal capacity and head pull-through capacity from ETA ( $\rho_k = 350 \text{ kg/m}^3$ )*

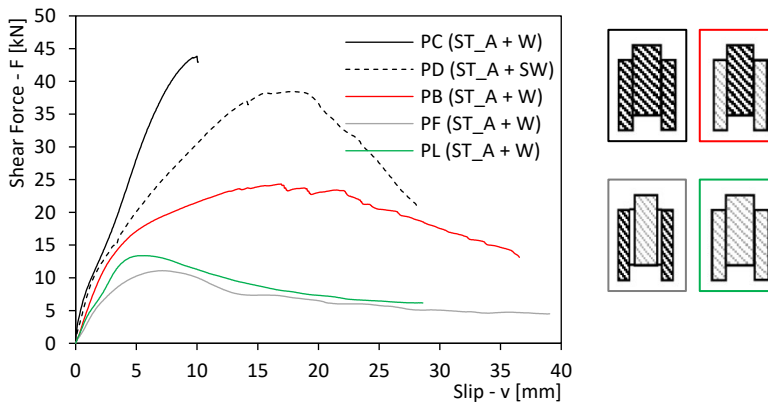
Test	Screw	L <sub>t1</sub> [mm]	D <sub>t1</sub> [mm]	f <sub>ax,k,45°</sub> [N/mm <sup>2</sup> ]	F <sub>ax,k,45°</sub> [kN]	R <sub>head,k</sub> [kN]
PI	DT <sub>A</sub> (L=150)	70	8	10.73	6.01	-
PM	DT <sub>B</sub> (L=190)	80	8.2	13.35	8.76	-
PL	ST <sub>A</sub> (L=220)	100	10	10.00	10.00	10.90
PN	ST <sub>B</sub> (L=200)	80	10	10.64	8.51	10.75

The capacity of connections made with DT screws is maximum when the two threads are evenly inserted in the two timber elements, as the withdrawal resistance is directly related to the thread length [30]. Therefore, for applications like TTC floors where the joists and the slab have significantly different heights, the connection capacity is limited by the height of the thinner element (i.e. the slab).

A possible solution to overcome this limit could be to have uneven fasteners where the reduced length of the rear thread is balanced by an improved head pull-through capacity (e.g. by having connectors with heads of larger sizes). However, to better understand the effects on the connection stiffness, further investigation is required.

### 3.3.4 COMPARISON PARAMETER: TIMBER PRODUCT ARRANGEMENT AND FAILURE MODE

As visible from Figure 3-14, a wide range of capacity values characterizes ST<sub>A</sub> screws when different configurations (types of washer or the arrangement of the timber components) are considered. As showed in Figure 3-15, this can be explained by analysing the different failure modes involved.



Test (connection)	$F_{\max,R}$ [kN]	$K_s$ [N/mm]	Failure mode
● PC ( $ST_A$ 45°+ W)	44.95	4924	Tensile strength
● PD ( $ST_A$ 45°+ SW)	38.91	4192	Splitting
● PB ( $ST_A$ 45°+ W)	25.34	5369	Head pull-through
● PF ( $ST_A$ 45°+ W)	11.13	3332	Thread withdrawal
● PL ( $ST_A$ 45°+ W)	13.75	3744	Thread withdrawal

Figure 3-14 Comparisons in terms of timber configurations and failure modes

The highest resistance registered (test PC) is related to the tensile strength of the screw shank (brittle failure). For the same timber configuration but replacing the washer (W) and the groove cut with the special washer (SW), a decrease of resistance is observed. In this case, at high stress levels (force exceeding value around 35 kN), the tooth on the bottom part of the special washer (Figure 3-2-A) started to act as a knife leading to failure because of splitting in the side timber elements.

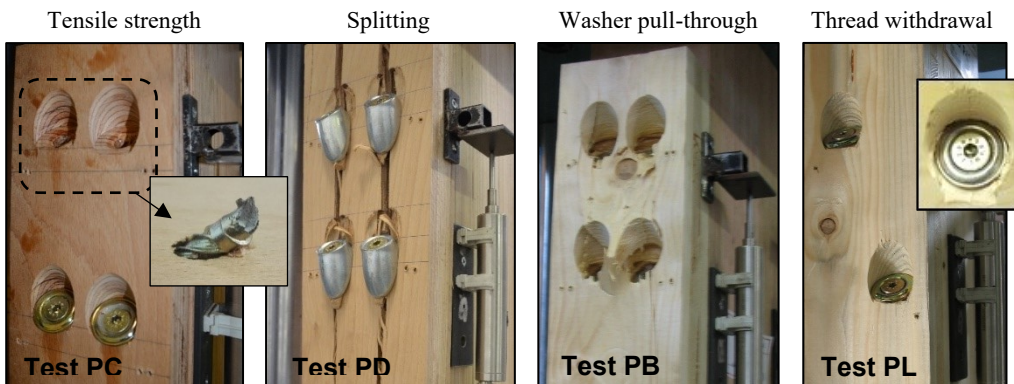


Figure 3-15 Single threaded screw: failure modes

As already mentioned, the lower values of resistance were obtained when the crisis involved the withdrawal capacity of the thread in the central element, independently of the type of side wooden element (tests PF and PL). It is worth mentioning that in case of failure involving thread withdrawal, the shape of the load-slip curve for slip values below 10 mm reflects the typical load-slip curve of axially loaded connectors [30]. An intermediate value of maximum capacity was registered for test PB, where pull-through failure of the washer was observed.

**3.3.5 COMPARISON PARAMETERS: DUCTILITY AND RESIDUAL STRENGTH**

The values of yield slip ( $v_y$ ), ultimate slip ( $v_u$ ) and ductility ( $D$ ) for each configuration are reported in Figure 3-16.

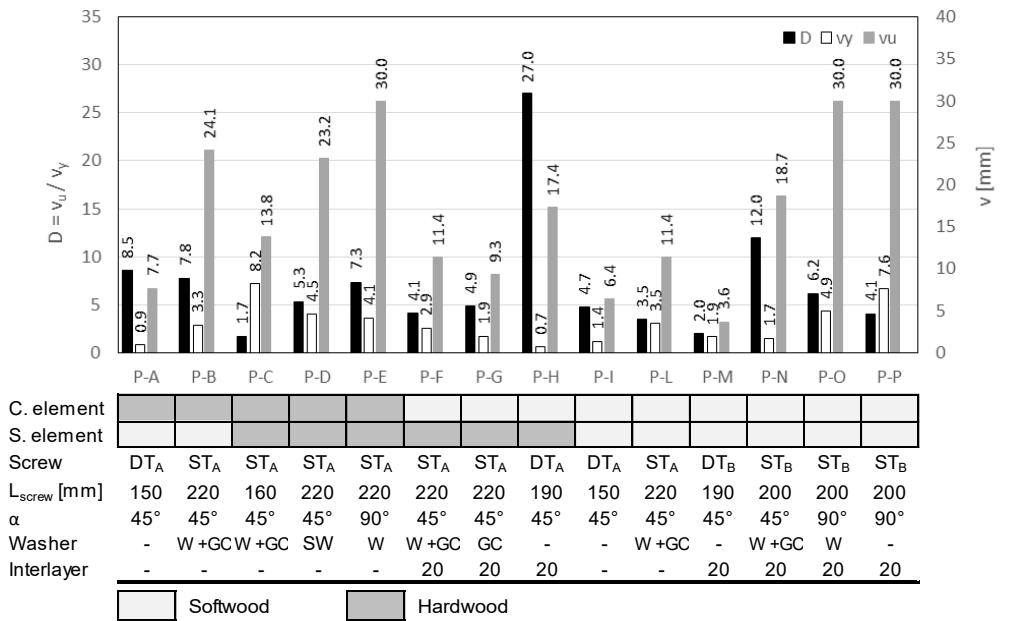


Figure 3-16 Experimental results in terms of yield slip, ultimate slip and ductility

The definition of ductility, described as the ratio between ultimate slip  $v_u$  and slip at yield  $v_y$ , reported in [16] gives comparable results for different timber connections only if the values of the yield slip are similar. As visible in Figure 3-16, the influence of parameters such as the screw inclination relative to the shear plane, the composition of timber members and the type of screws lead to high scattering of yield slip values. Therefore, a direct comparison between the ductility values obtained for all the tests might be misleading: for example, test PH showed the highest ductility value but it is

evident that its ability to accommodate large displacements was far from being at the highest level.

The definition of an absolute ductility parameter rather than a relative one [29], such as difference  $v_u - v_y$ , could better represent the “ductility concept” and permit to obtain comparable results for different types of timber connections (screws, bolts, nails, etc.). While the determination of ultimate slip  $v_u$  is substantially unaffected by ambiguities, the evaluation of the yield slip  $v_y$  is strongly dependent on the shape of the curve [28].

The upper bound limit of 30 mm suggested by [16] for the ultimate slip  $v_u$ , seems quite reasonable when the referenced connection is designed to be part of a hyperstatic system that most likely includes components that are incompatible with such large deformations. However, in case of screws arranged in the shear configuration ( $\alpha \approx 90^\circ$ ), this 30 mm limit has a significant impact on the ductility value that is calculated. In fact, the real ultimate slip of this type of connections largely exceeds the limit (especially for softwood elements) and this causes a significant underestimation of static ductility. By analysing the results of test PE (hardwood-hardwood), it can be noted that up to slip values exceeding the 30 mm threshold, no significant force reduction was registered. In this case, a decrease of strength equal to 20 % was observed for a mean slip value of 48.61 mm (Table 3-6), associated with a ductility equal to 11.80 (+ 61 % with respect to the value calculated with an ultimate slip of 30 mm). Higher values of ductility could be obtained for tests PO and PP (softwood-softwood) where the real ultimate displacements were not registered due to the set-up limits ( $v > v_{\max \text{ set-up}} = 90 \text{ mm}$ ).

Table 3-6 Residual strength

$V_{F_{\max R}}$	[mm]	3,4	17,1	11,1	16,3	33,1	6,8	5,3	7,1	1,4	5,7	1,9	10,9	47,6	70,6
$V_{0,8 F_{\max R}}$	[mm]	7,7	24,1		23,2	48,6	11,4	9,3	17,4	6,4	11,4	3,6	18,7	$V > V_{\max \text{ set-up}}$	$V > V_{\max \text{ set-up}}$
$V_{0,7 F_{\max R}}$	[mm]	15,7	29,7	Brittle failure	25,1	Specimens opening	12,8	10,6	22,0	8,3	13,0	4,8	23,2	$V > V_{\max \text{ set-up}}$	$V > V_{\max \text{ set-up}}$
$V_{0,6 F_{\max R}}$	[mm]	21,8	33,8		26,8		19,3	18,0	27,8	11,6	16,4	5,7	32,3	$V > V_{\max \text{ set-up}}$	$V > V_{\max \text{ set-up}}$
$V_{0,5 F_{\max R}}$	[mm]	36,6	39,6		28,1		26,3	27,7	31,4	20,9	22,0	8,7	43,5	$V > V_{\max \text{ set-up}}$	$V > V_{\max \text{ set-up}}$
Test		P-A	P-B	P-C	P-D	P-E	P-F	P-G	P-H	P-I	P-L	P-M	P-N	P-O	P-P
C. element															
S. element															
Screw		DT <sub>A</sub>	ST <sub>A</sub>	ST <sub>A</sub>	ST <sub>A</sub>	ST <sub>A</sub>	ST <sub>A</sub>	ST <sub>A</sub>	DT <sub>A</sub>	DT <sub>A</sub>	ST <sub>A</sub>	DT <sub>B</sub>	ST <sub>B</sub>	ST <sub>B</sub>	ST <sub>B</sub>
$L_{\text{screw}}$	[mm]	150	220	160	220	220	220	220	190	150	220	190	200	200	200
$\alpha$		45°	45°	45°	45°	90°	45°	45°	45°	45°	45°	45°	45°	90°	90°
Washer		-	W+GC	W+GC	SW	W	W+GC	GC	-	-	W+GC	-	W+GC	W	-
Interlayer		-	-	-	-	-	20	20	20	-	-	20	20	20	20

Softwood      Hardwood

The post-peak behaviours of the connections are described in Table 3-6, where the mean slip values associated with a strength loss of 20, 30, 40 and 50 % are reported.

For statically indeterminate structures, such data are required to determine how the load redistributes among the connectors once they have reached their peak capacity.

From the comparison between tests PI with tests PM, it can be observed how the specimens having  $DT_A$  screws are characterized by a more “gentle” post-peak strength loss than the specimen realized with  $DT_B$  screws. This might be attributed to the shorter thread pitch (for both  $p_{t1}$  and  $p_{t2}$ ) of  $DT_B$ .

It must be highlighted that all the considerations about ductility and residual strength are based on quasi-static monotonic testing. Therefore, cyclic testing is highly recommended in order to assess the behaviour of the connections under dynamic loading, especially with regard to dissipation capability.

### 3.4 CONSIDERATIONS ON PRACTICAL ISSUES

In this section, a brief discussion on practical considerations, especially regarding screw insertion into hardwood elements, is reported. According to [15], “...for all screws in hardwoods and for screws in softwoods with a diameter  $d \geq 6$  mm, pre-drilling is required (the lead hole for the threaded portion should have a diameter of approximately 70 % of the shank diameter)...”. This of course increases the challenge when both elements that have to be coupled require pilot holes. To avoid problem related to precision in overlapping, both central element and side element were clamped together during pre-drilling operations.



Figure 3-17 Practical issues: close up on broken insert bits, drill bits and on damaged bit-holes in screw heads

The high temperature generated by friction during hardwood predrilling can lead to problems on drill bits (see Figure 3-17), especially if long pilot holes are required. Working with TTC floors where hundreds of holes are necessary, drills and drill-bits with high performance are recommended. As an example of a suitable strategy to tackle

this challenge, during the experimental campaign, grease was used for screw insertion into beech LVL elements in order to reduce friction.

For the assembly of specimens with hardwood central elements, an impact driver was used in lieu of a “more traditional” (torque) drill. This was done in order to avoid overheating of the equipment (favoured by the particularly high torque level required to overcome friction) and to ensure a better tightening effect (i.e. to maximize the compression force developed by single thread connectors). Not rarely, the rupture of the insert drill bit occurred during the assembly phase (Figure 3-17). Damage to the bit-hole inside the screw head was also frequent.

It was demonstrated (test PF and PG) that for ST screws and hardwood side elements the use of washers is not necessary to increase connection stiffness and resistance. Therefore, the dimensions of groove cuts can be reduced or eliminated decreasing the time requested for joint fabrication.

### 3.5 CONCLUSIONS

The results of an extensive experimental campaign on timber screw connections is presented. Various timber products (i.e. softwood and hardwood in different forms: solidwood, glulam, crosslam, laminated veneer) connected by different types of screw fasteners were fabricated and tested.

The most significant outcomes can be summarized as follows:

- independently of the timber product arrangements, DT screws exhibited higher stiffness than ST screws, despite having a smaller diameter (Table 3-3);
- regarding the ST screws, the shear-tension load configurations ( $\alpha = 45^\circ$ ) resulted in stiffer and stronger connections when compared to the shear load configuration ( $\alpha = 90^\circ$ ). For test arrangements with side elements made of softwood, the use of ST screws with washers permitted to obtain significantly higher values of capacity than those exhibited by DT screws in similar configurations.”
- increases in both stiffness and maximum capacity were registered for test configurations employing hardwood (i.e. hardwood-hardwood and softwood-hardwood) when compared to traditional softwood-softwood configuration. This was particularly noticeable when hardwood was used for the central element because of the inhibition of the thread withdrawal from the hardwood element;

- 
- hardwood-hardwood specimens with inclined ST screws (45°) under shear-tension loading, failed due to tensile failure of the screw shank. The use of a connector with a larger diameter could therefore lead to an increase of the maximum capacity permitting the full exploitation of hardwood mechanical performance;
  - use of grease and an impact driver (instead of the traditional torque drill) significantly facilitates entry of the screws into engineered hardwood structural components.

### 3.6 ANNEX: FORMULAS AND PARAMETERS FOR THEORETICAL VALUES CALCULATION

#### 3.6.1 A: THEORETICAL LOAD-BEARING CAPACITY CALCULATION

The load-bearing capacity of the screws inserted at an angle  $\alpha$  with respect to the shear plane ( $0^\circ \leq \alpha \leq 90^\circ$ ) and subjected to shear-tension were calculated by adopting the model proposed by Bejtka and Blaß in [3]. As mentioned in the chapter 2.7, the following assumption was introduced: for those modes where the failure mechanism is mainly governed by the strength properties of just one of the two timber elements (i.e. modes a, b, d, e, Figure 3-7), the axial capacity of the fastener was calculated by considering only the screw-portion within the “actively involved element”. Hence, for failure modes a and d, the axial capacity is the minimum between the tensile strength of the shank and the head/washer pull-through capacity (or the thread pushing-in capacity when double threaded screws are concerned). For mode b and e, the axial capacity is the minimum between the tensile strength of the shank and the thread withdrawal capacity.

The characteristic load-carrying capacity  $F_{max,k,th}$  was calculated as the minimum value obtained from the following expression (see Figure 3-7):

$$R_a = R_{ax,k,1} \cdot \cos \alpha + f_{h,1,k} \cdot s_1 \cdot d_1 \cdot \sin \alpha \quad (A1)$$

$$R_b = R_{ax,k,2} \cdot \cos \alpha + f_{h,2,k} \cdot s_2 \cdot d_2 \cdot \sin \alpha \quad (A2)$$

$$R_c = R_{ax,k} \cdot (\mu \cdot \sin \alpha + \cos \alpha) + \frac{f_{h,1,k} \cdot s_1 \cdot d_1}{1 + \beta} \left(1 - \frac{\mu}{\tan \alpha}\right) \times \left[ \sqrt{\beta + 2\beta^2 \left[1 + \frac{s_2}{s_1} + \left(\frac{s_2}{s_1}\right)^2\right] + \beta^3 \left(\frac{s_2}{s_1}\right)^2} - \beta \left(1 + \frac{s_2}{s_1}\right) \right] \quad (A3)$$

$$R_d = R_{ax,k,1} \cdot (\mu \cdot \sin \alpha + \cos \alpha) + \frac{f_{h,1,k} \cdot s_1 \cdot d_1}{2 + \beta} \left(1 - \frac{\mu}{\tan \alpha}\right) \times \left[ \sqrt{2\beta(1 + \beta) + \frac{4\beta \cdot (2 + \beta) \cdot M_{y,k} \cdot \sin^2 \alpha}{f_{h,1,k} \cdot d_1 \cdot s_1^2}} - \beta \right] \quad (A4)$$

$$R_e = R_{ax,k,2} \cdot (\mu \cdot \sin \alpha + \cos \alpha) + \frac{f_{h,1,k} \cdot s_2 \cdot d_2}{1 + 2\beta} \left(1 - \frac{\mu}{\tan \alpha}\right) \times \left[ \sqrt{2\beta^2(1 + \beta) + \frac{4\beta \cdot (1 + 2\beta) \cdot M_{y,k} \cdot \sin^2 \alpha}{f_{h,1,k} \cdot d_2 \cdot s_2^2}} - \beta \right] \quad (A5)$$

$$R_f = R_{ax,k} \cdot (\mu \cdot \sin \alpha + \cos \alpha) + \left(1 - \frac{\mu}{\tan \alpha}\right) \sqrt{\frac{2\beta}{1 + \beta}} \sqrt{2 \cdot M_{y,k} \cdot f_{h,1,k} \cdot d_1 \cdot \sin^2 \alpha} \quad (A6)$$

Where  $\alpha$  is the *fastener-to-shear plane* angle;  $\mu$  is the friction coefficient for wood-to-wood surfaces assumed as equal to 0.25;  $s_i$  is the anchorage length of the screw inserted into element;  $d_i$  is the effective diameter of the screw part inserted into timber element ( $d_{shank}$  for ST screws;  $1.1 \cdot d_{core}$  for DT screws);  $f_{h,i,k}$  is the characteristic embedment strength of the relative timber element;  $\beta = f_{h,2,k}/f_{h,1,k}$ ; and  $M_{y,k}$  is the characteristic yield moment of the screw. In the absence of experimental data,  $M_{y,k}$  was determined according to the relevant technical approval (see Table 3-3).  $R_{ax,k,1}$  is the axial resistance of the screw part inserted in the lateral timber element. For ST screws,  $R_{ax,k,1}$  was assumed as equal to the minimum value between the characteristic head pull-through resistance ( $R_{head,k}$ ) and the characteristic tensile strength of the screw ( $R_{tens,k}$ ). Otherwise, for DT screws,  $R_{ax,k,1}$  was assumed as equal to the minimum value between the characteristic thread withdrawal resistance ( $R_{thread,k}$ ) and the characteristic tensile strength of the screw ( $R_{tens,k}$ ).  $R_{ax,k,2}$  is the axial resistance of the screw part inserted in the central timber element, corresponding to the minimum value between the characteristic thread withdrawal resistance ( $R_{thread,k}$ ) and the characteristic tensile strength of the screw ( $R_{tens,k}$ ). As regards equations (A3) and (A6),  $R_{ax,k} = \min\{R_{ax,k,1}; R_{ax,k,2}\}$ .

Every term in equations (A1) - (A6) was determined according to the provisions contained in the relevant product certificate ([22],[23],[24] and [25]). When missing, the formulations reported in the Eurocode 5 [15] were used.

When considering connections comprising hardwood elements, in the absence of specific indications from the literature, the thread withdrawal capacity ( $R_{thread,k}$ ) and the head-pull through capacity ( $R_{head,k}$ ) were considered to be greater than the tensile strength of the screws to better represent the experimental behaviour (e.g. brittle failure of the screw shank registered in P-C test).

The results of the theoretical load-bearing capacity calculation are summarized in Table A-1:

*Table A-1 Theoretical load-bearing capacity calculation*

	P-A	P-B	P-C	P-D	P-E	P-F	P-G
$R_{ax,k,1}$ [kN]	6,76	10,89	26,00	26,00	26,00	26,00	26,00
$R_{ax,k,2}$ [kN]	18,00	26,00	26,00	26,00	26,00	10,00	10,00
$f_{h,1,k}$ [N/mm <sup>2</sup> ]	15,01	15,22	25,66	25,66	44,90	25,66	25,66
$f_{h,2,k}$ [N/mm <sup>2</sup> ]	25,43	24,88	24,88	24,88	43,54	14,76	14,76
$M_{y,k}$ [Nmm]	20000	36000	36000	36000	36000	36000	36000
$F_{max,k,th}$ [kN]	7,06	11,28	23,61	23,61	11,29	10,49	10,49

	P-H	P-I	P-L	P-M	P-N	P-O	P-P
$R_{ax,k,1}$ [kN]	18,00	6,76	10,89	9,51	10,75	10,75	3,50
$R_{ax,k,2}$ [kN]	8,18	6,36	10,00	8,76	8,51	9,36	9,36
$f_{h,1,k}$ [N/mm <sup>2</sup> ]	25,30	15,01	15,22	14,94	15,25	26,69	26,69
$f_{h,2,k}$ [N/mm <sup>2</sup> ]	15,09	15,09	14,76	15,06	14,76	25,83	25,83
$M_{y,k}$ [Nmm]	20000	20000	36000	19500	35830	35830	35830
$F_{max,k,th}$ [kN]	8,32	6,59	10,32	8,73	8,98	5,97	4,50

### 3.6.2 B: THEORETICAL SLIP MODULUS CALCULATION

In order to evaluate the slip modulus of the connections where the screws were inserted at an angle  $\alpha$  with respect to the shear plane ( $0^\circ \leq \alpha \leq 90^\circ$ ), the formulation proposed by Tomasi et al. [4] was used:

$$K_{ser} = K_{lat} \cdot \sin \alpha (\sin \alpha - \mu \cdot \cos \alpha) + K_{ax} \cdot \cos \alpha (\cos \alpha - \mu \cdot \sin \alpha) \quad (B1)$$

Where  $K_{lat}$  and  $K_{ax}$  are, respectively, the axial and lateral slip moduli of the screw connection and  $\mu$  is the friction coefficient for wood to wood surfaces assumed as equal to 0.25.

The axial slip modulus  $K_{ax}$  of the DT screws was calculated considering the simultaneous pull-out of the two threaded parts of the connector as proposed by Kevarinmäki [31]. By analogy with the behaviour of two springs placed in series, the axial slip modulus can be calculated as followed:

$$K_{ax} = \frac{1}{1/K_{ax,1} + 1/K_{ax,2}} \quad (B2)$$

The same equation was employed for the connections where ST screws were used. In this case,  $K_{ax,2}$  corresponds to the axial stiffness due to the head penetration in the lateral timber and  $K_{ax,1}$  is the axial stiffness of the threaded part of the connector.

The axial stiffness related to the pull-out of the threaded part of screws was calculated as:

$$K_{ax,i} = c_1 \cdot d_i^{c_2} \cdot l_{ef,i}^{c_3} \quad (B3)$$

Where  $d$  is the outer thread diameter and  $l_{ef}$  is the penetration length of the threaded part into the timber member. The coefficients  $c_1$ ,  $c_2$  and  $c_3$  were assumed according to the relevant technical approvals ([22],[23],[24] and [25]).

Due to the lack of specific indications for evaluating the axial slip modulus associated with the ST head penetration into the lateral timber member tentative equation (B4) was used:

$$K_{ax} = E_\alpha \frac{\pi \cdot d_h^2 \cdot \sin \alpha}{4 \cdot t_{side}} \quad (B4)$$

Where  $d_h$  is the diameter of the screw head (or diameter of the washer when adopted),  $\alpha$  angle between the screw axis and the grain,  $t_{side}$  is the thickness of the lateral timber member and  $E_\alpha$  is the modulus of elasticity along direction  $\alpha$  with respect to the grain. The criterion proposed by Hankinson [32] was used:

$$E_\alpha = \frac{E_0 \cdot E_{90}}{E_0 \cdot \sin^2 \alpha + E_{90} \cdot \cos^2 \alpha} \quad (B5)$$

The lateral slip modulus  $K_{lat}$  was evaluated by considering the deformation occurring in both timber elements through the following relation:

$$K_{lat} = \frac{1}{1/K_{lat,1} + 1/K_{lat,2}} \quad (B6)$$

Where  $K_{lat,1}$  and  $K_{lat,2}$  are the lateral slip moduli (perpendicular to the screw shank) relative to the deformation of the single timber components. The lateral slip modulus was calculated as:

$$K_{lat,i} = 2 \left( \rho_m^{c_4} \cdot \frac{d^{c_5}}{c_6} \right) \quad (B7)$$

Which is consistent with the formulation recommended by EN 1995-1-1 [15] for steel-to-timber and concrete-to-timber connections (where the fastener part embedded into the concrete is assumed as rigid). It is worth noting that in cases where the two timber components are made from the same timber material,  $K_{lat}$  (B6) becomes equal to  $K_{ser}$  [15][13]. The coefficients  $c_4$ ,  $c_5$  and  $c_6$  were assumed in accordance with Table 7.1 of [15].

For tests PF, PG, PH, PN, PO, PP and PP where an interlayer made of timber boards was present, the lateral slip modulus  $K_{lat}$  was evaluated by considering the deformation of three separate contribution:

$$K_{lat} = \frac{1}{1/K_{lat,1} + 1/K_{int} + 1/K_{lat,2}} \quad (B8)$$

Where the lateral slip modulus relative to the interlayer was calculated as:

$$K_{int} = \rho_m^{c_4} \cdot \frac{d^{c_5}}{c_6} \quad (\text{B9})$$

The results of the theoretical slip modulus calculation are summarized in Table B-1:

*Table B-7 Theoretical slip modulus calculation*

	P-A	P-B	P-C	P-D	P-E	P-F	P-G
$K_{ax}$ [N/mm]	3253	3848	4987	4987	-	4574	2404
$K_{lat}$ [N/mm]	4948	4730	7830	7830	7830	1712	1712
$K_{ser}$ [N/mm]	3889	4179	6053	6053	7830	3501	2145

	P-H	P-I	P-L	P-M	P-N	P-O	P-P
$K_{ax}$ [N/mm]	3598	3253	3848	8536	3569	-	-
$K_{lat}$ [N/mm]	1406	3359	3474	1405	1484	1484	1484
$K_{ser}$ [N/mm]	2776	3293	3708	5862	2787	1484	1484

### 3.7 REFERENCES

- [1] Dietsch F., Brandner R. (2015) Self-tapping screws and threaded rods as reinforcement for structural elements. *Construction and Building Materials*, vol. 97, pp. 78 – 89.
- [2] Loss C., Piazza M., Zandonini R. (2016) Connections for steel–timber hybrid prefabricated buildings. Part I: Experimental tests. *Construction and Building Materials*, vol. 122, pp. 781 – 798.
- [3] Bejtka I., Blass H. J. (2002) Joints with inclined screws. *Proceedings from meeting thirty-five of the international council for building research studies and documentation*, CIB, Working Commission W18 – Timber Structure, Kyoto, Japan.
- [4] Tomasi R., Crosatti A., Piazza M. (2010) Theoretical and experimental analysis of timber-to-timber joints connected with inclined screws. *Construction and Building Materials*, vol. 24, pp. 1560 – 1571.

- [5] Giongo I., Schiro G., Piazza M., Tomasi R. (2016) Long-term out-of-plane testing of timber floors strengthened with innovative timber-to-timber solutions. *Proceedings of the World Conference on timber Engineering (WCTE)*, Vienna, Austria.
- [6] Ozarska B. (1999) A review of the utilization of hardwoods for LVL. *Wood Science and Technology*, vol. 33, pp. 341-351.
- [7] Aicher S., Christian Z., Dill-Langer G. (2014) Hardwood glulams – emerging timber products of superior mechanical properties. *Proceedings of the World Conference on timber Engineering (WCTE)*, Quebec City, Canada.
- [8] Knorz M., Van de Kuilen J.W. (2012) Development of a high-capacity engineered wood product – LVL made of European Beech. *Proceedings of the World Conference on timber Engineering (WCTE)*, Auckland, New Zealand.
- [9] Misconel A., Ballerini M., Van de Kuilen J.W. (2016) Steel-to-timber joints of beech-LVL with very high strength steel dowels. *Proceedings of the World Conference on timber Engineering (WCTE)*, Vienna, Austria.
- [10] Kobel P., Steiger R., Frangi A. (2014) Experimental analysis on the structural behaviour of connections with LVL made of Beech wood. *In Materials and Joints in Timber Structures*, RILEM Bookseries 9, Springer, pp. 211 – 220.
- [11] Celebi G., Kilic M. (2007) Nail and screw withdrawal strength of laminated veneer lumber made up hardwood and softwood layers. *Construction and Building Materials*, vol. 21, pp. 894–900.
- [12] Ali Taj M., Najafi S. K., Ebrahimi G. (2009) Withdrawal and lateral resistance of wood screw in beech, hornbeam and poplar. *European Journal of Wood and Wood Products*, vol. 67, pp. 135-140.
- [13] Sebastian W., Mudie J., Cox G., Piazza M., Tomasi R., Giongo I. (2016) Insight into mechanics of externally indeterminate hardwood–concrete composite beams. *Construction and Building Materials*, vol. 102, part 2, pp. 1029 – 1048.
- [14] Johansen KW. (1949) Theory of timber connections. *International association of bridge and structural engineering*, vol. 9, pp. 249 – 262.
- [15] European Committee for Standardization (2014). EN 1995-1-1:2004+A2:2014: Eurocode 5 - Design of timber structures, Part 1-1, General - Common rules and rules for buildings. CEN, Brussels, Belgium.
- [16] European Committee for Standardization (2001). EN 12512: Timber structures – Test methods – Cyclic testing of Joints made with mechanical fasteners. CEN, Brussels, Belgium.
- [17] European Committee for Standardization (1991). EN 26891: Timber structures – Joints made with mechanical fasteners – General principles for the determination of strength and deformation characteristics. CEN, Brussels, Belgium.

- [18] ETA (European Technical Approval) 14/0354: Glued laminated timber made of hardwood – Structural laminated veneer lumber made of beech.
- [19] European Committee for Standardization (2009). EN 338: Structural timber – Strength classes. CEN, Brussels, Belgium.
- [20] Certificate of performance No. 0672-CPR-0415 (MPA Stuttgart 0672).
- [21] ETA (European Technical Approval) 12/0347: X-Lam Dolomiti – CLT.
- [22] ETA (European Technical Approval) 11/0190: Würth self-tapping screws.
- [23] ETA (European Technical Approval) 11/0030: Rotho Blaas self-tapping screws
- [24] ETA (European Technical Approval) 12/0121: HECO-TOPIX-T and HECO-TOPIX-CC self-tapping screws.
- [25] ETA (European Technical Approval) 12/0063: SFS self-tapping screws WT
- [26] European Committee for Standardization (2005). EN 1990:2002+A1:2005: Eurocode - Basis of structural design. CEN, Brussels, Belgium.
- [27] Ballerini M. (2012) Experimental investigation on parallel-to-grain wood-to-wood joints with self-tapping screws. *Proceedings of the World Conference on timber Engineering (WCTE)*, Auckland, New Zealand.
- [28] Piazza M., Polastri A., Tomasi R. (2011) Ductility of timber joints under static and cyclic loads. *Proceedings of the Institutional of Civil Engineers, Structures and buildings* 164 April 2011 Issue SB2, pp. 79 - 90.
- [29] Jorissen A., Fragiaco M. (2011) General notes on ductility in timber structures. *Engineering Structures*, vol. 33, issue 11, pp. 2987-2997.
- [30] Stamatopoulos H., Malo K.A. (2015) Withdrawal capacity of threaded rods embedded in timber elements. *Construction and Building Materials*, vol. 94, pp. 387 – 397.
- [31] Kevarinmäki A. (2002) Joints with inclined screws. *Proceedings of meeting thirty-five of the international council for building research studies and documentations*, CIB, Working Commission W18 – Timber Structures, Kyoto, Japan.
- [32] Hankinson. R. L. (1921) Investigation of crushing strength of spruce at varying angles of grain. Air Service Information Circular No. 259, U.S. Air Service.



---

## 4 EXPERIMENTAL TESTS ON TIMBER-TO-TIMBER COMPOSITE FLOORS

### 4.1 INTRODUCTION

As stated in the introduction chapter, several research works are available in literature regarding the flexural behaviour (short-term and long-term) of timber-concrete composite (TCC) systems developed for a wide range of applications ([1], [3], [4] and [5]). Indeed, this construction technique is a well-established solution used both for the refurbishment of existing timber diaphragms ([1] and [2]) and for the realisation of new floors and bridges [6].

However, to the best knowledge of the author, a very limited number of works is available in literature on the mechanical behaviour of timber-to-timber composite (TTC) floors. A recent experimental campaign on TTC beams was carried out by Giongo et al. [7]. More specifically, four full-scale bending tests on TTC beams 7.5 m span, were performed by the authors and the results [7] have positively confirmed the potential of such technique.

On the basis of the experimental evidences provided by Giongo et al. ([7], [8] and [9]), seventeen full-scale tests on TTC floors (6.4 m span) assembled by means of the CP procedure were performed at the Laboratory of the Department of Civil, Environmental and Mechanical Engineering (DICAM) of the University of Trento (Italy). The results are presented and discussed in this Chapter.

Several aspects were investigated in this experimental campaign, including the applicability of the pre-stressing and cambering procedure, the validation of the numerical and the analytical models (see Chapter 2) and the out-of-plane flexural behaviour (bending stiffness and flexural capacity).

Essentially, the aims of these tests were two. The first aim was to investigate the mechanical behaviour of TTC beams designed for newly constructed high-performance diaphragms. Hybrid solutions, that coupled the lightness of softwood elements (spruce cross laminated panels), with the strength of hardwood components (beech laminated veneer lumber beams/panels) by means of different types of connectors, were compared with “more common” timber-to-timber solutions (exclusively made of softwood components). In addition, hardwood-hardwood configurations were studied. The second aim was to evaluate the performance of alternative strategies for retrofit interventions on timber diaphragms in historical heritage buildings affected by large deformations. Also in this case, the above-mentioned CP procedure, was considered.

All solutions were designed considering the following loads:

- Self-weight of permanent structural elements: accounted for separately for each floor solution;
- Self-weight of non-structural components (finishing layers and internal partitions):  $g_{2,k} = 3 \text{ kN/m}^2$ ;
- Characteristic service loads (live loads):  $q_k = 3 \text{ kN/m}^2$ .

According to the EN 1995 [15], the following deflection limit values were considered in the analysis for the Serviceability Limit States (SLS):

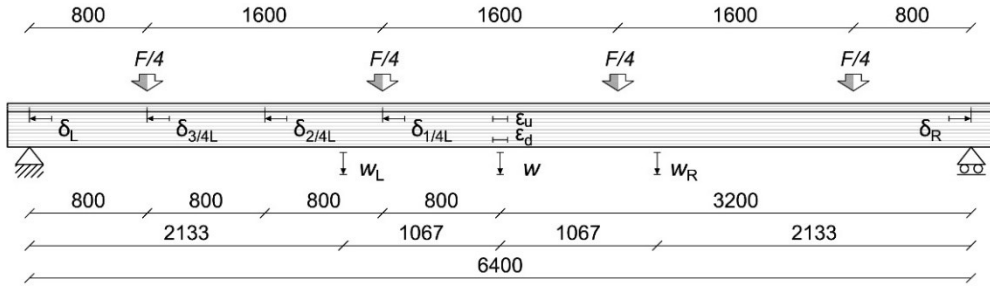
- Instantaneous deflection (live loads):  $w_{\text{inst,Q}} = L/400$
- Final deflection:  $w_{\text{net,fin}} = L/300$ .

In order to define the mechanical properties, in terms of stiffness, strength, static ductility and residual strength, of the connections selected for the realisation of the samples, several pushout tests were performed. The results of this preliminary experimental investigation were presented in the previous Chapter.

## 4.2 TEST SET-UP

In order to investigate both the applicability of the assembly procedure and the flexural performance of each TTC configuration, the experimental activity was divided into two steps:

1. Step 1: assembly of the TTC beams;
2. Step 2: bending test.



Instruments:

$\delta_L, \delta_{3/4L}, \delta_{2/4L}, \delta_{1/4L}, \delta_R$  : linear displacement transducer (LDT) – 50 mm

$w$  (2x),  $w_L, w_R$  : linear displacement transducer (LDT) – 300 mm

$\epsilon_u, \epsilon_d$  : Linear strain gauge sensor – 100 mm

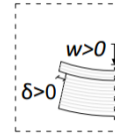


Figure 4-1 Instrument arrangement

With reference to the specimen assembly, a simply supported scheme was adopted for all tests. Figure 4-1 shows the instrument layout used both during the screw insertion (step 1) and during the bending tests (step 2). Details on the instrument layout are given in Chapter 2, where two tests (out of 17) from this experimental campaign were carefully analysed.

As concerns the bending tests, a six-point scheme was selected in order to better simulate a uniform distributed load acting on the floor. The vertical force was equally divided into four point loads by means of the load distributing system (see Figure 4-3). As shown in Figure 4-2, Polyethylene plates were fixed to 20 x 600 mm<sup>2</sup> steel plates and inserted between the setup and the upper elements of the composite beams in order to avoid local crushing perpendicular to the grain (by increasing the contact area) and to reduce friction phenomena.



Figure 4-2 Measuring instruments and Polyethylene plates

The load was applied to the specimens through a hydraulic actuator and was monitored by a 1000 kN load cell. According to the test protocol, each specimen was subjected to a monotonic quasi-static load under displacement control until failure of the specimen. The imposed displacement rate was set at 0.05 mm/s.

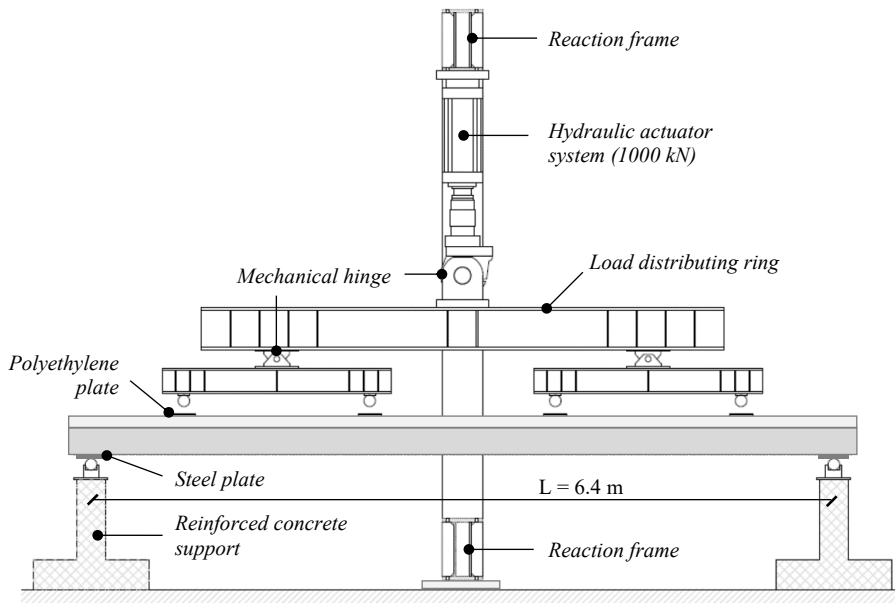


Figure 4-3 Test set-up

A picture taken from the top walk-way of the DICAM laboratory is shown in Figure 4-4. In particular, it is possible to see the steel reaction frame as well as the entire set-up used during the experimental campaign.



Figure 4-4 Laboratory of the Department of Civil, Environmental and Mechanical Engineering (DICAM) of the University of Trento (Italy)

### 4.3 TEST CONFIGURATIONS AND RESULTS

In this section, a description of all specimen configurations is provided. As stated in the introduction paragraph, different timber products obtained from both hardwood and softwood species were used for the construction of the TTC beams. The main mechanical properties of the beam elements, from both product documentations ([12], [14] and [15]) and international standards [13], are reported in Table 4-1.

Table 4-1 Mechanical properties of timber elements

	Beech LVL GL70	Spruce GL24h	Beech LVL panel	Spruce CLT panel
Reference:	[12]	[13]	[14]	[15]
$f_{m,k}$ [N/mm <sup>2</sup> ]	70	24	80	24
$f_{t,0,k}$ [N/mm <sup>2</sup> ]	55	19.2	60	14
$f_{t,90,k}$ [N/mm <sup>2</sup> ]	0.6	0.5	1.5	0.12
$f_{c,0,k}$ [N/mm <sup>2</sup> ]	59.4	24	57.5	21
$f_{c,90,k}$ [N/mm <sup>2</sup> ]	10.2	2.5	14	2.5
$f_{v,k}$ [N/mm <sup>2</sup> ]	4	3.5	8	3.3
$E_{0,mean}$ [N/mm <sup>2</sup> ]	16700	11500	16800	12000
$\rho_{mean}$ [kg/m <sup>3</sup> ]	≥ 740	420	800	450-500

The global modulus of elasticity as well as the mean density of all timber components were measured experimentally according to the EN 408 [16]. The results are reported in the result-sheets provided herein.

With references to the connection systems, two type of screws and washer were used (see Figure 4-5). Details on these fasteners are provided in Chapter 3 along with the results of an extensive experimental campaign aimed at defining the mechanical properties of several screw connections (Schiro et al. 2018 [10]).

The connection systems adopted for the assembly of the composite beams are shown in Figure 4-5. Throughout this Chapter, the acronym DT stands for double threaded screw, while ST refers to single threaded screw. With reference to the washers employed, W and SW are used to refer to traditional timber washer and washer mainly developed for steel-to-timber connection, respectively (Figure 4-5).

Some practical considerations on the screw insertion need to be made. Because beech LVL elements have a mean density that is approximately twice that of spruce elements, special attention has to be paid to the use of screw-type fasteners (that are mainly designed for softwood-softwood connections) in hardwood components.

Screw types:

(DT) – Double Threaded screw [18]



(ST) – Single Threaded screw [17]



Washer types:

(W) – Traditional Washer [17]



(SW) – “Special” Washer [17]



*Figure 4-5 Fastener and screw types*

From the analysis of the considerations presented in Chapter 3.4 (Schiro et al. 2018 [10]), the following technical precautions were taken:

- pilot holes were provided in all beech LVL elements;
- grease was used for screw insertion into beech LVL elements in order to reduce friction;
- high performance drill and drill-bits were used to reduce problems related to the high temperature generated by friction during hardwood predrilling;
- to avoid problems related to precision in overlapping, both lower element and upper element were clamped together during pre-drilling operations;

- an impact driver was used in lieu of a “more traditional” (torque) drill for the assembly of specimens with hardwood components. This was done in order to avoid overheating of the equipment (favoured by the particularly high torque level required to overcome friction) and to ensure a better tightening effect;
- for the specimens where single threaded screws were inserted with washers, groove cuts were prepared prior to the assembly of the beams, in order to have a wider contact area between the washer and the wood surface. Details on screw types and on the groove cuts are provided in the previous Chapter.

The results obtained from the experimental campaign are summarised in the following result sheets, subsequently to the description of each TTC beam configuration.

The following abbreviations were used in this Chapter:

- $w_{CP}$  : camber value at the end of the assembly procedure (when expected);
- $q_0$  : equivalent distributed load necessary to induce a midspan displacement variation equal (but in the opposite direction) to the camber value ( $\Delta w_{CP}$ );
- $(EJ)_0$  : flexural stiffness of composite beams with no interaction;
- $(EJ)_\infty$  : flexural stiffness of a composite beam with complete interaction;
- $(EJ)_{Exp}$  : experimental flexural stiffness (secant value at  $0.4 F_{max}$  );
- $(EJ)_{EC5}$  : effective bending stiffness according to EN 1995-1-1:2014 – Annex B: Mechanically jointed beams [15], defined as:

$$(EJ)_{EC5} = (EJ)_0 + \sum \gamma_i E_i A_i a_i^2$$

- $\eta$  : connection efficiency, defined as:  $\eta = \frac{(EJ)_{Exp} - (EJ)_0}{(EJ)_\infty - (EJ)_0}$
- $q_{(L/300)}$  : equivalent distributed load corresponding to a net vertical deflection ( $w$ ) with reference to a straight line between the supports equal to  $L/300 = 21.33$  mm;
- $w_{max}$  : vertical displacement (with reference to a straight line between the supports) at the maximum load;
- $F_{max}$  : maximum load reached;
- $q_{max}$  : uniformly distributed load equivalent to  $F_{max}$ .

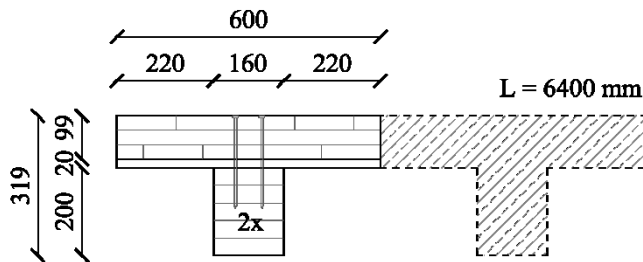
**TEST A1 | CONFIGURATION****Geometry**

Length: 6700 m (6400 mm span)

Upper element: Softwood CLT panel (3 layers)  
600 x 99 mm<sup>2</sup>

Interlayer: Non-structural floorboard (20 mm thick)

Lower element: Glulam beam GL24h  
160 x 200 mm<sup>2</sup>

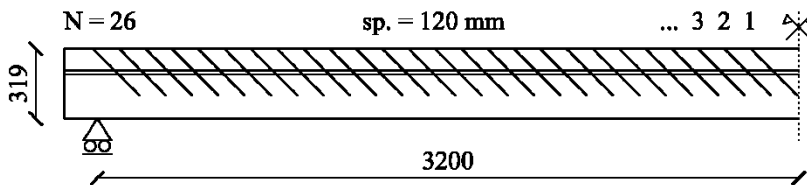
**Connection**

Screw type: Double threaded (DT) 8.5 x 300 mm<sup>2</sup>



Arrangement: Constant spacing (120 mm) | 45° | 2 rows

N. of fasteners: 104 screws

**Mechanical properties**

Upper element	$E_1$	11804	[N/mm <sup>2</sup> ]
	$\rho_1$	464.85	[kg/m <sup>3</sup> ]
Lower element	$E_2$	13052	[N/mm <sup>2</sup> ]
	$\rho_2$	471.08	[kg/m <sup>3</sup> ]
Connection (x1)	$k_s$	-	[N/mm]

Assembly method: CP procedure

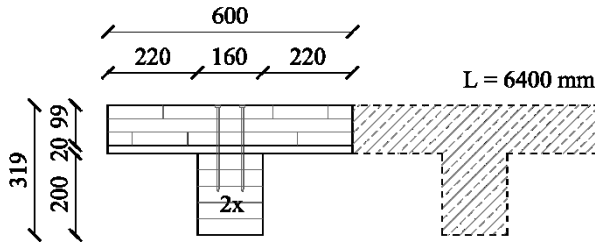
TEST A1

TEST A2   CONFIGURATION			
<b>Geometry</b>			
Length:	6700 m (6400 mm span)		
Upper element:	Softwood CLT panel (3 layers) 600 x 99 mm <sup>2</sup>		
Interlayer:	Non-structural floorboard (20 mm thick)		
Lower element:	Glulam beam GL24h 160 x 200 mm <sup>2</sup>		
<b>Connection</b>			
Screw type:	Single threaded (ST) 10 x 280 mm <sup>2</sup> + Washer (groove cut)		
Arrangement:	Constant spacing (120 mm)   45°   2 rows		
N. of fasteners:	104 screws		
<b>Mechanical properties</b>			
Upper element	E <sub>1</sub>	12866	[N/mm <sup>2</sup> ]
	ρ <sub>1</sub>	469.87	[kg/m <sup>3</sup> ]
Lower element	E <sub>2</sub>	12489	[N/mm <sup>2</sup> ]
	ρ <sub>2</sub>	443.10	[kg/m <sup>3</sup> ]
Connection (x1)	k <sub>s</sub>	-	[N/mm]

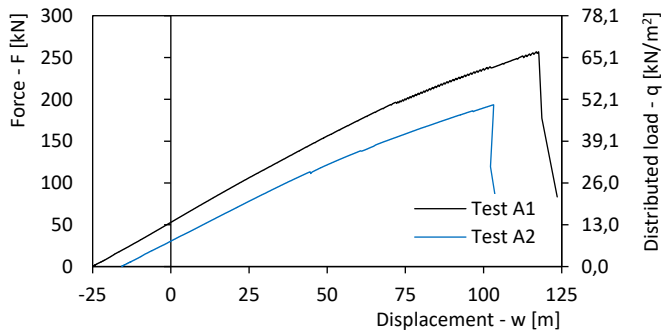
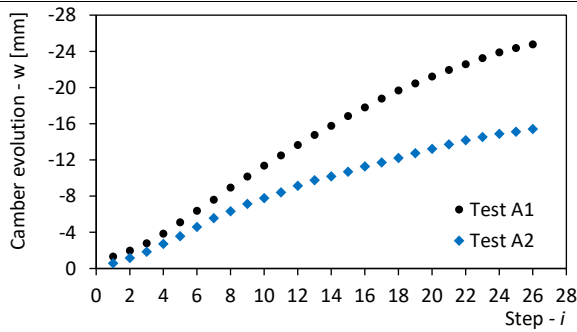
Assembly method: CP procedure

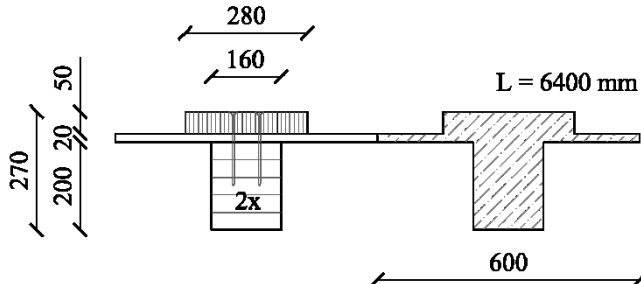
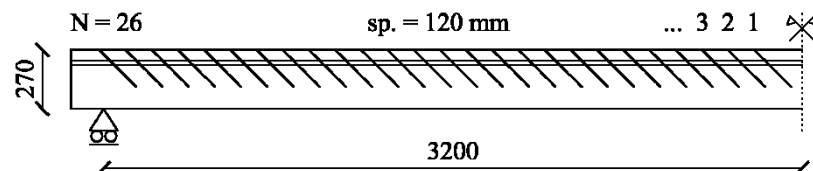
TEST A2

**TESTS A1 – A2 | RESULTS**



		Test A1	Test A2
$w_{CP}$	[mm]	-24.86	-15.50
	[L/...]	257	413
$q_0$	[kN/m <sup>2</sup> ]	13.76	7.92
$(EJ)_0$	[Nmm <sup>2</sup> ]	$1.94 \cdot 10^{12}$	$1.93 \cdot 10^{12}$
$(EJ)_\infty$	[Nmm <sup>2</sup> ]	$8.28 \cdot 10^{12}$	$7.37 \cdot 10^{12}$
$(EJ)_{ECS}$	[Nmm <sup>2</sup> ]	-	-
$(EJ)_{Exp}$	[Nmm <sup>2</sup> ]	$7.23 \cdot 10^{12}$	$6.38 \cdot 10^{12}$
$\eta$	[%]	83.38	69.08
$q_{(L/300)}$	[kN/m <sup>2</sup> ]	25.67	18.50
$w_{max}$	[mm]	116.89	103.22
$F_{max}$	[kN]	256.87	193.48
$q_{max}$	[kN/m <sup>2</sup> ]	66.89	50.39



<b>TEST B1   CONFIGURATION</b>	
<b>Geometry</b>	
Length:	6700 m (6400 mm span)
Upper element:	Beech LVL beam (on its side) 50 x 280 mm <sup>2</sup>
Interlayer:	Non-structural floorboard (20 mm thick)
Lower element:	Glulam beam GL24h 160 x 200 mm <sup>2</sup>
	
<b>Connection</b>	
Screw type:	Double threaded (DT) 8.5 x 190 mm <sup>2</sup>
	
Arrangement:	Constant spacing (120 mm)   45°   2 rows
N. of fasteners:	104 screws
	
<b>Mechanical properties</b>	
Upper element	$E_1$ 18333 [N/mm <sup>2</sup> ]
	$\rho_1$ 820.90 [kg/m <sup>3</sup> ]
Lower element	$E_2$ 12950 [N/mm <sup>2</sup> ]
	$\rho_2$ 443.10 [kg/m <sup>3</sup> ]
Connection (x1)	$k_s$ 13468 [N/mm]
<b>Assembly method:</b> CP procedure	
<b>TEST B1</b>	

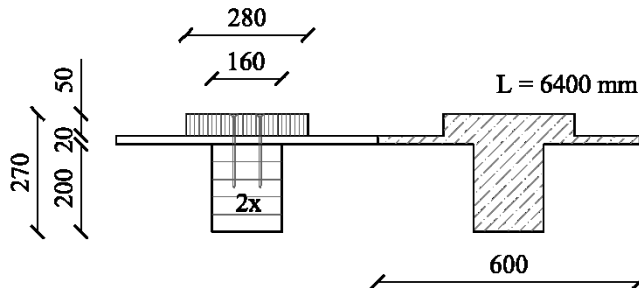
**TEST B2 | CONFIGURATION****Geometry**

Length: 6700 mm (6400 mm span)

Upper element: Beech LVL beam (on its side)  
50 x 280 mm<sup>2</sup>

Interlayer: Non-structural floorboard (20 mm thick)

Lower element: Glulam beam GL24h  
160 x 200 mm<sup>2</sup>

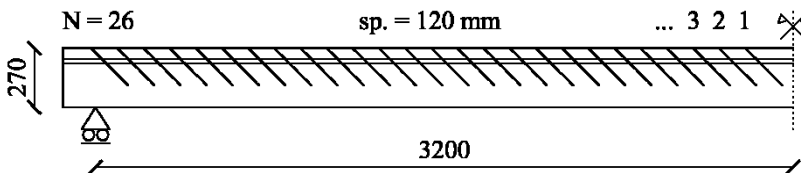
**Connection**

Screw type: Single threaded (ST) 10 x 240 mm<sup>2</sup> + Washer (groove cut)



Arrangement: Constant spacing (120 mm) | 45° | 2 rows

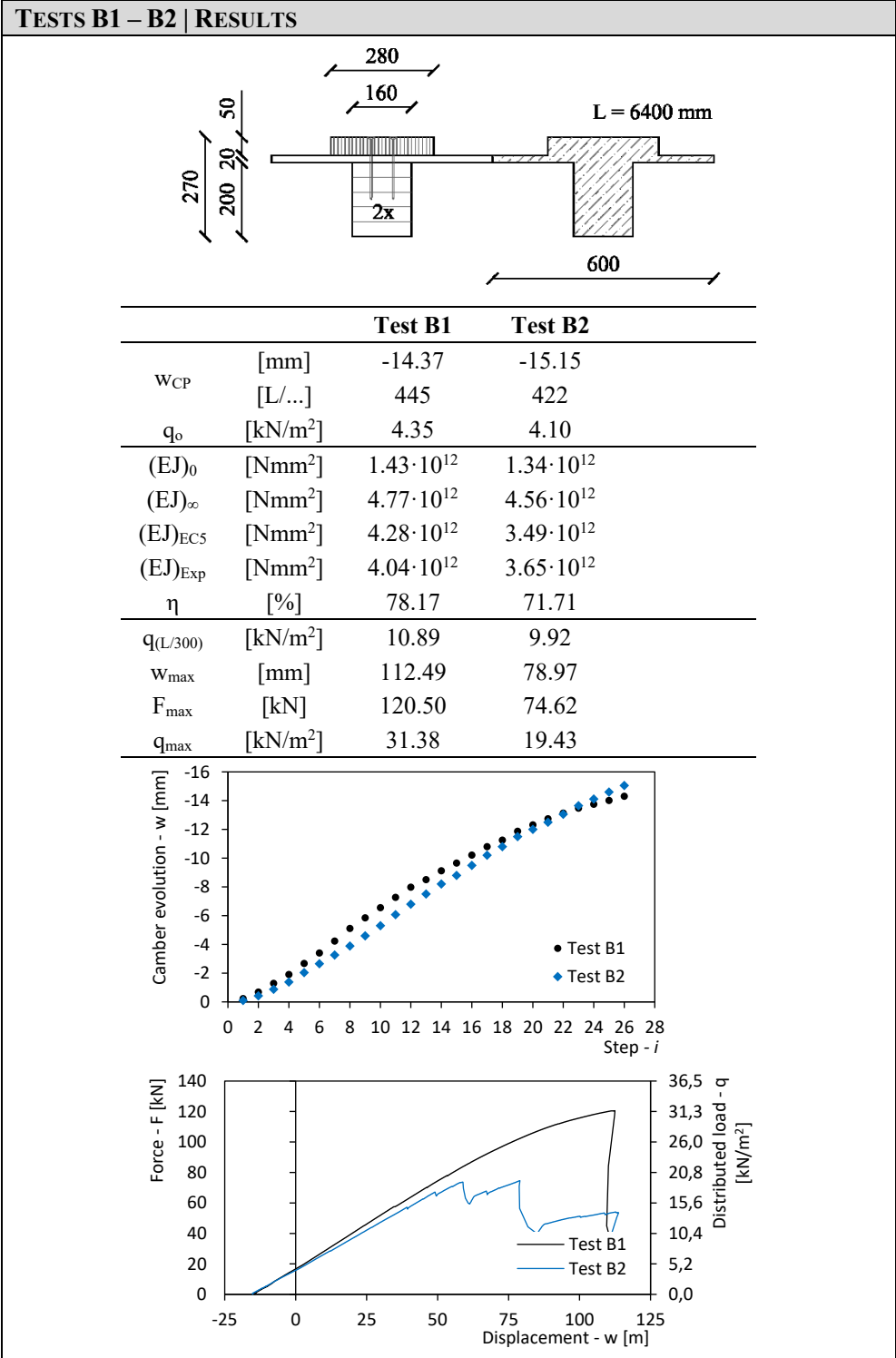
N. of fasteners: 104 screws

**Mechanical properties**

Upper element	$E_1$	18256	[N/mm <sup>2</sup> ]
	$\rho_1$	820.90	[kg/m <sup>3</sup> ]
Lower element	$E_2$	12017	[N/mm <sup>2</sup> ]
Connection (x1)	$\rho_2$	447.76	[kg/m <sup>3</sup> ]
	$k_s$	4472	[N/mm]

Assembly method: CP procedure

TEST B2



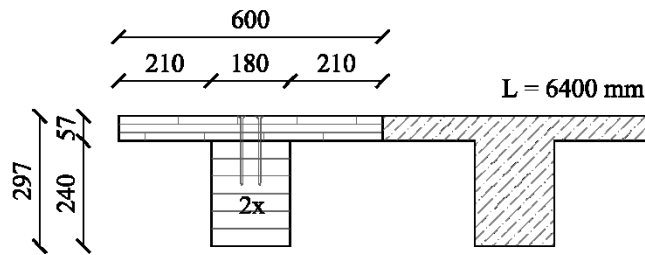
**TEST C1 | CONFIGURATION****Geometry**

Length: 6700 m (6400 mm span)

Upper element: Softwood CLT panel (3 layers)  
600 x 57 mm<sup>2</sup>

Interlayer: -

Lower element: Glulam beam GL24h  
180 x 240 mm<sup>2</sup>

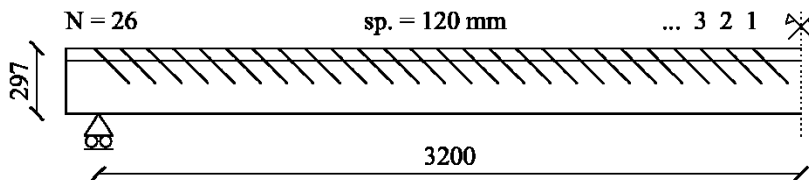
**Connection**

Screw type: Double threaded (DT) 8.5 x 150 mm<sup>2</sup>



Arrangement: Constant spacing (120 mm) | 45° | 2 rows

N. of fasteners: 104 screws

**Mechanical properties**

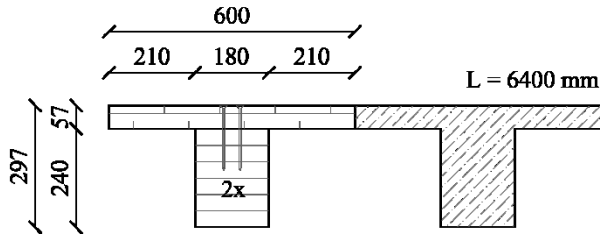
Upper element	$E_1$	11353	[N/mm <sup>2</sup> ]
	$\rho_1$	458.24	[kg/m <sup>3</sup> ]
Lower element	$E_2$	9638	[N/mm <sup>2</sup> ]
	$\rho_2$	418.05	[kg/m <sup>3</sup> ]
Connection (x1)	$k_s$	9773	[N/mm]

Assembly method: CP procedure

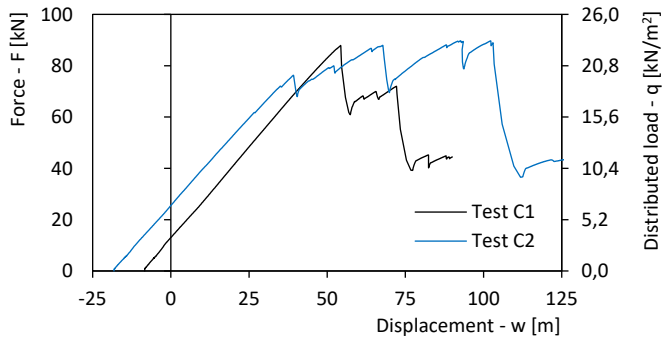
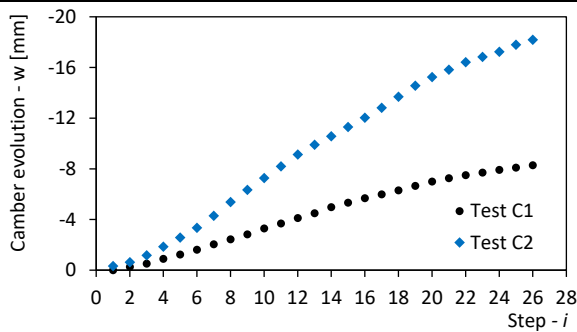
TEST C1

TEST C2   CONFIGURATION			
<b>Geometry</b>			
Length:	6700 m (6400 mm span)		
Upper element:	Softwood CLT panel (3 layers) 600 x 57 mm <sup>2</sup>		
Interlayer:	-		
Lower element:	Glulam beam GL24h 180 x 240 mm <sup>2</sup>		
<b>Connection</b>			
Screw type:	Single threaded (ST) 10 x 220 mm <sup>2</sup> + Washer (groove cut)		
Arrangement:	Constant spacing (120 mm)   45°   2 rows		
N. of fasteners:	104 screws		
<b>Mechanical properties</b>			
Upper element	$E_1$	11708	[N/mm <sup>2</sup> ]
	$\rho_1$	458.24	[kg/m <sup>3</sup> ]
Lower element	$E_2$	9530	[N/mm <sup>2</sup> ]
	$\rho_2$	421.50	[kg/m <sup>3</sup> ]
Connection (x1)	$k_s$	3744	[N/mm]
<b>Assembly method:</b> CP procedure			
<b>TEST C2</b>			

**TESTS C1 – C2 | RESULTS**



		Test C1	Test C2
$w_{CP}$	[mm]	-8.35	-18.20
	[L/...]	766	352
$q_0$	[kN/m <sup>2</sup> ]	3.38	6.64
$(EJ)_0$	[Nmm <sup>2</sup> ]	$2.10 \cdot 10^{12}$	$2.08 \cdot 10^{12}$
$(EJ)_\infty$	[Nmm <sup>2</sup> ]	$5.62 \cdot 10^{12}$	$5.65 \cdot 10^{12}$
$(EJ)_{EC5}$	[Nmm <sup>2</sup> ]	$4.95 \cdot 10^{12}$	$4.28 \cdot 10^{12}$
$(EJ)_{Exp}$	[Nmm <sup>2</sup> ]	$4.92 \cdot 10^{12}$	$4.65 \cdot 10^{12}$
$\eta$	[%]	80.23	71.86
$q_{(L/300)}$	[kN/m <sup>2</sup> ]	11.20	14.24
$w_{max}$	[mm]	54.32	92.69
$F_{max}$	[kN]	87.90	89.72
$q_{max}$	[kN/m <sup>2</sup> ]	22.89	23.37



<b>TEST D1   CONFIGURATION</b>	
<b>Geometry</b>	
Length:	6700 m (6400 mm span)
Upper element:	Beech LVL panel (type S) 600 x 40 mm <sup>2</sup>
Interlayer:	-
Lower element:	Beech LVL beam GL70 160 x 240 mm <sup>2</sup>
<b>Connection</b>	
Screw type:	Single threaded (ST) 10 x 220 mm <sup>2</sup>
Arrangement:	Constant spacing (120 mm)   45°   2 rows
N. of fasteners:	104 screws
<b>Mechanical properties</b>	
Upper element	$E_1$ 21744 [N/mm <sup>2</sup> ]
	$\rho_1$ 851.99 [kg/m <sup>3</sup> ]
Lower element	$E_2$ 19604 [N/mm <sup>2</sup> ]
	$\rho_2$ 789.02 [kg/m <sup>3</sup> ]
Connection (x1)	$k_s$ 4924 [N/mm]
<b>Assembly method:</b> CP procedure	
<b>TEST D1</b>	

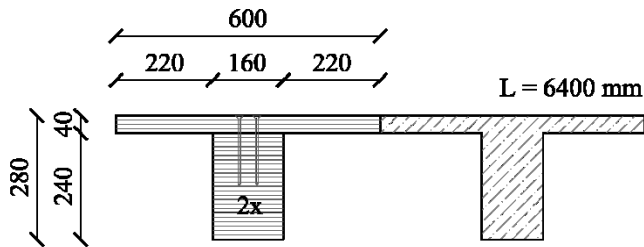
**TEST D2 | CONFIGURATION****Geometry**

Length: 6700 m (6400 mm span)

Upper element: Beech LVL panel (type S)  
600 x 40 mm<sup>2</sup>

Interlayer: -

Lower element: Beech LVL beam GL70  
160 x 240 mm<sup>2</sup>

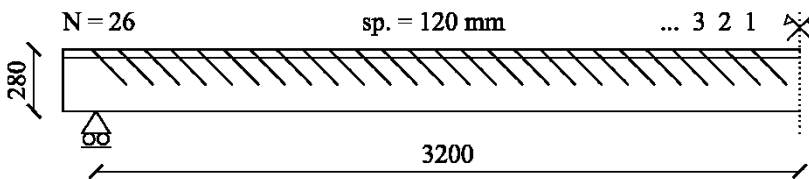
**Connection**

Screw type: Single threaded (ST) 10 x 220 mm<sup>2</sup> + Washer (45°)



Arrangement: Constant spacing (120 mm) | 45° | 2 rows

N. of fasteners: 104 screws

**Mechanical properties**

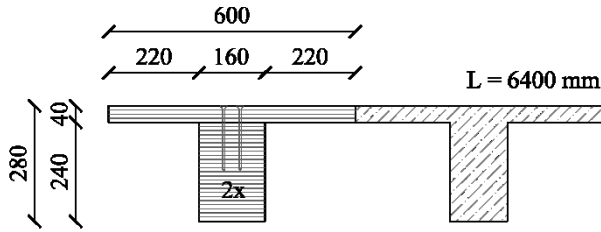
Upper element	$E_1$	20949	[N/mm <sup>2</sup> ]
	$\rho_1$	839.55	[kg/m <sup>3</sup> ]
Lower element	$E_2$	16711	[N/mm <sup>2</sup> ]
Connection (x1)	$\rho_2$	789.02	[kg/m <sup>3</sup> ]
	$k_s$	4192	[N/mm]

Assembly method: CP procedure

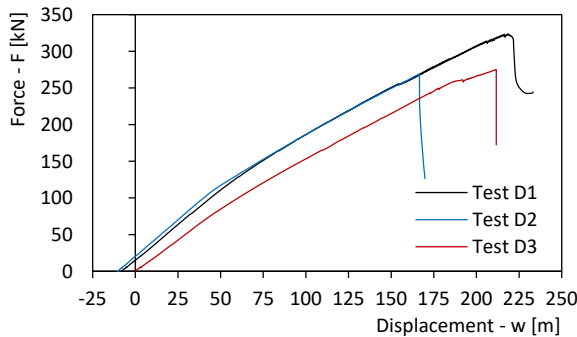
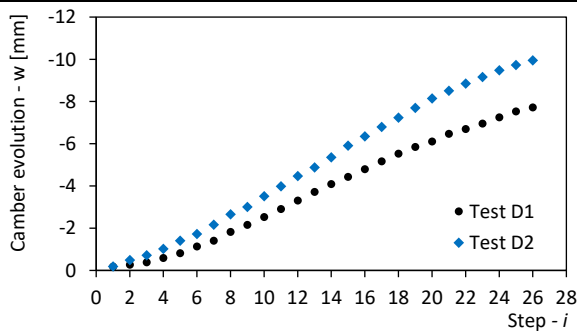
TEST D2

<b>TEST D3   CONFIGURATION</b>	
<b>Geometry</b>	
Length:	6700 m (6400 mm span)
Upper element:	Beech LVL panel (type S) 600 x 40 mm <sup>2</sup>
Interlayer:	-
Lower element:	Beech LVL beam GL70 160 x 240 mm <sup>2</sup>
<b>Connection</b>	
Screw type:	Single threaded (ST) 10 x 220 mm <sup>2</sup>
Arrangement:	Constant spacing (120 mm)   45°   2 rows
N. of fasteners:	104 screws
<b>Mechanical properties</b>	
Upper element	$E_1$ 21993 [N/mm <sup>2</sup> ]
	$\rho_1$ 845.77 [kg/m <sup>3</sup> ]
Lower element	$E_2$ 17154 [N/mm <sup>2</sup> ]
Connection (x1)	$\rho_2$ 800.68 [kg/m <sup>3</sup> ]
	$k_s$ 4924 [N/mm]
<b>Assembly method:</b> Traditional (no CP procedure)	
<b>TEST D3</b>	

**TESTS D1 – D2 – D3 | RESULTS**



	Test D1	Test D2	Test D3
$w_{CP}$ [mm]	-7.72	-9.96	-
$w_{CP}$ [L/...]	829	642	-
$q_0$ [kN/m <sup>2</sup> ]	3.96	5.31	-
$(EJ)_0$ [Nmm <sup>2</sup> ]	$3.68 \cdot 10^{12}$	$3.15 \cdot 10^{12}$	$3.23 \cdot 10^{12}$
$(EJ)_\infty$ [Nmm <sup>2</sup> ]	$9.72 \cdot 10^{12}$	$8.67 \cdot 10^{12}$	$8.98 \cdot 10^{12}$
$(EJ)_{EC5}$ [Nmm <sup>2</sup> ]	$6.85 \cdot 10^{12}$	$5.95 \cdot 10^{12}$	$6.32 \cdot 10^{12}$
$(EJ)_{Exp}$ [Nmm <sup>2</sup> ]	$6.73 \cdot 10^{12}$	$6.97 \cdot 10^{12}$	$5.94 \cdot 10^{12}$
$\eta$ [%]	50.40	69.17	47.18
$q_{(L/300)}$ [kN/m <sup>2</sup> ]	14.68	16.31	9.37
$w_{max}$ [mm]	218.50	166.55	211.61
$F_{max}$ [kN]	323.82	269.05	275.11
$q_{max}$ [kN/m <sup>2</sup> ]	84.33	70.07	71.64



<b>TEST E1   CONFIGURATION</b>	
<b>Geometry</b>	
Length:	6700 m (6400 mm span)
Upper element:	Beech LVL panel (type S) 600 x 40 mm <sup>2</sup>
Interlayer:	-
Lower element:	Beech LVL beam GL70 120 x 200 mm <sup>2</sup>
<b>Connection</b>	
Screw type:	Single threaded (ST) 10 x 220 mm <sup>2</sup>
Arrangement:	Constant spacing (120 mm)   45°   2 rows
N. of fasteners:	104 screws
<b>Mechanical properties</b>	
Upper element	E <sub>1</sub> 20478 [N/mm <sup>2</sup> ]
	ρ <sub>1</sub> 845.77 [kg/m <sup>3</sup> ]
Lower element	E <sub>2</sub> 16652 [N/mm <sup>2</sup> ]
	ρ <sub>2</sub> 796.02 [kg/m <sup>3</sup> ]
Connection (x1)	k <sub>s</sub> 4924 [N/mm]
<b>Assembly method:</b> CP procedure	
<b>TEST E1</b>	

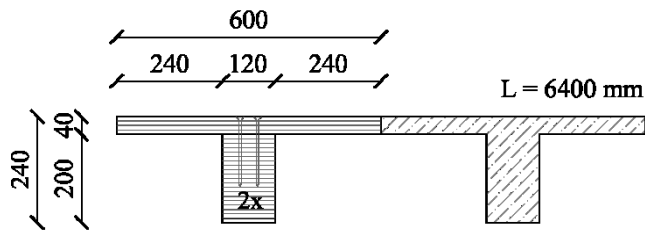
**TEST E2 | CONFIGURATION****Geometry**

Length: 6700 m (6400 mm span)

Upper element: Beech LVL panel (type S)  
600 x 40 mm<sup>2</sup>

Interlayer: -

Lower element: Beech LVL beam GL70  
120 x 200 mm<sup>2</sup>

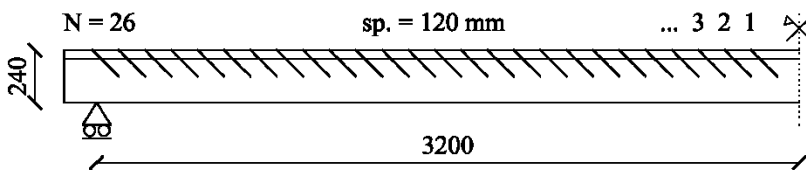
**Connection**

Screw type: Single threaded (ST) 10 x 220 mm<sup>2</sup> + Washer (45°)



Arrangement: Constant spacing (120 mm) | 45° | 2 rows

N. of fasteners: 104 screws

**Mechanical properties**

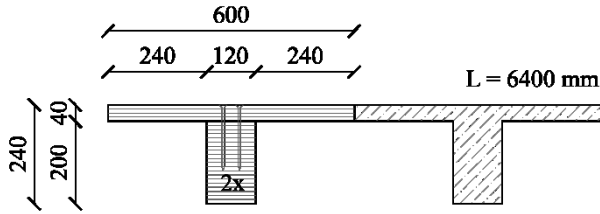
Upper element	$E_1$	21588	[N/mm <sup>2</sup> ]
	$\rho_1$		[kg/m <sup>3</sup> ]
Lower element	$E_2$	17238	[N/mm <sup>2</sup> ]
	$\rho_2$		[kg/m <sup>3</sup> ]
Connection (x1)	$k_s$	4192	[N/mm]

Assembly method: CP procedure

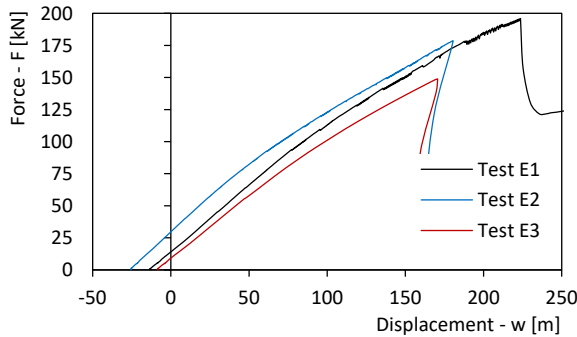
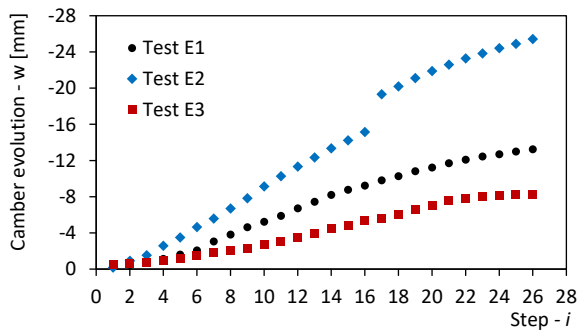
**TEST E2**

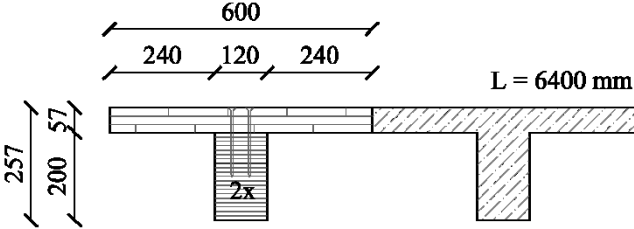
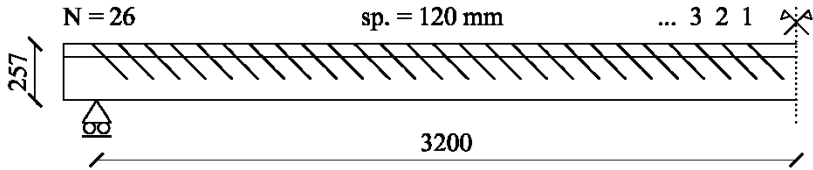
TEST E3   CONFIGURATION			
<b>Geometry</b>			
Length:	6700 m (6400 mm span)		
Upper element:	Beech LVL panel (type S) 600 x 40 mm <sup>2</sup>		
Interlayer:	-		
Lower element:	Beech LVL beam GL70 120 x 200 mm <sup>2</sup>		
<b>Connection</b>			
Screw type:	Single threaded (ST) 10 x 220 mm <sup>2</sup>		
Arrangement:	Constant spacing (120 mm)   45°   2 rows		
N. of fasteners:	104 screws		
<b>Mechanical properties</b>			
Upper element	$E_1$	21344	[N/mm <sup>2</sup> ]
	$\rho_1$	845.68	[kg/m <sup>3</sup> ]
Lower element	$E_2$	16652	[N/mm <sup>2</sup> ]
	$\rho_2$	796.02	[kg/m <sup>3</sup> ]
Connection (x1)	$k_s$	4924	[N/mm]
<b>Assembly method:</b> Traditional (no CP procedure)		<b>TEST E3</b>	

**TESTS E1 – E2 – E3 | RESULTS**



		Test E1	Test E2	Test E3
$w_{CP}$	[mm]	-13.25	-25.51	-8.28
	[L/...]	483	251	773
$q_0$	[kN/m <sup>2</sup> ]	3.65	7.72	2.40
$(EJ)_0$	[Nmm <sup>2</sup> ]	$1.40 \cdot 10^{12}$	$1.45 \cdot 10^{12}$	$1.40 \cdot 10^{12}$
$(EJ)_\infty$	[Nmm <sup>2</sup> ]	$4.57 \cdot 10^{12}$	$4.76 \cdot 10^{12}$	$4.63 \cdot 10^{12}$
$(EJ)_{EC5}$	[Nmm <sup>2</sup> ]	$3.32 \cdot 10^{12}$	$3.30 \cdot 10^{12}$	$3.35 \cdot 10^{12}$
$(EJ)_{Exp}$	[Nmm <sup>2</sup> ]	$3.65 \cdot 10^{12}$	$3.68 \cdot 10^{12}$	$3.40 \cdot 10^{12}$
$\eta$	[%]	70.87	67.24	61.92
$q_{(L/300)}$	[kN/m <sup>2</sup> ]	9.38	13.94	7.75
$w_{max}$	[mm]	223.43	180.57	170.64
$F_{max}$	[kN]	195.98	178.61	148.88
$q_{max}$	[kN/m <sup>2</sup> ]	51.04	46.51	38.77



<b>TEST F1   CONFIGURATION</b>	
<b>Geometry</b>	
Length:	6700 m (6400 mm span)
Upper element:	Softwood CLT panel (3 layers) 600 x 57 mm <sup>2</sup>
Interlayer:	-
Lower element:	Beech LVL beam GL70 120 x 200 mm <sup>2</sup>
	
<b>Connection</b>	
Screw type:	Double threaded (DT) 8.5 x 150 mm <sup>2</sup>
	
Arrangement:	Constant spacing (120 mm)   45°   2 rows
N. of fasteners:	104 screws
	
<b>Mechanical properties</b>	
Upper element	$E_1$ 12819 [N/mm <sup>2</sup> ]
	$\rho_1$ 475.69 [kg/m <sup>3</sup> ]
Lower element	$E_2$ 16716 [N/mm <sup>2</sup> ]
Connection (x1)	$\rho_2$ 796.02 [kg/m <sup>3</sup> ]
	$k_s$ 13234 [N/mm]
<b>Assembly method:</b> CP procedure	
<b>TEST F1</b>	

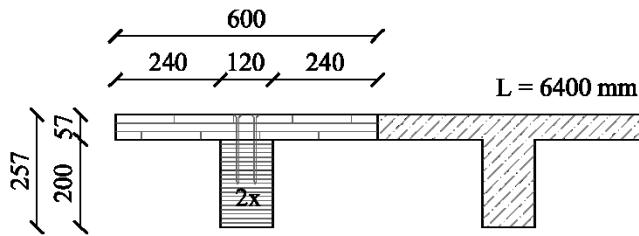
**TEST F2 | CONFIGURATION****Geometry**

Length: 6700 m (6400 mm span)

Upper element: Softwood CLT panel (3 layers)  
600 x 57 mm<sup>2</sup>

Interlayer: -

Lower element: Beech LVL beam GL70  
120 x 200 mm<sup>2</sup>

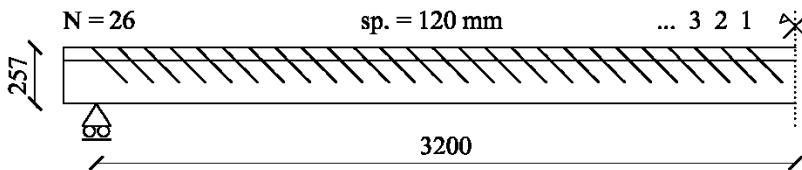
**Connection**

Screw type: Single threaded (ST) 10 x 220 mm<sup>2</sup> + Washer (groove cut)



Arrangement: Constant spacing (120 mm) | 45° | 2 rows

N. of fasteners: 104 screws

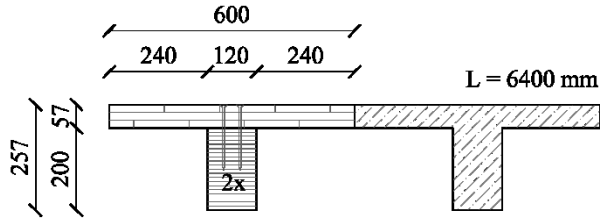
**Mechanical properties**

Upper element	$E_1$	11529	[N/mm <sup>2</sup> ]
	$\rho_1$	562.60	[kg/m <sup>3</sup> ]
Lower element	$E_2$	17300	[N/mm <sup>2</sup> ]
	$\rho_2$	802.24	[kg/m <sup>3</sup> ]
Connection (x1)	$k_s$	5369	[N/mm]

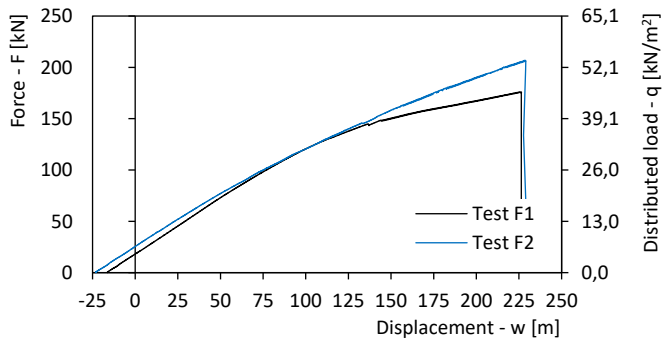
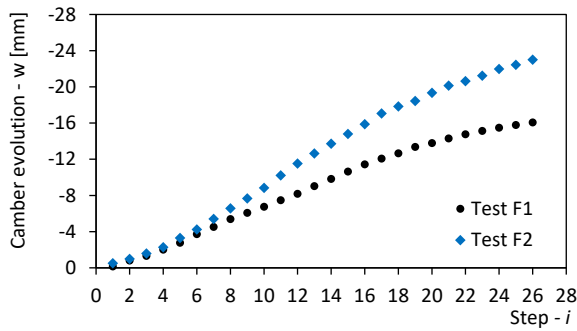
Assembly method: CP procedure

**TEST F2**

**TESTS F1 – F2 | RESULTS**



		Test F1	Test F2
$w_{CP}$	[mm]	-16.20	-23.04
	[L/...]	395	278
$q_o$	[kN/m <sup>2</sup> ]	4.70	6.62
$(EJ)_0$	[Nmm <sup>2</sup> ]	$1.45 \cdot 10^{12}$	$1.49 \cdot 10^{12}$
$(EJ)_\infty$	[Nmm <sup>2</sup> ]	$4.24 \cdot 10^{12}$	$4.14 \cdot 10^{12}$
$(EJ)_{EC5}$	[Nmm <sup>2</sup> ]	$3.81 \cdot 10^{12}$	$3.34 \cdot 10^{12}$
$(EJ)_{Exp}$	[Nmm <sup>2</sup> ]	$3.85 \cdot 10^{12}$	$3.66 \cdot 10^{12}$
$\eta$	[%]	85.73	81.85
$q_{(L/300)}$	[kN/m <sup>2</sup> ]	10.76	12.55
$w_{max}$	[mm]	225.54	228.56
$F_{max}$	[kN]	176.02	207.03
$q_{max}$	[kN/m <sup>2</sup> ]	45.84	53.91



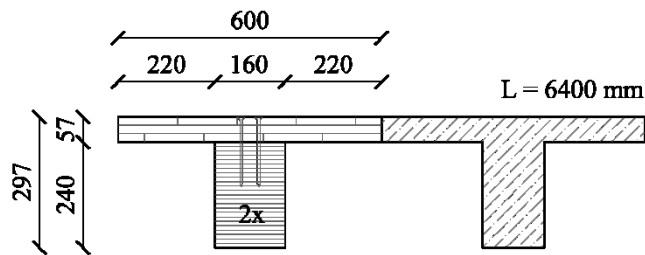
**TEST G1 | CONFIGURATION****Geometry**

Length: 6700 m (6400 mm span)

Upper element: Softwood CLT panel (3 layers)  
600 x 57 mm<sup>2</sup>

Interlayer: -

Lower element: Beech LVL beam GL70  
160 x 240 mm<sup>2</sup>

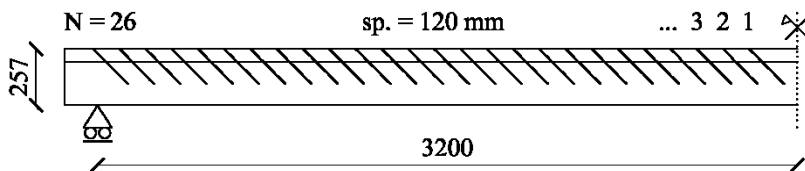
**Connection**

Screw type: Double threaded (DT) 8.5 x 150 mm<sup>2</sup>



Arrangement: Constant spacing (120 mm) | 45° | 2 rows

N. of fasteners: 104 screws

**Mechanical properties**

Upper element	$E_1$	12984	[N/mm <sup>2</sup> ]
	$\rho_1$	466.96	[kg/m <sup>3</sup> ]
Lower element	$E_2$	17154	[N/mm <sup>2</sup> ]
Connection (x1)	$\rho_2$	785.14	[kg/m <sup>3</sup> ]
	$k_s$	13234	[N/mm]

Assembly method: CP procedure

TEST G1

<b>TEST G2   CONFIGURATION</b>	
<b>Geometry</b>	
Length:	6700 m (6400 mm span)
Upper element:	Softwood CLT panel (3 layers) 600 x 57 mm <sup>2</sup>
Interlayer:	-
Lower element:	Beech LVL beam GL70 160 x 240 mm <sup>2</sup>
<b>Connection</b>	
Screw type:	Single threaded (ST) 10 x 220 mm <sup>2</sup> + Washer (groove cut)
Arrangement:	Constant spacing (120 mm)   45°   2 rows
N. of fasteners:	104 screws
<b>Mechanical properties</b>	
Upper element	E <sub>1</sub> 12112 [N/mm <sup>2</sup> ]
	ρ <sub>1</sub> 458.24 [kg/m <sup>3</sup> ]
Lower element	E <sub>2</sub> 17292 [N/mm <sup>2</sup> ]
Connection (x1)	ρ <sub>2</sub> 796.80 [kg/m <sup>3</sup> ]
	k <sub>s</sub> 5369 [N/mm]
<b>Assembly method:</b> CP procedure	
<b>TEST G2</b>	

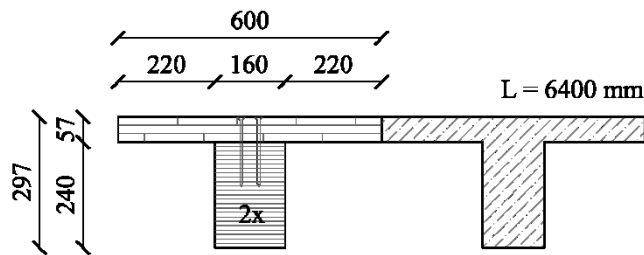
**TEST G3 | CONFIGURATION****Geometry**

Length: 6700 m (6400 mm span)

Upper element: Softwood CLT panel (3 layers)  
600 x 57 mm<sup>2</sup>

Interlayer: -

Lower element: Beech LVL beam GL70  
160 x 240 mm<sup>2</sup>

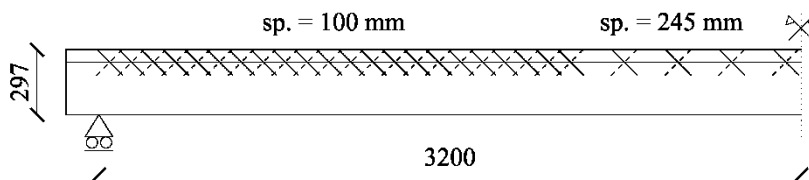
**Connection**

Screw type: Double threaded (DT) 8.5 x 150 mm<sup>2</sup>



Arrangement: Variable spacing (100/245 mm) | X | 2 rows

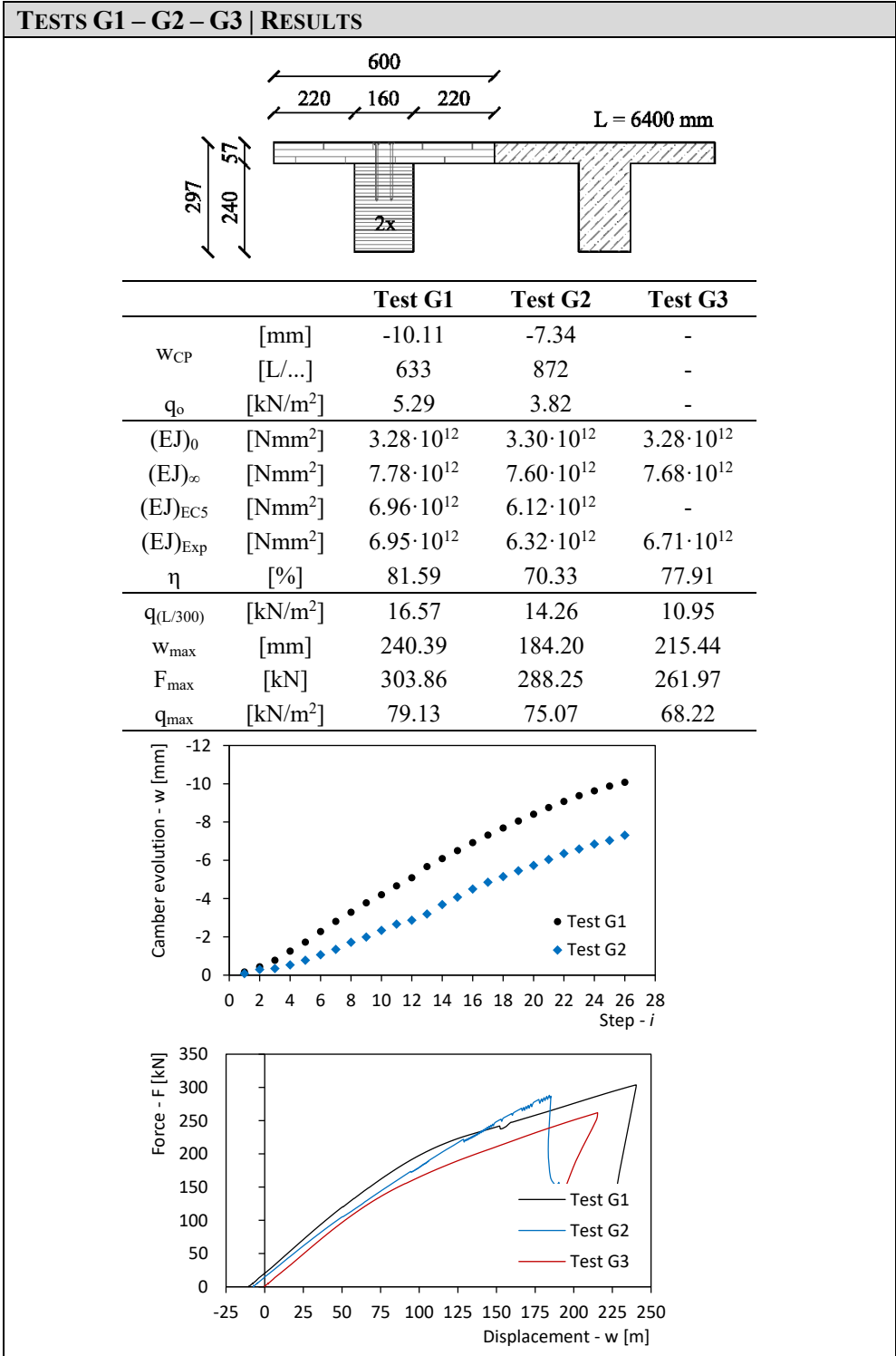
N. of fasteners: 104 screws

**Mechanical properties**

Upper element	$E_1$	12539	[N/mm <sup>2</sup> ]
	$\rho_1$	466.96	[kg/m <sup>3</sup> ]
Lower element	$E_2$	17194	[N/mm <sup>2</sup> ]
	$\rho_2$	800.68	[kg/m <sup>3</sup> ]
Connection (x1)	$k_s$	-	[N/mm]

**Assembly method:** Traditional (no CP procedure)

**TEST G3**



## 4.4 RESULT COMPARISON

Seventeen timber-to-timber composite floor solutions were investigated in this Chapter. As mentioned before, these samples were designed considering different application fields. More specifically, solutions for newly constructed high-performance diaphragms (made both of hardwood and softwood) were compared with timber-based technique for retrofit interventions on existing timber diaphragms. As expected, these composite systems exhibited significantly different mechanical performances, in terms of both pre-stress, camber value and flexural behaviour.

As it can be seen in Figure 4-6, the final uplift  $w_{CP}$  ranged from -7.34 mm (L/872) to -25.51 mm (L/251). The maximum camber value was obtained for test E2 where, as a consequence of a problem occurred during the screw insertion (step 16), a retightening of all fasteners was done. Additional studies on the effects introduced by a final retightening of all devices are provided in the next Chapter, where the development of high-performance solutions for prefabricated timber-to-timber composite floor modules to be realized by using laminated veneer lumber (LVL) made of beech wood is presented.

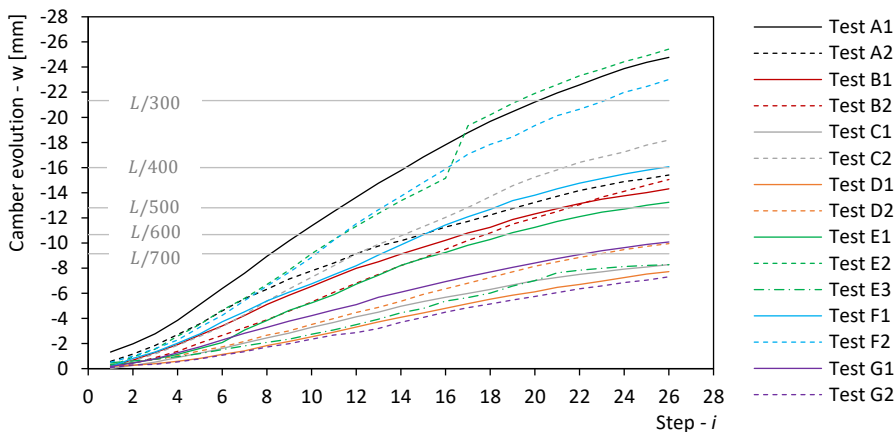


Figure 4-6 Result comparison in terms of camber evolution

The results of the six-point bending tests are presented in Figure 4-7 in terms of force Vs. displacement curves.

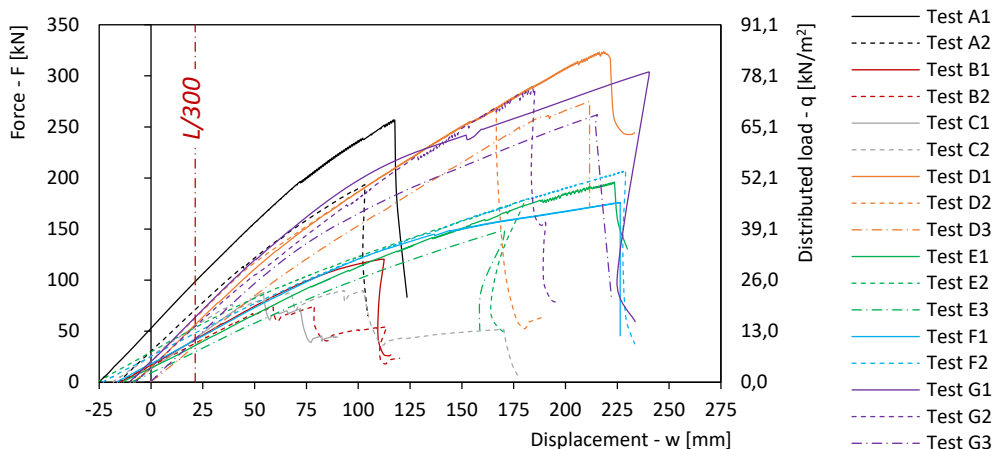


Figure 4-7 Result comparison in terms of force Vs. displacement curves

As shown in Figure 4-7, the test program outcome was characterized by a large variability in the specimen performance. With reference to the load-carrying capacity, the ultimate limit state (ULS) did not constitute a limiting criterion. Not surprisingly, higher values of capacity were registered for the specimens where hardwood elements were employed, with the exception of test A1 where a softwood CLT panel 99 mm thick was used. All specimens showed a failure mode related to the bending stress at the bottom of the joist cross section (see Figure 1 12).



Figure 4-8 Failure modes

By focusing the attention on the displacement range between  $w_{CP}$  and the limit value assumed for the service limit state ( $w_{SLS} = L/300$ ), it is possible to note how all TTC beams assembled with the CP procedure showed an equivalent distributed load  $q_0$  (necessary to induce a midspan displacement variation equal to  $\Delta w_{CP}$ ) greater than  $3 \text{ kN/m}^2$ .

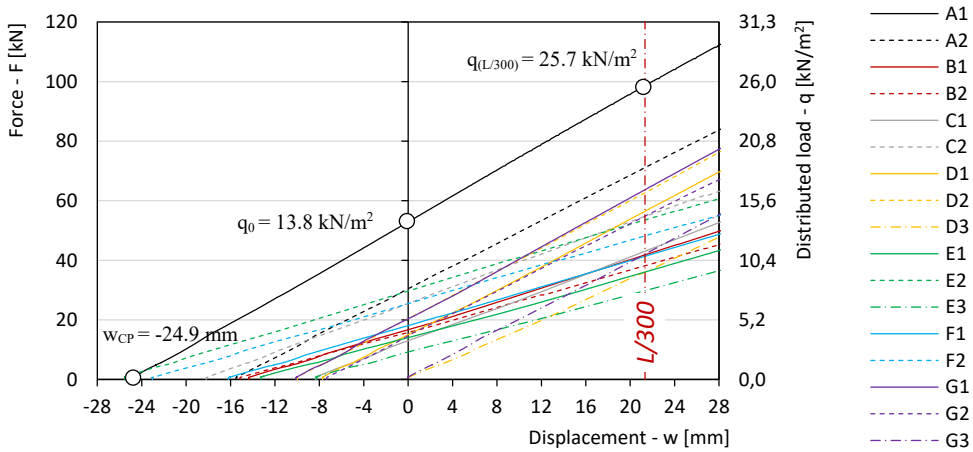


Figure 4-9 Result comparison in terms of force Vs. displacement curves ( $w_{CP} < w < w_{SLS}$ )

As illustrated in Figure 4-9, thanks to the use of relatively long DT screws (8.5 x 300 mm<sup>2</sup>) and a softwood CLT panel 99 mm thick, test A1 exhibited the highest values of  $q_0$  and  $q_{(L/300)}$ . On the other hand, without considering the tests where the CP procedure was not applied (i.e. D3 and G3), test E3 showed the worst performance. As it will be illustrated in the following, a problem occurred during the screw insertion for specimen E3.

The results of Figure 4-6 and Figure 4-9 are summarised in the histograms of Figure 4-10 and Figure 4-11.

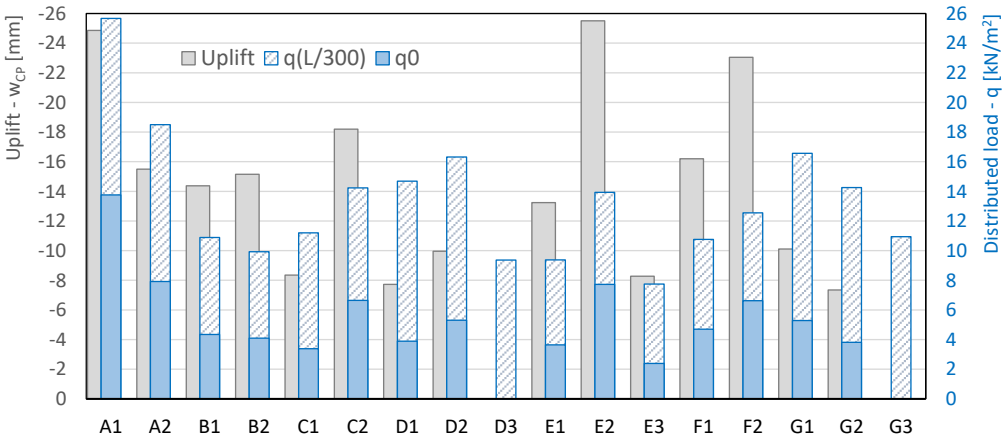


Figure 4-10 Result comparison: camber values at the end of the assembly phase (left) and flexural performances (right)

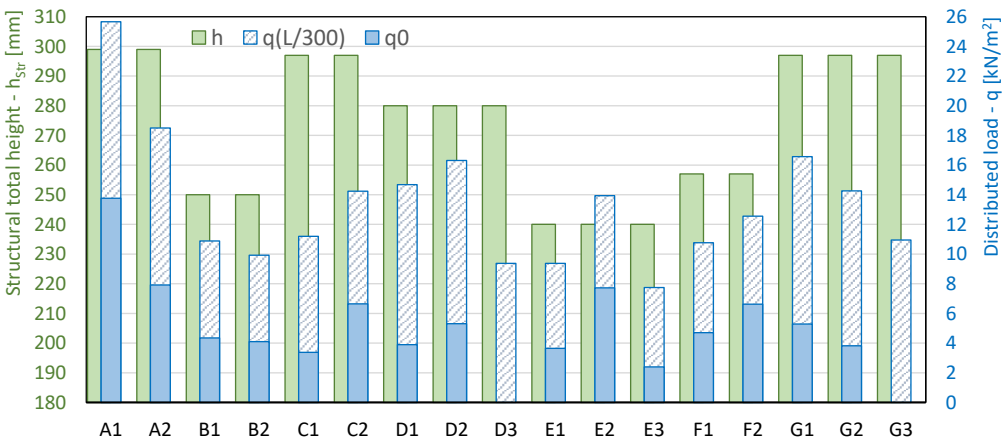


Figure 4-11 Result comparison: structural total height of the TTC solutions (left) and flexural performances (right)

With the aim of analysing the bending stiffness of the TTC beams, a rigid translation of all force-displacement curves was provided in Figure 4-12, where  $w^*$  refers to the vertical displacement measured with reference to the deformed configuration at the end of the CP procedure. Essentially, the curves can be divided into two main groups. Thanks to a greater structural height ( $L/h = 21.4 \div 22.9$ ), tests A, D and G exhibited a significant bending stiffness ranging from  $5.94 \cdot 10^{12}$  to  $7.93 \cdot 10^{12}$  Nmm<sup>2</sup>. On the other hand, due to the smaller size of the timber components ( $L/h = 24.9 \div 26.7$ ), tests B, E and F showed a flexural stiffness values between  $3.40 \cdot 10^{12}$  and  $4.05 \cdot 10^{12}$  Nmm<sup>2</sup>. An intermediate behaviour was registered for tests C where, despite a length/height ratio of 25.6, the values of bending stiffness ranged between  $4.65 \cdot 10^{12}$  and  $4.92 \cdot 10^{12}$  Nmm<sup>2</sup>.

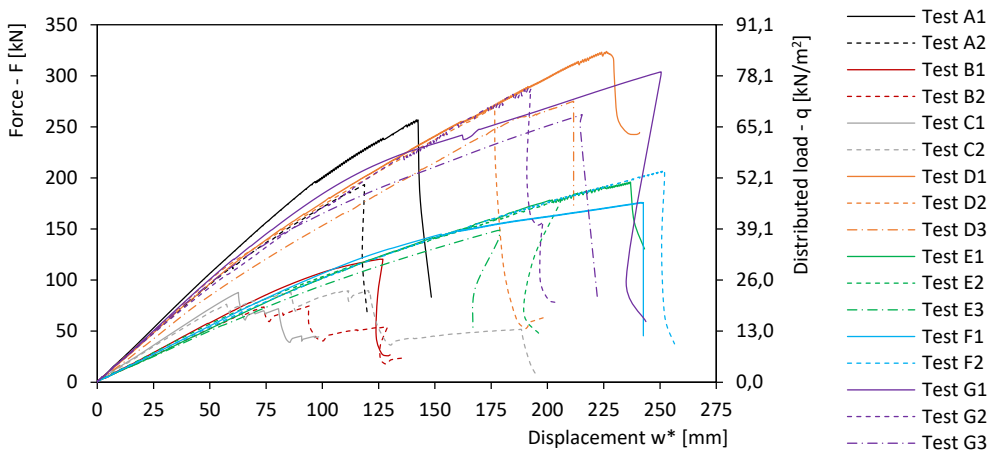


Figure 4-12 Result comparison in terms of force Vs. displacement\* curves

The flexural stiffness  $(EJ)_{Exp}$  (the secant value at  $0.4 F_{max}$  was considered) and the efficiency  $\eta$  of the connection system are reported in the histogram below.

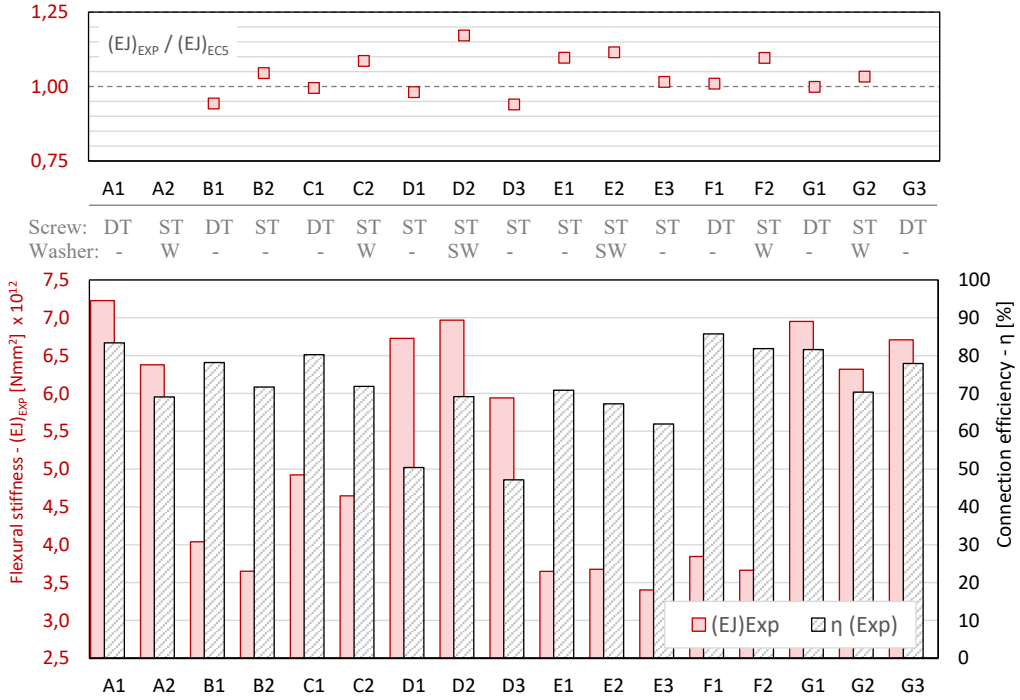


Figure 4-13 Result comparison: flexural stiffness (left) and connection efficiency (right)

In the upper part of Figure 4-13, a comparison between the stiffness experimentally measured and the value  $(EJ)_{EC5}$  calculated in accordance with the Eurocode 5 [15] is also proposed. Since the slip modulus  $k_s$  of the connection is a key parameter for the estimation of  $(EJ)_{EC5}$ , in those configurations where  $k_s$  was not experimentally measured (see Chapter 3), the value of  $(EJ)_{EC5}$  was omitted.

The connection efficiency was calculated as:

$$\eta = \frac{(EJ)_{Exp} - (EJ)_0}{(EJ)_\infty - (EJ)_0} \quad (\text{Eq. 26})$$

The highest efficiency was found for tests F1 (85.73) and A1 (83.38) while the lower values were registered in tests D3 (47.18) and D1 (50.40). Generally, thanks to the higher value of slip modulus exhibited by DT screws with respect to ST screws, a greater efficiency was observed in those configurations where DT screws were adopted (considering the same timber elements).

With reference to the stiffness ratio presented in Figure 4-13, with the exception of test B1, values close to unity were found for all tests assembled with double threaded screws. On the other hand, values of  $(EJ)_{Exp}/(EJ)_{EC5}$  greater than one were observed for tests with single threaded screws. The highest values were reached in tests D2 (1.17) and E2 (1.12), characterised by having a “special washer” (see Figure 4-14). This extra stiffness appeared to be related to the high level of pressure exerted by this fastener type. Furthermore, from the comparison of test D1 with test D3 (same element size and type of fasteners), a +13.30 % variation in bending stiffness was observed in test D1, where the assembly procedure was correctly applied (specimen D3 was assembled without respecting the correct order specified by the CP procedure). More details on the correlation between the beam flexural stiffness and the screw pressure are given in the next Chapter.

#### 4.4.1 HARDWOOD-HARDWOOD SOLUTIONS

Six TTC floors entirely made of beech LVL components were tested. With regard to the geometry of the samples, two configurations were taken into account. More specifically, while the same beech LVL panel (40 mm thick) was used for all tests, two beam sizes were considered: 160 x 240 mm<sup>2</sup> (tests D) and 120 x 200 mm<sup>2</sup> (tests E). The connection system was realized by using the same number (104) and type of single threaded screws (10 x 220 mm<sup>2</sup>) but considering different washer arrangements.

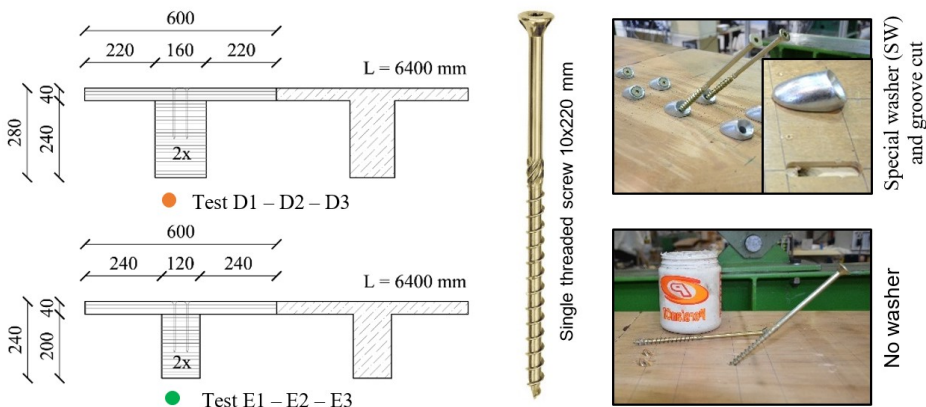


Figure 4-14 Hardwood-hardwood configurations

The results from the hardwood-hardwood specimens are reported below. As expected, D tests exhibited higher load capacity and flexural stiffness (Figure 4-15). Conversely, the adoption of a slender beam (as in tests E) permits to obtain greater camber values (up to 25.52 mm). This resulted in a more effective solution within the range of interest

( $0 < w < w_{SLS}$ ). Despite tests E are characterised by a relatively low structural height ( $L/h = 26.7$ ), a large load capacity was observed in all tests ( $q_{max} > 38 \text{ kN/m}^2$ ).

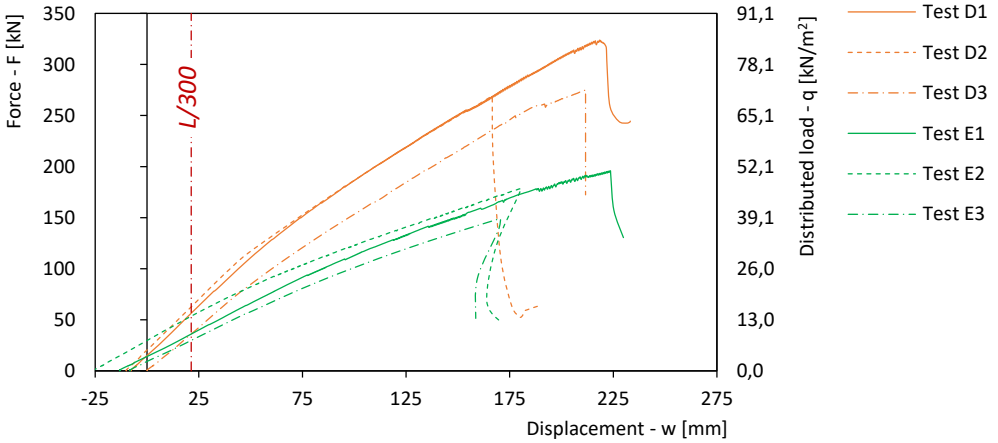


Figure 4-15 Result comparison: hardwood - hardwood solutions

As highlighted in Figure 4-16, the use of a washer (SW) mainly designed for steel-to-timber connection (tests D2 and E2) has proven to be the best solution in terms of both camber value and flexural stiffness. Therefore, the development of an optimised washer for timber-to-timber inclined connections could result in the complete elimination of the groove cuts and in a performance increase. With reference to Figure 4-15, test E3 exhibited a smaller uplift because of local misalignments between the predrilled holes in the panel and in the beam. Such misalignment resulted in a decreased compression force exerted by several of the fasteners. For this reason, test E3 was not considered in the comparison of Figure 4-16.

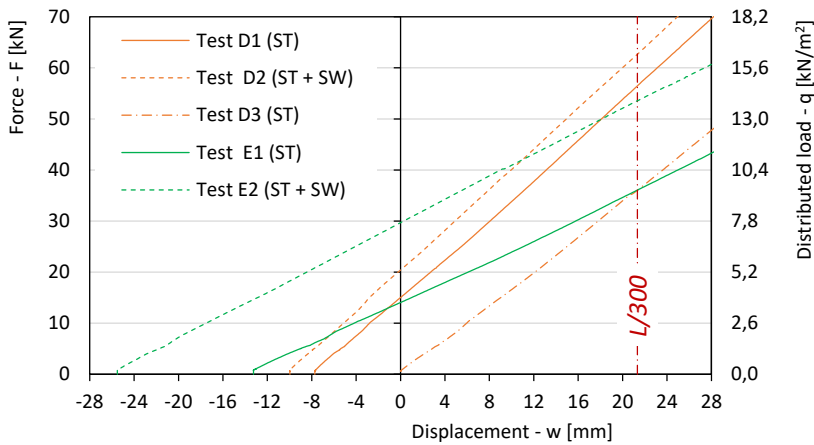


Figure 4-16 Result comparison: hardwood - hardwood solutions ( $w_{CP} < w < w_{SLS}$ )

From the comparison of test D3 (“traditional” assembly method) with tests D1 and D2 (CP procedure), the benefits introduced by the pre-stressing and cambering procedure appeared to be evident, especially for  $w < w_{SLS}$ , where for example test E2 performed better than tests D1 and D2, despite a “more slender” joist.

Figure 4-17 shows some pictures of the TTC beams where it is possible to note the large deformation occurred in these tests before reaching the failure condition.



Figure 4-17 Hardwood - hardwood composite solutions

#### 4.4.2 SOLUTIONS FOR RETROFIT INTERVENTION ON TIMBER DIAPHRAGMS

In this section, three alternative strategies for retrofit interventions on existing timber diaphragms are examined. The existing floor was simulated by using two different softwood beam cross-sections:  $160 \times 200 \text{ mm}^2$  (tests A and B) and  $180 \times 240 \text{ mm}^2$  (test

C). A layer of timber boards (20 mm thick) was placed in between the joist and the panel (only for tests A and B) to simulate the existing flooring (non-structural element).

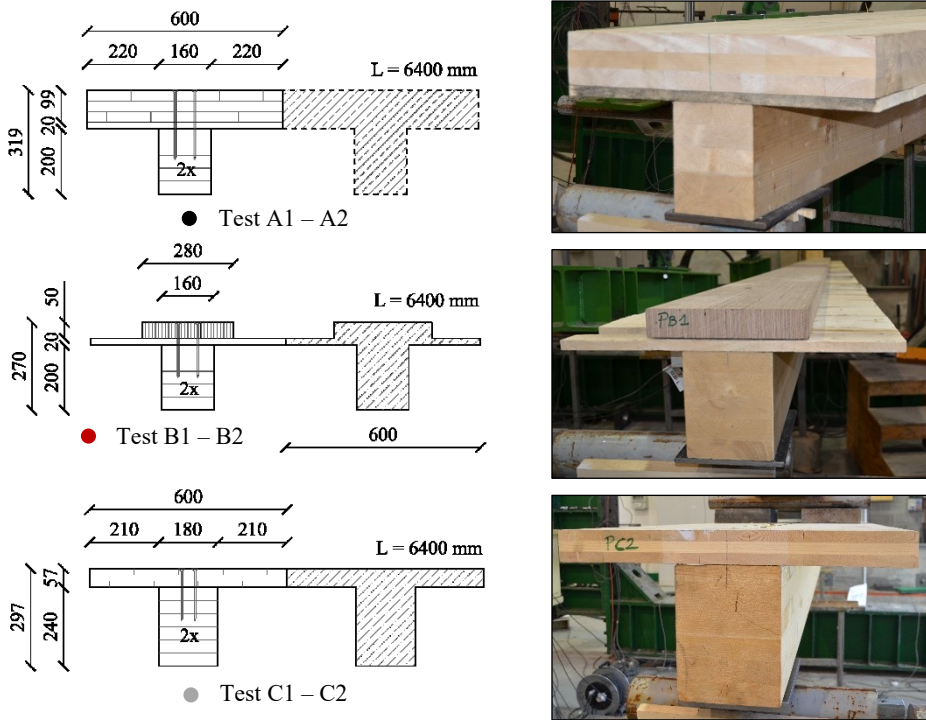


Figure 4-18 Solutions for retrofit intervention

The bending test results from all specimens are presented in Figure 4-19. Despite solution A can be used to camber existing beams affected by large deformation, tests A1 and A2 were designed to prove the potentiality of the assembly procedure. In fact, thanks to the larger panel thickness (if compared to test type C) longer DT screws can generating a higher compression force can be adopted. As a result, camber values ranging between 18.50 mm to 25.67 mm ( $L/257$ ) were registered. With reference to test A1, an equivalent distributed load  $q_0$  (required to eliminate the upward deflection induced by the CP procedure) greater than  $13.5 \text{ kN/m}^2$  was observed.

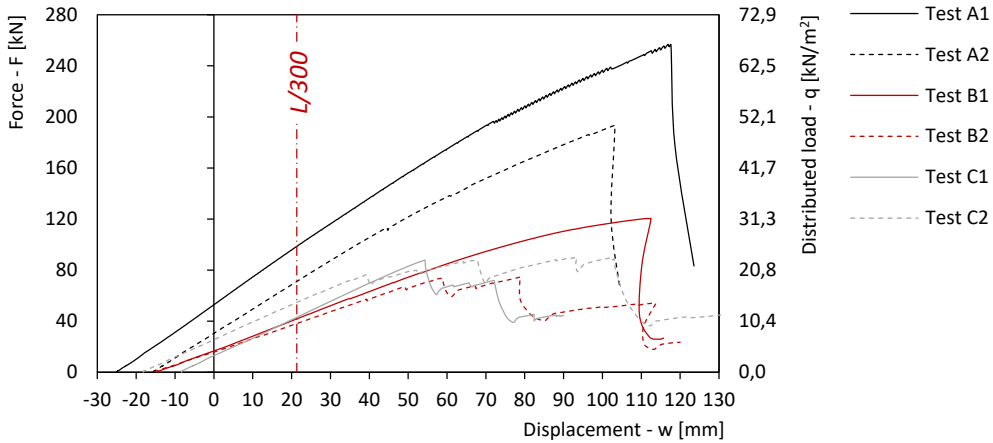


Figure 4-19 Result comparison: retrofit solutions

For  $w < L/300$ , a similar qualitative behaviour was obtained for tests B1, B2 and C1 (Figure 4-20). With respect to test C1, the adoption of single threaded screws in test C2 permitted to increase the camber value (+117.96 %) and also the  $q_0$  value (+96.45 %). Conversely, for thicker panels (as in A configurations) the use of double threaded screws appeared to be more effective.

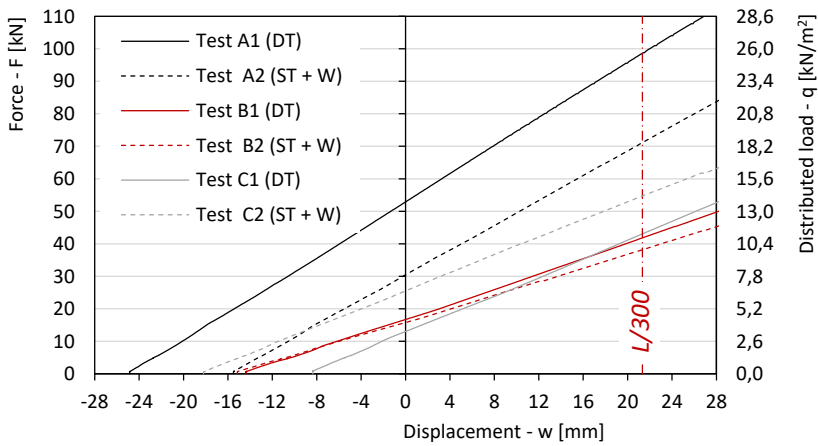


Figure 4-20 Result comparison: retrofit solutions ( $w_{CP} < w < w_{SLS}$ )

### 4.4.3 HYBRID SOLUTIONS VS. HARDWOOD-HARDWOOD SOLUTIONS

Four different configurations are considered in this paragraph. Two of these (tests D and E) are entirely made of beech LVL components, while the other two solutions (tests G and F) are characterized by having a softwood CLT panel (57 mm thick) instead of a beech LVL panel (40 mm thick).

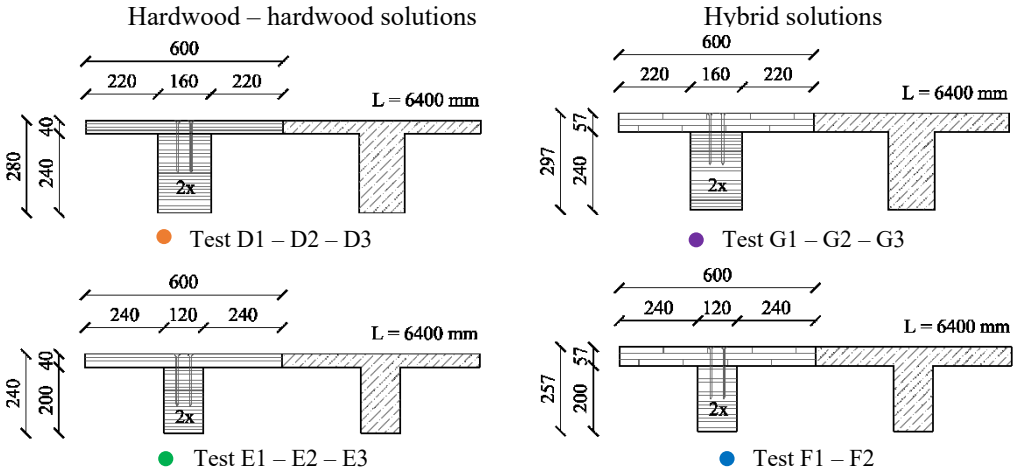


Figure 4-21 Hardwood-hardwood and softwood-hardwood configurations

### TESTS D VS. TESTS G

As shown in

Figure 4-22, tests D and tests G (the same joist element was used) exhibited a similar flexural behaviour both in terms of bending stiffness and load capacity. As already shown in the previous section, for hardwood-hardwood configurations the best results in term of camber values (-9.96 mm) and  $q_0$  (5.31 kN/m<sup>2</sup>) were found for test D2, where single threaded screws coupled with washers mainly designed for steel-to-timber connections (SW) were adopted (Figure 4-23). With reference to the hybrid configurations, the use of double threaded screws has proven to be the best solution. For midspan displacement values not exceeding ~50 mm, tests G1 and D2 showed approximately the same behaviour.

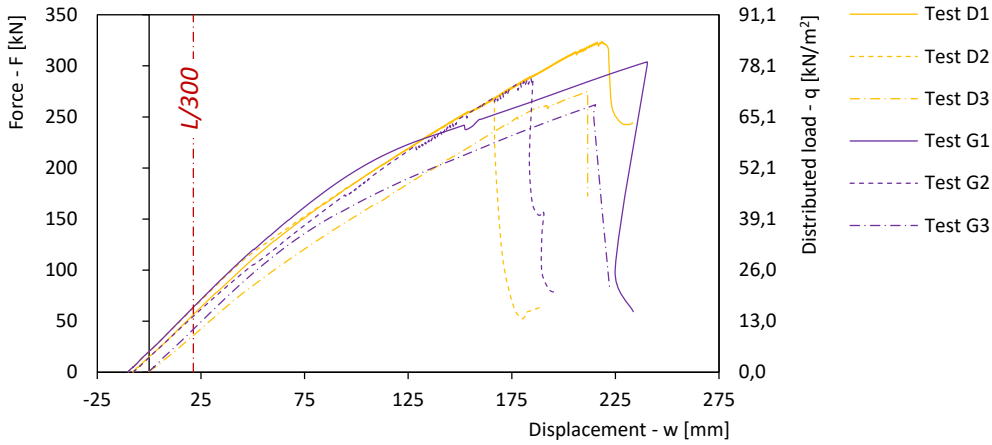


Figure 4-22 Result comparison: tests D Vs. tests G

Double threaded fasteners were not used in hardwood-hardwood configurations (tests D and E) due to the small thickness of the beech LVL panels (40 mm). Indeed, the effectiveness of this type of device is strictly related to the thickness of the coupled elements.

As can be seen in Figure 4-23, the adoption of the CP procedure permitted to increase the performance of all configurations, maintaining unchanged the total number of fasteners (it is worth reminding that the CP procedure was not adopted for test D3 and test G3).

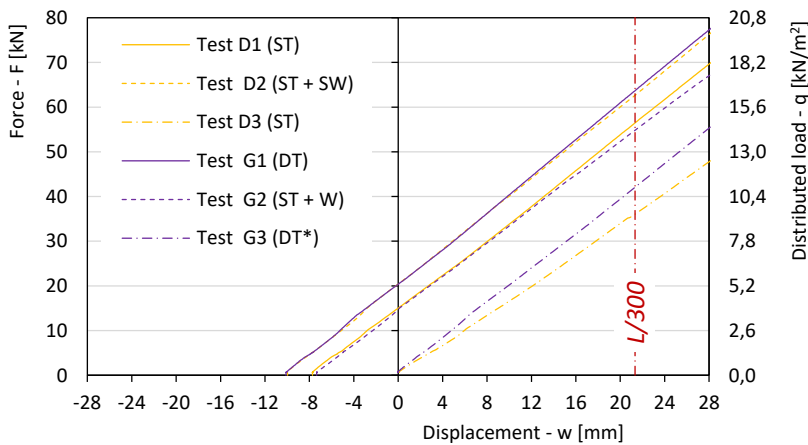


Figure 4-23 Result comparison: tests D Vs. tests G ( $w_{CP} < w < w_{SLS}$ )

In conclusion, despite a similar level of performance was observed for tests D2 and G1, the hybrid configuration where a softwood panel is coupled with a hardwood joist by means of DT screws appeared to be the best solution for the following reasons:

- Weight decrease: softwood CLT panel 57 mm thick is lighter than Beech LVL panel 40 mm thick (~25 %);
- Cost reduction (softwood CLT panels are usually less expensive than beech LVL panels);
- Time consuming: no groove cuts are required for DT screws.

### TESTS E VS. TESTS F

Similarly to what observed for tests D and G, a consistent behaviour was found from the comparison of the hardwood-hardwood solutions (tests E) with the hybrid solutions (tests E), for the configurations designed to have a reduced joist height (for tests E and F the SLS limit criterion can only be met by taking into account the camber). The use of single threaded screws coupled with the “special” washer confirmed to be the best solution in order to exploit the remarkable mechanical properties of beech LVL elements in hardwood-hardwood configurations (test E2).

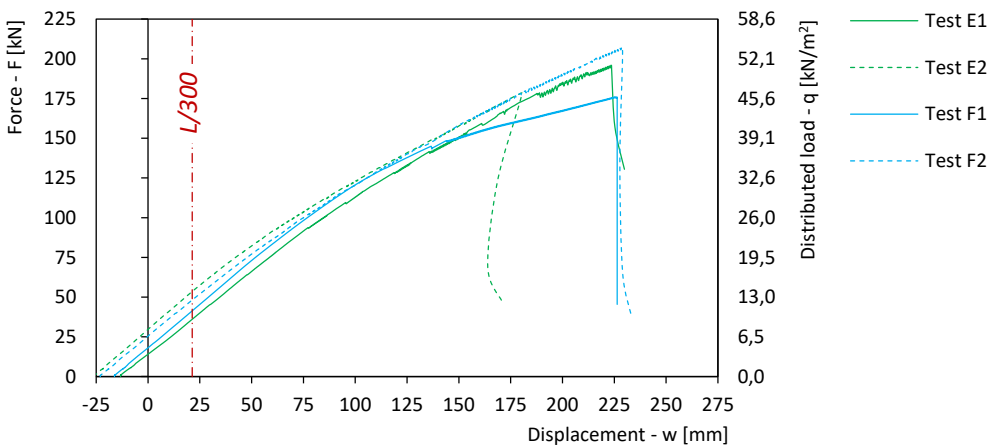


Figure 4-24 Result comparison: tests E Vs. tests F

Differently from what observed from the analysis of the G hybrid configurations, for test F (also hybrid) the use of single threaded screws (test F2) permitted to obtain the maximum value of camber (Figure 4-25), despite the same type and size (8.5 x 150 mm<sup>2</sup>) of double threaded screws were used in both tests F1 and G1.

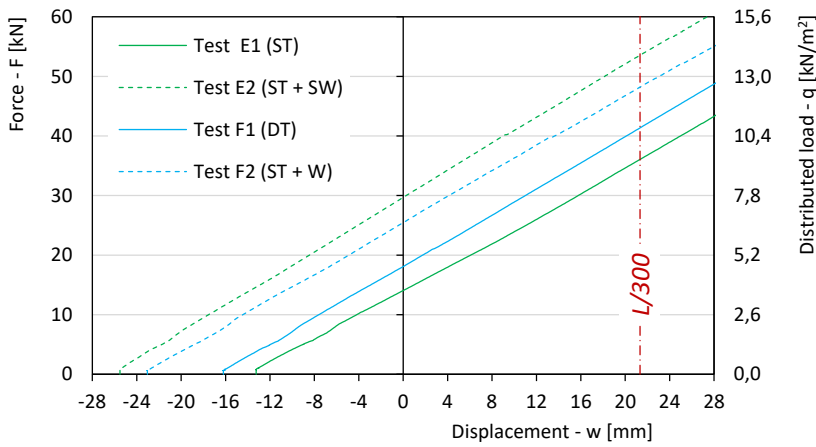


Figure 4-25 Result comparison: tests E Vs. tests F ( $w_{CP} < w < w_{SLs}$ )

However, the best performance in terms of bending stiffness was reached by test F1 ( $3.85 \cdot 10^{12}$  Nmm<sup>2</sup>), confirming the reliability of the hybrid system assembled by means of double threaded screws.



Figure 4-26 Hybrid configuration: Test F2

## 4.5 REFERENCES

- [1] Turrini, G., Piazza, M. (1983) A technique for stiffness and strength upgrading of wooden floors. *Recuperare*, vol. 5, pp. 224–237 (in Italian).
- [2] Turrini, G., Piazza, M. (1983a) Static behaviour of timber-concrete composite structures. *Recuperare*, vol. 6, pp. 214–225 (in Italian).
- [3] Ceccotti, A. (1995) Timber-concrete composite structures. *Timber engineering STEP 2*, H. Blass, et al., ed., 1st Ed., Centrum Hout, Netherlands, E13/1–E13/12.
- [4] Jorge L. F., Schänzlin J., Lopes S. M. R., Cruz H., Kuhlmann U. (2010) Time-dependent behaviour of timber lightweight concrete composite floors. *Engineering Structures*, vol. 32, pp. 3966–3973.
- [5] Yeoh, D., Fragiaco M., Deam B. (2011) Experimental behaviour of LVL–concrete composite floor beams at strength limit state. *Engineering Structures*, vol. 33 pp. 2697–2707.
- [6] Rautenstrauch K., Mueller J., Simon A. (2010) The first timber-concrete composite road bridge in Germany. *Proceedings of the World Conference on timber Engineering (WCTE)*, Riva del Garda, Italy.
- [7] Giongo I., Piazza M., Tomasi R. (2012) Out of plane refurbishment techniques of existing timber floors by means of timber to timber composite structures. *Proceedings of the World Conference on timber Engineering (WCTE)*, Auckland, New Zealand.
- [8] Giongo I., Piazza M., Tomasi R. (2012) Cambering of timber composite beams by means of screw fasteners. *Journal of Heritage Conservation*, vol. 32, pp. 133–136.
- [9] Giongo I., Schiro G., Piazza M., Tomasi R. (2016) Long-term out-of-plane testing of timber floors strengthened with innovative timber-to-timber solutions. *Proceedings of the World Conference on timber Engineering (WCTE)*, Vienna, Austria.
- [10] Schiro G., Giongo I., Sebastian W., Riccadonna D., Piazza M. (2018) Testing of timber-to-timber screw-connections in hybrid configurations. *Construction and Building Materials*, vol. 171, pp. 170–186.
- [11] European Committee for Standardization (2014). EN 1995-1-1:2004+A2:2014: Eurocode 5 - Design of timber structures, Part 1-1, General - Common rules and rules for buildings. CEN, Brussels, Belgium.
- [12] ETA (European Technical Approval) 14/0354: Glued laminated timber made of hardwood – Structural laminated veneer lumber made of beech.
- [13] European Committee for Standardization (2013). EN 14080: Timber structures – Glued laminated timber and glued solid timber. CEN, Brussels, Belgium.

- [14] Certificate of performance No. 0672-CPR-0415 (MPA Stuttgart 0672).
- [15] ETA (European Technical Approval) 12/0347: X-Lam Dolomiti – CLT.
- [16] European Committee for Standardization (2010) EN 408: Timber Structures – Structural timber and glued laminated timber – Determination of some physical and mechanical properties. CEN, Brussels, Belgium.
- [17] ETA (European Technical Approval) 11/0190: Würth self-tapping screws.
- [18] ETA (European Technical Approval) 12/0121: HECO-TOPIX-T and HECO-TOPIX-CC self-tapping screws.

# 5 NEW HIGH-PERFORMANCE TTC FLOOR-MODULES REALIZED WITH BEECH LVL: DESIGN AND TESTING

## 5.1 INTRODUCTION

Starting from the results achieved in the previous sections, in this chapter the development of high-performance solutions for prefabricated timber-to-timber composite floor modules to be realised by using laminated veneer lumber (LVL) made of beech wood is presented.

The Cambering-Prestressing (CP) procedure, previously analysed in Chapter 2 and used in Chapter 4, is considered in this section to maximise floor efficiency and to exploit the remarkable strength properties of hardwood products.

*Table 5-1 Mechanical properties of different timber elements*

Element type and grading			Beech LVL	Spruce	Beech LVL	Spruce
			GL70	Glulam GL24	panel	CLT panel
			[3]	[4]	[5]	[6]
Bending:	$f_{m,k}$	[N/mm <sup>2</sup> ]	70	24	80	24
Tension:	$f_{t,0,k}$	[N/mm <sup>2</sup> ]	55	19.2	60	14
	$f_{t,90,k}$	[N/mm <sup>2</sup> ]	0.6	0.5	1.5	0.12
Compression:	$f_{c,0,k}$	[N/mm <sup>2</sup> ]	59.4	24	57.5	21
	$f_{c,90,k}$	[N/mm <sup>2</sup> ]	10.2	2.5	14	2.5
Shear:	$f_{v,k}$	[N/mm <sup>2</sup> ]	4	3.5	8	3.3
MoE	$E_{0,mean}$	[N/mm <sup>2</sup> ]	16700	11500	16800	12000
Density:	$\rho_{mean}$	[kg/m <sup>3</sup> ]	≥ 740	420	800	450-500

To better understand the potentialities of this “new engineered wood product” ([1] and [2]), a comparison of the main mechanical properties (from product documentation and international standards) of different wood products is proposed in Table 5-1.

As this table evidences, beech LVL exhibits an extremely high strength if compared to a traditional softwood product ( $f_{m,k} = +191.68\%$ ). Despite this, the increase in MoE (+45.22%) is not so pronounced when compared to the increase in mean density ( $\geq 76.19\%$ ). Therefore, to exploit the material qualities, pre-stressing of the modules was adopted by using the CP assembly procedure presented in Chapter 2. Figure 5-1 shows the static efficiency of different wood products compared with structural steel grade S355. Also in this case, the “*specific strength*” (strength-to-weight ratio) shown by hardwood elements confirmed the structural potentialities of this “new engineered wood product”.

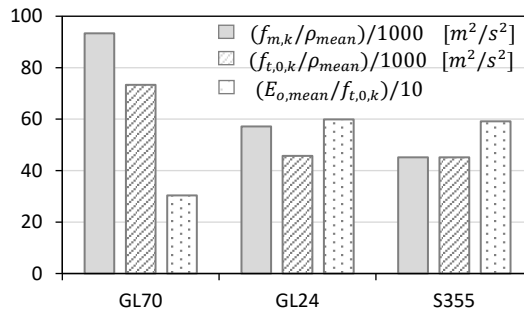


Figure 5-1 Static efficiency comparison

The research program was divided in three steps. The first phase was dedicated to the analysis and comparison of the mechanical performance (see Chapter 3) of a wide range of fastener typologies, not necessarily timber fasteners only. The results of the experimental tests aimed at defining the mechanical behaviour of the screw anchor fastener that was selected as optimal (Figure 5-3) are reported in the next sections.

The second phase was focused on designing the element sections for realizing pre-fabricated floor modules. Numerical modelling and analytical procedures were based on the experimental inputs from the testing campaign on the connections.

Two structural applications were considered:

- 6 m long diaphragms for residential buildings (Eurocode 1 [8] – Cat. A);
- 10 m long diaphragms for office areas, schools, restaurants, hall (Eurocode 1 [8] – Cat. B, C1).

The last phase of this research activity was dedicated to the full-scale testing of the solutions defined in the design phase. The tests, performed by assuming a four-point loading scheme (six-point bending test), consisted in monotonic loading up to the beam failure for the 6 m long modules and semi-cyclic loading (up to a load level twice as much the design load at ultimate limit state conditions) for the 10 m long modules.

The study presented in this chapter was part of the research project “FLOORitHARDWOOD”. It involved the partnership between the Department of Civil, Environmental and Mechanical Engineering (DICAM) of the University of Trento, the Italian Ministry of University and Research (MIUR), Pollmeier GmbH & Co. KG and Heco Italia Efg Srl.



*Figure 5-2 FLOORitHARDWOOD project*

## 5.2 CONNECTION TESTING

To define an optimal fastener, multiple aspects had to be considered [8]: strength, stiffness, ability to develop a compression force (CP procedure), ease of assembly, cost effectiveness. Furthermore, the definition of such parameters strongly depend on the connection configuration (angle between the fastener and the load direction) and the density of the elements to be connected (for timber-timber connections).

The screw type fasteners available on the market, which are usually developed for use in softwood elements, have demonstrated to perform “poorly” when employed in hardwood components, as proved by the experience of Schiro et. al [8] (see Chapter 3). For these reasons, the connector device that was selected as optimal is a screw anchor [8] that was designed for use in concrete. As shown in Heco Multi-monti MMS-S 12 [7], this fasteners has a shank diameter equal to 9.4 mm and a thread diameter of 12 mm. The total length is 180 mm while the threaded part in 120 mm long. Having been developed for application in high-density material, such connector is not fitted with a tip and therefore all fasteners were inserted with a predrill of diameter 10 mm,

thoroughly cleaned before the insertion of the screw anchors. The hexagon head permits to exert high level of torque moment avoiding problems on the bit-hole inside the screw head. Moreover, for the reasons that will be presented in the following, a flat washer ( $\varnothing$  24 mm) was used.

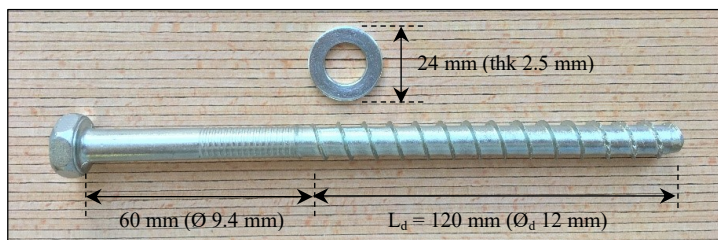


Figure 5-3 Heco Multi-monti MMS-S 12 [7]

The correct evaluation of the slip modulus of the connection (both for the shear-tension and shear-compression configuration), and the value of “compressive pre-load” that the fastener is able to induce in the two jointed timber elements is crucial to the correct design of TTC floor assembled with the CP procedure. For this reason, three types of test were performed:

- Pull-out tests;
- Screw pressure tests;
- Push-out tests.

The results of the experimental tests aimed at defining the mechanical behaviour of the screw anchor fastener that was selected for the realisation of the samples (Figure 2 1) are reported below.

### 5.2.1 PULL-OUT TESTS

Every test specimen was subjected to quasi-static monotonic loading under displacement control, maintaining a constant rate of slip of 0.05 mm/s in accordance with EN 12512 [10]. The load, introduced by a hydraulic actuator (universal testing machine), was monitored with a 100 kN load cell. The fastener relative displacement was measured as the difference between the machine displacement (in addition to the machine’s own measuring system, a LVDT transducer was used in order to have a redundant measure) and the timber specimen uplift (monitored with an AEP transducer).

The investigated test parameters were:

- Embedment depth of the threaded part  $L_d$ : 40 – 60 – 80 – 100 – 120 mm (full thread);
- Screw-to-grain angle  $\alpha$ : 90° – 45°;
- Use of grease for screw insertion: with or without grease.



Figure 5-4 Pull-out test setup for 90° and 45° screw-to-grain angle

**CONFIGURATION A |  $\alpha = 90^\circ$  - WITHOUT GREASE**

The test results in terms of load-displacements curves are reported in Figure 5-5:

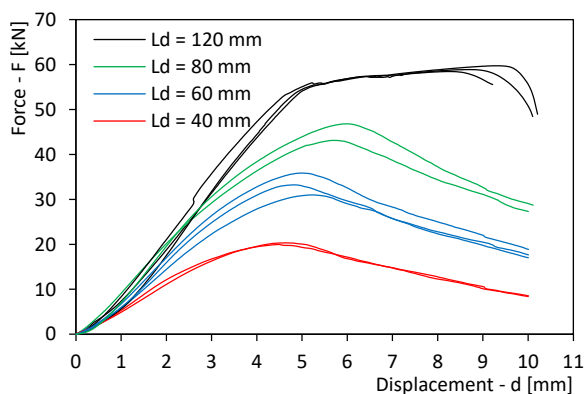


Figure 5-5 Load-displacement curves for 90° screw-to-grain angle - without grease

Positive correlations between embedment depth ( $L_d$ ) and withdrawal capacity ( $F_{ax}$ ) or axial stiffness ( $K_{ax}$ ) were registered (see Figure 5-6, with  $L_d$  in mm,  $F_{ax}$  in kN and  $K_{ax}$

in N/mm). The  $R^2$  values (square of the Pearson's product-moment correlation coefficient) are reported in the graphs of Figure 5-6. Both  $F_{ax}$  and  $K_{ax}$  were calculated according to the EN 12512 [10].

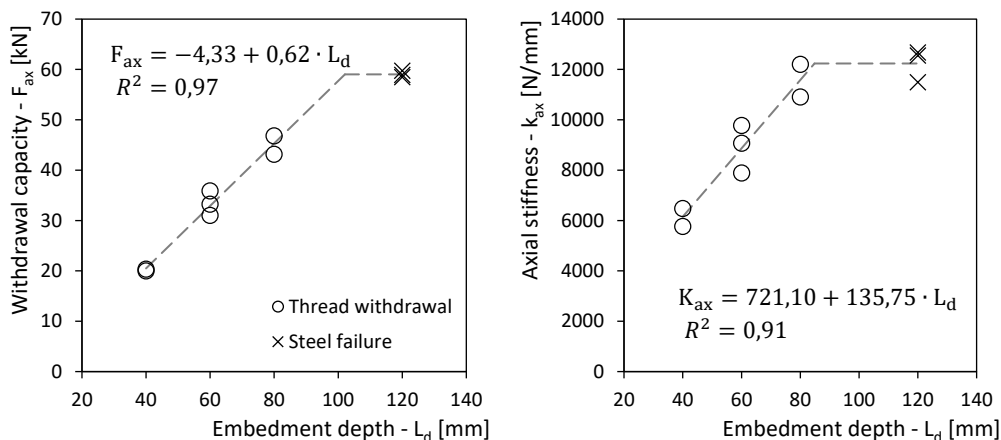


Figure 5-6 Withdrawal capacity and axial stiffness for 90° screw-to-grain angle - without grease

For embedment depths between 40 and 80 mm, thread withdrawal was observed. Differently, for  $L_d = 120\text{ mm}$  steel failure in screw shank was registered. Consistently with the mean tensile resistance of MMS-12 anchors ( $N_{R,mean} = 60\text{ kN}$ ) provided by the producer [7], a maximum axial load equal to 59.5 kN was registered (steel failure) for a penetration length of 120 mm.

**CONFIGURATION B |  $\alpha = 45^\circ$  - WITHOUT GREASE**

The test results in terms of load-displacements curves are reported in Figure 5-7:

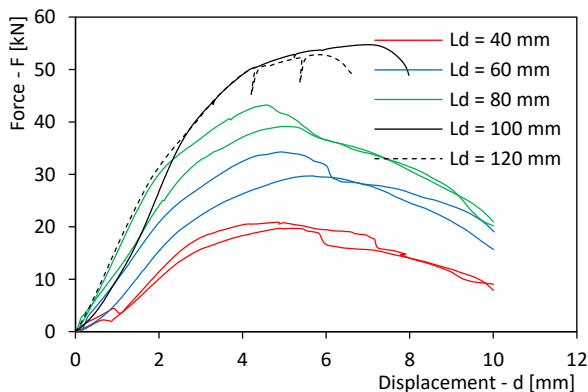


Figure 5-7 Load-displacement curves for 45° screw-to-grain angle without grease

Positive correlations between embedment depth ( $L_d$ ) and withdrawal capacity ( $F_{ax}$ ) or axial stiffness ( $K_{ax}$ ) were registered (see Figure 5-8, with  $L_d$  in mm,  $F_{ax}$  in kN and  $K_{ax}$  in N/mm). The  $R^2$  values are reported in the graphs of Figure 5-8.

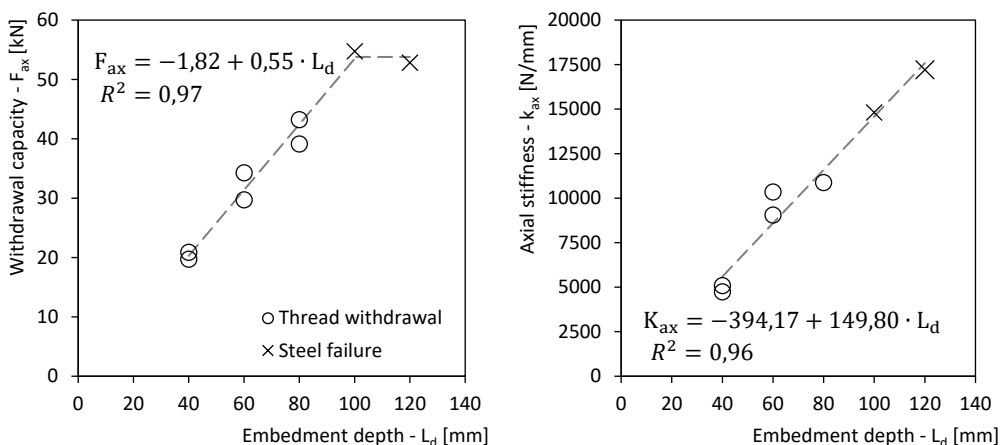


Figure 5-8 Withdrawal capacity and withdrawal stiffness for 45° screw-to-grain angle without grease

Also in this case, for embedment depths between 40 and 80 mm, thread withdrawal was observed. Differently, for  $L_d$  equal to 100 mm and 120 mm steel failure in screw shank was shown.

**CONFIGURATION C |  $\alpha = 45^\circ$ - WITH GREASE**

The test results in terms of load-displacements curves are reported in Figure 5-9:

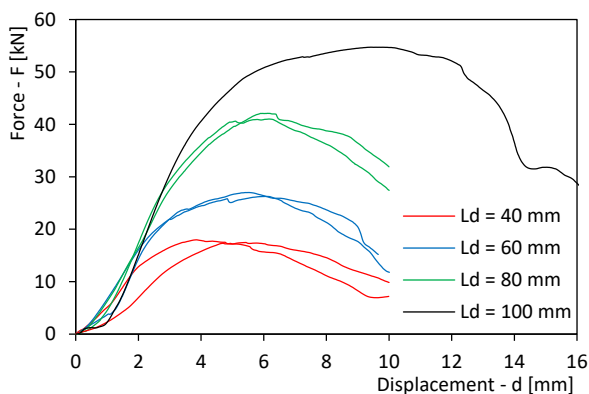


Figure 5-9 Load-displacement curves for 45° screw-to-grain angle with grease

Positive correlations between embedment depth ( $L_d$ ) and withdrawal capacity ( $F_{ax}$ ) or axial stiffness ( $K_{ax}$ ) were registered (see Figure 5-10, with  $L_d$  in mm,  $F_{ax}$  in kN and  $K_{ax}$  in N/mm). The  $R^2$  values are reported in the graphs of Figure 5-10.

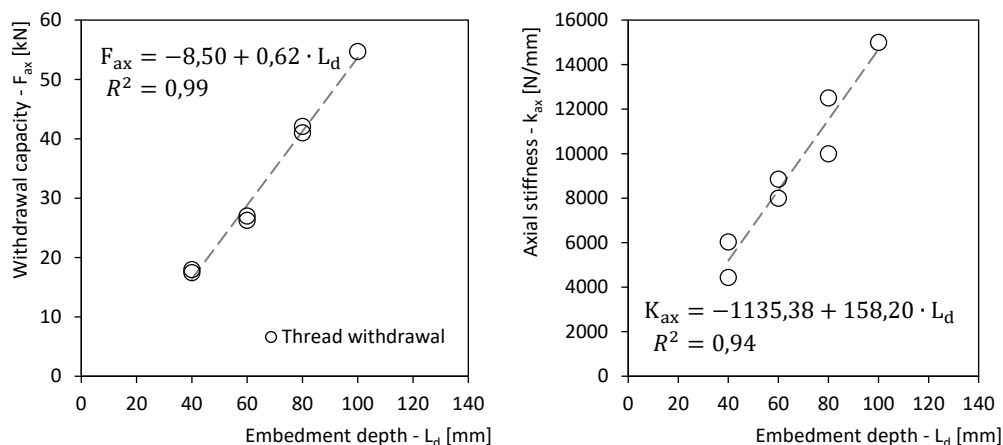


Figure 5-10 Withdrawal capacity and withdrawal stiffness for  $45^\circ$  screw-to-grain angle with grease

With reference to the failure modes, thread withdrawal was observed for all tests ( $40 \text{ mm} \leq L_d \leq 100 \text{ mm}$ ).

## RESULT COMPARISON

Generally, for an embedment depth of the threaded part greater than 100 mm, failure modes characterized by tensile rupture of the screw shank were observed. For embedment depths smaller than 100 mm, failure modes related to the thread withdrawal were instead registered. A comparison of the outcomes from the pull-out tests is given in Figure 5-11.

Tests with a screw-to-grain angle of  $45^\circ$  exhibited a lower maximum load with respect to the  $90^\circ$  tests. As concerns the  $45^\circ$  configurations, tests with grease showed lower withdrawal capacity than the tests without grease. This difference appeared to be more pronounced for limited values of the embedment depth of the threaded part.

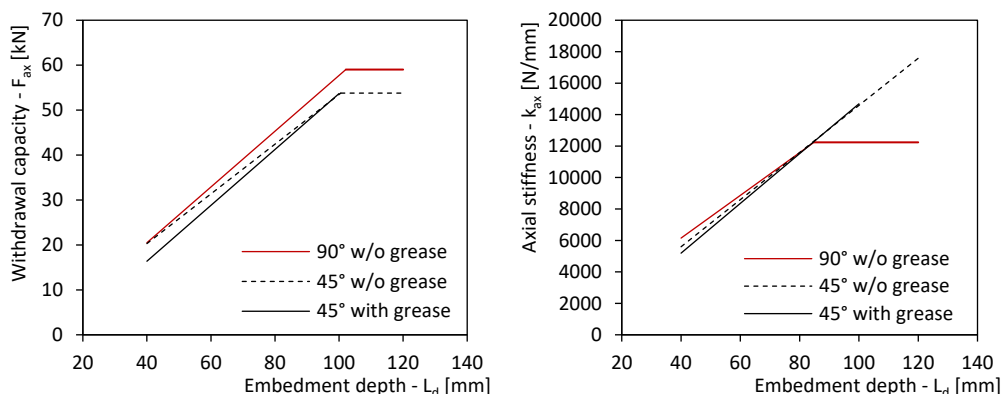


Figure 5-11 Withdrawal capacity and axial stiffness for all the configurations analysed

With regard to the withdrawal stiffness, 90° tests presented a plateau for embedment depth higher than 80 mm, while for 45° tests, both with or without grease, the axial stiffness value continue to increase also for embedment depth higher than 80 mm. This could be related to the different failure mode associated with the thread withdrawal that was observed for the two configurations, as can be seen from Figure 5-12.

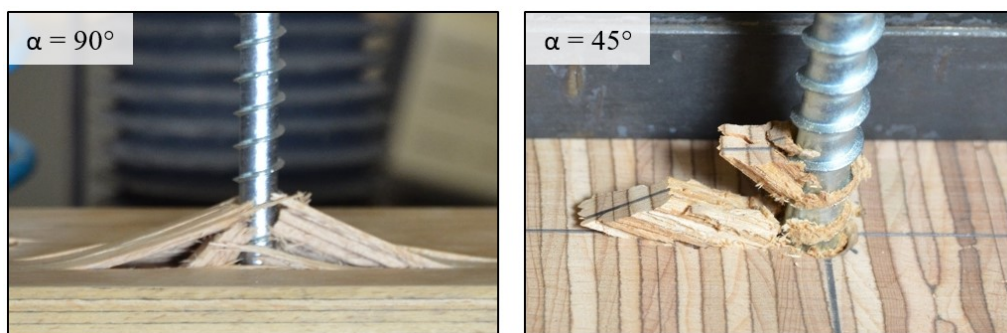


Figure 5-12 Failure modes for 90° and 45° configurations

## 5.2.2 FASTENER PRELOAD TESTS

As shown in Figure 5-13, to estimate the compressive force induced by the fastener, a 100 kN load cell was placed between the two timber elements. All tests were performed considering an embedment depth of the threaded part equal to 120 mm (corresponding to the maximum threaded length for the fastener used in the experimental campaign).

The axial force generated by the fastener was monitored for a period of approximately two minutes ( $F_{stab}$ ) after reaching the peak load ( $F_{Max}$ ). Three tests were also monitored for a period of three days in order to investigate the load relaxation over time

for different screw configurations. If not differently specified, a flat steel washer was used ( $\text{Ø} = 24 \text{ mm}$ , 2.5 mm thick).

The investigated parameters of these tests are:

- Fastener-to-grain angle  $\alpha$ :  $90^\circ - 45^\circ$ ;
- Use of different types of screwdriver.
- Use of grease for screw insertion: with or without grease;
- Use of washer: with or without washer ( $\text{Ø} 24 \text{ mm}$ ).



Figure 5-13 Screw preload test setup for  $90^\circ$  and  $45^\circ$  screw-to-grain angle

### FASTENER-TO-WOOD GRAIN ANGLE (WITH GREASE)

No significant differences in terms of compressive pre-load induced by the single fastener were noticed ( $F_{stab}$ ) when varying the fastener-to-grain angle (see Figure 5-14). In all tests a pneumatic gun was employed for the screw insertion.

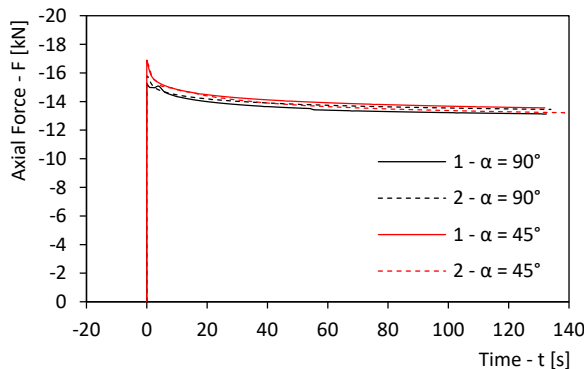


Figure 5-14 Compressive pre-load for  $90^\circ$  and  $45^\circ$  fastener-to-grain angle configurations

The results are summarized in *Table 5-2*:

Table 5-2 Compression force exerted by the fasteners (with grease)

	$\alpha = 90^\circ$		$\alpha = 45^\circ$	
	F <sub>Max</sub> [kN]	F <sub>stab</sub> [kN]	F <sub>Max</sub> [kN]	F <sub>stab</sub> [kN]
1°	15.22	13.40	16.86	13.92
2°	15.77	13.74	16.69	13.59
Mean	15.50	13.57	16.75	13.76

**TORQUE-AXIAL FORCE RELATION (WITHOUT GREASE)**

By using a torque wrench, a linear relation between the insertion torque [Nm] and the maximum axial force [kN] generated by the fastener was found. The tests were performed without grease for the fastener insertion. As shown in Figure 5-15, no differences were observed from 90° to 45° configurations.

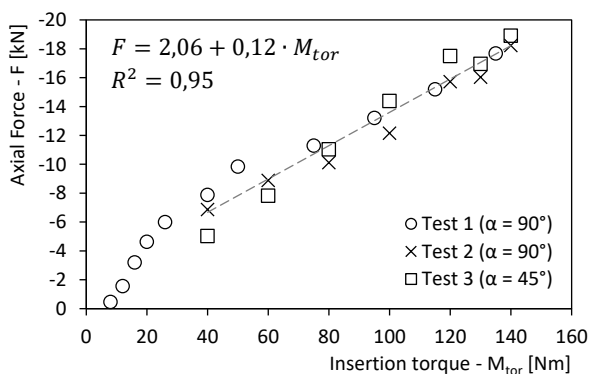


Figure 5-15 Compressive preload and insertion torque relation

A maximum torsional moment equal to 140 Nm was applied during testing. Despite this value exceeds the nominal capacity of the connector (120 Nm), no screw failure was experienced. This was attributed to the fact that a considerable amount of torque is required to overcome friction. Besides, a significant part of the torsional stress dissipates as soon as the insertion is completed. Anyways, for the design a maximum torque of approximately 90 Nm was considered, which should guarantee an adequate safety margin.

### POWER DRIVEN TOOLS (90° - WITH GREASE)

The compression force exerted by three different types of power driven tools is analysed in this section. Grease was used in all tests to ease the insertion procedure. A fastener-to-grain angle of 90° was considered.

The tools tested are (Figure 5-15):

- Drill A: Impact screwdriver (*mod. Milwaukee HD 18 HIW*);
- Drill B: Torque drill (*mod. Milwaukee HDE 13 RQD*);
- Drill C: Air impact wrench (*mod. Chicago Pneumatic RP 9540-B*).



A: Milwaukee HD 18 HIW  
([www.milwaukeetool.com](http://www.milwaukeetool.com))



B: Milwaukee HDE 13 RQD  
([www.milwaukeetool.com](http://www.milwaukeetool.com))



C: Chicago Pneumatic RP 9540-B  
([www.cp.com](http://www.cp.com))

Figure 5-16 Driven tools

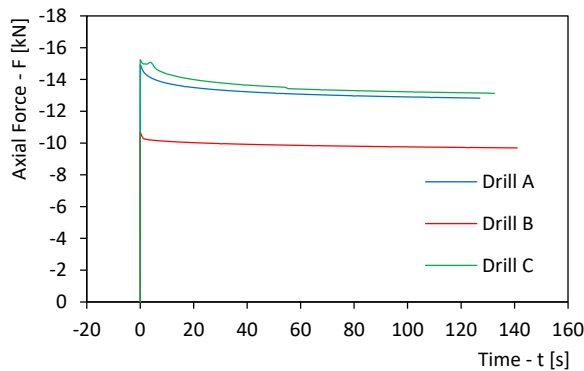


Figure 5-17 Drill comparison for 90° fastener-to-grain angle, with washer and with grease configuration

The results (mean values) are shown in Figure 5-17 and summarized in Table 5-3.

Table 5-3 Compression force exerted by the fasteners (different driven tools was used)

Drill	F <sub>Max</sub> [kN]	F <sub>stab</sub> [kN]
A	14.92	13.08
B	10.65	9.85
C	15.22	13.40

As a result, the air impact wrench (Drill C) proved to be the best tool to achieve highest possible values of axial force, as it presents the advantage of having no limitations due to overheating or battery discharge.

### USE OF LUBRICANT

As presented in Figure 5-18, the use of a lubricant (i.e. common industrial grease), thanks to the reduced friction during the insertion, permitted to obtain higher values of axial force than the cases where the lubricant was not used (F<sub>stab</sub> = + 38.01%).

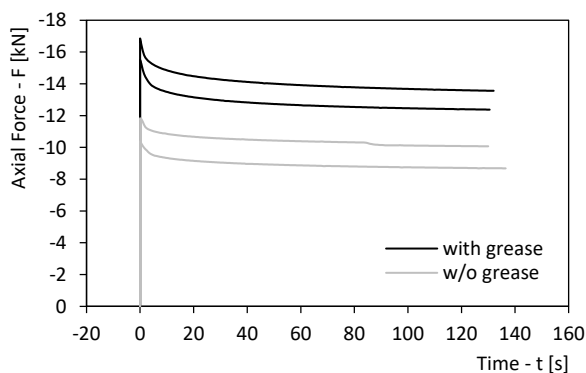


Figure 5-18 Compressive pre-load registered with grease and without grease

The results are reported in Table 5-4:

Table 5-4 Compression force exerted by the fasteners (with or without grease)

	With grease		Without grease	
	F <sub>Max</sub> [kN]	F <sub>stab</sub> [kN]	F <sub>Max</sub> [kN]	F <sub>stab</sub> [kN]
1°	16.86	13.92	10.39	8.87
2°	15.51	12.66	11.83	10.39
Mean	16.19	13.29	11.11	9.63

### COMPRESSION FORCE RELAXATION OVER TIME

In order to obtain preliminary information on the compression force relaxation over time, data from three tests were acquired continuously for a period of three days. Every test was assembled by using the air impact wrench (Drill C) and considering fastener-to-grain angle of  $45^\circ$ .

In particular, three different configurations were analysed:

- A: with grease, with washer;
- B: without grease, with washer;
- C: with grease, without washer.

The experimental evidences are reported in Figure 5-19 and Table 5-5.

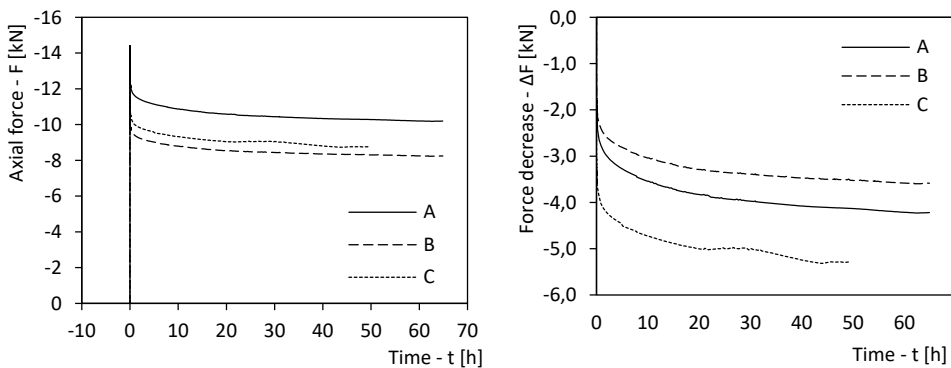


Figure 5-19 Compression force relaxation over time: long-term monitoring

As expected, tests with grease (A and C) exhibited significantly higher values of compression force than the test where no grease was used. However, the long term behaviour appeared not to be influenced by the use of lubricant. After 50 hours,  $\sim 30\%$  force decrease was observed for both the test with grease (A) and the test without (B). Otherwise, test without washer exhibited similar value of maximum axial force with respect to the test A, but greater relaxation over time ( $\sim 38\%$  after 50 hours).

Table 5-5 Compression force relaxation over time: long-term monitoring

Time	Test:	A	B	C
0 s	$F_{\text{Max}}$ [kN]	14.41	11.83	14.05
60 s	$F_{\text{stab}}$ [kN]	12.74 (-11.59%)	10.43 (-11.83%)	11.18 (-20.43%)
24 h	$F_{\text{LT}}$ [kN]	10.51 (-27.06%)	8.49 (-28.23%)	9.05 (-35.59%)
50 h	$F_{\text{LT}}$ [kN]	10.28 (-28.66%)	8.30 (-29.84)	8.76 (-37.65%)

Consequently, in order to maximise the compression force and minimize relaxation phenomena over time, the best solution was found to be the adoption of both lubricant and washer. It is worth noting that the force-reduction over time rate appeared to decrease rapidly. All the specimens in fact presented at the 50<sup>th</sup> hour of monitoring an almost horizontal force vs. time curve.

### 5.2.3 PUSH-OUT TESTS

The instrument arrangements and the experimental setup used in this section are shown in Chapter 3. Every specimen was subjected to quasi-static monotonic loading under displacement control maintaining a constant rate of slip of 0.05 mm/s (according to EN 12512 [10]). The load, introduced by a universal testing machine through a hydraulic actuator, was monitored with a 1000 kN cell. Two linear variable differential transducers (LVDTs) were employed to monitor the slip between the central and side elements and the total slip value was taken as the mean of the two measurements (Figure 5-20).

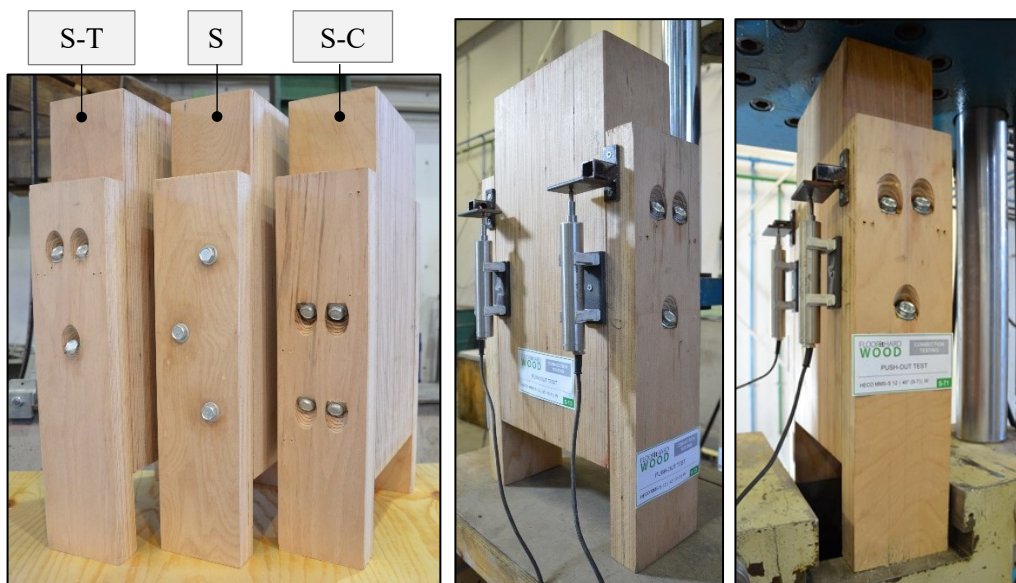


Figure 5-20 Push-out configurations

Three different fastener configurations were studied during this experimental campaign (three tests were performed for each configuration):

- Shear-tension (*S-T*): the fasteners were inserted at an angle of  $45^\circ$  with respect to the shear plane and were loaded under a shear-tension configuration;
- Shear-compression (*S-C*): the fasteners were inserted at an angle of  $-45^\circ$  with respect to the shear plane and were loaded under a shear-compression configuration;
- Shear (*S*): the fasteners were inserted at an angle of  $90^\circ$  with respect to the shear plane.

The results of the experimental campaign are reported in the graphs below.

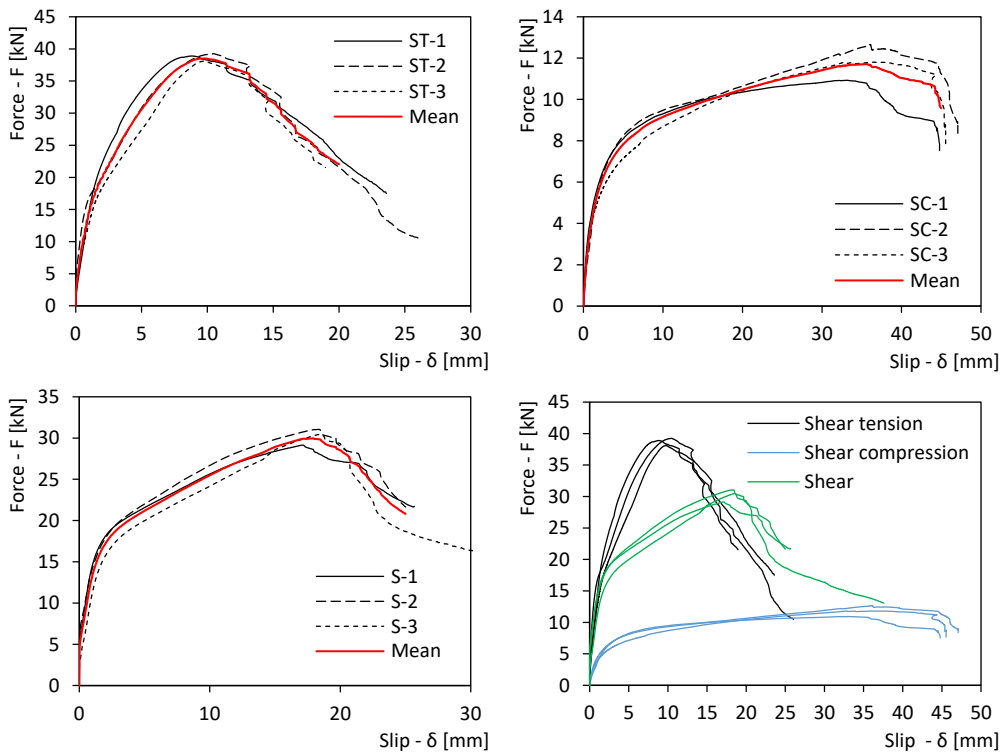


Figure 5-21 Push-out tests: load-slip curves

According to the EN 12512 [10] and EN 26891 [11], the mechanical properties of the connection systems were determined. The results are reported in Table 5-6.

Table 5-6 Push-out test results in terms of maximum load, slip modulus, yield point and ductility

Configuration		$F_{max}$ [kN]	$k_s$ [N/mm]	$F_y$ [kN]	$\delta_y$ [mm]	D
S-T	Mean	38.74	12572	20.66	1.48	11.3
	CoV	1.2%	18.5%	22.0%	28.7%	35.1%
S-C	Mean	11.80	3159	6.23	1.81	25.6
	CoV	6.0%	13.4%	8.8%	16.3%	14.8%
S	Mean	30.20	11807	17.95	1.34	17.9
	CoV	2.6%	20.5%	2.9%	21.1%	21.6%

Where  $F_{max}$  is the actual maximum load reached in each test,  $K_s$  is the slip modulus and  $F_y$  is the yield force. The slip modulus  $K_s$  of the connections (corresponding to the slip modulus  $K_{ser}$  provided by EN 1995-1-1 [12]) was calculated by means of the following equation [11]:

$$K_s = \frac{0.4 \cdot F_{max} - 0.1 \cdot F_{max}}{v_{0.4} - v_{0.1}} \quad (\text{Eq. 2})$$

where  $v_{0.1}$  and  $v_{0.4}$  are the connection slips (evaluated for each specimen) corresponding to loads equal to  $0.1 \cdot F_{max}$  and  $0.4 \cdot F_{max}$  respectively.

The ductility  $D$  was calculated as the ratio between ultimate slip and yield slip according to [10], where the ultimate slip  $\delta_u$  was assumed as the slip at 0.8 times  $F_{max}$  on the descending branch of the load-slip curve.

### 5.3 DESIGN PARAMETERS

Several aspects aimed at obtaining manifold objectives were considered in the design approach, including: material efficiency (taking into account product size availability), versatility of use, competitiveness when compared to non-composite floors or standard composite floors, ease of assembly, reduction of milling operations (e.g. groove cuts, pre-drills) and connection efficiency (i.e. reduced number of fasteners).

The international standards adopted to design the TTC floors here presented are:

- EN 1990: Basis of structural design [13];
- EN 1991: Actions on structures [9];
- EN 1995: Design of timber structures [12].

In the following sections, the permanent non-structural loads and the service loads considered in the design process of the innovative TTC floor modules are presented.

### DESIGN LOADS | PERMANENT LOADS

Self-weight of non-structural components applied to the floor modules:

Components	[kN/m <sup>3</sup> ]	[mm]	[kN/m <sup>2</sup> ]
Floor finish			0.35
Lightweight concrete screed	18	40	0.72
Water proofing layer			0.04
Gypsum-fiber panels (fire protection)	12	30	0.36
		Tot =	1.47

Self-weight of partitions: 1 kN/m<sup>2</sup> (self-weight  $\leq$  2.5 kN/m wall length), according to [9].

Total permanent non-structural load:  $g_{2,k} = 2.47$  kN/m<sup>2</sup>.

The self-weight of permanent structural elements was accounted for separately for each module solution.

### DESIGN LOADS | SERVICE LOADS

With reference to the characteristic service loads (live loads), according to the Table 6.1 of EN 1991 [9], two different categories were considered:

- TTC floor module 6 m span:  $q_k = 2$  kN/m<sup>2</sup> (Cat. A – Areas for domestic and residential activities);
- TTC floor module 10 m span:  $q_k = 3$  kN/m<sup>2</sup> (Cat. B and C1 – Office areas, schools, restaurants, dining halls, reading room).

### DESIGN PARAMETERS

According to the EN 1995 [12], the following deflection limit values were considered in the analysis for the Serviceability Limit States (SLS):

- Instantaneous deflection (live loads):  $w_{inst,Q} = L/400$ ;
- Final deflection:  $w_{net,fin} = L/300$ .

Where  $w_{inst,Q}$  is the instantaneous deflection due to the characteristic combination of the live loads (no permanent loads were considered) and  $w_{net,fin}$  is the final net deflection

measured from a straight line drawn between the supports due to the quasi-permanent combination of actions (see

Figure 5-22).

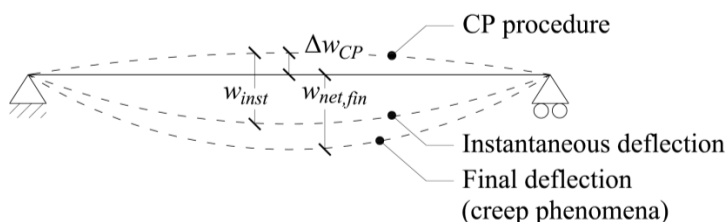


Figure 5-22 Components of deflection

As it will be presented in the following, thanks to the mechanical properties of beech LVL the satisfaction of the Ultimate Limit States (ULS) safety requirements does not represent a limiting factor in the design of the floor modules. Nonetheless, all safety checks prescribed in section 6 of EN 1995 [12] were verified and requirements satisfaction was ensured.

## 5.4 NUMERICAL AND ANALYTICAL MODELS

In order to define the optimal cross section of the timber elements as well as the number and the spacing of the fasteners, both the assembly and the loading phases had to be considered. To this aim, two design approaches were considered for the definition of the effects produced by the assembly procedure: a finite element simulation and an analytical model proposed by Giongo et al. (see Chapter 2). For the analysis of the mechanical behaviour of the prefabricated floors under vertical loads the results of the FE model was compared with the outcomes of the simplify model ( $\gamma$ -method) proposed in the Annex B of the Eurocode 5 [12].

As shown in Figure 5-23, a series of numerical analyses were conducted by using SAP2000 [14] finite element software package. Timber joists were simulated by using linear elastic frame elements, while the timber slab was modelled with two-dimensional shell elements characterized by orthotropic elastic behaviour. The connectors were schematized with nonlinear link elements. The load-slip curve adopted in the model for the connection system reproduced exactly the results of the push-out tests presented in the previous section, as shown in Figure 5-23. The compression force exerted by the fasteners was simulated by a self-balanced force system, parallel to the connector axis.

Vertical inextensible rods were introduced in order to maintain the distance between the frame elements and the shell elements unaltered during the analysis (deformation orthogonal to the grain is neglected). The “temporal sequentiality” of the CP procedure was obtained by adopting the non-linear staged construction available in SAP2000 [14] and defining different analysis steps for each location where the screws were driven in.

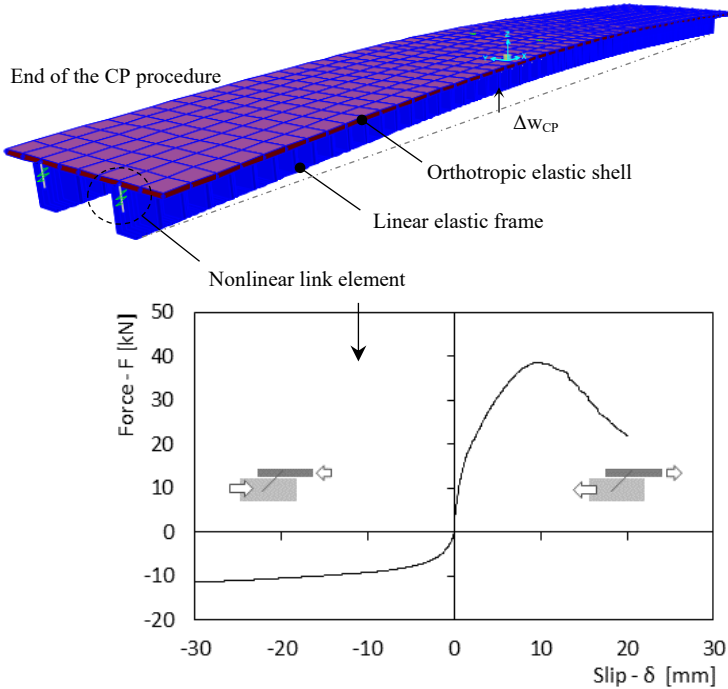


Figure 5-23 Force - slip curve of the screw connection

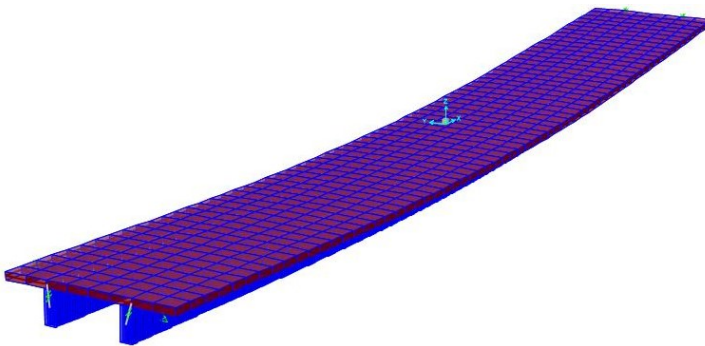


Figure 5-24 Deformed shape (magnifying factor: 2) of the model for the 6 m span module (constant fastener spacing) under 15 kN/m<sup>2</sup> loading

## 5.5 FLOOR MODULE DESIGN

### DESIGN 1 | FLOOR MODULE FOR RESIDENTIAL BUILDINGS

The solutions presented in this section were designed considering a total floor length of 6 m and an imposed load equal to 2.00 kN/m<sup>2</sup>, according to the Cat. A of EN 1991 [9][8]. Each module was composed of a beech LVL panel type Q 900 x 6000 mm<sup>2</sup> (40 mm thick) and two beech LVL beams, 450 mm spaced. According to the certificate provided by the supplier [5], beech LVL panel type Q has 15% of cross layers (layers perpendicular to the principal direction of the panel).

In order to analyse the benefits introduced by the adoption of the CP procedure, three different scenarios were considered in the design process of the floor module:

- Scenario 1A – Pre-stressed composite floor: cambering pre-stressing procedure was considered for the module assembly (numerical model);
- Scenario 1B – Standard composite floor: designed according to the Annex B of the EN 1995 [12]: Mechanically jointed beams;
- Scenario 1C – Traditional floor: only the joists were considered as primary elements (panels can be oriented perpendicularly to the beam axis; nevertheless, minimum panel-joist connection has to be provided).

The outcomes of the design process are summarized in Table 5-7. Details on the design of the pre-stressed module are given in the following paragraphs.

*Table 5-7 Floor module for Residential buildings*

1A: Pre-stressed Composite Module	1B: Standard Composite Module (EC5)	1C: Traditional Timber Floor
Panel: 40 x 900 mm <sup>2</sup>	Panel: 40 x 900 mm <sup>2</sup>	Panel: 40 mm thick (non-structural)
Joist: 60 x 160 mm <sup>2</sup> (2x)	Joist: 100 x 200 mm <sup>2</sup> (2x)	Joist: 120 x 280 mm <sup>2</sup> (2x)
Connection: Heco Multi-monti MMS-S 12 x 180 mm <sup>2</sup>	Connection: Heco Multi-monti MMS-S 12 x 180 mm <sup>2</sup>	Connection: Screw fasteners @ ≈ 300 mm
Fastener spacing: 150 mm	Fastener spacing: 150 mm	
Height: 200 mm (L/30)	Height: 240 mm (L/25)	Height: 320 mm (L/19)
Timber volume*: 6.1 m <sup>3</sup>	Timber volume*: 10.4 m <sup>3</sup>	Timber volume*: 11.5 m <sup>3</sup>

\* a surface of 100 m<sup>2</sup> was considered

## DESIGN 2 | FLOOR MODULE FOR OFFICE AREAS, SCHOOLS AND RESTAURANTS

The solutions presented in this section were designed considering a total floor length of 10 m and an imposed load equal to  $3.00 \text{ kN/m}^2$ , according to the Cat. B and C1 of EN 1991 [9]. Each module was composed of a beech LVL panel type Q  $1800 \times 10000 \text{ mm}^2$  (40 mm thick) and two beech LVL beams, 900 mm spaced. According to the certificate provided by the supplier [5], beech LVL panel type Q has 15% of cross layers (layers perpendicular to the principal direction of the panel).

In order to analyse the benefits introduced by the adoption of the CP procedure, three different scenarios were considered in the design process of the floor module:

- Scenario 2A – Pre-stressed composite floor: cambering pre-stressing procedure was considered for the module assembly (numerical model);
- Scenario 2B – Standard composite floor: designed according to the Annex B of the EN 1995 [12]: Mechanically jointed beams;
- Scenario 2C – Traditional floor: only the joists were considered as primary elements (panels can be oriented perpendicularly to the beam axis; nevertheless, minimum panel-joist connection has to be provided).

The outcomes of the design process are summarized in Table 5-8. Details on the design of the pre-stressed module are given in the following paragraphs.

*Table 5-8 Floor module for Office areas, Schools and Restaurants*

2A: Pre-stressed Composite Module	2B: Standard Composite Module (EC5)	2C: Traditional Timber Floor
Panel: $40 \times 1800 \text{ mm}^2$	Panel: $40 \times 1800 \text{ mm}^2$	Panel: 40 mm thick (non-structural)
Joist: $200 \times 320 \text{ mm}^2$ (2x)	Joist: $200 \times 400 \text{ mm}^2$ (2x)	Joist: $240 \times 440 \text{ mm}^2$ (2x)
Connection: Heco Multi-monti MMS-S $12 \times 180 \text{ mm}^2$	Connection: Heco Multi-monti MMS-S $12 \times 180 \text{ mm}^2$	Connection: Screw fasteners @ $\approx 300 \text{ mm}$
Fastener spacing: 200 mm	Fastener spacing: 200 mm	
Height: 360 mm (L/28)	Height: 440 mm (L/23)	Height: 480 mm (L/21)
Timber volume*: $11.1 \text{ m}^3$	Timber volume*: $12.9 \text{ m}^3$	Timber volume*: $15.7 \text{ m}^3$

\* a surface of  $100 \text{ m}^2$  was considered

## CONSIDERATIONS

The test outcomes appeared as promising especially when the floor modules were compared to more “traditional solutions”. The potential material saving for both floor modules was estimated in Table 5-7 and Table 5-8 by considering a surface of  $100 \text{ m}^2$ .

With reference to the standard composite solutions (Annex B of the EN 1995 [12]), the adoption of the cambering and pre-stressing procedure permitted to reduce significantly the total timber volume: -40% for the 6 m span module and -14% for the 10 m span module.

The A solutions (pre-stressed cambered modules) are by far the most efficient in terms of floor structural height for both 6 m and 10 m spanning modules. It is worth noting that the number of fasteners per joist (e.g. 50 fastener/joist for the 10 m long module) can be considered “relatively small” if compared to typical timber-timber composite floors where crossed disposition of the fasteners is commonly adopted. It is worth remembering that a certain number of fasteners avoiding slab-joist separation, is required even when the floor slab contribution is not considered. A visual comparison of the structural solutions designed for the three aforementioned scenarios, is proposed below:

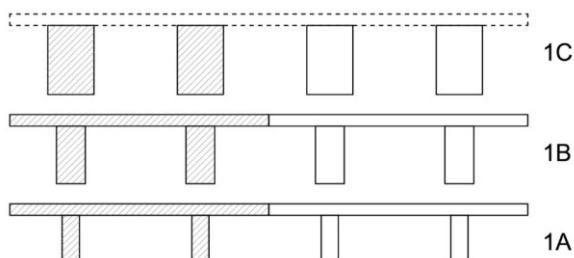


Figure 5-25 Floor modules for residential buildings ( $L=6\text{ m}$ )

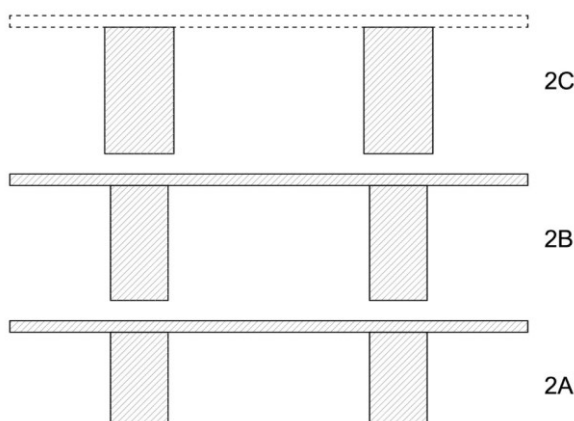
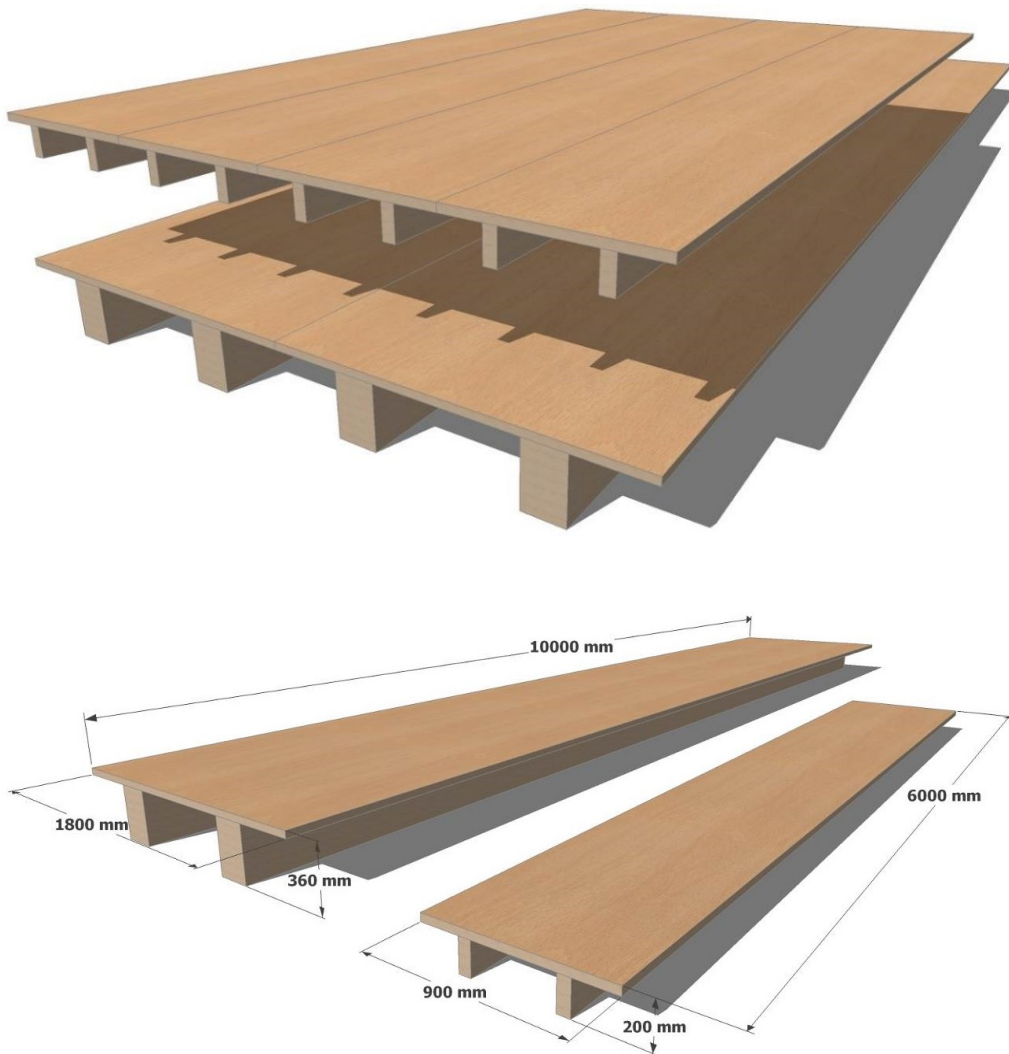


Figure 5-26 Floor modules for office buildings, schools and restaurants ( $L=10\text{ m}$ )

A rendering of the two floor modules designed in this chapter is showed below.



*Figure 5-27 Floor module rendering*

## 5.6 FULL SCALE TESTING

### 5.6.1 FLOOR MODULES FOR RESIDENTIAL BUILDINGS (L = 6 M)

Four full-scale test specimens (6 m span) were tested up to failure under quasi-static monotonic loading. Each module was comprised of a beech LVL panel type Q 900 x 6000 mm<sup>2</sup> (40 mm thick) and two beech LVL beams 60 x 160 mm<sup>2</sup> spaced at 450 mm. The screw anchor *Heco Multi-monti MMS-S 12* [7] was selected for realising the joist-to-slab connection of all the specimens.

Test 6A, 6B and 6C were realised with constant fastener spacing of 150 mm along the joist axis. A total of 80 screws were used to realise each module. Such spacing, determined from the numerical modelling and the analytical formulation (see Chapter 2), permitted to optimise the connection costs and to maximise the camber value. Test 6D was characterised by variable fastener spacing along the joist axis (the same total number of screws as per test 6A, 6B and 6C was used). The varied spacing should result in a slightly decreased camber value but an improved module response to the external loading. Differently from the other tests, sample 6A was assembled by assuming an incorrect application of the CP procedure. In particular, the screw fasteners were inserted for  $\approx 80\%$  of the fastener length by following the correct insertion order (i.e. alternately with respect to the module centre, starting from the midspan). Subsequently the remaining  $\approx 20\%$  of the fastener length (where the screw pressure is developed) was driven in by starting from one module end and proceeding towards to the opposite end.

Table 5-9 reports the geometry and the fastener layout of the four modules tested:

*Table 5-9 Geometry and details of the four tested specimens (L = 6 m)*

	Test 6A	Test 6B	Test 6C	Test 6D
Panel	900 x 40	900 x 40	900 x 40	900 x 40
Joist	60 x 160 (2x)			
CP procedure	No	Yes	Yes	Yes
Fasteners n°	80	80	80	80
Fasteners spacing	Uniform Sp: 150 mm	Uniform Sp: 150 mm	Uniform Sp: 150 mm	Variable Sp: 100 + 200 mm

The fastener arrangements considered for the realization of the four TTC modules are showed in Figure 5-28.

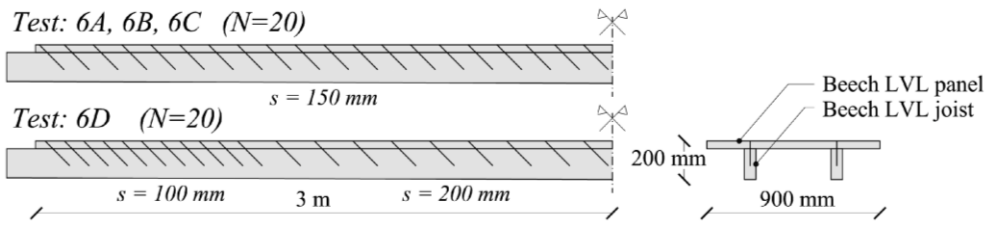


Figure 5-28 Fasteners spacing for tests 6A, 6B, 6C (uniform) and 6D (variable)

Prior to the execution of the full-scale tests, a series of preliminary investigations were performed to determine the MoE and the density of the timber elements. The results are reported in Table 5-10.

Table 5-10 Modulus of elasticity (MoE) and mean density of the timber elements ( $L = 6\text{ m}$ )

		Test 6A	Test 6B	Test 6C	Test 6D
$E_{\text{panel}}$	[N/mm <sup>2</sup> ]	16798	16591	16205	16401
$E_{\text{joist},1}$	[N/mm <sup>2</sup> ]	18211	18629	18225	18381
$E_{\text{joist},2}$	[N/mm <sup>2</sup> ]	18390	18561	18851	18481
$\rho_{\text{panel}}$	[kg/m <sup>3</sup> ]	824.1	805.6	796.3	824.1
$\rho_{\text{joist},1}$	[kg/m <sup>3</sup> ]	820.7	820.7	820.7	820.7
$\rho_{\text{joist},2}$	[kg/m <sup>3</sup> ]	820.7	820.7	820.7	820.7

### CAMBERING AND PRE-STRESSING ASSEMBLY PROCEDURE

As presented in Chapter 2, the cambering and pre-stressing (CP) assembly procedure relies on the ability of the fasteners to exert a compression force on the timber elements. Such compression force can be effectively exploited for improving the floor performance (by creating a pre-stressed condition that results in an upward camber) only when the fasteners are inserted with an inclination to the grain as shown in Figure 5-28.

For the specimen assembly, it was decided to adopt a simply supported scheme where the supports were positioned at 1/3 of the module span. This, in order to have the element self-weight positively incrementing CP procedure effectiveness. Figure 5-29 reports the test setup and the instruments arrangement adopted to monitor the assembly of the specimens. The vertical displacement ( $w_M$ ,  $w_{M,b}$ ,  $w_L$  and  $w_R$ ) was monitored by four linear displacement transducers (LDTs). The camber value was calculated as the difference between the mean value from the midspan displacements ( $w_M$ ,  $w_{M,b}$ ) and the mean value from the displacements at the supports ( $w_L$ ,  $w_R$ ). The panel-to-joists interface slips ( $\delta_L$ ,  $\delta_{L,b}$ ,  $\delta_R$ ,  $\delta_{R,b}$ ,  $\delta_{3/4L}$ ,  $\delta_{2/4L}$ ,  $\delta_{1/4L}$ ) were measured by means of seven

LDTs. The instruments  $\delta_{3/4L}$ ,  $\delta_{2/4L}$  and  $\delta_{1/4L}$  were positioned at equally spaced intervals in order to obtain the slip profile along the beam axis. For test 6A and 6B, seven linear strain gauges ( $\epsilon_{M,u}$ ,  $\epsilon_{M,m}$ ,  $\epsilon_{M,d}$ ,  $\epsilon_{1/3,u}$ ,  $\epsilon_{1/3,d}$ ,  $\epsilon_{2/3,u}$ ,  $\epsilon_{2/3,d}$ ) were provided to estimate the strain distribution in three different cross sections of the joist element. The axial force and bending moment diagrams on the joist were inferred by calculating the tension stress distribution by using the MoE previously measured (Table 5-10).

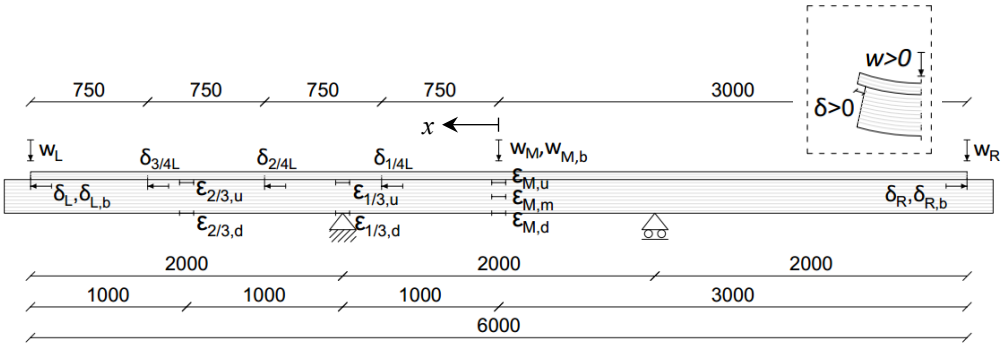


Figure 5-29 Test setup and instruments arrangement for the CP procedure of 6m modules and sign convention for slip and vertical displacement

The setup used for the assembly of the modules are reported in Figure 5-30.



Figure 5-30 Test setup used for the CP assembly procedure

Figure 5-31 summarizes the camber values at the end of the CP procedure and the camber values after the re-tightening of the fasteners (subsequently to the insertion of

the last fastener, all the screws were re-tightened starting from the midspan location to the module ends, similarly to the insertion scheme adopted for CP procedure).

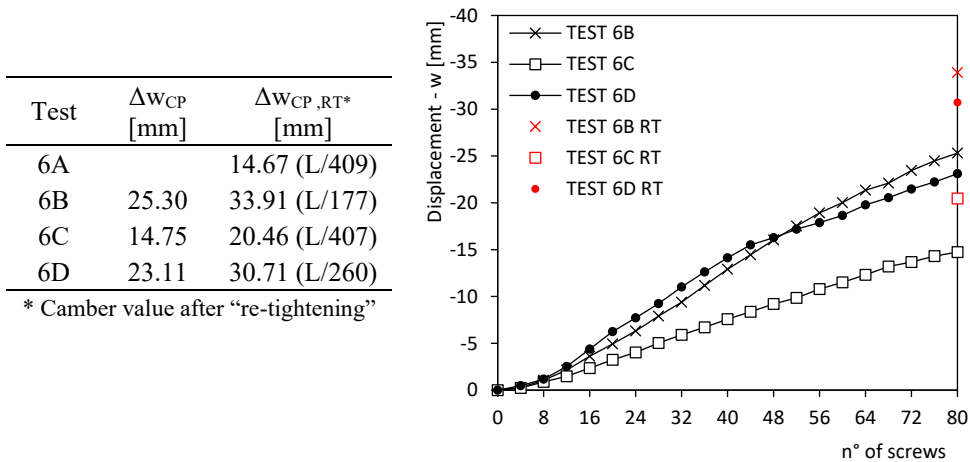


Figure 5-31 Midspan uplift values at the end of the assembly procedure (left) and camber evolution (right)

Differently from the graphs presented in Chapter 2 where the camber evolution was firstly analysed, on the x-axis of Figure 5-31 and following, the total number of screw inserted at each step was indicated. Hence, by dividing the number of fasteners by 4 is possible to define the *i*-th step number ( $N = 20$ ).

Test 6A was not reported in Figure 5-31 because for this test the fasteners were tightened proceeding from one floor end to the other (differently from the correct CP procedure) and the camber evolution do not follow a determined law. Test 6C exhibited a smaller uplift because of local misalignments between the predrilled holes and the groove cuts required to accommodate the fastener heads. Such misalignment resulted in decreased compression force exerted by several fasteners.

Figure 5-32 shows the results of test B in terms of camber value (left) recorded during the screw insertion and after the re-tightening, and the fasteners effectiveness (right) with respect to the final camber value.

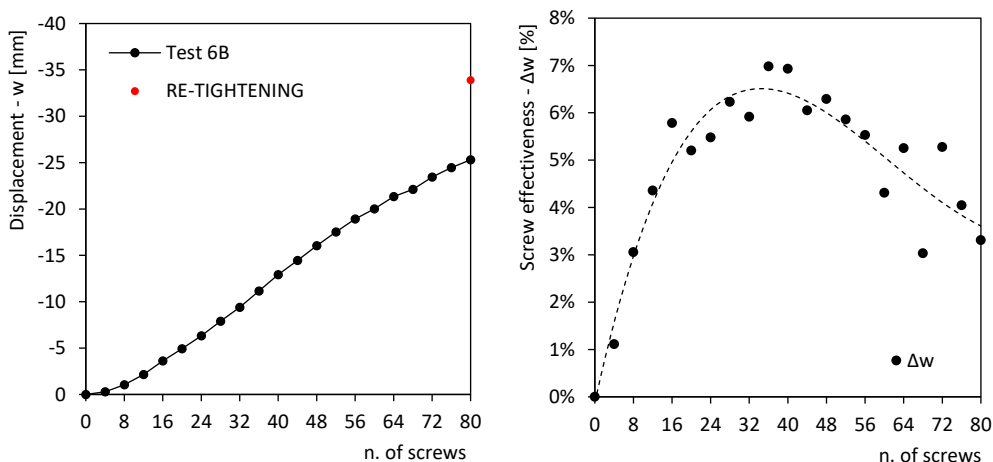


Figure 5-32 Test 6B: camber evolution (left) and screw effectiveness with respect to the final value of camber (right)

Figure 5-34 (left) presents the slip profile recorded by the four AEP transducers ( $\delta_L$ ,  $\delta_{3/4L}$ ,  $\delta_{2/4L}$ ,  $\delta_{1/4L}$ ) positioned at the joist-panel interface. The grey lines represent the slip profile after the insertion of each 4-screw set, for a total number of twenty lines ( $N = 20$ ) considering also the solid black lines representing the last 4-screw set inserted; the black dashed line reveals the value of slip in a certain position at the exact moment of the fastener insertion in that position. Hence, the actual slip endured by the fasteners during the CP procedure can be estimated as the difference between the solid black line and the dashed black line (Figure 5-34 - right). A particular of the transducer arrangement ( $\delta_L$ ,  $\delta_{3/4L}$ ,  $\delta_{2/4L}$ ,  $\delta_{1/4L}$ ) is proposed in Figure 5-33.

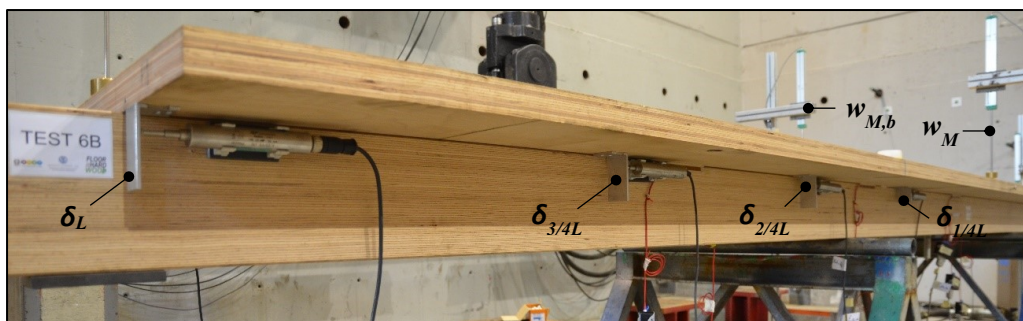


Figure 5-33 Particular of the transducers (LDT) used to monitor the panel-to-joist slip

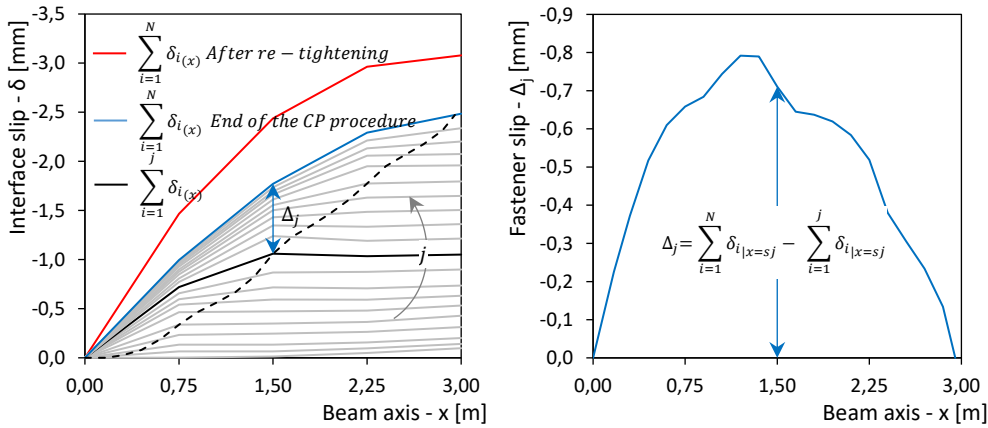


Figure 5-34 Slip profile plotted along half beam axis: total slip registered at the joist-panel interface (left) and actual slip endured by the fasteners (right)

Figure 5-35 (left) reports the slip profile registered at the end of the assembly of test 6A and at the end of re-tightening of test 6B, 6C and 6D. Figure 5-35 (right) shows the actual slip of the fasteners obtained as explained above. The reference system assumed in this chapter to describe the vertical deflection and the joist-panel interface slips is illustrated in Figure 5-29. Generally, the displacements were considered as positive when related to a downward deflection of the composite beam.

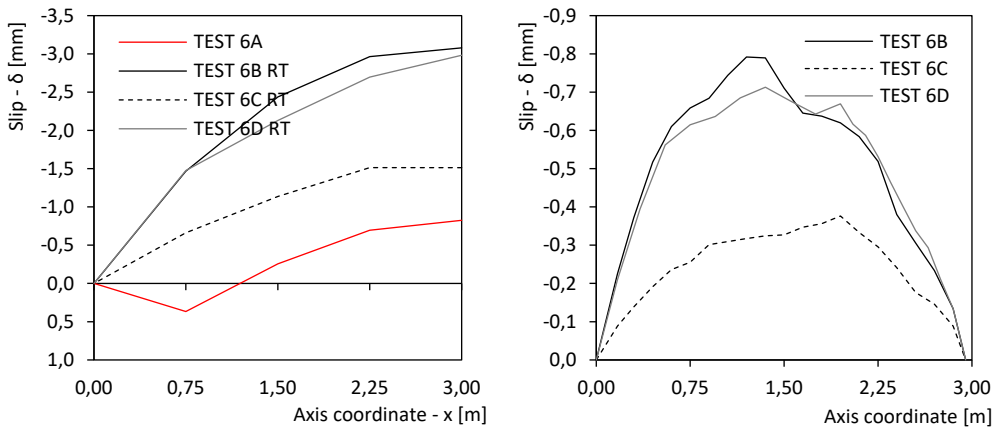


Figure 5-35 Total slip profile of the four specimens at the end of the CP procedure or assembly (left) and actual screw slip of test 6B, 6C and 6D (right)

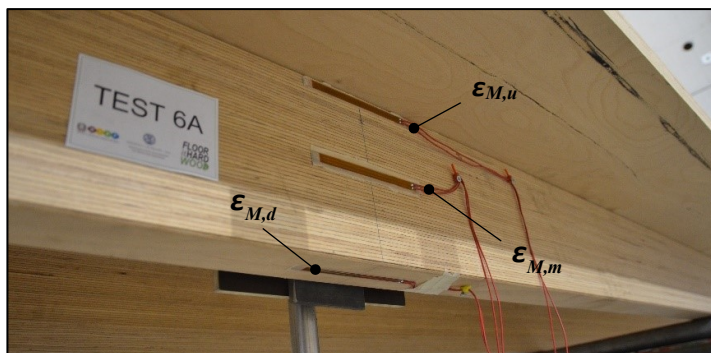


Figure 5-36 Close-up of the strain gauges positioned at the joist midspan

Figure 5-37 reports the axial force and bending moment diagrams calculated for the joist elements of test 6A and 6B. The positive sign of the axial force indicates traction while the positive sign of the bending moment is referred to the sagging moment (compression at the top of the section and tension at the bottom).

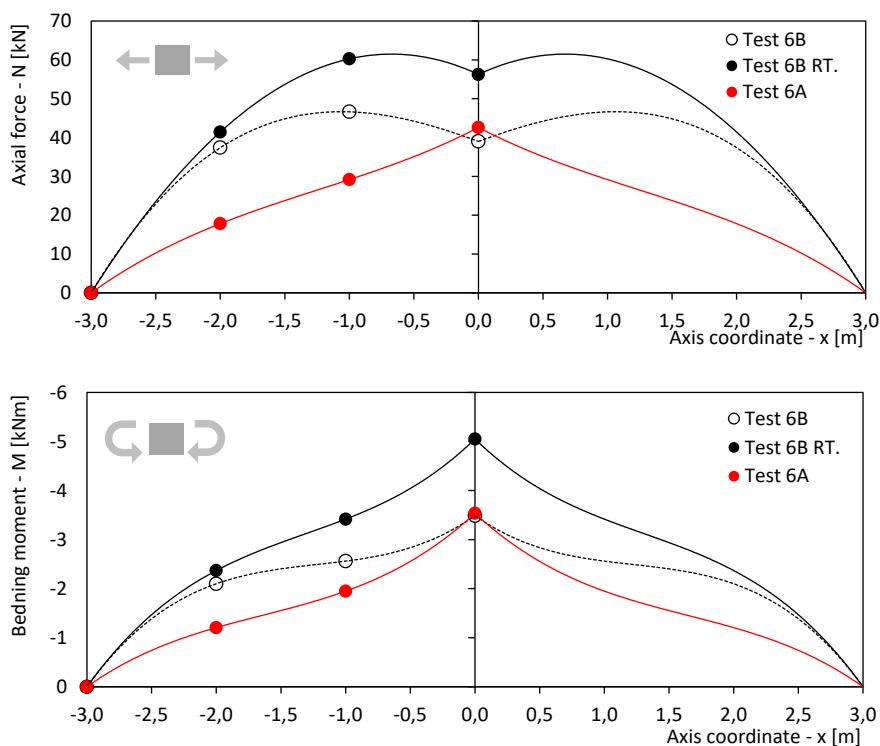
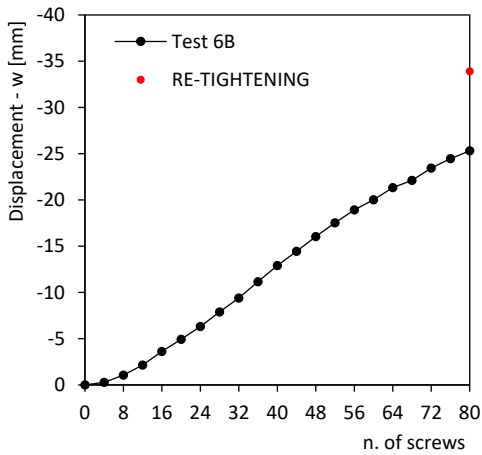


Figure 5-37 Axial force and bending moment diagrams calculated for test 6A and 6B (circles are referred to the value of  $N$  and  $M$  registered in correspondence of the strain gauges)

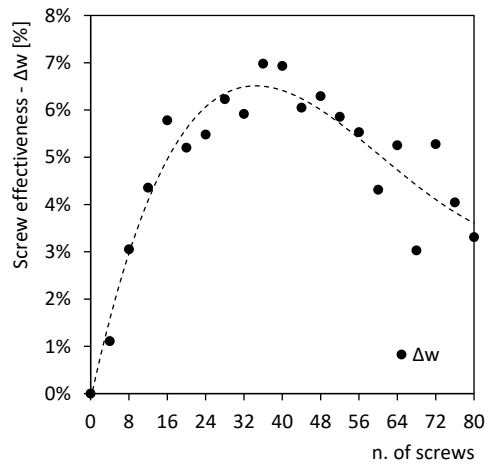
From the comparison of the internal actions at the midspan section of test 6A and 6B, a + 31.99% variation of the axial force followed by + 45% of the bending moment (absolute values) was observed in test B, where the composite beam was assembled by assuming a correct application of the CP procedure (same element sections and fasteners arrangement)

**TEST 6B**

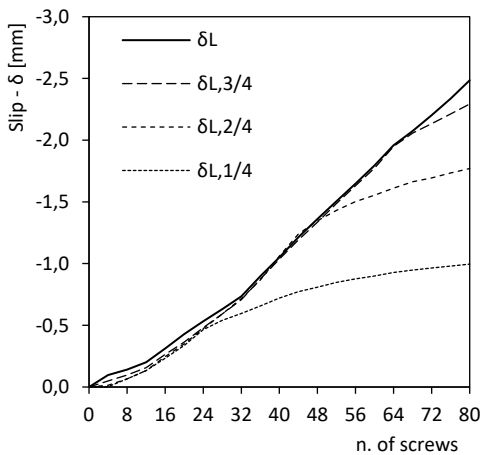
Readings from all the instruments are reported in the graphs below.



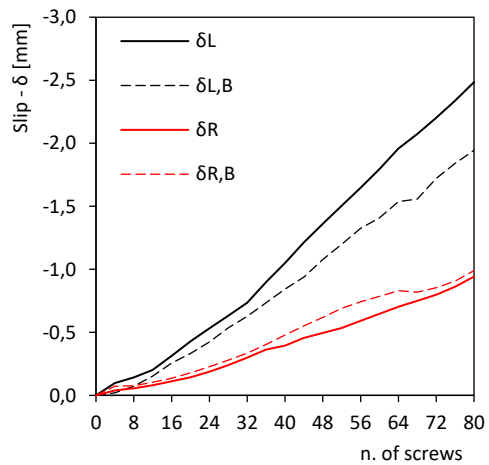
a)



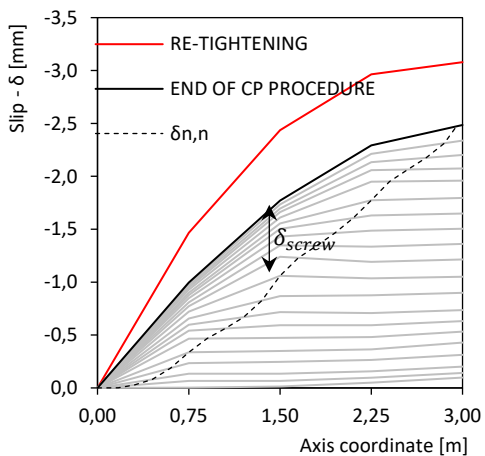
b)



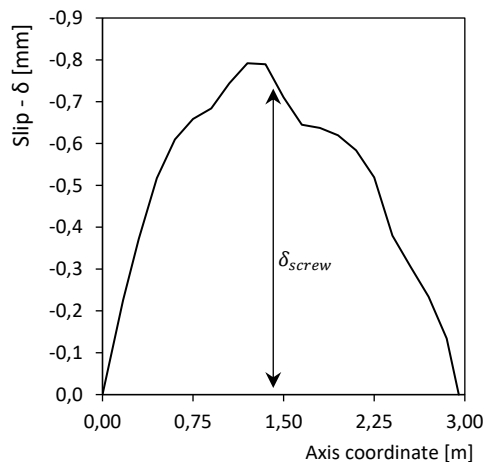
c)



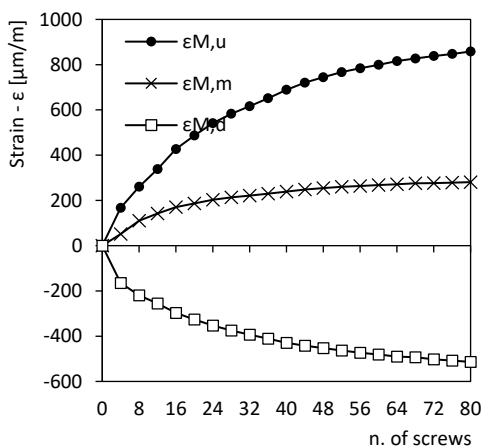
d)



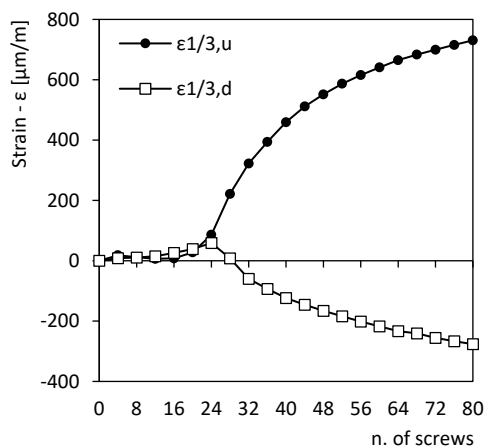
e)



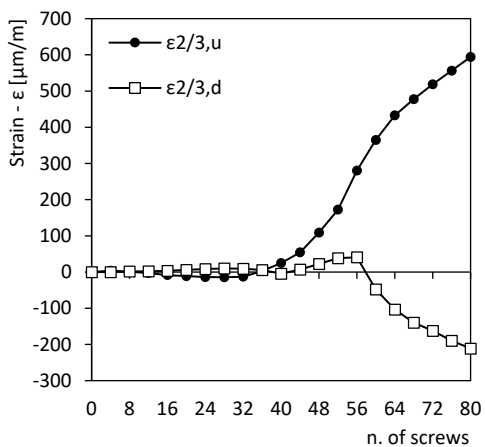
f)



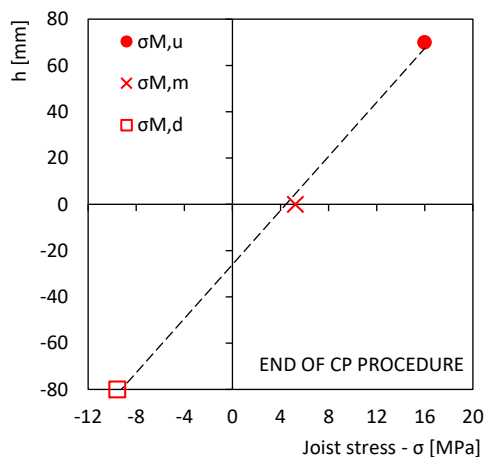
g)



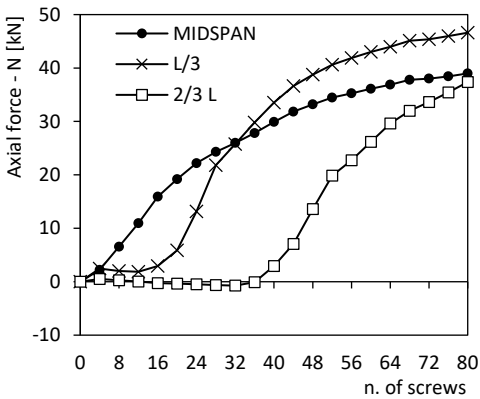
h)



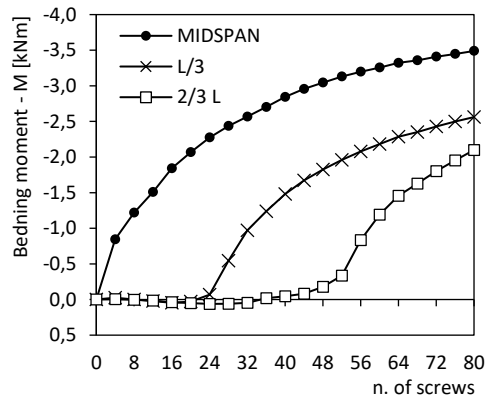
i)



j)



k)

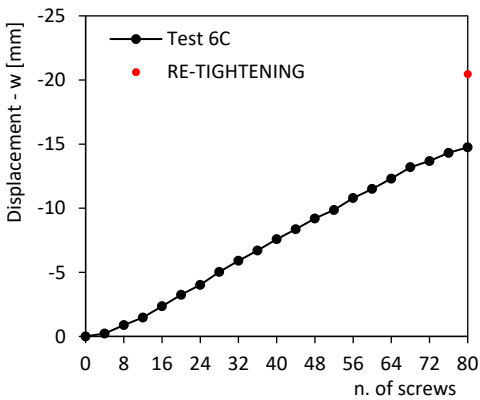


l)

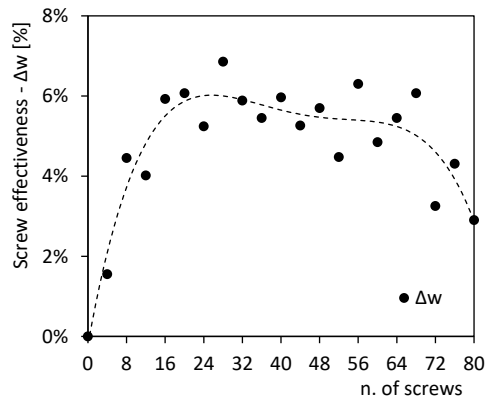
Figure 5-38 Test 6B: results of the CP procedure

**TEST 6C**

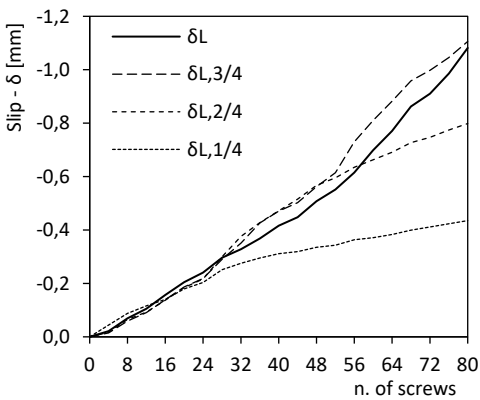
Readings from all the instruments are reported in the graphs below.



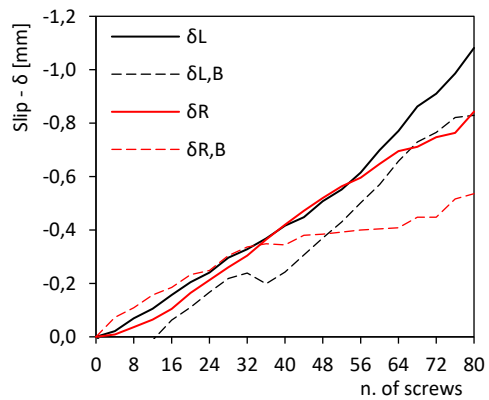
a)



b)



c)



d)

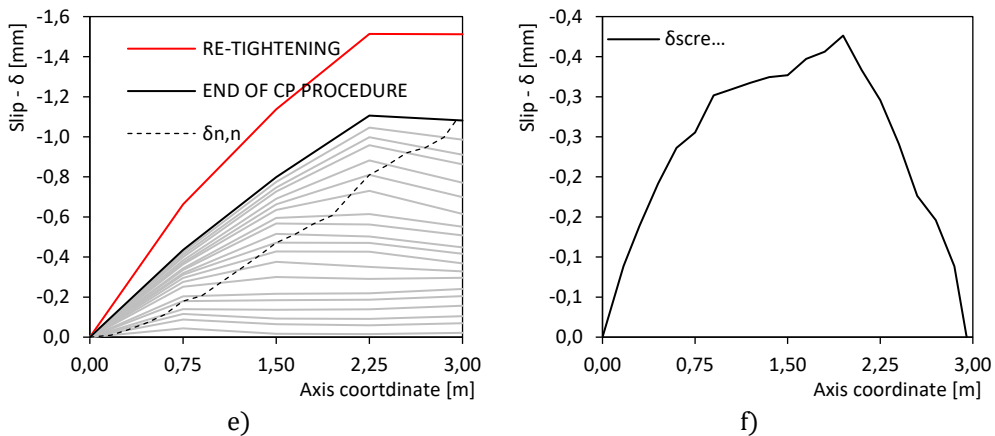
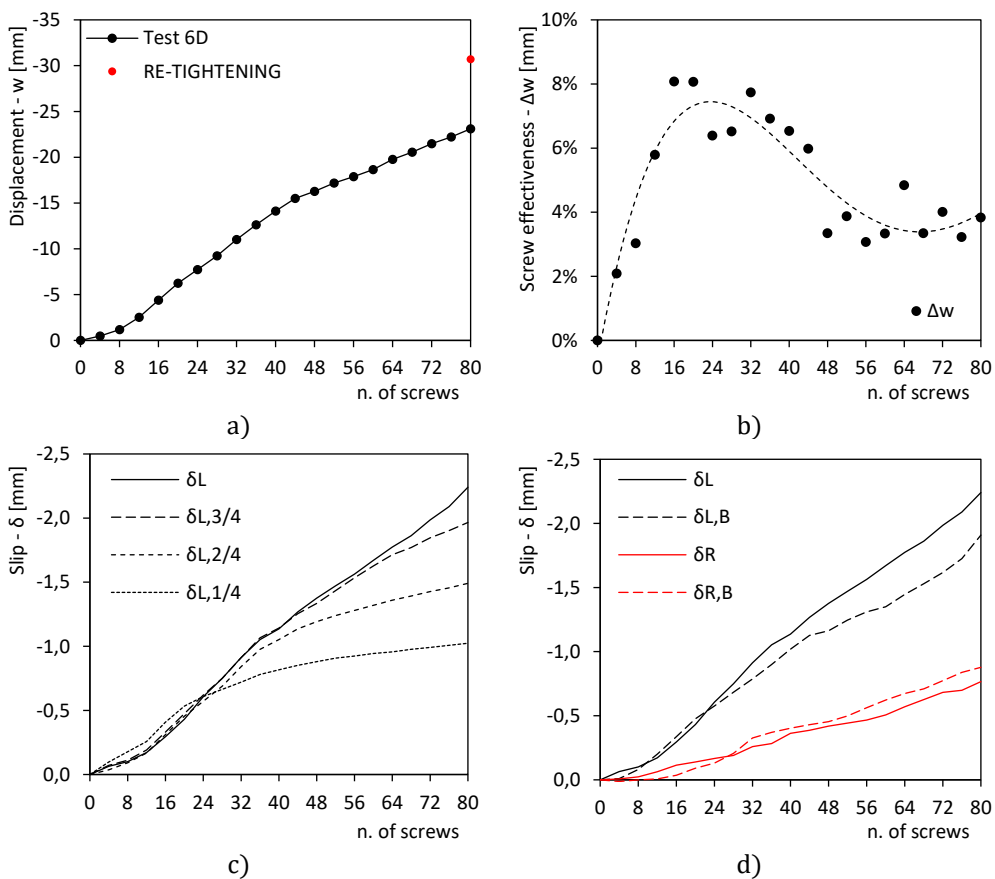


Figure 5-39 Test 6C: results of the CP procedure

### TEST 6D

Readings from all the instruments are reported in the graphs below.



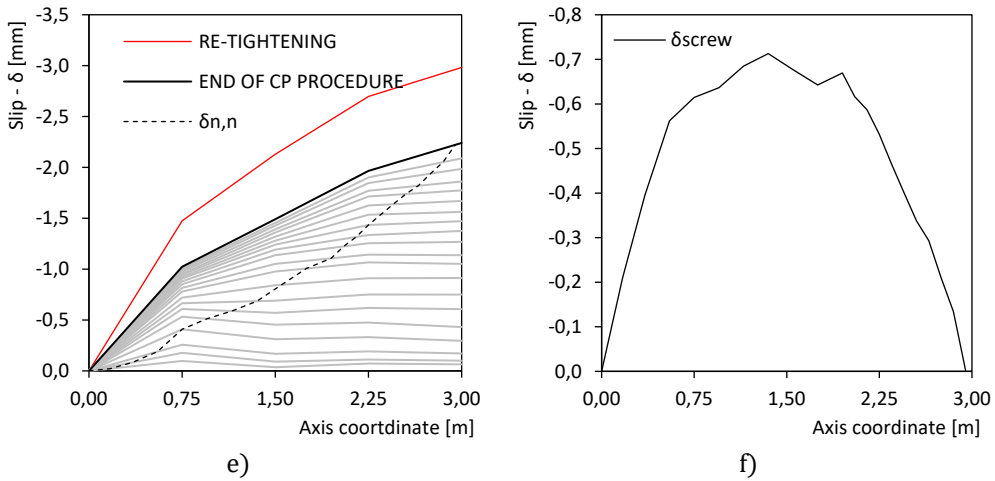


Figure 5-40 Test 6D: results of the CP procedure

**SIX-POINT BENDING TESTS**

Each specimen was subjected to a monotonic quasi-static load under displacement control until failure of the sample. A six-point bending test scheme was selected in order to better simulate a uniform distributed load acting on the floor. The test setup and the instruments layout for the loading phase are shown in Figure 5-41 and Figure 5-42. The instruments arrangement is the same used for the CP procedure with the exception of the  $w_L$  and  $w_R$  transducers, for obvious reasons.

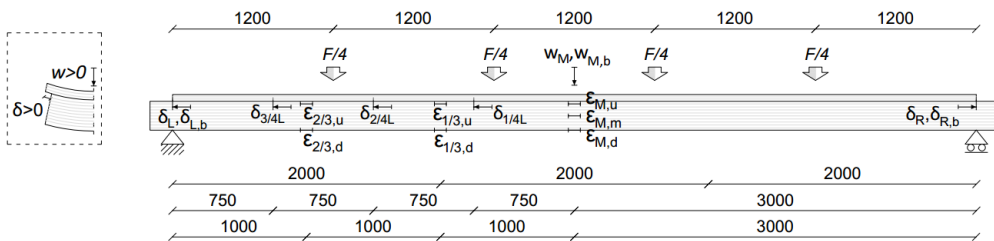


Figure 5-41 Test setup and instruments layout for the loading of the 6m modules. Sign convention for slip and vertical displacement is also reported

The load was applied through a hydraulic actuator and was monitored by a 1000 kN load cell. The imposed displacement rate was set to 0.05 mm/s.



Figure 5-42 Test setup for the loading procedure of the samples ( $L = 6\text{ m}$ )

Figure 5-43. presents the results of the six-point bending tests in terms of force Vs. displacement at the midspan. The effect of the assembly procedure is reflected by having the starting points on the negative side of x-axis.

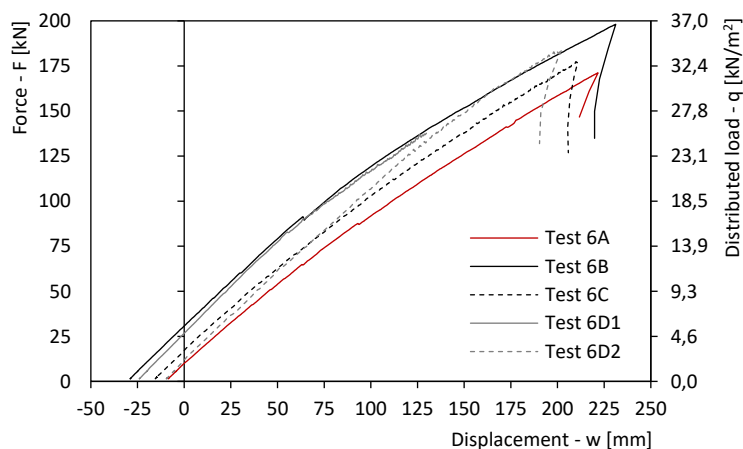


Figure 5-43 Six-point bending test results: load-displacement curves

A malfunction in the loading system occurred during the Test 6D. Consequently, the test (6D<sub>1</sub>) was stopped and then repeated up to failure (6D<sub>2</sub>). The results are summarized in Table 5-11, where:

- $F_{max}$  : maximum load reached;
- $q_{max}$  : uniformly distributed load equivalent to  $F_{max}$ ;
- $q_0$  : equivalent distributed load necessary to induce a midspan displacement variation equal to the camber value ( $\Delta w_{CP}$ );
- $q_{(\Delta w=L/400)}$  : equivalent distributed load necessary to induce a midspan displacement variation ( $\Delta w$ ) equal to  $L/400 = 15 \text{ mm}$ ;
- $q_{(w=L/300)}$  : equivalent distributed load corresponding to a net vertical deflection ( $w$ ) below a straight line between the supports equal to  $L/300 = 30 \text{ mm}$ ;
- $\Delta w_{inst,Q}$  : midspan deflection caused by characteristic load combination of the live loads ( $q_k = 2 \text{ kN/m}^2$ ).

Table 5-11 Failure loads and SLS displacements of the modules ( $L = 6 \text{ m}$ )

Test	$F_{max}$ [kN]	$q_{max}$ [kN/m <sup>2</sup> ]	$q_0$ [kN/m <sup>2</sup> ]	$q_{(\Delta w=L/400)}$ [kN/m <sup>2</sup> ]	$\Delta w_{inst,Q}$ [mm]	$q_{(w=L/300)}$ [kN/m <sup>2</sup> ]
6A	171.12	31.70	1.85	2.91	9.46	5.22
6B	198.11	36.70	5.68	3.11	8.84	9.37
6C	177.33	32.80	3.17	3.05	9.20	6.72
6D	184.24	34.10	4.94	3.21	8.36	8.83
Requests		> 6.25		> 2.00	< 15.00	

As can be seen in Table 5-11, the ultimate limit state (ULS) did not represent a design limitation for the pre-stressed composite modules developed in this Chapter. All tested samples exhibited failure loads exceeding  $30 \text{ kN/m}^2$ . As reference to Test 6A, which is the Test where the “minimum” failure load was registered, it exhibited a flexural strength capacity ( $q_{max}$ ) five times higher than the required value ( $> 6.25 \text{ kN/m}^2$  according to [9] and [13]). Such large “over-strength” might prove extremely useful in order to satisfy fire safety requirements. Given that in fire condition, the limitation of floor deformation is not a crucial parameter, the “over-strength” should guarantee that the modules retain adequate load-bearing capability even when the effective joist cross-section is significantly reduced by the fire action. Despite this large “over-strength”, gypsum-fiber panels for the fire protection were considered in the analysis of the self-weight non-structural components.

A remarkable equivalent distributed load  $q_0$  necessary to induce a midspan displacement variation equal to the camber value  $\Delta w_{CP}$  was recorded for all specimens. More

specifically, a value of  $q_0$  equal to  $5.68 \text{ kN/m}^2$  was registered in Test 6B, approximately three times the value reached in Test 6A (no CP procedure).



Figure 5-44 Specimen 6B during the loading phase

With reference to the instantaneous deflection due to the application of the live loads (characteristic combination), a limit value equal to  $\Delta w_{inst,Q} = L/400 = 15 \text{ mm}$  was required. All TTC floor modules satisfied the demands, as showed in Table 5-11.

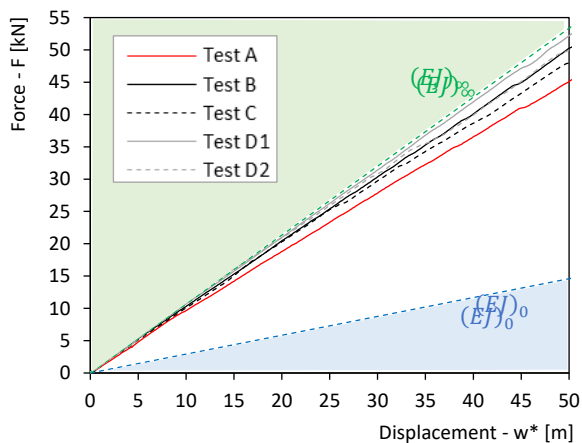


Figure 5-45 Six-point bending test results: load-displacement\* curves

Figure 5-45 presents the results from the six-point bending tests. A rigid translation of the curves along the x-axis equal to the actual camber value at the end of the CP procedure was considered in the graph (i.e. for the sake of stiffness comparison all curves start from the 0 displacement value). As expected, on equal number of total fasteners, Test 6A exhibited the minor bending stiffness.

With reference to the results of Test 6B (Figure 5-46), the flexural stiffness of the specimen was observed to be higher than the stiffness derived from both the numerical model (pushover curve) and the method provided by the Eurocode 5 – Annex B [12].

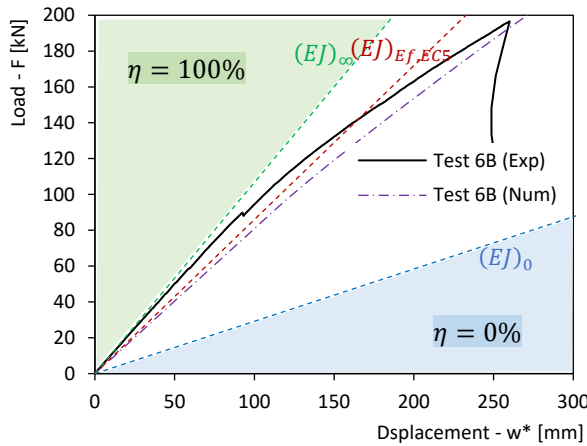
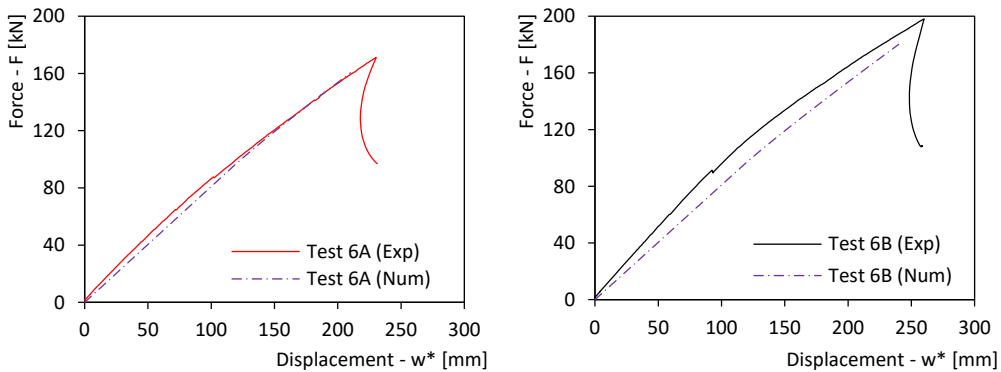


Figure 5-46 Test 6B: load-displacement\* curves

Figure 5-47 presents the comparisons between the experimental results (starting from the end of the CP procedure) and the numerical models (pushover curve). It can be noted that the specimens assembled with the CP procedure (6B, 6C and 6D) exhibited a stiffer response ( $\approx 20\%$ ) than the stiffness predicted with the numerical models. The extra-stiffness appeared to be related to the magnitude of pre-stress applied



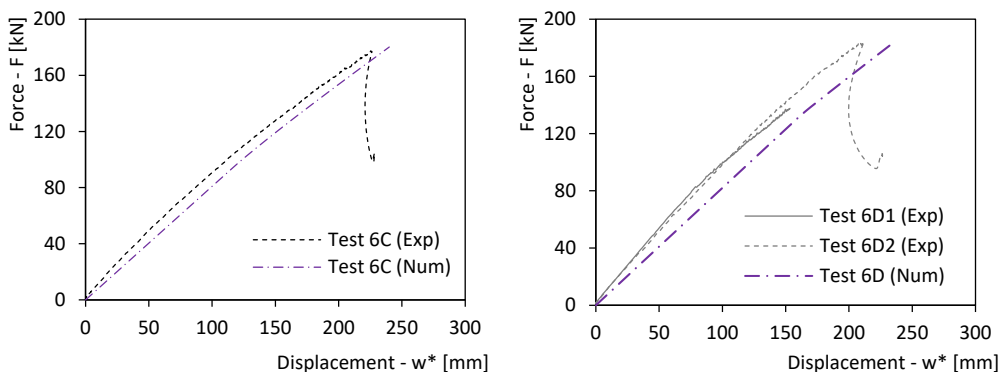


Figure 5-47 Comparisons of the experimental load-displacement curves and the pushover curves obtained from the numerical models

Test 6D was stopped at a total force level of 135 kN (6D1) and then repeated up to failure (6D 2). As shown in Figure 5-47, the curves representing the two 6D tests match closely to each other, showing no detrimental effects due to test repetition. Moreover, the optimisation of the fastener spacing along the joist axis (for a fixed number of screw fasteners) proved to have limited effectiveness (+ 4% stiffness increase). Adoption of constant fastener spacing appears therefore preferable.

Figure 5-48 compared the slip profiles measured at the beginning of the specimen loading (black curves, consistent with the slip profiles registered at the end of the CP procedure) with the slips profiles at the failure of the modules (red curves).

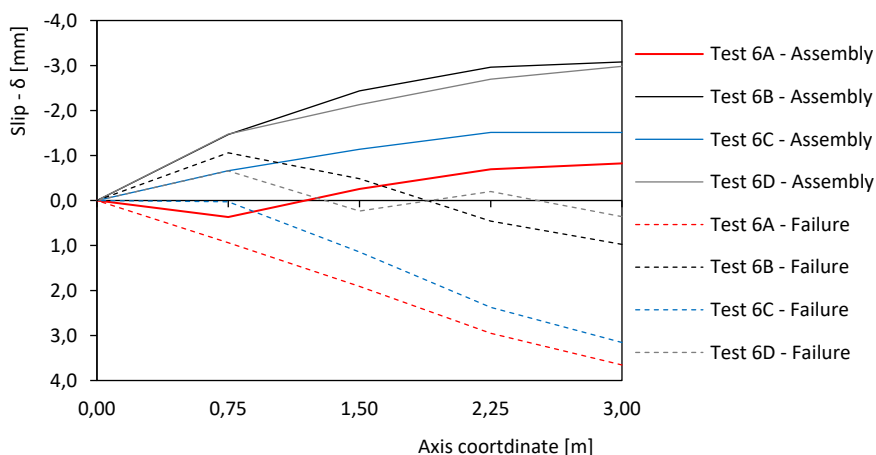


Figure 5-48 Panel-to-joist interface slip profiles of the tested specimens ( $L = 6$  m) at the end of the CP procedure and at the failure of the samples

In Figure 5-49 and Figure 5-50, axial force and bending moment diagrams recorded from the “front joist” during the loading of the samples 6A and 6B are compared. As expected the joists were subjected to combined tension and bending. Differently from the assembly phase, the maximum bending moment during the bending test was registered in a cross section which is 1 m away from the centre.

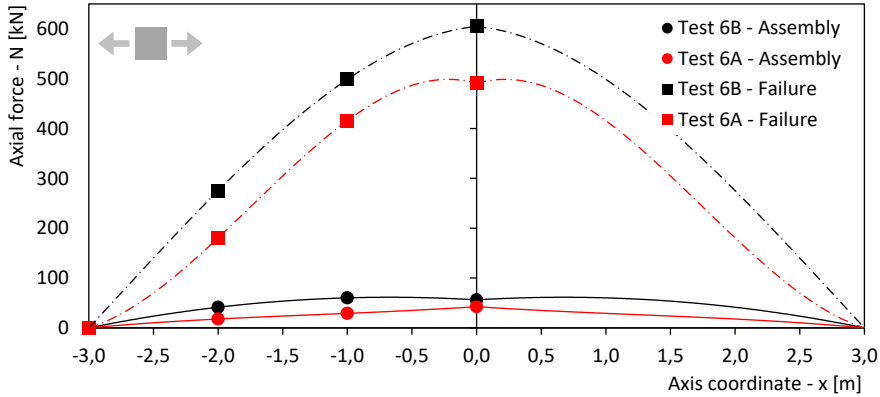


Figure 5-49 Axial force diagrams calculated for test 6A and 6B at the end of the assembly procedure and at the failure of the samples

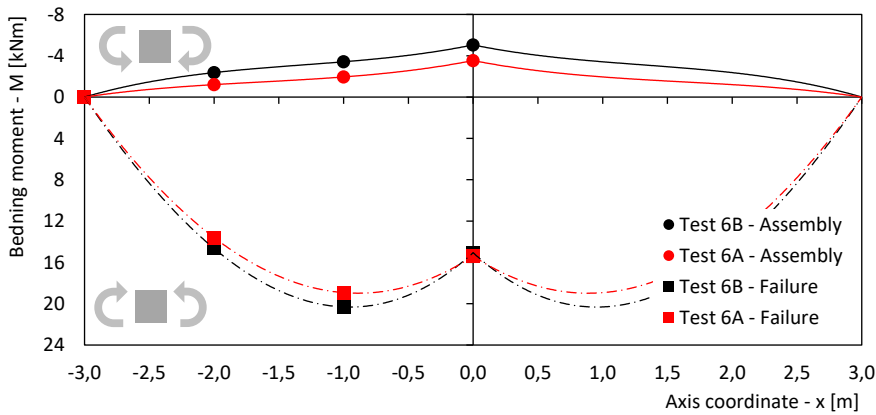


Figure 5-50 Bending moment diagrams calculated for test 6A and 6B at the end of the assembly procedure and at the failure of the samples

With reference to Test 6B, the axial force and bending moment acting on the joist element during the six-point bending test are shown in Figure 5-51 and Figure 5-52.

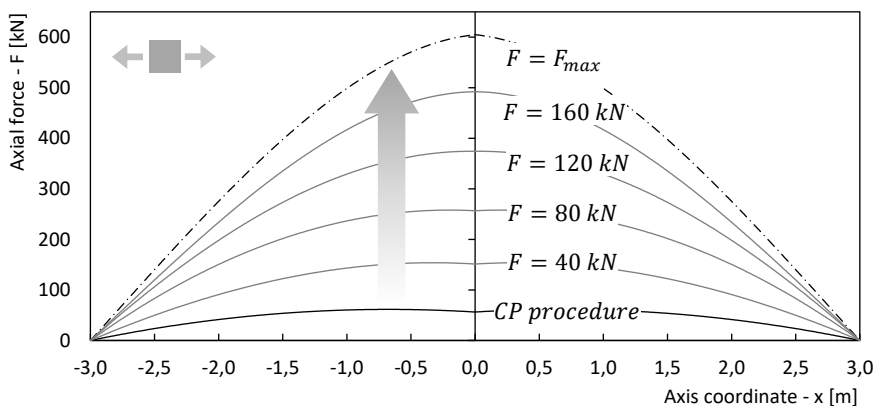


Figure 5-51 Test 6B: axial force diagrams during the loading phase

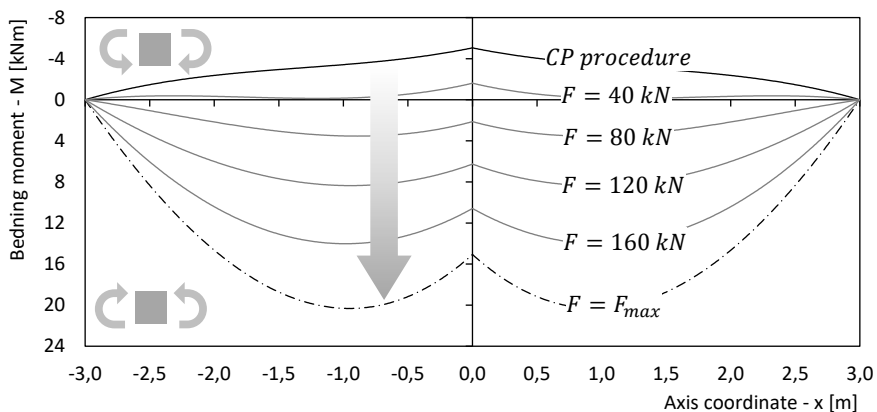


Figure 5-52 Test 6B: bending moment diagrams during the loading phase

A failure mode similar to that reported in Figure 5-53 was detected for all tests. Specifically, the collapse was related to the bending stress at the bottom of the joist cross section.



Figure 5-53 Test 6B: collapse occurred in the joist element for a combined action of tension and bending stresses

With reference to the Test 6B, Figure 5-54 plots the normal stress profile  $\sigma$  in the joist element at midspan starting from the end of the assembly phase up to the failure ( $F_{\max} = 198.05$  kN).

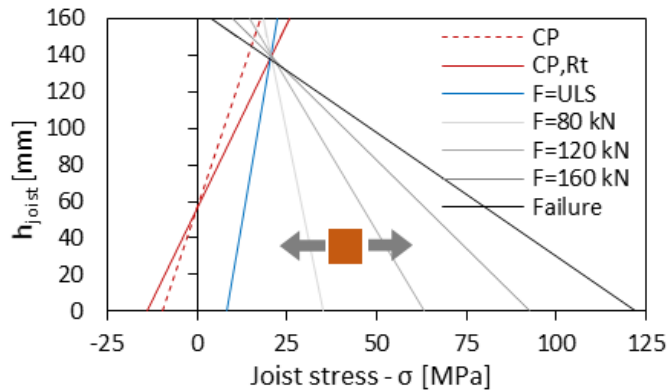


Figure 5-54 Normal stress in the joist element of Test 6B at the midspan

At the end of the assembly procedure, despite the presence of the axial tension force in the joist element (induced by the pre-stressing), the bottom side is compressed ( $\sigma = -13.87$  MPa) due to the effect produced by the negative bending moment. With regards

to the flexural behaviour of TCC or TTC composite beams under vertical loads, the ultimate loading capacity of such systems is commonly reached when a crack starts to develop at the bottom edge of the mid-span section. Consequently, the stress state resulting from the adoption of the assembly technique determines an increase in the bending capacity of the composite structure. The maximum stress value registered right before reaching  $F_{\max}$  was equal to 121.86 MPa (111.21 MPa for Test 6A).

Table 5-12 gives the stress values at the beam bottom surface derived from the strain gauge measures (with reference to test 6B) for load levels corresponding to SLS and ULS conditions. In the table, the stress values from the pre-stressed 6B specimen (scenario A) are compared with the values calculated for “standard TTC” floors (no CP assembly procedure; scenario B) and “non-compound” floors (slab contribution is neglected; scenario C) characterized by having the same joist/slab cross-section among each other. From the results the beneficial effect of the CP assembly procedure appears as evident, with the beam bottom surface being under compression at SLS load condition. The midspan displacement variation  $\Delta w_{\text{ULS}}$  caused by a force level equivalent to the USL design load is also reported.

*Table 5-12 Stress and deformation comparison for design scenarios A, B and C (A = pre-stressed TTC; B = standard TTC; C = beam only). Joist cross-section (60 x 160 mm) and spacing (450 mm) and slab thickness (40 mm) were considered as constant for all scenarios*

		Pre-stressed TTC module	Standard TTC module	Only beams
$\sigma_{\text{inf SLS}}$	[N/mm <sup>2</sup> ]	-7.1	7.7	15.8
$\sigma_{\text{inf ULS}}$	[N/mm <sup>2</sup> ]	6.5	24.9	49.4
$\Delta w_{\text{ULS}}$	[mm]	33.4	50.9	152.6

Where:

- $\sigma_{\text{inf,SLS}}$  : beam stress at the bottom surface with reference to the SLS design load level (positive if traction);
- $\sigma_{\text{inf,ULS}}$  : beam stress at the bottom surface with reference to the ULS design load level;
- $\Delta w_{\text{ULS}}$  : midspan displacement variation produced by the ULS design load level.

## CONNECTION EFFICIENCY

In this section, the connection efficiency of the TTC floor modules is analysed. The dimensionless parameter  $\eta$  quantifies the “level of interaction” between the upper panel and the joist elements. Hence,  $\eta \approx 1$  relies on composite structures where the interface slip between the elements is negligible. Conversely, a composite structure where no shear fasteners are provided has a connection efficiency  $\eta = 0$ .

As reference to the Test 6B, the numerical model showed an initial efficiency of 66.44%. Differently, the experimental test exhibited an initial efficiency of 99.31% (+ 49.47%). In Figure 5-55 is reported a comparison between the experimental results (Test 6B) and the numerical model (pushover analysis), in terms of load-displacement curves (a) and connection efficiency (b). The efficiency was calculated by considering the secant bending stiffness (between 0 and F).

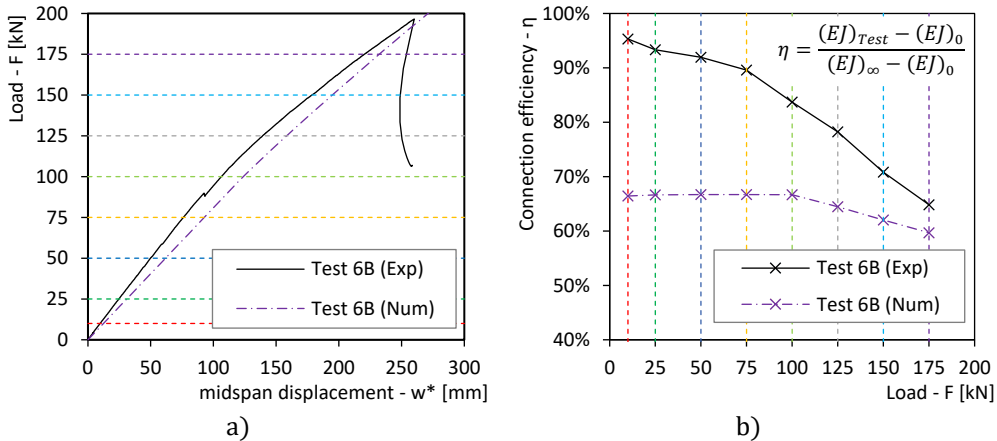


Figure 5-55 Test 6B: a) force-displacement curves; b) connection efficiency

The discrepancy showed in Figure 5-56 can be related to the high level of interaction developed by the connection system. As reported in Figure 5-56-b, no significant slips were observed in Test 6B until reaching  $F \approx 75$  kN ( $13.89$  kN/m<sup>2</sup>). The compression force exerted by the screw type fasteners resulted in non-negligible friction phenomena that considerably increased the shear stiffness of the connection.

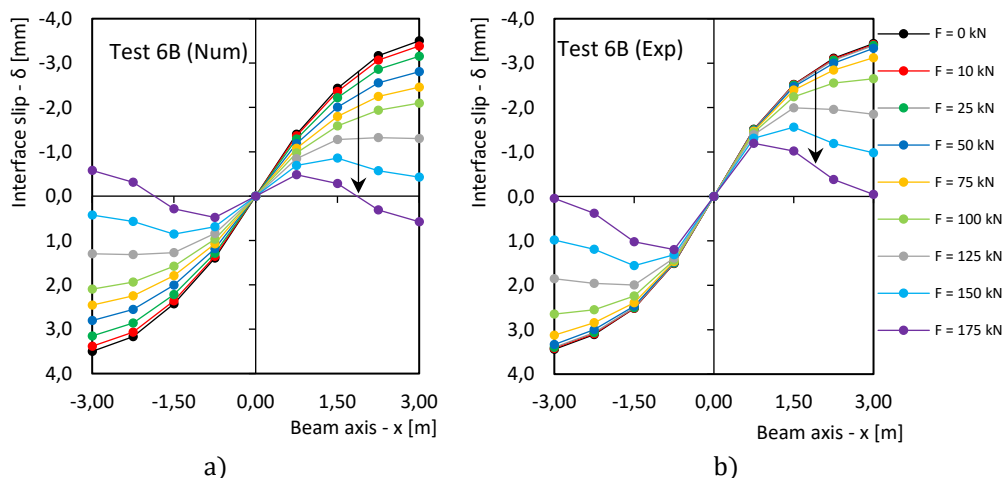


Figure 5-56 Test 6B: slip profiles – a) experimental test; b) numerical model

### 5.6.2 FLOOR MODULE FOR OFFICE AREAS, SCHOOLS AND RESTAURANTS ( $L = 10$ M)

Two full-scale test specimens, 10 m span, were tested under quasi-static monotonic loading procedure. Each module is composed of a beech LVL panel type Q 1800 x 10000 mm (40 mm thick) and two beech LVL beams 200 x 320 mm spaced at 900 mm. The screw anchor *Heco Multi-monti MMS-S 12* [7] was selected for the connection of all the samples.

The two specimens differ from each other for the fastener spacing. Test 10A was characterised by a constant spacing of 200 mm. From the analytical and numerical models, such fastener configuration was expected to ensure the exact floor performance needed to satisfy SLS requirements. Therefore, to increase the SLS safety margin, fastener spacing was further optimised for test 10B where a variable spacing was assumed (Table 5-13).

Table 5-13 Geometry and details of the two tested modules ( $L = 10$  m)

	Test 10A	Test 10B
Panel	1800 x 40	1800 x 40
Joist	200 x 320 (2x)	200 x 320 (2x)
CP procedure	Yes	Yes
Fasteners n°	100	116
Fasteners spacing	Uniform Sp: 200 mm	Variable Sp: 100 + 200 mm

The fastener arrangements considered for the realisation of the two TTC modules are showed in Figure 5-57:

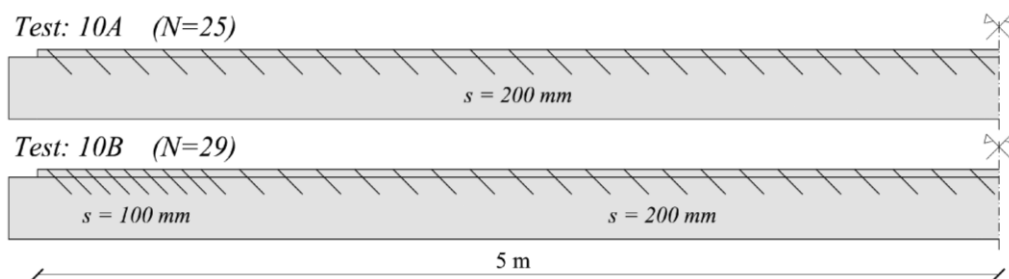


Figure 5-57 Fasteners spacing of test 10A (uniform) and 10B (variable)

Prior to the execution of the full-scale tests, a series of preliminary investigations were performed to determine the MoE and the density of the timber elements. The results are reported in Table 5-14.

Table 5-14 Modulus of elasticity and mean density of the timber elements ( $L = 10$  m)

		Test 10A	Test 10B
$E_{\text{pane},1}$	[N/mm <sup>2</sup> ]	16612	15791
$E_{\text{joist},1}$	[N/mm <sup>2</sup> ]	16640	16796
$E_{\text{joist},2}$	[N/mm <sup>2</sup> ]	15651	15738
$\rho_{\text{panel}}$	[kg/m <sup>3</sup> ]	816.7	816.7
$\rho_{\text{joist},2}$	[kg/m <sup>3</sup> ]	807.8	804.8
$\rho_{\text{joist},2}$	[kg/m <sup>3</sup> ]	803.4	803.4

A picture of the movement of the TTC module inside the laboratory of the Department of Civil, Environmental and Mechanical Engineering of the University of Trento is showed below.

### CAMBERING AND PRE-STRESSING ASSEMBLY PROCEDURE

The test setup and the instruments arrangement adopted for the CP procedure of the 10 m floor modules were the same used for the 6 m specimens (Figure 5-29). Also in this case, for the specimen assembly, it was decided to adopt a simply supported scheme where the supports were positioned at 1/3 of the module span. This, in order to have element self-weight positively increment CP procedure effectiveness.



*Figure 5-58 Movement of the sample*

The vertical displacement ( $w_M$ ,  $w_{M,b}$ ,  $w_L$  and  $w_R$ ) was monitored by four linear displacement transducers (LDTs). The camber value was calculated as the difference between the mean value from the midspan displacements ( $w_M$ ,  $w_{M,b}$ ) and the mean value from the displacements at the supports ( $w_L$ ,  $w_R$ ). The panel-to-joists interface slips ( $\delta_L$ ,  $\delta_{L,b}$ ,  $\delta_R$ ,  $\delta_{R,b}$ ,  $\delta_{3/4L}$ ,  $\delta_{2/4L}$ ,  $\delta_{1/4L}$ ) were measured by means of seven LDTs. The instruments  $\delta_{3/4L}$ ,  $\delta_{2/4L}$  and  $\delta_{1/4L}$  were positioned at equally spaced intervals in order to obtain the slip profile along the beam axis. For test 10A were used six linear strain gauge sensors ( $\epsilon_{M,u}$ ,  $\epsilon_{M,d}$ ,  $\epsilon_{1/3,u}$ ,  $\epsilon_{1/3,d}$ ,  $\epsilon_{2/3,u}$ ,  $\epsilon_{2/3,d}$ ) to estimate the strain distribution in three different cross sections of one joist. The axial force and bending moment diagrams on the joist were inferred by calculating the tension stress distribution by means of the MoE previously measured (Table 5-14).

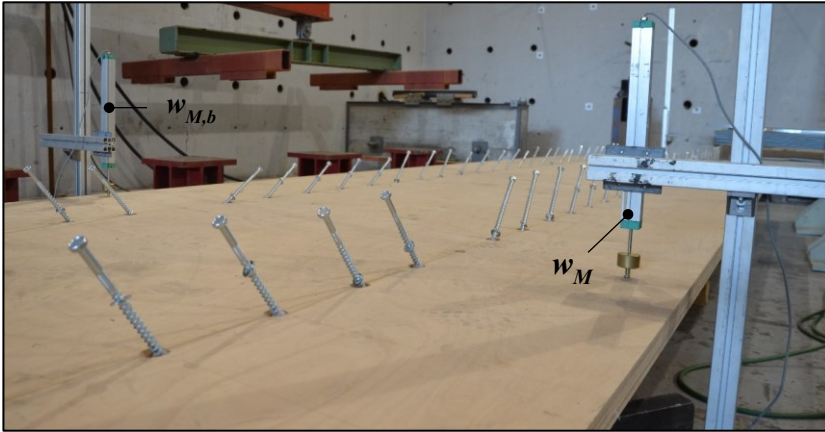


Figure 5-59 Detail of the fasteners insertion at the module midspan

Figure 5-60 summarises the camber values at the end of the CP procedure and the camber values after the re-tightening of the fasteners (subsequently to the insertion of the last fastener, all the screws were re-tightened starting from the midspan location to the module ends, similarly to the insertion scheme adopted for CP procedure). As expected, no significant increment on the camber value was found in test 10B, where four screw rows were added in the external parts of the sample (+16 screws). Almost the same camber evolution was observed for tests 10A and 10B until the insertion of the 84<sup>th</sup> screw (before spacing change in test 10B), indicating an appropriate repeatability of the adopted procedure.

Test	$\Delta w_{CP}$ [mm]	$\Delta w_{CP,RT}^*$ [mm]
10A	10.94	14.78 (L/677)
10B	10.72	15.09 (L/663)

\* Camber value after “re-tightening”

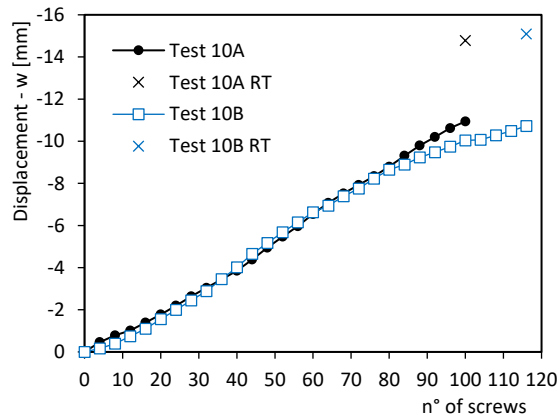
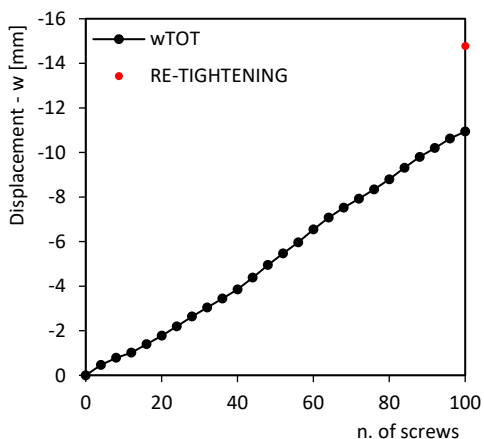


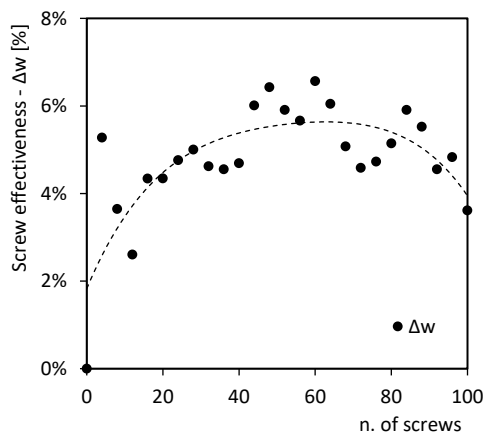
Figure 5-60 Midspan uplift values at the end of the assembly procedure (left) and camber evolution (right)

Despite the remarkable weight and moment of inertia of the beam element, a final camber value greater than 14.78 mm ( $\sim L/680$ ) was registered for both TTC modules (10 m span). The main experimental results are presented in the following graphs.

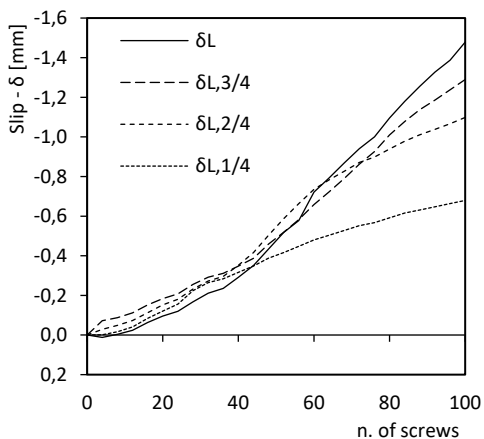
**TEST 10A**



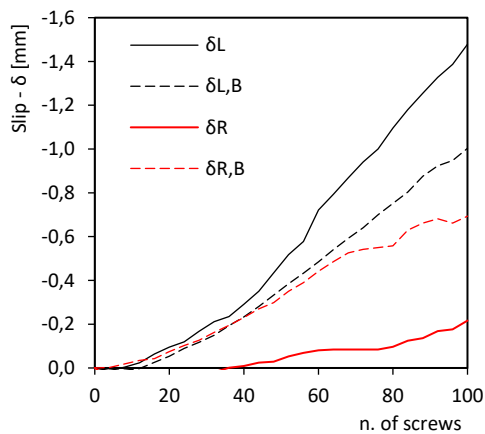
a)



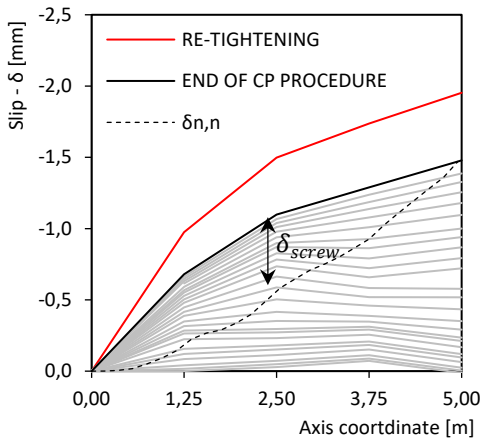
b)



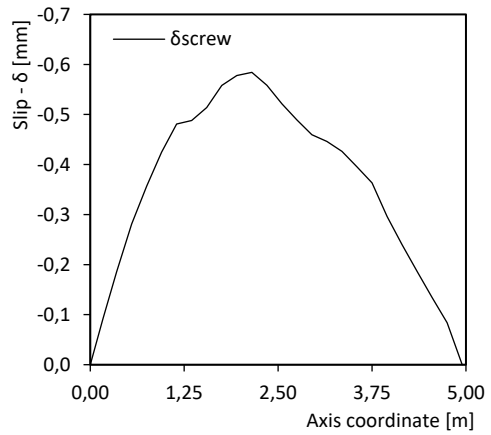
c)



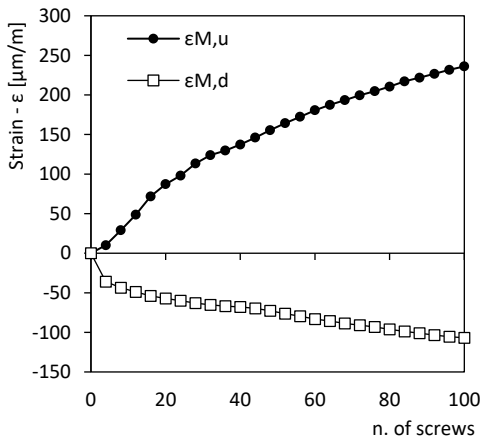
d)



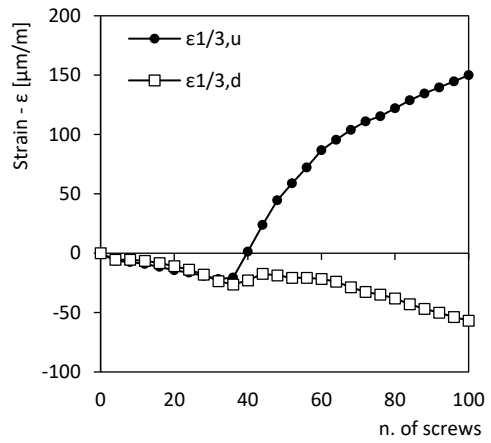
e)



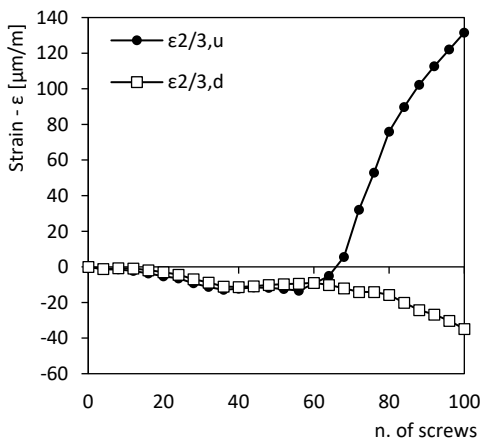
f)



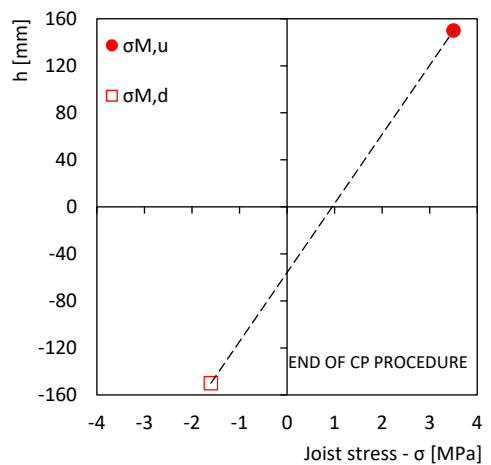
g)



h)



i)



j)

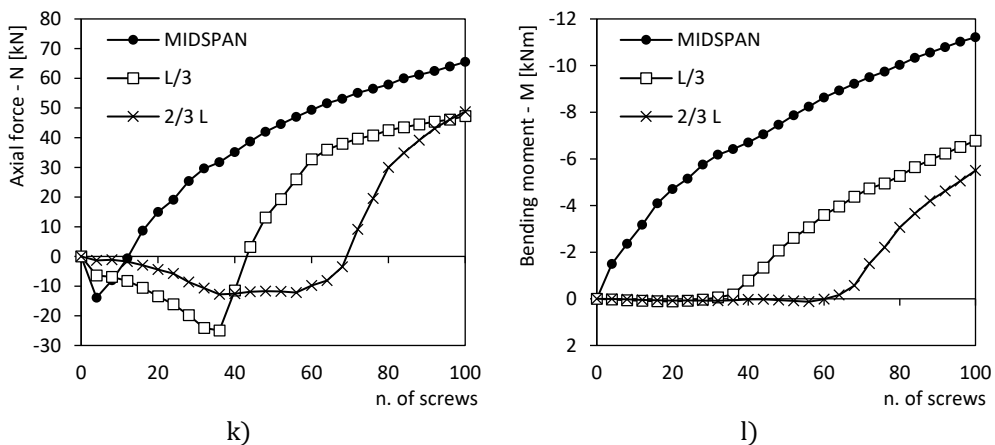


Figure 5-61 Test 10A: results of the CP procedure

Figure 5-62 reports the axial force and bending moment diagrams calculated for the joist elements of Test 10A at the end of the CP procedure.

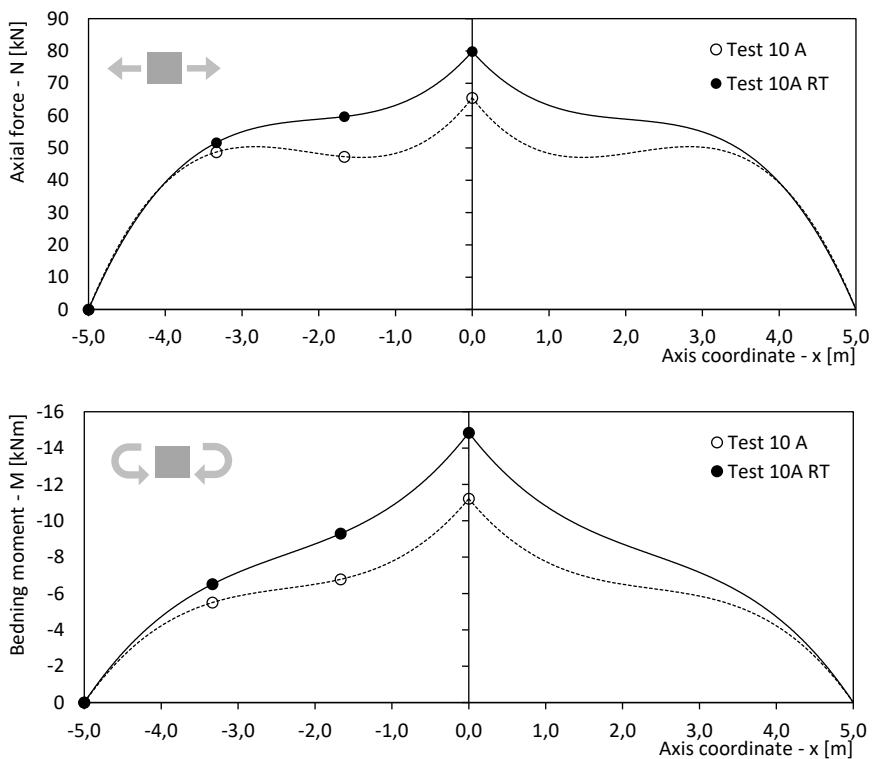
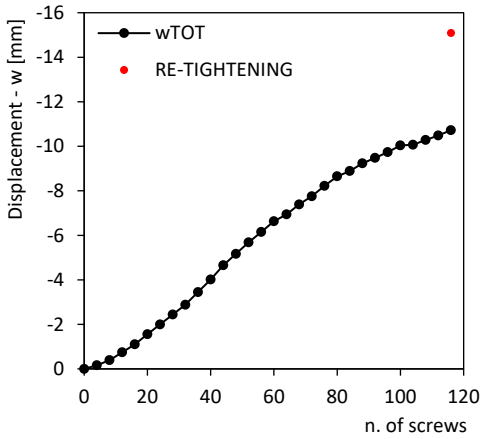


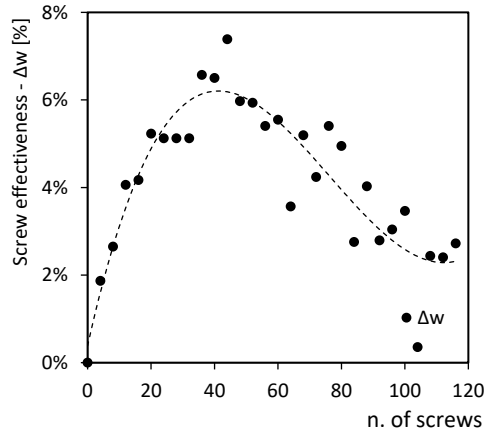
Figure 5-62 Axial force and bending moment diagrams calculated for test 10A (circles are referred to the value of  $N$  and  $M$  registered in correspondence of the strain gauges)

The positive sign of the axial force indicates traction while the positive sign of the bending moment is referred to the sagging moment (compression at the top of the section and tension at the bottom).

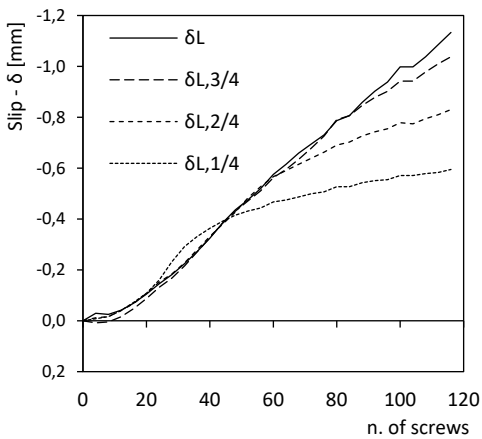
**TEST 10B**



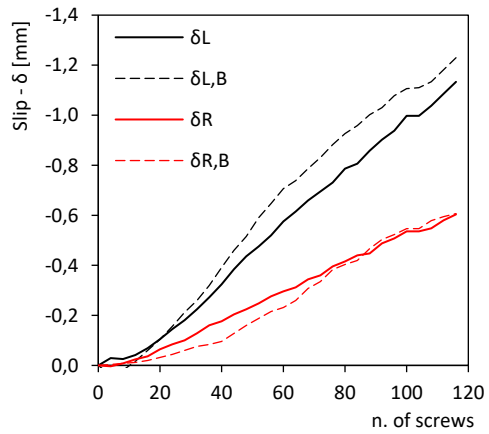
a)



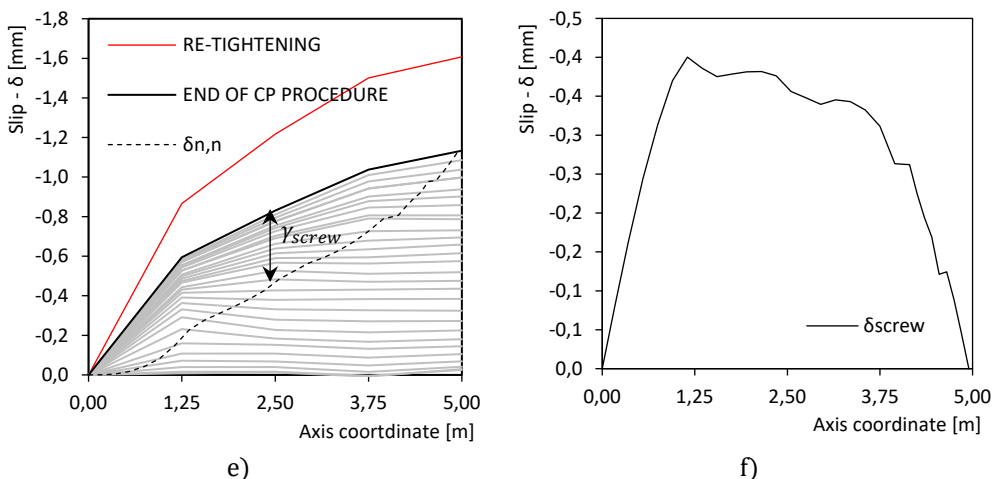
b)



c)



d)



e) f)  
Figure 5-63 Test 10B: results of the CP procedure

### SIX-POINT BENDING TESTS

Each specimen was subjected to a monotonic quasi-static load under displacement control, performing a six-point bending test. The failure load of the module, estimated by the numerical model and equal to approximately 850 kN, exceeds the maximum safe load of the test setup. For that reason, “semi-cyclic” test loading under displacement control was adopted: each specimen was repeatedly loaded and unloaded according to a predetermined loading scheme. The selected load steps are reported in Table 5-15.

Table 5-15 Load steps for the “semi-cyclic” testing of the 10 m modules

Load step	q [kN/m <sup>2</sup> ]	F [kN]	Repetitions
0.5 SLS	2.75	49.5	1
SLS	5.50	99.0	3
ULS	7.75	139.5	3
2 ULS	15.50	279.0	1
2.5 ULS	19.38	348.75	1*

SLS: characteristic load combination of actions

ULS: fundamental load combination of actions

\* only for Test 10B



Figure 5-64 Test setup for the loading procedure of the specimens ( $L = 10$  m)

The instruments layout was the same adopted for the CP assembly procedure,  $w_L$  and  $w_R$  transducers excluded. The loading was applied through a hydraulic actuator and was monitored by a 1000 kN load cell. The imposed displacement rate was set to 0.05 mm/s. The loading scheme considered for the six-point bending tests is showed in Figure 5-65:

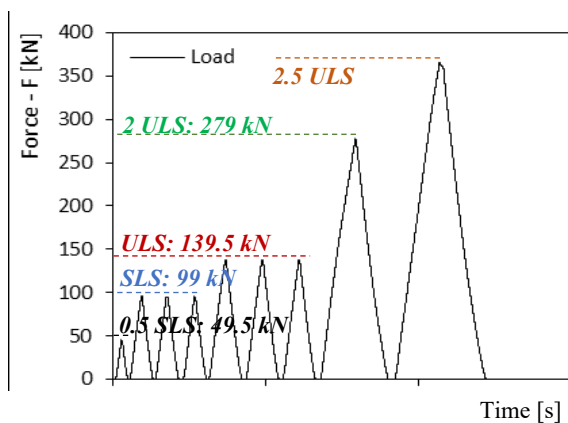


Figure 5-65 Loading scheme for the six-point bending tests

### Test 10A

Figure 5-66 reports the force recorded during testing of specimen 10A (the load was applied under displacement control).

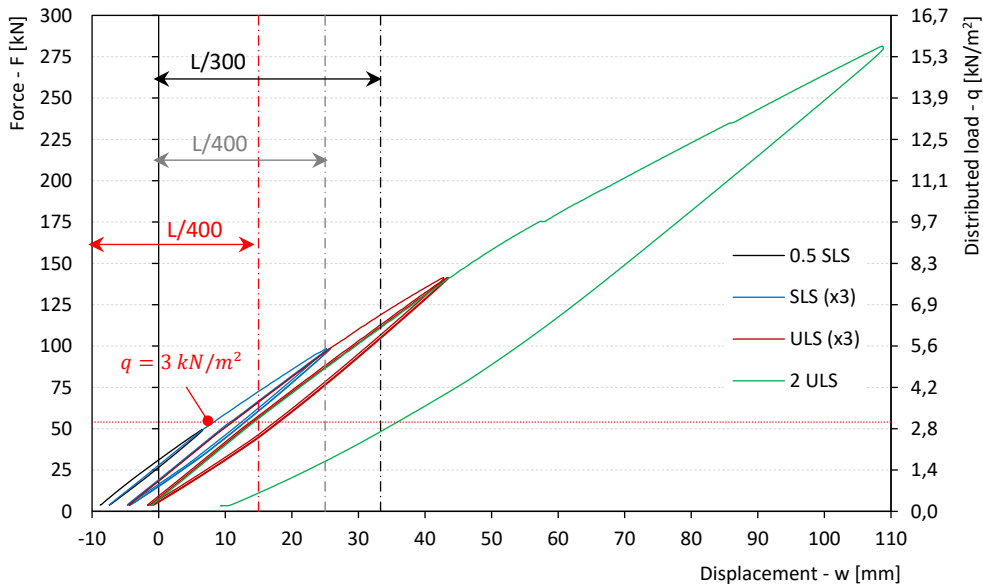


Figure 5-66 Test 10A: Load-displacement curve. Negative values on the x-axis derive from the module camber obtained through the CP assembly procedure



Figure 5-67 Specimen 10 A under loading ( $F = 148.0 \text{ kN}$  - ULS limit threshold exceeded)

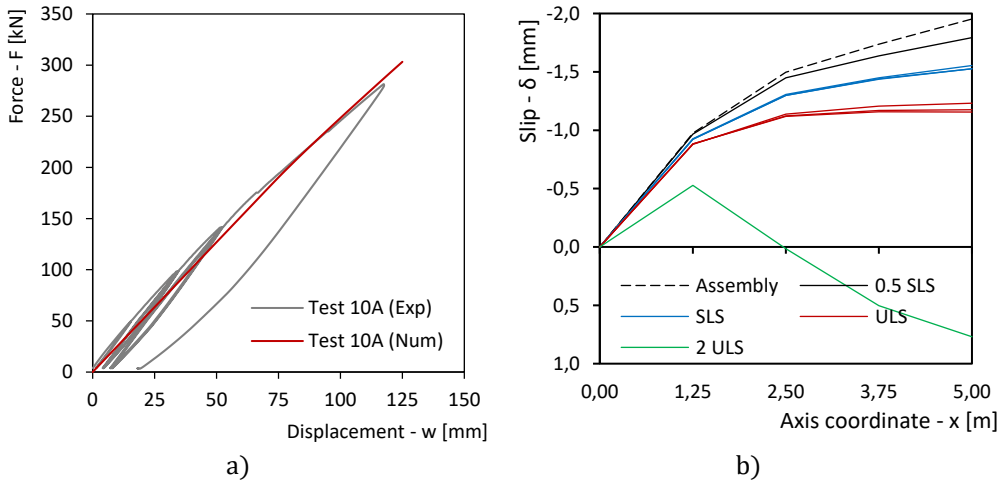


Figure 5-68 Test 10A: a) comparison between experimental load-displacement curve and numerical pushover curve; b) interface slip profiles at different loading stages

With reference to Test 10A, the axial force and bending moment acting on the joist element during the six-point bending test are shown in Figure 5-69 and Figure 5-70.

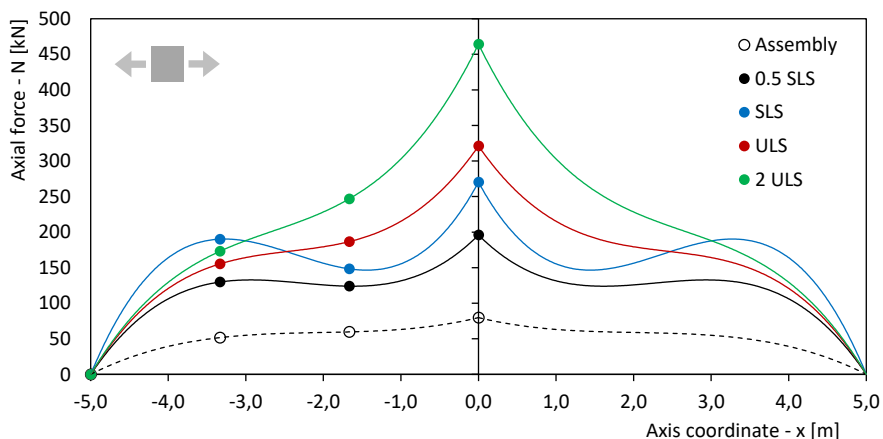


Figure 5-69 Test 10A: axial force diagrams during the loading phase

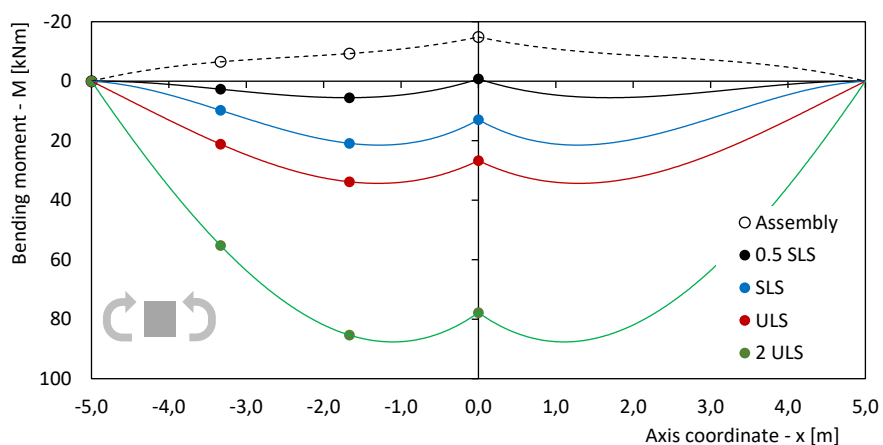


Figure 5-70 Test 10A: bending moment diagrams during the loading phase

### TEST 10B

Figure 5-71 reports the force recorded during testing of specimen 10B (the load was applied under displacement control).

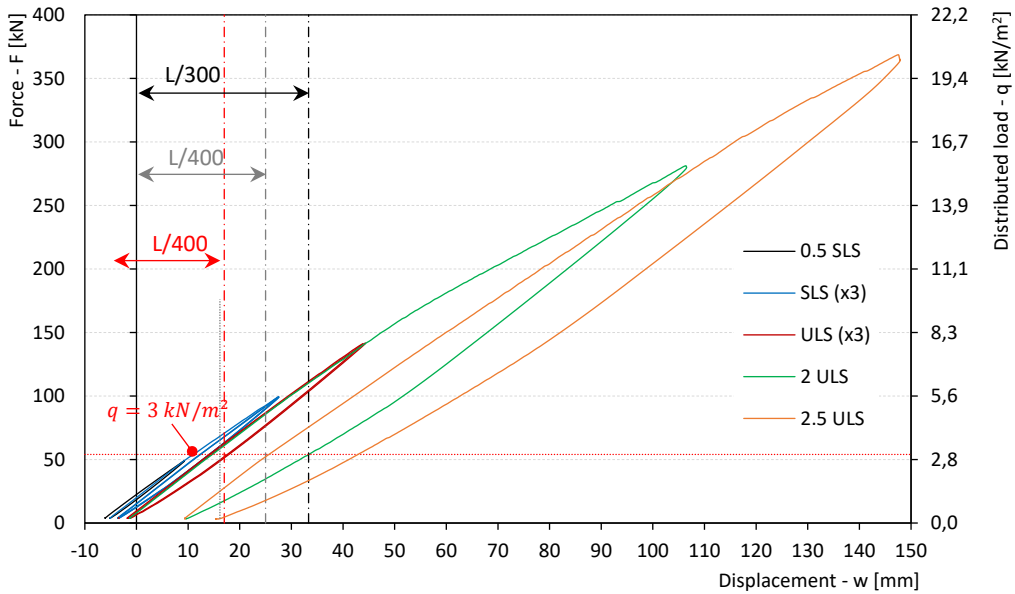


Figure 5-71 Test 10B: Load-displacement curve. Negative values on the x-axis derive from the module camber obtained through the CP assembly procedure

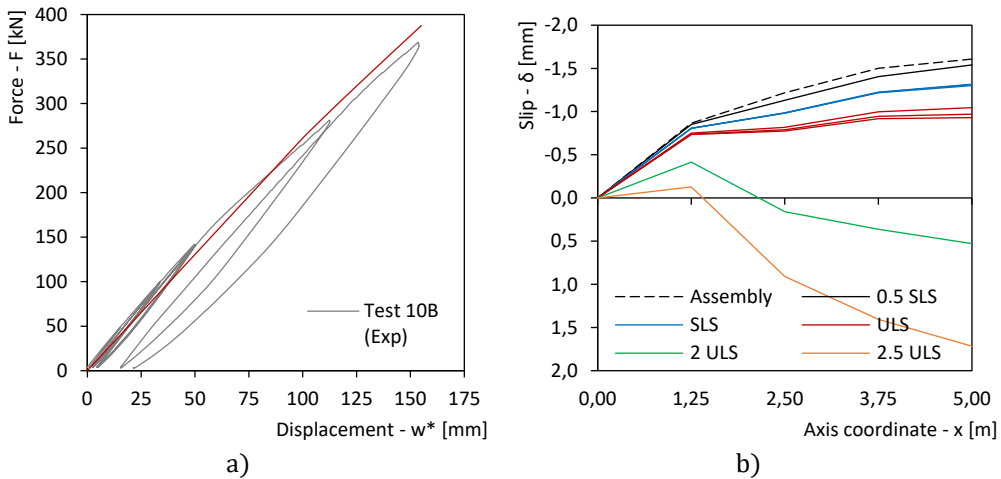


Figure 5-72 Test 10B: a) comparison between experimental load-displacement curve and numerical pushover curve; b) interface slip profiles at different loading stages

## RESULT COMPARISON

As shown in Figure 5-66 and Figure 5-71, both specimens largely satisfied the SLS and the ULS requirements. Despite a load equal to 2.5 times the fundamental combination of actions (ULS) was applied to 10B test, no damage or significant bending stiffness reduction were observed.

From the comparison of the experimental curves with the relevant pushover curve (Figure 5-68-a and Figure 5-72-a), a markedly higher ( $\approx 17\%$ ) flexural stiffness was registered in the experimental tests. The extra-stiffness appeared to be related to the magnitude of pre-stress applied.

As reported Table 5-16, the floor specimens exhibited neither stiffness degradation nor strength loss due to cyclic loading (up to load levels exceeding ULS conditions). A residual camber was registered also after the removal of the load corresponding to the ULS ( $q = 7.75 \text{ kN/m}^2$ ).

*Table 5-16 Test results: force Vs. displacement registered at every load step*

Step	F [kN]	Test 10A w [mm]	Test 10B w [mm]
0.5×SLS	3.85	-8.78	-6.09
	49.50	6.55	9.28
1° SLS	3.85	-7.39	-5.10
	99.00	25.18	27.34
2° SLS	3.85	-4.67	-3.62
	99.00	25.76	27.39
3° SLS	3.85	-4.36	-3.56
	99.00	25.83	27.41
1° ULS	3.85	-4.36	-3.47
	139.5	41.88	42.62
2° ULS	3.85	-1.52	-1.80
	139.50	42.69	43.12
3° ULS	3.85	-1.09	-1.44
	139.50	42.88	43.42
2×ULS	3.85	-0.87	-1.28
	279.00	107.37	105.26
2.5×ULS	3.85	9.33	9.48
	348.75	-	137.69
	3.85	-	15.53

3.85 kN: self-weight of the steel plates arranged above the timber panels

The backbone force Vs. displacement relationships from test TA and test TB are compared in Figure 5-73.

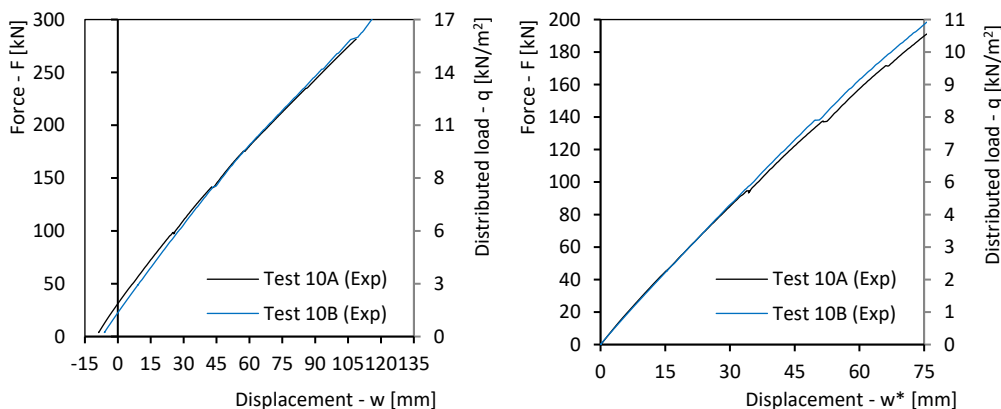


Figure 5-73 Result comparison in terms of force Vs. displacement backbone curves

As result, the optimization of the fastener spacing along the joist axis (with a 15% increase in the number of fasteners) determined no appreciable improvements (both in terms of floor stiffness and midspan camber). Adoption of constant fastener spacing appears therefore preferable. Table 5-17 gives the stress values at the beam bottom surface derived from the strain gauge measures (with reference to test 10A) for load levels corresponding to SLS and ULS conditions. In the table, the stress values from the pre-stressed 10A specimen (scenario A) are compared with the values calculated for “standard TTC” floors (no CP assembly procedure; scenario B) and “non-compound” floors (slab contribution is neglected; scenario C) characterised by having the same joist/slab cross-section among each other. As already seen for the 6 m span modules, the results show a significant stress reduction thanks to the adoption of the CP assembly. The midspan displacement variation ( $\Delta w_{ULS}$ ) caused by a force level equivalent to the ULS design load is also reported.

Table 5-17 Stress and deformation comparison for design scenarios A, B and C (A = pre-stressed TTC; B = standard TTC; C = beam only). Joist cross-section (200 x 320 mm) and spacing (900 mm) and slab thickness (4 mm) were considered as constant for all scenarios

	Pre-stressed TTC module	Standard TTC module	Only beams
$\sigma_{inf\ SLS}$ [N/mm <sup>2</sup> ]	3.4	6.8	9.9
$\sigma_{inf\ ULS}$ [N/mm <sup>2</sup> ]	11.8	18.3	25.5
$\Delta w_{ULS}$ [mm]	51.5	65.8	109.5

Where:

- $\sigma_{\text{inf,SLS}}$  : beam stress at the bottom surface with reference to the SLS design load level, positive if traction ( $q = 5.50 \text{ kN/m}^2$ );
- $\sigma_{\text{inf,ULS}}$  : beam stress at the bottom surface with reference to the ULS design load level ( $q = 7.75 \text{ kN/m}^2$ );
- $\Delta w_{\text{ULS}}$  : midspan displacement variation produced by the ULS design load level ( $q = 7.75 \text{ kN/m}^2$ ).

## 5.7 CONCLUSIONS

The research work presented in this chapter was aimed at developing high-performance solutions for prefabricated timber-to-timber composite floor modules to be realised by using laminated veneer lumber made of beech LVL. To exploit the material strength qualities, pre-stressing of the modules was adopted by using the CP assembly procedure presented in Chapter 2. Two modules characterised by different span and service load were designed and tested. Testing of the connection system, that was regarded as the most suited to guarantee the best floor performance (at reasonable economical costs), was also performed.

Decision making during the design process was mainly governed by the limitations ensuing from the Serviceability Limit State (SLS) requirements satisfaction. The deformation limits were selected according to EN 1995. More specifically, the maximum allowable midspan displacement values are:

- Instantaneous deformation:  $w_{\text{inst,Q}} = L/400$
- Final deformation:  $w_{\text{net,fin}} = L/300$

Where  $w_{\text{inst,Q}}$  is the instantaneous midspan displacement calculated for the characteristic combination of the live loads (no permanent loads) and  $w_{\text{net,fin}}$  is the final net deflection (midspan displacement measured from a straight line drawn across the beam supports) due to the quasi-permanent combination of the loads.

Table 5-18 Instantaneous midspan displacement of the tested specimens and relative SLS value

Test	Experimental results		Design values		
	$\Delta w_{inst,Q}$ [mm]	$q_{L/400}$ [kN/m <sup>2</sup> ]	L/400 [mm]	$q_{SLS,design}$ [kN/m <sup>2</sup> ]	SLS
6A	9.46	2.90	15.00	2.00	✓
6B	8.84	3.11	15.00	2.00	✓
6C	9.20	3.06	15.00	2.00	✓
6D	8.36	3.25	15.00	2.00	✓
10A	18.51	4.22	25.00	3.00	✓
10B	18.45	4.24	25.00	3.00	✓

$\Delta w_{inst,Q}$  = midspan displacement variation produced by a vertical force equivalent to the floor service load

$q_{L/400}$  = distributed load level necessary to induce a midspan displacement variation equal to L/400

From the test results (summarised in Table 5-18) it is possible to draw the following remarks.

Floor modules for residential buildings (L = 6 m):

- All tested floor specimens satisfied the SLS and ULS requirements;
- The application of the CP assembly procedure permitted to obtain relatively high values of camber ( $\approx L/200$ , note that the final deformation limit was established at L/300);
- A non-negligible amount of camber ( $\approx L/430$ ) was registered even for the specimen assembled adopting a non-optimal fastener insertion order;
- An equivalent distributed load  $q_0$  necessary to induce a midspan displacement variation equal to the camber value ( $\Delta w_{CP}$ ) ranged between 1.85 kN/m<sup>2</sup> (Test 6A – no Cp procedure) and 5.68 kN/m<sup>2</sup> (Test 6B) was registered;
- Stiffness of the tested specimens assembled with the CP procedure was observed to be higher than the stiffness derived from the pushover curves obtained from the numerical models ( $\approx 20\%$  variation). The extra-stiffness appeared to be related to the magnitude of pre-stress applied (see  $q_{L/400}$  values in Table 5-18);
- The adoption of the CP procedure determined a significant stress reduction with respect to the stress level for “standard” TTC conditions;

- Optimisation of the fastener spacing along the joist axis (for a fixed number of screw fasteners) proved to have limited effectiveness (+ 4% stiffness increase). Adoption of constant fastener spacing appears therefore preferable;
- All tested specimens exhibit failure loads exceeding  $30 \text{ kN/m}^2$ , while the estimated ULS load, accordingly to EN 1991, is  $6.25 \text{ kN/m}^2$ . Such over-strength could prove quite useful when dealing with fire safety (no deformation limits).

Floor modules for office areas, schools and restaurants ( $L = 10 \text{ m}$ ):

- All tested floor specimens satisfied the SLS (and ULS) requirements;
- Due to the high inertia of the module cross section, CP procedure demonstrated to be less effective in terms of upward camber (camber values of approximately  $L/600$ ) when compared to the 6 m module outcome. However, the force required to eliminate the upward deformation introduced by the cambering procedure corresponded to  $1.5 \text{ kN/m}^2$  (0.5 times the characteristic service loads);
- Stiffness of the tested specimens was markedly higher ( $\approx 17\%$ ) than the stiffness derived from the pushover curves obtained from the numerical models. The extra-stiffness appeared to be related to the magnitude of pre-stress applied;
- The adoption of the CP procedure determined a significant stress reduction with respect to the stress level for “standard” TTC conditions;
- Optimisation of the fastener spacing along the joist axis (with a 15% increase in the number of fasteners) determined no appreciable improvements (both in terms of floor stiffness and midspan camber). Adoption of constant fastener spacing appears therefore preferable;
- The floor specimens exhibited neither stiffness degradation nor strength loss due to cyclic loading (up to load levels exceeding ULS conditions)

As discussed in Chapter 2, for any given total number of connectors, a reduction in the central screw spacing should produce an increase in the camber. Conversely shorter spacing values at the floor supports should increase the module out-of-plane performance when subjected to the external loads.

## 5.8 REFERENCES

- [1] Dill-Langer G., Aicher S. (2014) Glulam Composed of Glued Laminated Veneer Lumber Made of Beech Wood: Superior Performance in Compression Loading. *Materials and Joints in Timber Structures*, RILEM Bookseries 9, 603 DOI: 10.1007/978-94-007-7811-5\_55.
- [2] Knorz M., Van de Kuilen J-W. (2012) Development of a high-capacity engineered wood product - LVL made of European beech (*Fagus Sylvatica L.*). *Proceeding of the World Conference on Timber Engineering (WCTE) 2012*, Auckland, New Zealand.
- [3] ETA (European Technical Approval) 14/0354: Glued laminated timber made of hardwood – Structural laminated veneer lumber made of beech.
- [4] European Committee for Standardization (2013). EN 14080: Timber structures – Glued laminated timber and glued solid timber. CEN, Brussels, Belgium.
- [5] Certificate of performance No. 0672-CPR-0415 (MPA Stuttgart 0672).
- [6] ETA (European Technical Approval) ETA-12/0347: X-Lam Dolomiti – CLT.
- [7] ETA (European Technical Approval) ETA-05/0010: Concrete screw made of galvanised steel for use in concrete.
- [8] Schiro G., Giongo I., Sebastian W., Riccadonna D., Piazza M. (2018) Testing of timber-to-timber screw-connections in hybrid configurations. *Construction and Building Materials*, vol. 171, pp. 170-186.
- [9] European Committee for Standardization (2002). EN 1991-1-1:1991: Eurocode 1 - Eurocode 1: Actions on structures - Part 1-1: General actions - Densities, self-weight, imposed loads for buildings. CEN, Brussels, Belgium
- [10] European Committee for Standardization (2001). EN 12512: Timber structures – Test methods – Cyclic testing of Joints made with mechanical fasteners. CEN, Brussels, Belgium.
- [11] European Committee for Standardization (1991). EN 26891: Timber structures – Joints made with mechanical fasteners – General principles for the determination of strength and deformation characteristics. CEN, Brussels, Belgium.
- [12] European Committee for Standardization (2014). EN 1995-1-1:2004+A2:2014: Eurocode 5 - Design of timber structures, Part 1-1, General - Common rules and rules for buildings. CEN, Brussels, Belgium.
- [13] European Committee for Standardization (2005). EN 1990:2002+A1:2005: Eurocode - Basis of structural design. CEN, Brussels, Belgium.
- [14] CSI [Computers and Structures Inc.] (2004) CSI Analysis Reference Manual for SAP2000®, ETABS®, and SAFE®. CSI, Berkele.

---

## 6 LONG-TERM OUT-OF-PLANE TESTING OF PRE-STRESSED TIMBER COMPOSITE FLOORS

### 6.1 INTRODUCTION

A relatively “simple” method for cambering and pre-stressing timber-to-timber composite beams was presented in Chapter 2. The applicability, as well as the effectiveness of this technique, was thoroughly studied in Chapters 2, 4 and 5. In such sections, the maximum capacity and the instantaneous flexural stiffness of TTC beams (and modules) assembled with the above-mentioned procedure were investigated through six-point bending tests. The results, showed that the ultimate limit state (short-term conditions) verifications did not seem to represent a limitation criterion for the design of this type of elements.

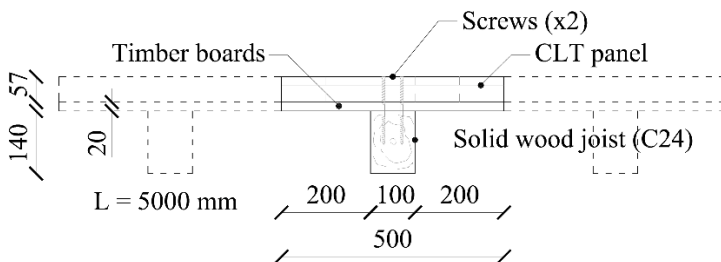
According to international design codes, such as the Eurocode 5 [13], timber structures have to satisfy both ultimate limit state (ULS) and serviceability limit state (SLS) design requirements under short-term and long-term loading scenarios. Consequently, in order to determine the actual applicability of the cambering/pre-stressing (CP) procedure, the rheological behaviour needs to be studied. To this purpose, four experimental tests on the long-term behaviour (out-of-plane) of timber-to-timber composite (TTC) floors were performed in the climatic chamber of the University of Trento (Italy). The environmental parameters T and R.H. (temperature and relative humidity respectively) were kept constant during the whole test period. In particular, a temperature of 20° C and a relative humidity of 60% were set in order to guarantee a service class 1, in accordance with Eurocode 5 [13]: “*moisture content in the materials corresponding to a temperature of 20°C and the relative humidity of the surrounding air only exceeding 65 % for a few weeks per year*”.

## 6.2 TEST CONFIGURATIONS

As visible in Figure 6-1, the specimen geometry reproduces a 0.5 m wide floor module. The span choice (5 m) was determined by the physical constraint of the climatic chamber size (6.5 m x 3.6 m, length x width). The joist cross-section was selected to simulate an existing floor that did not comply with the current Standard provisions and therefore needed to be strengthened. When refurbishing timber diaphragms in traditional masonry buildings, the choice of the strengthening solution is often influenced by the need of having the finished surface level after the intervention compatible with the existing openings. Hence, the thickness of the reinforcing panels adopted in the experimental campaign corresponds to the minimum available on the market for CLT panels (i.e. 57 mm). Such solution, previously checked in accordance with the  $\gamma$ -method contained in the B Annex of Eurocode 5 [13], meets the safety requirements as far as the Ultimate Limit State is concerned (details on the design loads are given in the section 6.2.3), but exceeds the deformability limit under serviceability conditions. The adoption of the CP procedure could therefore be greatly beneficial, provided that its long-term effectiveness is proved.

### 6.2.1 SPECIMEN CONFIGURATIONS

The geometry of the specimens is shown in Figure 6-1. As mentioned before, due to the physical constraint of the climatic chamber, the length of the composite floor was equal to 5000 mm. The floor specimens were realised by coupling a softwood 3-layers cross laminated timber panel (500 x 5000 mm<sup>2</sup>; 57 mm thick) with a solid wood joist grade C24 (100 x 140 mm<sup>2</sup>). A layer of timber boards (20 mm thick) was placed in between the joist and the panel to simulate the existing flooring (non-structural element).



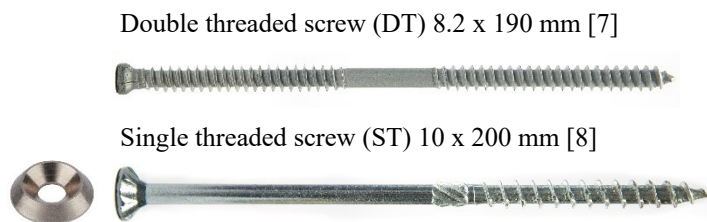


Figure 6-1 Specimen geometry and screw types

According to the relevant European Technical Assessment (ETA - [5]) and the international standard EN 338:2009 [4], the main mechanical properties of the timber elements are those provided in Table 6-1.

Table 6-1 Strength and stiffness properties of the timber elements according to the standards

Element type and grading			Spruce solid wood (C24) [4]	CLT Panel [5]
Bending	$f_{m,k}$	[N/mm <sup>2</sup> ]	24	24
Tension	$f_{t,0,k}$	[N/mm <sup>2</sup> ]	19.2	14
	$f_{t,90,k}$	[N/mm <sup>2</sup> ]	0.5	0.12
Compression	$f_{c,0,k}$	[N/mm <sup>2</sup> ]	24	21
	$f_{c,90,k}$	[N/mm <sup>2</sup> ]	2.5	2.5
Shear	$f_{v,k}$	[N/mm <sup>2</sup> ]	3.5	3.3
MoE	$E_{0,mean}$	[N/mm <sup>2</sup> ]	11500	12000
Density	$\rho_{mean}$	[kg/m <sup>3</sup> ]	420	450-500

Prior to the execution of the full-scale tests, a series of preliminary investigations were performed to determine the MoE and the density of the timber elements. Specifically, the global modulus of elasticity of each timber member was measured experimentally according to EN 408 [6]. The results are summarised in Table 6-2 along with the measured density values.

Table 6-2 Experimental mechanical properties of the timber elements

Element			Test T1	Test T2	Test T3	Test T4
Panel	MoE	[N/mm <sup>2</sup> ]	14224	11813	11803	11520
	$\rho_m$	[kg/m <sup>3</sup> ]	470.4	455.2	456.1	450.6
Joist	MoE	[N/mm <sup>2</sup> ]	8774	11366	8591	10284
	$\rho_m$	[kg/m <sup>3</sup> ]	462.5	459.7	489.2	485.7

By assuming a fixed number of fasteners for each test (i.e. 64), four different screw configurations were addressed by the experimental campaign. As reported in Figure 6-2, for the first two tests (T1 and T2), a constant screw spacing (150 mm) was adopted. In particular, double threaded (DT) screws (8.2 x 190 mm [7]) were used for test T1, while single threaded (ST) screws (10 x 200 mm [8]) were used for test T2. For the T2 configuration, grooves were cut to ensure an adequate contact surface to the washers (W) employed to increase the contact area (see Figure 6-3). The fasteners and the washer used in this experimental campaign are shown in Figure 6-1.

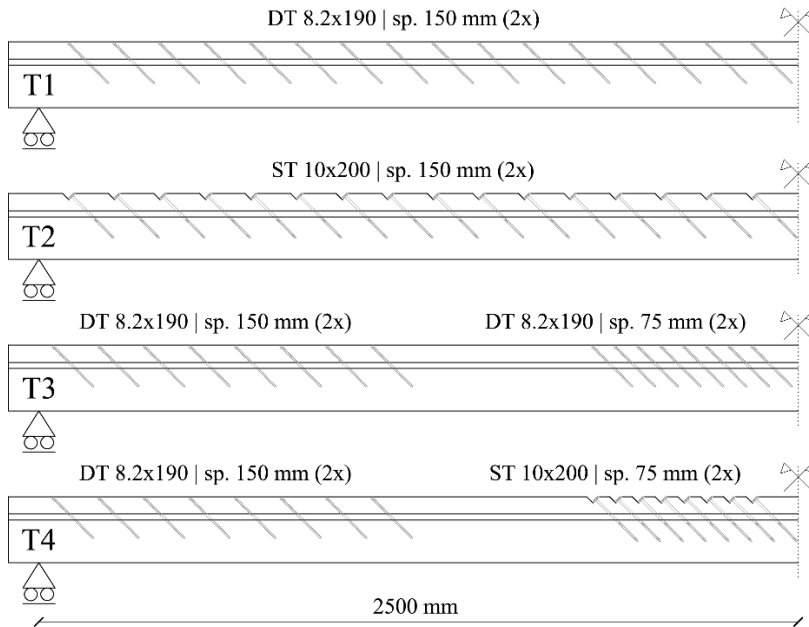


Figure 6-2 Fastener configurations

The influence of variable screw spacing was analysed in test T3 and T4. More specifically, the sample T3 was realized by using the same number of DT screws as for test T1 but with a halved spacing in the central half span (see Figure 6-2). T4 configuration differs from T3 for the use of ST screws in the central part of the beam instead of the DT fasteners. The purpose of test T4 was to couple the high compression force exerted by ST screws (increases camber value) with the higher shear stiffness of DT screws (increases flexural behaviour).

Details on the fastener insertion are given in Figure 6-3.

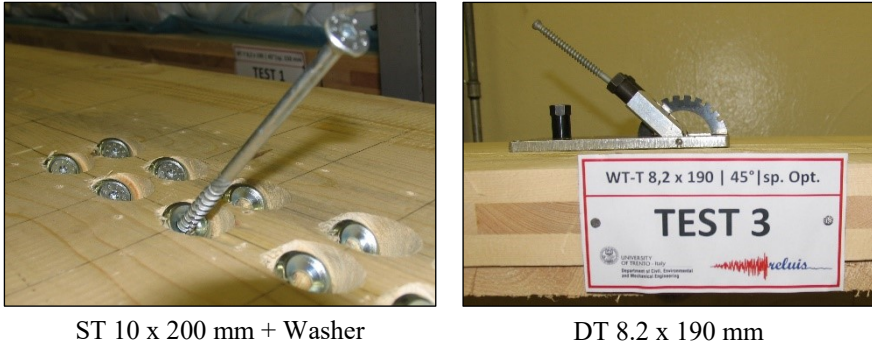


Figure 6-3 Connection details

### 6.2.2 CONNECTION PROPERTIES

10 pushout tests were performed to investigate the mechanical behaviour of the connection systems (Figure 6-4). The screw configurations reproduced the two arrangements selected for the floor specimens. Timber boards were inserted between the central solid wood element and the lateral CLT elements to simulate the existing flooring. The load, introduced by a universal testing machine was monitored with a 100 kN load cell. Two inductive transducers (LVDTs) were employed to measure the relative displacements between the timber components. These tests are a part (test PM and PN) of a larger experimental campaign [24] on the mechanic behaviour of screw-type connector already presented in the document. For a more detailed explanation, please refer to Chapter 3.

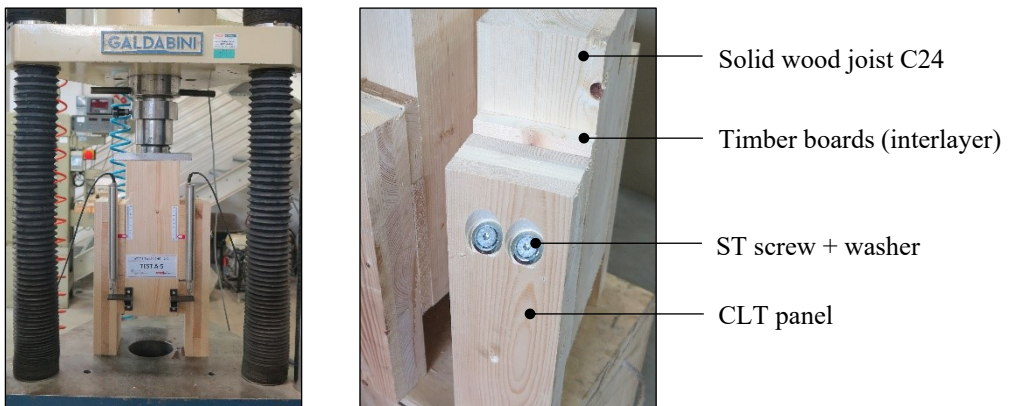


Figure 6-4 Push-out tests

Table 6-3 summarises the main mechanical properties of the connections considered in this section, where  $F_{\max}$  is the mean value of the maximum force registered for all test repetitions associated with each configuration;  $K_s$  is the slip modulus (shear-tension configuration) of the connections (corresponding to the slip modulus  $K_{\text{ser}}$  provided by EN 1995-1-1 [13]) and  $F$  is the compression force generated by the screws. The standards adopted as reference documents for the evaluation of the connection performance parameters were EN 12512 [9] and EN 26891 [10]. In the absence of experimental data on the compression forces  $F$  exerted by the fasteners, the formulation proposed by Giongo et al. in [11] was considered.

Table 6-3 Connection properties (single screw)

		DT 8.2 x 190   45°	ST 10 x 200   45°
$F_{\max}$	[kN]	9.06	12.37
$K_s$	[N/mm]	7835	5700
$F$	[kN]	4.26	5.18

In Figure 6-5 the experimental results from the push-out tests are plotted in terms of connection shear force (per single fastener) versus slip (average value from both specimen sides).

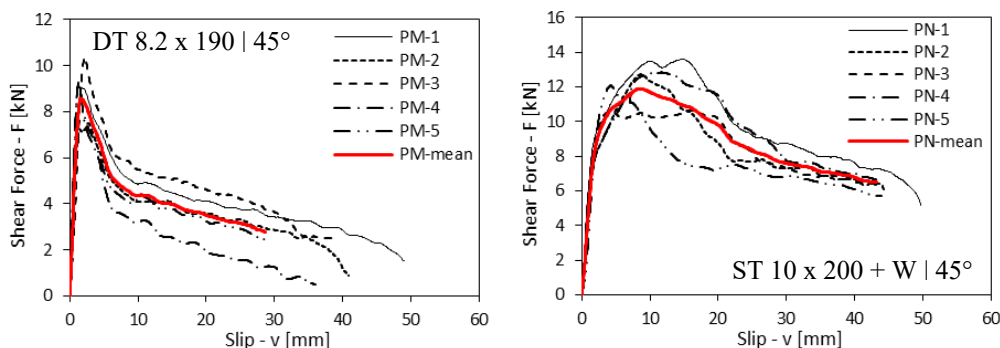


Figure 6-5 Push-out results (Chapter 3)

As expected, ST screws exhibited lower values of slip modulus  $K_s$  (shear-tension configuration) and higher [11] compression force values ( $F$ ) enabling a more effective application of the assembly procedure.

### 6.2.3 DESIGN LOADS AND PARAMETERS

According to EN 1991 [12], the solutions presented in this section were tested out-of-plane considering the following loads:

Permanent non-structural loads (self-weight of non-structural components applied to the floor and self-weight of partitions):

Table 6-4 Permanent non-structural loads

Components	[kN/m <sup>3</sup> ]	[mm]	[kN/m <sup>2</sup> ]
Floor finish		20	0.50
Lightweight concrete screed	16	30	0.48
Insulation panel	2.5	40	0.10
Screed	18	50	0.72
Internal partitions			1.2
$g_{2,k} =$			3.00

Characteristic service load (Cat. A – Areas for domestic and residential activities):  $q_k = 2 \text{ kN/m}^2$ .

With reference to the EN 1995 [12], the following deflection limit values were considered for the Serviceability Limit States (SLS):

- Instantaneous deflection:  $w_{inst} = L/300 = 16.67 \text{ mm}$ ;
- Final deflection (creep phenomena):  $w_{net,fin} = L/350 = 14.29 \text{ mm}$ .

Where  $w_{inst}$  is the instantaneous deflection due to the characteristic combination of actions ( $Q_{Ch.} = 5.43 \text{ kN/m}^2$ ) and  $w_{net,fin}$  is the final net deflection due to the quasi-permanent combination of actions with reference to a straight line drawn between the supports ( $Q_{Q.P.} = 4.03 \text{ kN/m}^2$ ).

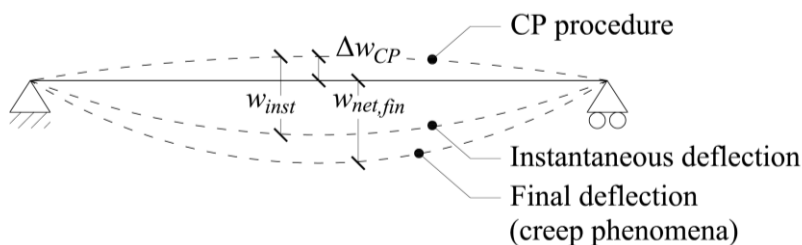


Figure 6-6 Components of deflection

As previously mentioned, the ultimate capacity of the specimens was evaluated during the design phase through the gamma method from the EN 1995. Consequently, every TTC floor met the Ultimate Limit State safety requirements [13].

### 6.3 TEST SET-UP AND INSTRUMENT ARRANGEMENT

As presented in the opening paragraph, the experimental tests were performed in the climatic chamber of the University of Trento. The environmental parameters T and R.H. (room temperature and relative humidity) were kept constant at values of respectively 20°C and 60% for the whole testing period (except for a short period due to malfunctioning of the control system, see Figure 6-7). This assumption allowed to neglect the mechano-sorptive deformation of the timber elements ([14] and [15]), reducing the variables that influence the long-term behaviour of composite floors. More specifically, it was possible to analyse the influence of screw compression force relaxation over time on the viscous deformation of the timber elements and the overall “compound response”.

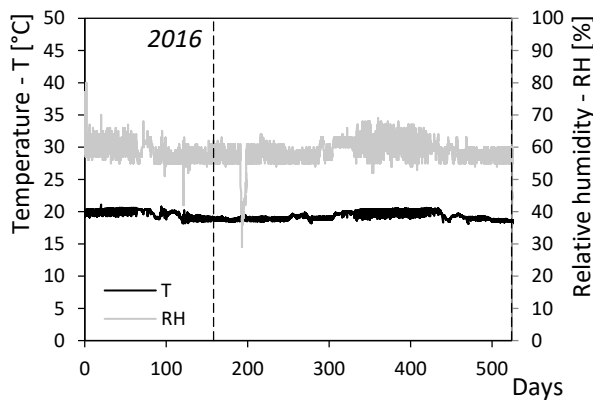


Figure 6-7 Temperature and relative humidity values over the entire testing period

With reference to the instrument layout, the midspan deflection ( $w$ ) and the interface slip at the beam ends ( $\delta_L$  and  $\delta_R$ ) were measured during all the testing phases. The sign convention assumed is reported in Figure 6-8). In addition (see Figure 6-9 right), for test T4 the stress distribution at the midspan cross section of the joist was evaluated by means of two linear strain gauge sensors ( $\epsilon_u$  and  $\epsilon_d$ ).

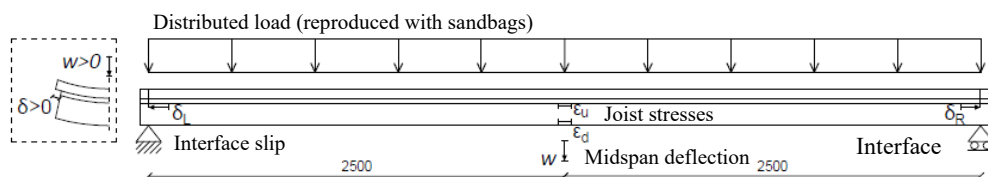


Figure 6-8 Test set-up and instruments arrangement

During an initial period of two weeks, inductive transducers (LVDTs) and string potentiometers were used. After this period, the digital instruments were replaced with analog instruments (see Figure 6-9: long-term monitoring).

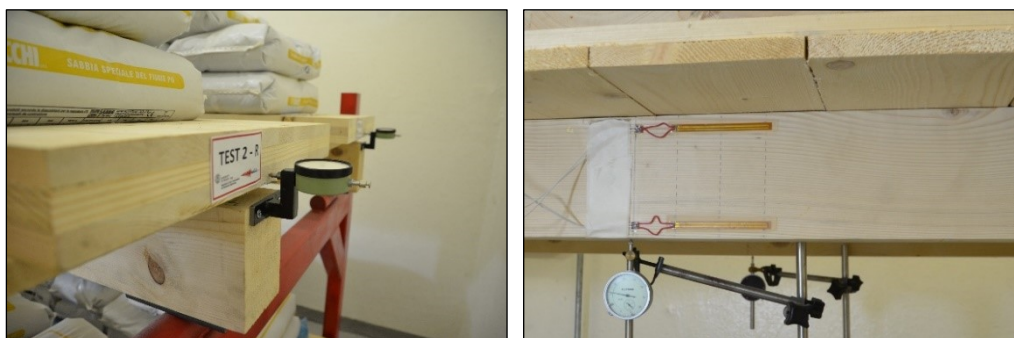


Figure 6-9 Analog instruments (left and right) used for long-term monitoring and midspan strain gauge sensors (right)

To reproduce the vertical loads acting on the floor structure, sandbags were used. To facilitate the specimen loading and unloading, the sandbags were 25 kg each. In order to avoid weight variation because of moisture absorption, the bag tightness was carefully checked before commencing the loading phase. When needed the seal was secured with waterproof duct tape.

The experimental work was comprised of five testing phases (see Figure 6-14):

1. Cambering of the specimen by means of the CP procedure;
2. Loading of the specimen (characteristic combination:  $Q_{Ch}$ );
3. Unloading of the specimen and measurement of the instantaneous elastic regain;
4. Re-loading of the specimen (quasi-permanent combination:  $Q_{QP}$ );
5. Long-term monitoring of midspan deflection and interface slips.

## 6.4 EXPERIMENTAL RESULTS

### 6.4.1 ASSEMBLY PROCEDURE

In this section, the results of the assembly procedure are presented. Figure 6-10 plots the midspan uplift evolution registered during the screw insertion. Differently from the graphs used in Chapter 2 to describe the camber evolution, on the x-axis of Figure 6-10 the total number of screw inserted at each step was indicated. Hence, by dividing the fastener number by 4 is possible to define the *i*-th step number ( $N = 16$ ).

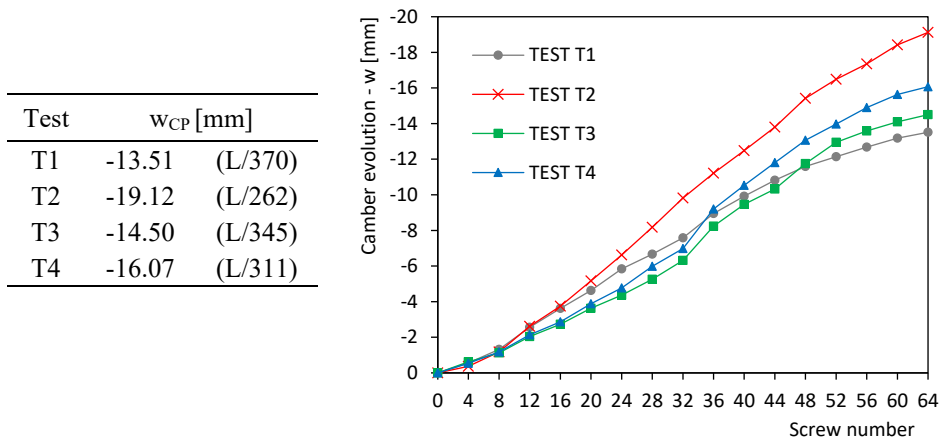


Figure 6-10 Midspan uplift evolution

All the specimens exhibited a significant uplift. The midspan deflection values were comparable (but in the opposite direction) with the deformation corresponding to the serviceability limit state (L/350). Test T2 showed the best performance, thanks to the higher pressure developed by the ST screws coupled with washers (see [11] for insight about the compression force generated by different screw connectors). By comparing the uplift values from T3 and T1, a 7.4% camber increase can be noted. The substitution of the central DT screws with ST screws (T3 vs. T4) produced a further 10.8% of improvement.

At the end of the CP procedure, all tests were kept unloaded for a period of 15 hours. As results, test T1 exhibited a further 3.36 % increase in midspan uplift (from 13.51 mm to 13.96 mm). No variation in the camber value was instead observed for test T2 during the above mentioned 15h. The actual camber variation recorded for specimens T1 and T2 is given in Figure 6-11.

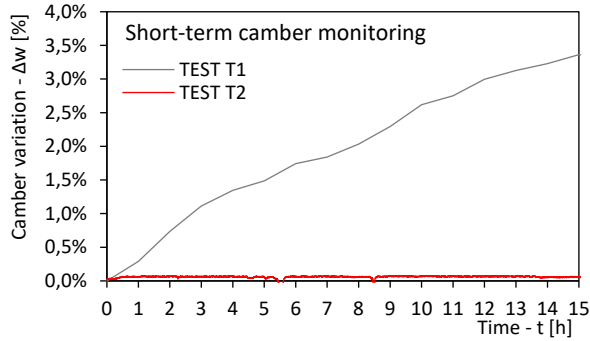
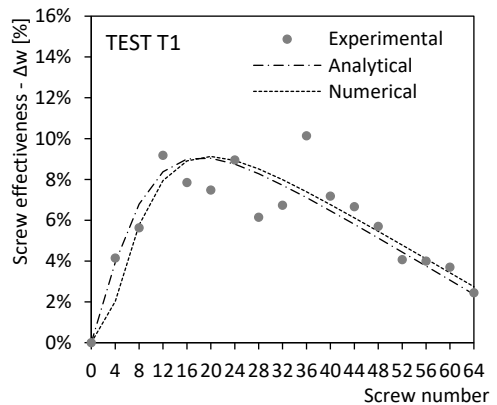
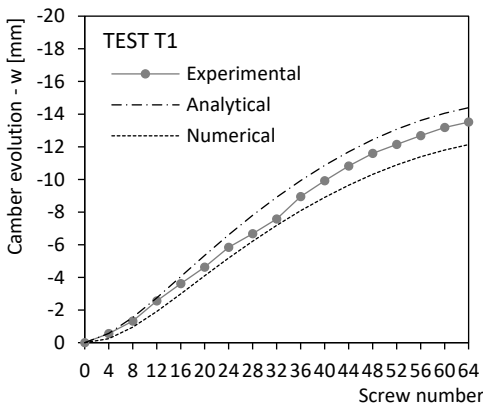


Figure 6-11 Test T1 and T2: camber variation at the end of the CP procedure (without load applied)

These findings can be explained by analysing the different screw typology used for test T1 and test T2. Giongo et al. [11] in fact observed a gain in the level of compression force exerted by double threaded screws when monitoring the short-term pressure variation of self-tapping screws connecting two timber elements. This delayed, post-assembly increase in the compression force appears to be a reasonable explanation for the short-term camber rise observed from test T1.

In the following graphs, for each test, the experimental camber at the midspan (solid line) is compared to the prediction obtained from the numerical model (dashed line) and the analytical formulation (dash-dot line). Specifications on the both the numerical model and the analytical formulation are provided in Chapter 2. The analytical formulation assumes a uniform connection stiffness and consequently cannot be applied to tests T3 and T4 where the spacing was variable.



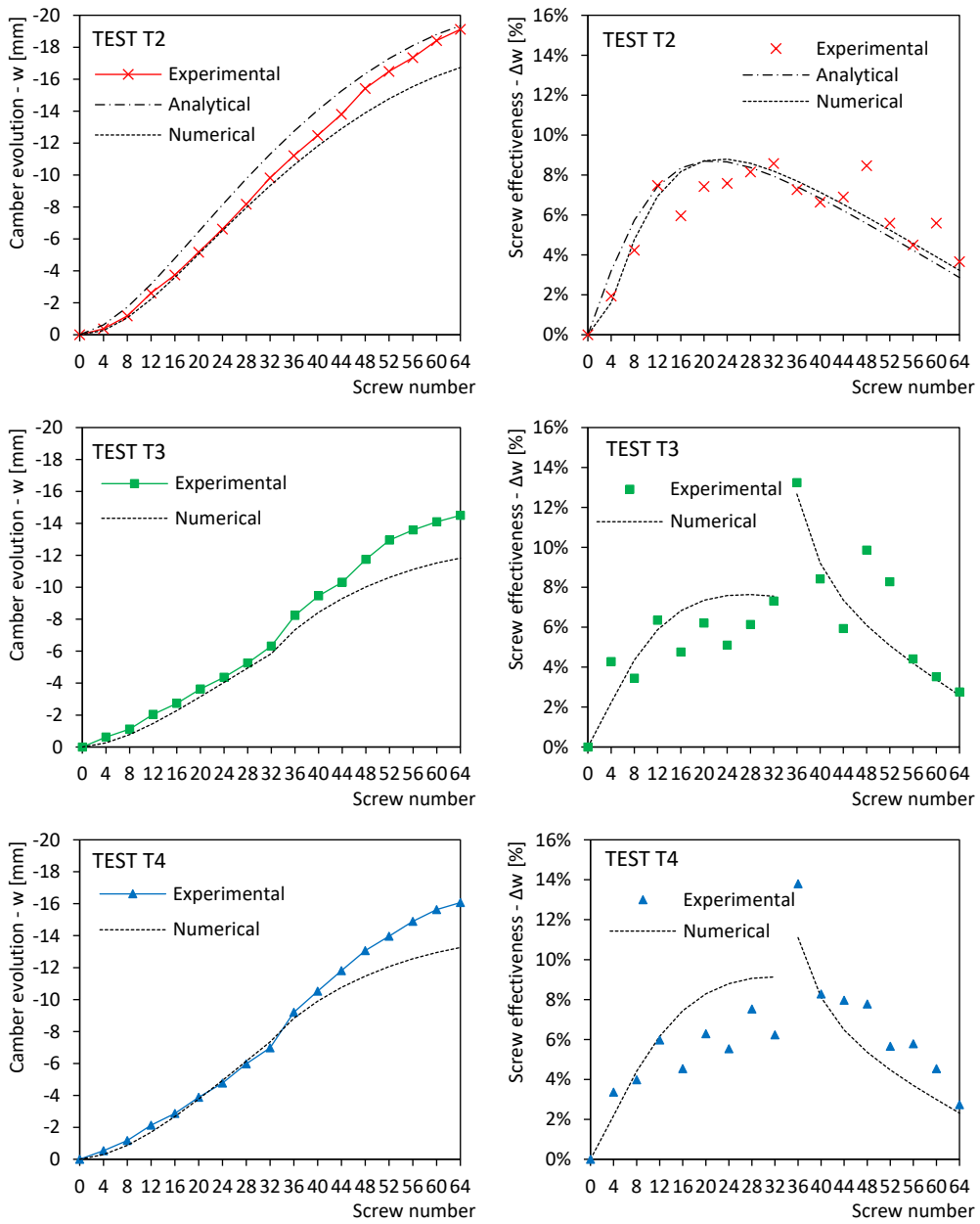


Figure 6-12 Comparison of the experimental outcomes with the analytical and numerical models in terms of camber evolution and screw effectiveness

As can be appreciated from Table 6-5, where the comparison regards the final midspan uplift, a good correlation between the experimental and analytical data was registered.

On the other hand, a general underestimation of the camber value was highlighted by comparing the numerical prediction to the experimental outcomes, especially where a variable screw spacing was adopted (test T3 and T4).

*Table 6-5 Experimental uplift values at the end of the CP procedure and comparison with numerical and analytical predictions*

Test	Experimental	Numerical		Analytical	
	$w_{Exp}$ [mm]	$w_{Num}$ [mm]		$w_{Th}$ [mm]	
T1	-13.51	-12.13	-10.18 %	-14.4	+6.56 %
T2	-19.12	-16.73	-12.52 %	-19.4	+1.18 %
T3	-14.50	-11.82	-18.46 %	-	-
T4	-16.07	-1326	-17.52 %	-	-

#### 6.4.2 SPECIMEN LOADING (SHORT-TERM)

Once the assembly was completed (phase 1), each specimen was loaded (

Figure 6-13) with a number of sandbags reproducing the uniform load distribution as per the characteristic combination ( $Q_{Ch} = 5.43 \text{ kN/m}^2$ ). The load was removed after a period of about half-hour (phase 2).



*Figure 6-13 Specimen loading*

Subsequent to the specimen unloading (phase 3) and the elastic regain of the camber, the specimens were reloaded with the quasi-permanent load (phase 4,  $Q_{QP} = 4.03 \text{ kN/m}^2$ ) and set for long-term monitoring (phase 5). The experimental outcomes from phase 1

to phase 4 are presented in Table 6-6, where  $w$  is the midspan deflection measured from a straight line between the supports (positive if downwards).

Table 6-6 Test results from phase 1 to phase 4

Phase	$w$		T1	T2	T3	T4
1°	$w_{CP}^*$	[mm]	-13.96	-19.13	-14.55	-16.33
2°	$w_{Ch.}$	[mm]	5.58	-3.95	5.22	0.74
	$\Delta w_{Ch.}$	[mm]	19.54	15.18	19.77	17.07
3°	$w_{Unload}$	[mm]	-13.12	-18.5	-14.2	-15.8
4°	$w_{Q.P.}$	[mm]	0.50	-7.43	0.12	-3.46
	$\Delta w_{Q.P.}$	[mm]	13.62	11.07	14.32	12.34

$w_{CP}^*$ : camber value after ~15 h from the end of the CP procedure

As an example, in Figure 6-14 the variation of the midspan displacement  $w$  during the various testing phases up to one week after the application of the permanent loading is reported for test T2.

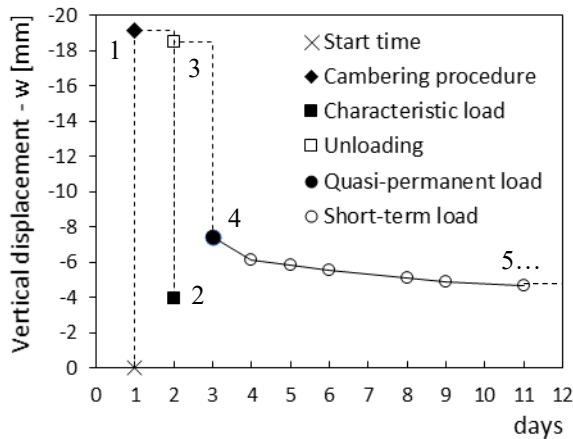


Figure 6-14 Test T2: representation of the testing protocol

Test T2 exhibited an instantaneous midspan deflection  $\Delta w_{Ch}$  due to the characteristic load combination lower than  $L/300$ . Moreover, T2 test showed a residual camber of -3.95 mm even after the application of the characteristic load. Subsequent to the unloading of the specimens, no significant residual deformations were registered in all specimens, thereby proving that the effects of the assembly procedure persist also after a loading-unloading test. At the end of phase 4 when the samples were loaded with the quasi-permanent combination of actions, tests T2 and T4 showed a significant residual

upward deflection (-7.42 mm for T2 test). However, a downward deflection smaller than 0.50 mm was observed for tests T1 and T3 even after the load imposition.

From the comparison of the instantaneous deflection values ( $\Delta w_{Ch}$  and  $\Delta w_{QP}$ ), it can be observed that test T1 and T3 showed a lower bending stiffness despite the use of DT screws. This behaviour can be attributed to a combination of factors: 1) the smaller MoE of solid wood joists used for specimens T1 and T3 (Table 6-2); 2) a possible underestimation of ST screw stiffness. Specifically, the contribution of friction to the slip modulus in the pushout tests (reported in Chapter 3) might have been decreased by a minimal surface separation at the timber element interface because of the force lever arm (see Figure 6-4a)

### 6.4.3 SPECIMEN LOADING (LONG-TERM)

Figure 6-15 gives the deformation development starting from the date when test T1 was assembled (T1 test was started approximately three months before the other specimens were assembled). In the same graph, the variation of the relative humidity is also reported. As already mentioned, malfunctioning of the control system regulating the humidifier was experienced at days 198-199. During that period the relative humidity decreased to approximately 30 % before the system rebooted and could restore the normal 60 % ( $\pm 5$  %).

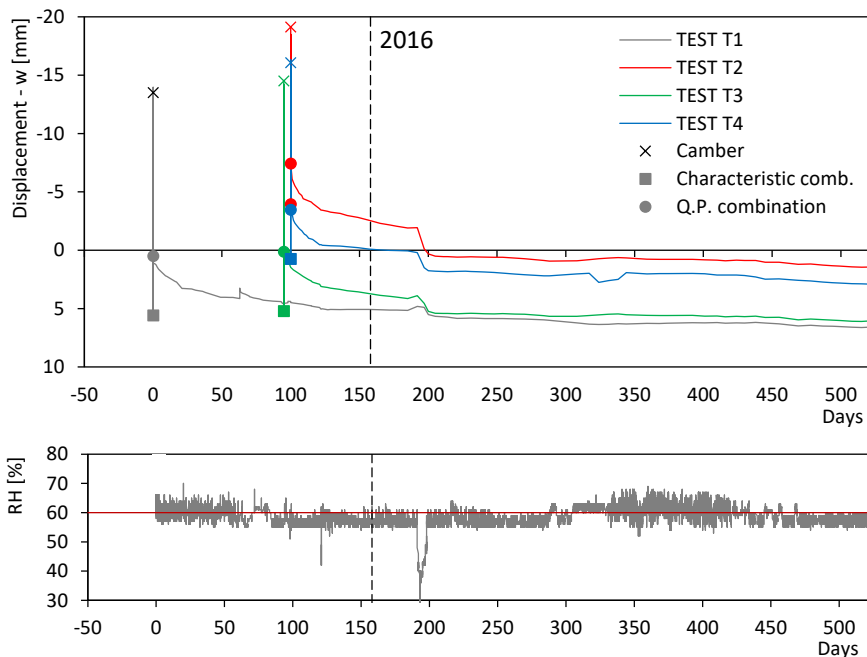


Figure 6-15 Phase 5: long term monitoring

This meant a remarkable, almost instantaneous, deformation increase for all the specimens except for T1 (Figure 6-15) that besides a momentary settling, appeared to be unaffected by the temporary humidity variation.

It is common knowledge that long-term behaviour of wood is significantly influenced by the environmental conditions (external temperature and relative humidity). More specifically, wood is affected by phenomena such as creep, shrinkage, swelling, thermal strain and mechano-sorptive creep [15]. This last contribution is related to cycles of moisture content (MC) variation. In general, to a moisture content change corresponds a dimensional variation of the timber element section. Being the pull-through stiffness/resistance of the rear part of the ST fasteners strongly dependent on the effectiveness of contact between the screw-head/washer and the wood surface, it appears evident that ST screws are more sensitive to wood dimensional changes than DT screws (Figure 6-16).

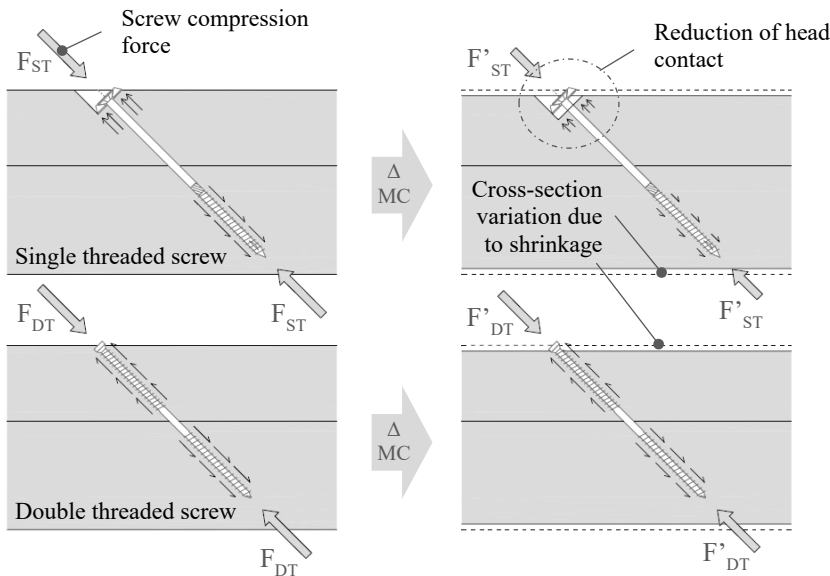


Figure 6-16 Schematic representation of the correlation between timber dimensional changes and compression force exerted by ST/DT screws

It is worth noting that despite the effects of the aforementioned malfunctioning, the performance of all specimens largely satisfy the most restrictive requisites by Eurocode 5 [12] in terms of final deflection ( $w_{fin,net} < L/500$  for all specimen configurations).

Figure 6-17 shows the specimen layout within the climatic chamber. By arranging the specimens on two levels, it was possible to optimize the space and create a lateral

corridor to facilitate the data collection from the analogue instruments. The floor specimen supports were realized by using steel tubular elements. Steel cylinders were welded to the support frame to ensure “simply supported beam” boundary conditions. Steel plates were fixed to the joists to distribute the contact stresses and avoid local crushing of the wood fibers.

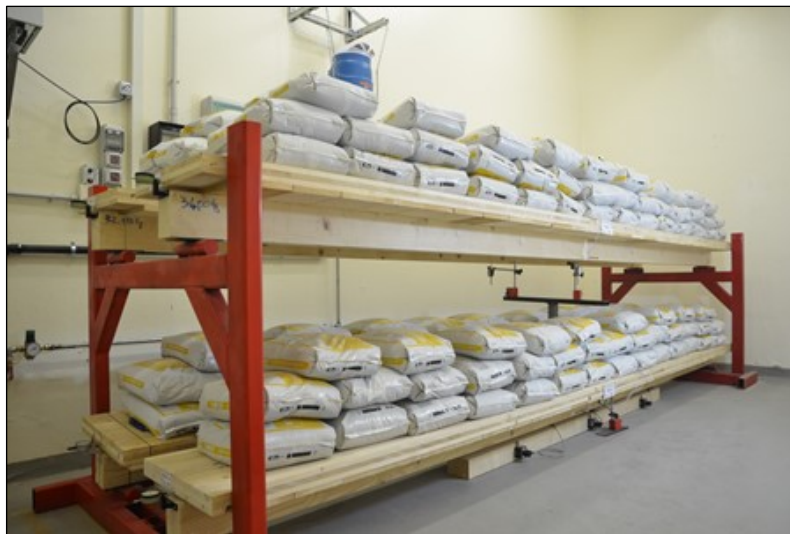


Figure 6-17 Long term testing under quasi-permanent load combination (test setup)

## 6.5 PREDICTION OF THE LONG-TERM BEHAVIOUR

In this section, the outcomes of the experimental campaign are compared with a predictive model for the long-term evaluation of the flexural behaviour of timber composite structures.

An extremely simplified method that permits to estimate the final deformation (50 years) of a composite structure is proposed by the Eurocode 5 [13]. In particular, according to point 2.3.2.2 of [13], “for serviceability limit state, if the structure consists of members or components having different time-dependent properties, the final mean value of modulus of elasticity  $E_{mean,fin}$ , shear modulus  $G_{mean,fin}$  and slip modulus  $K_{ser,fin}$  which are used to calculate the long-term deformation due to the quasi-permanent combination of actions should be taken from the following expression:”

$$E_{mean,fin,i} = \frac{E_{mean,i}}{1 + k_{def}} \quad (\text{Eq. 1})$$

$$K_{ser,fin} = \frac{K_{ser}}{1 + k_{def}} \quad (\text{Eq. 2})$$

Where  $k_{def}$  is a coefficient for the evaluation of the “final” creep deformation that depends on the relevant service class and the material type. For solid timber/glued laminated timber/LVL in service class 1,  $k_{def} = 0.6$  [13]. The conventional reduction factors used for the evaluation of the final moduli of elasticity allows to account for the global creep behaviour by assuming a fictitious time dependency of this parameter. Indeed, the real value of modulus of elasticity is not time dependent [17].

As presented in [15], at any moment  $t$  the mechanical properties can be evaluated by referring to the following formulae:

$$E_{mean,i}(t) = \frac{E_{mean,i}}{1 + \phi_{t,i}(t - t_0)} \quad (\text{Eq. 3})$$

$$K_{ser}(t) = \frac{K_{ser}}{1 + \phi_{t,con}(t - t_0)} \quad (\text{Eq. 4})$$

Where  $\phi_t(t - t_0)$  is the time-dependent creep coefficient, while  $t$  and  $t_0$  are the final and initial instant of the analysis respectively.

In the predictive model presented in this paragraph, the creep coefficient proposed by Toratti [16] was used:

$$\begin{aligned} \phi_t(t - t_0) &= \phi_{tc}(t - t_0) + \phi_{tms}(t - t_0) = \\ &= \left(\frac{t - t_0}{t_d}\right)^m + \phi^\infty \left[1 - e^{-c \frac{2\Delta u}{100\Delta t}(t - t_0)}\right] \end{aligned} \quad (\text{Eq. 5})$$

Where:

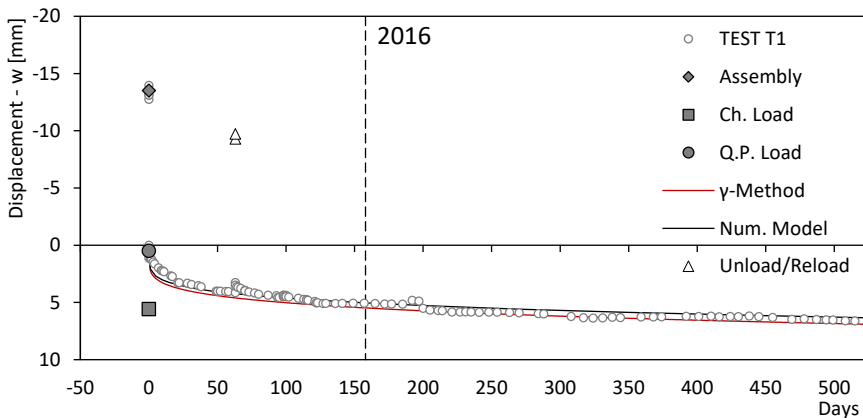
- $\phi_{tc}(t - t_0)$  : creep part of the total creep;
- $\phi_{tms}(t - t_0)$  : mechano-sorptive part of the total creep;
- $m$  : coefficient equal to 0.21 for spruce elements;
- $c$  : coefficient equal to 2.5 for spruce elements;
- $t_d$  : is the doubling time of creep, which for spruce it corresponds to 29500 days;
- $\phi^\infty$  : coefficient equal to 0.7 for spruce element;
- $\Delta u$  : is the maximum variation of the moisture content.

Since the environmental parameters T and R.H. were kept constant for the whole testing period (except for a short time period) the mechano-sorptive deformation of timber elements can be neglected ([14] and [15]).

The modulus of elasticity of the timber elements  $E_{mean,i}(t)$  (Eq. 3) and the slip modulus of the connection  $K_{ser}(t)$  (Eq. 4) were used in the numerical model (a full description of the numerical model and its properties is provided in Chapter 2) to calculate the long-term deformation. With reference to tests T1 and T2 (constant fastener spacing) where the analytical prediction of the long-term behaviour was attempted by referring to the  $\gamma$ -method proposed by the Annex B of EN 1995 [13], the time-dependent parameters  $E_{mean,i}(t)$  and  $K_{ser}(t)$  were also used. .

Despite the Eurocode 5 [13] suggestion to double the connection creep coefficient if the system is made of timber elements with the same time-dependent behaviour (joist elements and CLT panels are made of spruce), the same creep coefficient was used for timber elements and connection ( $\phi_{t,i}(t - t_0) = \phi_{t,con}(t - t_0)$ ). As it will be shown in the following, this assumption has proven to better reproduce the experimental evidence.

Figure 6-18 compares the results from the predictive models for long-term behaviour of composite structure (obtained by employing Toratti’s coefficient) with the experimental curves.



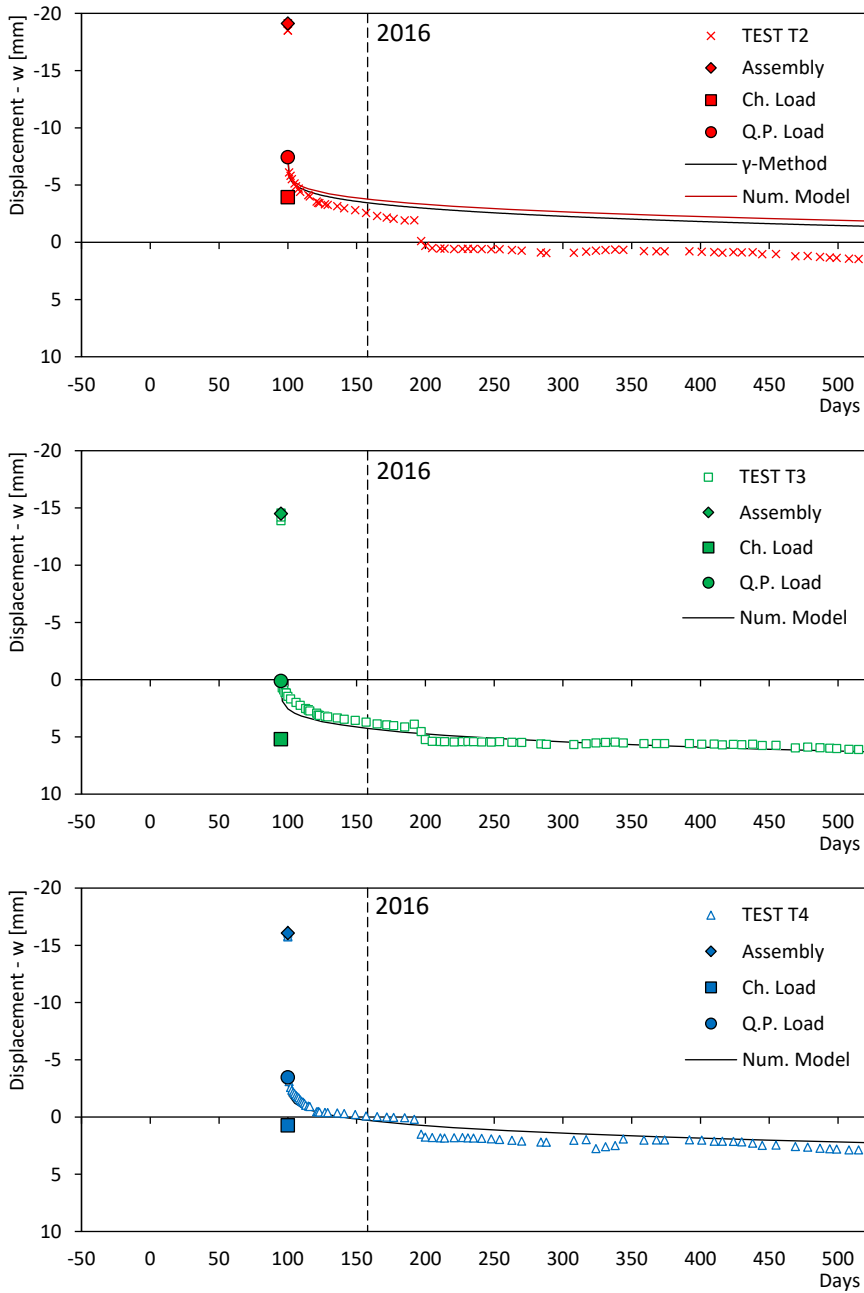
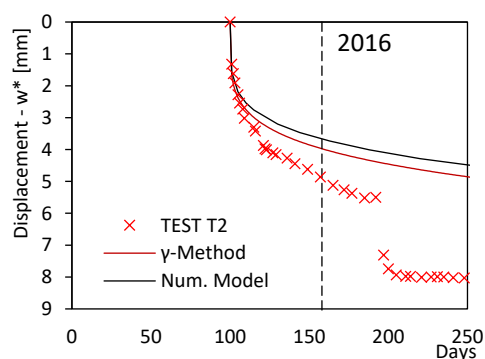
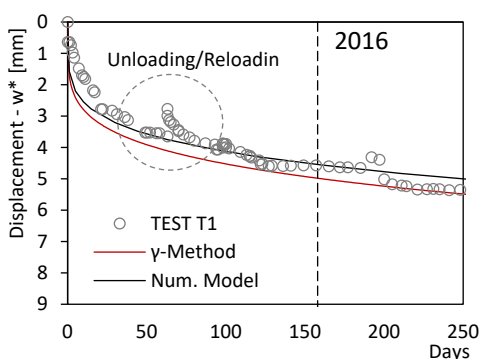


Figure 6-18 Long-term behaviour: experimental data Vs. predictive models

With reference to test T1, it can be observed how both the predictive models (numerical model and  $\gamma$ -method) closely reproduce the experimental behaviour. This denotes that, despite the inevitable reduction over time of the compression force generated by the screws (see [11]), the beneficial effects of the CP procedure are overall stable. The numerical model, in fact, considers only viscous phenomena at the material and connection level ( $\phi_{t,i}(t - t_0), \phi_{t,con}(t - t_0)$ ) and does not take into account changes in the “composite action” due to a possible “screw pressure” decrease. Similar considerations can be made for T3 and T4. It can be noted how before and after the deflection shift induced by the RH spike, the slope of the two curve branches is perfectly consistent and the experimental lines are parallel to the predictive curves. The flexural behaviour of the samples in correspondence to the RH variation (days 198-199) is examined in Figure 6-19 ( $w^*$  starts after the application of the quasi-permanent combination of actions – point 4 in Figure 6-14).

Regarding test T2, the midspan deflection exceeded the expected value, even prior to the RH spike, showing dissimilar performance of ST connections with respect to DT connections. Further study is required to determine whether the deformation increase is to be attributed to the connection stiffness reduction, or to the alteration of the force exchanged at the interface deriving from a loss of screw compression force.

Two months after the assembly of the sample (day 63), test T1 was unloaded and, after four hours, reloaded with the same number of sandbags. As a result, the specimen exhibited an instantaneous elastic regain equal to 13.40 mm, followed by a further delayed-regain of 0.47 mm. The total uplift observed in this phase ( $w_{Unload} = 13.87$  mm) is comparable to the camber value ( $w_{CP^*} = 13.96$  mm). After the reloading of the composite beam, no deformation shifts were observed and the experimental data continued to match the original predictive curve.



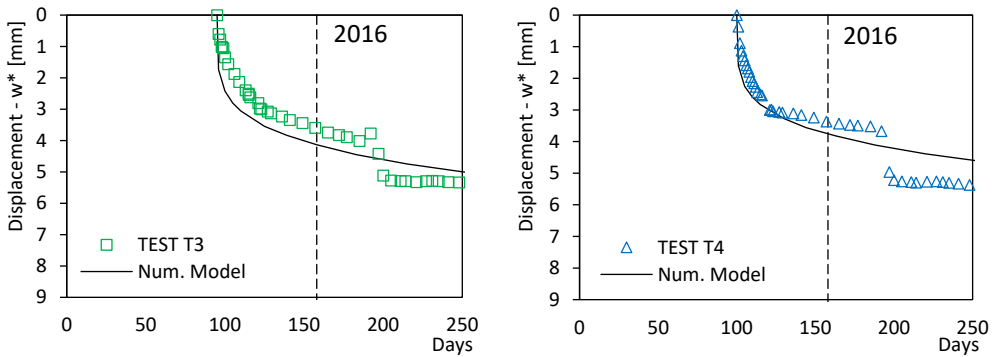


Figure 6-19 Flexural behaviour of the specimens in correspondence to the RH variation (days 198-199)

## 6.6 CONCLUSIONS

An experimental campaign on the long-term performance (out-of-plane) of timber diaphragms strengthened with crosslam panels fixed to the joists by employing to the cambering/pre-stressing procedure proposed in Chapter 2, was presented. Four specimens 5.4 m long (5 m net span) were subjected to long-term loading in controlled environmental conditions at the University of Trento.

The main outcomes of the experimental work can be summarized as follows:

- Despite the inevitable reduction over time of the compression force generated by the screws, the benefits of adopting the CP procedure when realizing timber-to-timber strengthening solution appeared to be persistent over time;
- After a monitoring period of two years, all TTC solutions exhibited a final net deformation  $w_{fin,net}$  under a quasi-permanent load combination of actions well below  $L/500$  (the limit value provided by the Eurocode 5 [13] ranges between  $L/250$  and  $L/350$ );
- Thanks to a higher compression force and a lower stiffness, the ST screws coupled with washers permitted to obtain higher camber values than the DT screws;
- On the other hand, T2 test, assembled with ST screws, exhibited a higher creep rate than the specimens constructed with DT screws;
- ST screw connections showed a more sensitive response to wood moisture content changes than DT screw connections;

- The combined use of both ST and DT fasteners as in T4 test, appeared to be promising. However, further testing on the long-term behaviour of such mixed connection system is strongly recommended;
- A general good correlation between the predictive models (numerical model and  $\gamma$ -method) and the experimental data was observed.

## 6.7 REFERENCES

- [1] Giongo I., Piazza M., Tomasi R. (2012) Cambering of timber composite beams by means of screw fasteners. *Journal of Heritage Conservation*, vol. 32, pp. 133-136.
- [2] Giongo I., Schiro G., Piazza M., Tomasi R. (2016) Long-term out-of-plane testing of timber floors strengthened with innovative timber-to-timber solutions. Proceedings of the World Conference on timber Engineering (WCTE), Vienna, Austria.
- [3] CEN (2014) EN 1995-1-1: Design of timber structures – Common rules and rules for buildings. CEN, Brussels, Belgium.
- [4] European Committee for Standardization (2009). EN 338: Structural timber – Strength classes. CEN, Brussels, Belgium.
- [5] ETA (European Technical Approval) 12/0347: X-Lam Dolomiti – CLT
- [6] European Committee for Standardization (2010) EN 408: Timber Structures – Structural timber and glued laminated timber – Determination of some physical and mechanical properties. CEN, Brussels, Belgium.
- [7] ETA (European Technical Approval) 12/0063: SFS self-tapping screws WT
- [8] ETA (European Technical Approval) 11/0030: Rotho Blaas self-tapping screws
- [9] European Committee for Standardization (2001). EN 12512: Timber structures – Test methods – Cyclic testing of Joints made with mechanical fasteners. CEN, Brussels, Belgium.
- [10] European Committee for Standardization (1991). EN 26891: Timber structures – Joints made with mechanical fasteners – General principles for the determination of strength and deformation characteristics. CEN, Brussels, Belgium.
- [11] Giongo I., Piazza M., Tomasi R. (2013) Investigation on the self-tapping screws capability to induce internal stress in timber elements. *Advanced Material Research*, vol. 778, pp. 604-611.

- [12] European Committee for Standardization (2002). EN 1991-1-1:1991: Eurocode 1 - Eurocode 1: Actions on structures - Part 1-1: General actions - Densities, self-weight, imposed loads for buildings. CEN, Brussels, Belgium.
- [13] European Committee for Standardization (2014). EN 1995-1-1:2004+A2:2014: Eurocode 5 - Design of timber structures, Part 1-1, General - Common rules and rules for buildings. CEN, Brussels, Belgium.
- [14] Mohager S., Toratti T. (1993). Long term bending creep of wood in cyclic relative humidity. *Wood science and technology*, vol. 27, pp.49-59.
- [15] Fragiacomio M., Ceccotti A. (2006). Simplified approach for the long-term behaviour of timber-concrete composite beams according to the eurocode 5 provisions. International council for research and innovation in building and construction (CIB-W18/39-9-1). Meeting thirty-nine, Florence Italy.
- [16] Toratti T. (1992). Creep of timber beams in a variable environment. PhD. Thesis ISBN 951-22-1251-X. Helsinki University of Technology, Finland.
- [17] Ceccotti, A. (1995). "Timber-concrete composite structures." Timber Engineering, Step 2, First Edition, Centrum Hout, The Netherlands, E13/1-E13/12.

## 7 CONCLUSIONS

The main objective of the research work presented herein was to deepen the understanding of the out-of-plane mechanical behaviour of timber-to-timber composite (TTC) floors obtained by relying on dry connection systems (with incomplete interaction). To this purpose, several types and arrangements of connections and different timber products, made from both softwood and hardwood species, were considered for the development and testing of technical solutions suitable for a wide range of structural applications.

To optimise the performance of these structural systems, an original assembly procedure (CP procedure), developed at the University of Trento, was considered. This method allows the designers to pre-stress and camber composite timber elements by simply relying on screw type connectors arranged in a specific configuration (no additional external supports are required). The potentiality shown by this technique makes it a valid option for the retrofit of vintage timber floors. Basically, by applying this assembly method it is possible to reduce the effects of irreversible deformation and to improve the out-of-plane response of existing diaphragms without significantly increasing the weight. In addition, use of this technique seems to be even more promising when it aimed at the development new timber diaphragms characterized by extremely high mechanical performance.

In order to predict the effects resulting from the implementation of this procedure, an analytical formulation suitable for describing both the stress and the strain state was described in Chapter 2. Successively, a numerical model was developed through a finite element software. The nonlinear staged construction analysis was employed to reproduce the sequential insertion of the connectors during the assembly procedure. A general good correlation was observed between the results from the analytical formulation and the numerical model. Furthermore, a parametric study was performed in order to better understand the effects of different fastener configurations on the mechanical behaviour of composite systems assembled with the CP procedure. The

configuration with the fasteners equally distributed along the beam axis has proved to be the most performing solution, considering both the benefits introduced by the assembly procedure and the flexural behaviour of the system under vertical load.

A total of twenty-seven full scale tests on timber-to-timber composite floors (from 5.4 m to 10 m span) were carried out at the laboratory of the Department of Civil, Environmental and Mechanical Engineering (DICAM) of the University of Trento. The outcomes positively contributed to the calibration and validation of this assembly technique, confirming the method applicability. Furthermore, the test results were consistent with the predictions from the numerical and analytical models, in terms of uplifts, stress levels and overall mechanical performance.

In contrast to connectors typically used in steel structures, there is currently no harmonized standard that establishes the requirements for structural timber screw connections. As a consequence, there are several typologies of self-tapping screw available on the market that differ from each other for geometry, type of thread, head and tip. Currently, the mechanical properties provided by the producers in the product standards permit to characterize the performance of these connections only when used in “standard” configurations (typically orthogonal to the grain and inserted in softwood elements). As the extrapolation of the results from other “similar” fastener types and configurations is inadvisable, an experimental campaign was performed by focusing on the short-term mechanical performance of those connection configurations deemed as suitable for creating pre-stressed/pre-cambered timber-to-timber composite structures, where the fasteners are inserted at an angle to the grain other than  $90^\circ$  and may connect different timber products. The research activity on timber fastener connections consisted of fifty-eight specimens laid out in fourteen arrangements. Each sample was tested under quasi-static monotonic loading. Result comparisons regarding connection stiffness, strength, static ductility, residual strength and failure mode were presented and discussed. The data obtained from these tests provided paramount input parameters that were used in the design process of all timber-to-timber composite floors investigated in this document.

Seventeen configurations of TTC floors spanning 6.4 m were analysed in Chapter 4. The aims of these tests were two. Specifically, the first goal was to investigate the mechanical behaviour of composite beams designed for newly constructed high-performance diaphragms. The second aim of this experimental campaign was to evaluate the performance of alternative strategies for retrofit interventions on timber diaphragms in historical heritage buildings affected by large deformations. Hybrid solutions, that coupled the lightness of softwood elements, with the strength of hardwood components by means of different types of connectors, were compared with

“more common” timber-to-timber solutions. Hardwood-hardwood configurations were also investigated. The outcome of the test program was characterized by a large variability in the specimen performance, in terms of both pre-stress, camber value and flexural behaviour. Final uplift  $w_{CP}$  ranging from  $L/872$  to  $L/251$  was registered. The maximum values of flexural capacity were observed for those specimens where hardwood joists were employed. However, the ultimate limit state (ULS) design conditions did not constitute a limiting criterion for any of the tested structures. Generally, thanks to the higher value of slip modulus exhibited by double threaded (DT) screws with respect to single threaded (ST) screws, a greater efficiency was observed in those configurations where DT screws were adopted (considering same-size timber elements). By comparing hardwood-hardwood configurations with different joist cross-sections, greater camber values were registered for the specimens characterised by having slenderer beams. This resulted in the “slender solutions” being more effective within the range of interest ( $0 < w < w_{SLS}$ ).

The development of high-performance solutions for prefabricated timber-to-timber composite floor modules to be realized by using laminated veneer lumber (LVL) made of beech wood was presented. In this case, the cambering and pre-stressing (CP) procedure was used to maximize the floor efficiency and exploit the remarkable strength properties of hardwood products. Two modules characterised by different span (6 m and 10m) and service load were designed and tested out-of-plane. Testing of the connection system, that was regarded as the most suited to guarantee the best floor performance (at reasonable economical costs), was also performed. All tested floor specimens largely satisfied both the service limit state and the ultimate limit state requirements. The application of the CP assembly procedure permitted to obtain relatively high values of camber. Moreover, a remarkable equivalent distributed load necessary to eliminate the upward deformation introduced in the specimens was recorded for all specimens. Stiffness of the tested specimens assembled with the assembly procedure was observed to be higher than the stiffness derived from the pushover curves obtained from the numerical models. The extra-stiffness appeared to be related to the magnitude of pre-stress applied.

The last phase of the research activity was dedicated to the study of the rheological behaviour of timber-to-timber composite beams assembled with the innovative technique thoroughly analysed in this thesis. To this purpose, four composite specimens made of softwood elements, were assembled and then loaded out-of-plane and subjected to continuous monitoring under controlled environmental conditions (in a climatic chamber). Despite the inevitable reduction of the compression force generated by the screws, the benefits of adopting the CP procedure appeared to be persistent over time. A general good correlation between the predictive models (numerical and analytical

models) and the experimental data was observed. Different screw types and configurations were investigated in this experimental campaign. As result, thanks to a higher compression force and a lower stiffness, the single threaded screws coupled with washers permitted to obtain higher camber values than the double threaded screws. On the other hand, the specimen assembled with single threaded screws exhibited a higher creep rate and a mechanical behaviour more sensitive to moisture content changes in the timber elements than the specimens constructed by using double threaded screws. The combined use of both connector types appeared to be the most promising solution.